Flight Testing the Piper PA-32 Saratoga and PA-31 Navajo

A Thesis Presented for the

Master of Science

Degree

The University of Tennessee, Knoxville

Matthew John DiMaiolo

May 2015

Copyright © 2015 by Matthew DiMaiolo

All rights reserved.

DEDICATION

I dedicate this thesis to my family for always supporting me and encouraging me to follow my dreams.

ACKNOWLEDGEMENTS

I would like to express my great appreciation for everyone in the Aviation Systems and Flight Research Department who helped me in the creation, execution, and completion of this thesis. I would like to thank Dr. Steve Brooks, my advisor, for his guidance in writing this document, Dr. Peter Solies for providing the theoretical knowledge of flight mechanics, and Dr. Borja Martos for providing the applied knowledge of flight testing and acting as a test pilot. I would also like to extend my gratitude to Greg Heatherly for his time and patience as the primary test pilot and his knowledge of flying, to Jacob Bowman for his support and knowledge of aircraft systems, and Jonathan Kolwyck for his assistance with calibrations and knowledge of test systems. I would also like to thank Kristopher Oegema and Jorge Parra Martinez for their patience and support in assisting with flight tests and data reduction. I thank everyone for their willingness to wake up early for pre-sunrise briefings. I would also like to thank my family and friends for all of their continued support; I never would have made it to this point without them.

ABSTRACT

The purpose of this thesis was to flight test the University of Tennessee Space Institute's PA-32 Saratoga and PA-31 Navajo and provide baseline data for future students to reference. Flight tests consisted of both performance and stability and control parameters using a variety of flight test techniques. The tests selected represent the fundamentals that are taught in classes and short courses at the university, beginning with the air data system calibration, proceeding to cruise and climb performance, to stall performance and characteristics, and to static and dynamic stability.

After an introduction and description of the aircraft and flight test program, the selected flight tests are discussed with theory, flight test techniques, and data reduction methods. For many of the flight tests, only a single technique was used to gather data. However, a number of tests include the use of multiple techniques and/or data reduction methods; this provides students with exposure to varying methods that may be used with a range of aircraft. The results of each flight test are discussed and recommendations for future tests provided.

TABLE OF CONTENTS

CHAPTER 1 INTRODUCTION 1
1.1 Purpose 1
1.2 Flight Testing Background 1
CHAPTER 2 PROGRAM DESCRIPTION 3
2.1 Flight Test Plan 3
2.2 Aircraft Description 4
CHAPTER 3 FLIGHT TEST TECHNIQUES 6
3.1 Air Data System Calibration 6
3.2 Cruise Performance 8
3.3 Climb Performance 11
3.4 Stalls 12
3.5 Longitudinal Static Stability 14
3.6 Longitudinal Maneuvering Stability 17
3.7 Longitudinal Dynamic Stability 20
3.8 Lateral-Directional Static Stability 22
3.9 Lateral-Directional Dynamic Stability 24
CHAPTER 4 RESULTS AND DISCUSSION 26
4.1 Air Data System Calibration 26
4.1.1 Saratoga – GPS 4 Leg Method 26
4.1.2 Navajo – GPS 4 Leg Method 26
4.2 Cruise Performance 27
4.2.1 Saratoga – PIW-VIW Method 27
4.2.2 Saratoga – W/δ Method 28
4.2.3 Navajo – PIW-VIW Method 29
4.2.4 Navajo – W/δ Method 30
4.3 Climb Performance 31
4.3.1 Saratoga – Sawtooth Climb Method 31
4.3.2 Saratoga – Level Accel Method 31
4.3.3 Navajo – Sawtooth Climb Method 32
4.3.4 Navajo – Level Accel Method 33
4.4 Stalls 34
4.4.1 Saratoga – Stalls 34
4.4.2 Navajo – Stalls 35
4.5 Longitudinal Static Stability 37
4.5.1 Saratoga – Stabilized Method 37
4.5.2 Saratoga – Level Accel/Decel Method 39
4.5.3 Navajo – Stabilized Method 40
4.5.4 Navajo – Level Accel/Decel Method 42
4.6 Longitudinal Maneuvering Stability 44
4.6.1 Saratoga – Stabilized Load Factor Method 44
4.6.2 Navajo – Stabilized Load Factor Method 45
4.7 Longitudinal Dynamic Stability 45
4.7.1 Saratoga – Phugoid 45
4.7.2 Saratoga – Short Period 46

4.7.3 Navajo – Phugoid 47
4.7.4 Navajo – Short Period 47
4.8 Lateral-Directional Static Stability 48
4.8.1 Saratoga – Steady Heading Sideslip Method 48
4.8.2 Navajo – Steady Heading Sideslip Method 50
4.9 Lateral-Directional Dynamic Stability 51
4.9.1 Saratoga – Spiral Mode 51
4.9.2 Saratoga – Roll Mode 51
4.9.3 Saratoga – Dutch Roll Mode 52
4.9.4 Navajo – Spiral Mode 52
4.9.5 Navajo – Roll Mode 53
4.9.6 Navajo – Dutch Roll Mode 53
CHAPTER 5 CONCLUSION 55
5.1 Overview 55
5.2 Recommendations 55
BIBLIOGRAPHY 57
APPENDICES 59
APPENDIX A FIGURES 60
APPENDIX B TABLES 136
APPENDIX C LOCATION OF ADDITIONAL DOCUMENTATION 139
APPENDIX D METHODS FOR DETERMINING DAMPING RATIO 140
D.1 Subsidence Ratio Method or Log Decrement Method 140
D.2 Transient Peak Ratio Method 142
D.3 Time Ratio Method 144
D.4 Log Decrement Equation Method 147
VITA 149

LIST OF TABLES

Table 2.1 – Flight Test Parameter Details 136
Table 4.1 – Comparison of Saratoga Values of Rate of Climb Using the Sawtooth Climb Method 137
Table 4.2 – Comparison of Navajo Values of Rate of Climb Using the Sawtooth Climb Method 137
Table 4.3 – Saratoga Stall Speeds in Clean Configuration 137
Table 4.4 – Saratoga Stall Speeds in Landing Configuration 137
Table 4.5 – Saratoga Stall Speeds in 30° Bank, Clean Configuration 138
Table 4.6 – Navajo Stall Speeds in Clean Configuration 138
Table 4.7 – Navajo Stall Speeds in Landing Configuration 138
Table 4.8 – Navajo Stall Speeds in 30° Bank, Clean Configuration 138

LIST OF FIGURES

Figure 2.1 – Piper PA-32 Saratoga 60
Figure 2.2 – Saratoga Factory Pitot-Static Mast 60
Figure 2.3 – Saratoga Test Air Data System 61
Figure 2.4 – Saratoga Test Fuselage Static Port 61
Figure 2.5 – Piper PA-31 Navajo 62
Figure 2.6 – Navajo Factory Pitot Tube 62
Figure 2.7 – Navajo Static Ports 63
Figure 2.8 – Navajo Test Air Data System 64
Figure 4.1 – Position Error Correction Coefficient vs. Indicated Airspeed for N22UT 65
Figure 4.2 – Velocity Position Error Correction vs. Indicated Airspeed for N22UT 65
Figure 4.3 – Altitude Position Error Correction vs. Indicated Airspeed for N22UT 66
Figure 4.4 – Position Error Correction Coefficient vs. Indicated Airspeed for N11UT 66
Figure 4.5 – Velocity Position Error Correction vs. Indicated Airspeed for N11UT 67
Figure 4.6 – Altitude Position Error Correction vs. Indicated Airspeed for N11UT 67
Figure 4.7 – PIW vs. VIW for N22UT 68
Figure 4.8 – Normalized PIW vs. VIW for N22UT 68
Figure 4.9 – Pressure Altitude vs. Manifold Pressure for N22UT 69
Figure 4.10 – Density Altitude vs. True Airspeed for N22UT 69
Figure 4.11 – Drag Coefficient vs. Lift Coefficient Squared for N22UT 70
Figure 4.12 – Drag Polar for N22UT 70
Figure 4.13 – Specific Range Using the PIW-VIW Method for N22UT 71
Figure 4.14 – Specific Endurance Using the PIW-VIW Method for N22UT 71
Figure 4.15 – Equivalent Shaft Horsepower vs. Equivalent Airspeed for N22UT 72
Figure 4.16 – Normalized Equivalent Shaft Horsepower vs. Equivalent Airspeed for N22UT 72
Figure 4.17 – Fuel Flow vs. Calibrated Airspeed for N22UT 73
Figure 4.18 – Referred Fuel Flow vs. Referred Shaft Horsepower for N22UT 73
Figure 4.19 – Shaft Horsepower Specific Fuel Consumption vs. Referred Shaft Horsepower for N22UT .. 74
Figure 4.20 – Specific Range Using W/δ Method for N22UT 74
Figure 4.21 – Specific Endurance Using W/δ Method for N22UT 75
Figure 4.22 – PIW vs. VIW for N11UT 75
Figure 4.23 – Normalized PIW vs. VIW for N11UT 76
Figure 4.24 – Pressure Altitude vs. Manifold Pressure for N11UT 76
Figure 4.25 – Density Altitude vs. True Airspeed for N11UT 77
Figure 4.26 – Drag Coefficient vs. Lift Coefficient Squared for N11UT 77
Figure 4.27 – Drag Polar for N11UT 78
Figure 4.28 – Specific Range Using PIW-VIW Method for N11UT 78
Figure 4.29 – Specific Endurance Using PIW-VIW Method for N11UT 79
Figure 4.30 – Equivalent Shaft Horsepower vs. Equivalent Airspeed for N11UT 79
Figure 4.31 – Normalized Equivalent Shaft Horsepower vs. Equivalent Airspeed for N11UT 80
Figure 4.32 – Fuel Flow vs. Calibrated Airspeed for N11UT 80
Figure 4.33 – Referred Fuel Flow vs. Referred Shaft Horsepower for N11UT 81

Figure 4.34 – Shaft Horsepower Specific Fuel Consumption vs. Referred Shaft Horsepower for N11UT.. 81
Figure 4.35 – Specific Range Using W/δ Method for N11UT 82
Figure 4.36 – Specific Endurance Using W/δ Method for N11UT 82
Figure 4.37 – Rate of Climb vs. Calibrated Airspeed Using Sawtooth Climbs for N22UT 83
Figure 4.38 – PIW vs. CIW for N22UT 83
Figure 4.39 – Density Altitude vs. Rate of Climb Using Sawtooth Climb for N22UT 84
Figure 4.40 – True Airspeed vs. Time for N22UT 84
Figure 4.41 – Specific Excess Power vs. True Airspeed for N22UT 85
Figure 4.42 – Pressure Altitude vs. Indicated Airspeed for N22UT 85
Figure 4.43 – Rate of Climb vs. Calibrated Airspeed Using Level Accel for N22UT 86
Figure 4.44 – Density Altitude vs. Rate of Climb Using Level Accel for N22UT 86
Figure 4.45 – Rate of Climb vs. Calibrated Airspeed Using Sawtooth Climb for N11UT 87
Figure 4.46 – PIW vs. CIW for N11UT 87
Figure 4.47 – Density Altitude vs. Rate of Climb Using Sawtooth Climb for N11UT 88
Figure 4.48 – True Airspeed vs. Time for N11UT 88
Figure 4.49 – Specific Excess Power vs. True Airspeed for N11UT 89
Figure 4.50 – Pressure Altitude vs. Indicated Airspeed for N11UT 89
Figure 4.51 – Rate of Climb vs. Calibrated Airspeed Using Level Accel for N11UT 90
Figure 4.52 – Density Altitude vs. Rate of Climb Using Level Accel for N11UT 90
Figure 4.53 – Stall Testing in a Clean Configuration for N22UT 91
Figure 4.54 – Stall Testing in a Power Approach Configuration for N22UT 92
Figure 4.55 – Stall Testing in a 30° Turn for N22UT 93
Figure 4.56 – Stall Testing in a Clean Configuration for N11UT 94
Figure 4.57 – Stall Testing in a Power Approach Configuration for N11UT 95
Figure 4.58 – Stall Testing in a 30° Turn for N11UT 96
Figure 4.59 – Elevator Deflection vs. Calibrated Airspeed Using Stabilized Method for N22UT 97
Figure 4.60 – Elevator Deflection vs. Lift Coefficient Using Stabilized Method for N22UT 97
Figure 4.61 – Stick-Fixed Neutral Point Determination Using Stabilized Method for N22UT 98
Figure 4.62 – Stick-Fixed Neutral Point vs. Lift Coefficient Using Stabilized Method for N22UT 98
Figure 4.63 – Elevator Force vs. Calibrated Airspeed Using Stabilized Method for N22UT 99
Figure 4.64 – Elevator Force vs. Lift Coefficient Using Stabilized Method for N22UT 99
Figure 4.65 – Stick-Free Neutral Point Determination Using Stabilized Method for N22UT 100
Figure 4.66 – Stick-Free Neutral Point vs. Lift Coefficient Using Stabilized Method for N22UT 100
Figure 4.67 – Elevator Deflection vs. Calibrated Airspeed Using Level Accel/Decel for N22UT 101
Figure 4.68 – Elevator Deflection vs. Lift Coefficient Using Level Accel/Decel for N22UT 101
Figure 4.69 – Stick-Fixed Neutral Point Determination Using Level Accel/Decel for N22UT 102
Figure 4.70 – Stick-Fixed Neutral Point vs. Lift Coefficient Using Level Accel/Decel for N22UT 102
Figure 4.71 – Elevator Force vs. Calibrated Airspeed Using Level Accel/Decel for N22UT 103
Figure 4.72 – Elevator Force vs. Lift Coefficient Using Level Accel/Decel for N22UT 103
Figure 4.73 – Stick-Free Neutral Point Determination Using Level Accel/Decel for N22UT 104
Figure 4.74 – Stick-Free Neutral Point vs. Lift Coefficient Using Level Accel/Decel for N22UT 104
Figure 4.75 – Elevator Deflection vs. Calibrated Airspeed Using Stabilized Method for N11UT 105
Figure 4.76 – Elevator Deflection vs. Lift Coefficient Using Stabilized Method for N11UT 105

Figure 4.77 – Stick-Fixed Neutral Point Determination Using Stabilized Method for N11UT 106
Figure 4.78 – Stick-Fixed Neutral Point vs. Lift Coefficient Using Stabilized Method for N11UT 106
Figure 4.79 – Elevator Force vs. Calibrated Airspeed Using Stabilized Method for N11UT 107
Figure 4.80 – Elevator Force vs. Lift Coefficient Using Stabilized Method for N11UT 107
Figure 4.81 – Stick-Free Neutral Point Determination Using Stabilized Method for N11UT 108
Figure 4.82 – Stick-Free Neutral Point vs. Lift Coefficient Using Stabilized Method for N11UT 108
Figure 4.83 – Elevator Deflection vs. Calibrated Airspeed Using Level Accel/Decel for N11UT 109
Figure 4.84 – Elevator Deflection vs. Lift Coefficient Using Level Accel/Decel for N11UT 109
Figure 4.85 – Stick-Fixed Neutral Point Determination Using Level Accel/Decel for N11UT 110
Figure 4.86 – Stick-Fixed Neutral Point vs. Lift Coefficient Using Level Accel/Decel for N11UT 110
Figure 4.87 – Elevator Force vs. Calibrated Airspeed Using Level Accel/Decel for N11UT 111
Figure 4.88 – Elevator Force vs. Lift Coefficient Using Level Accel/Decel for N11UT 111
Figure 4.89 – Stick-Free Neutral Point Determination Using Level Accel/Decel for N11UT 112
Figure 4.90 – Stick-Free Neutral Point vs. Lift Coefficient Using Level Accel/Decel for N11UT 112
Figure 4.91 – Elevator Deflection vs. Load Factor for N22UT 113
Figure 4.92 – Stick-Fixed Maneuvering Point Determination for N22UT 113
Figure 4.93 – Elevator Force vs. Load Factor for N22UT 114
Figure 4.94 – Stick-Free Maneuvering Point Determination for N22UT 114
Figure 4.95 – Elevator Defection vs. Load Factor for N11UT 115
Figure 4.96 – Stick-Fixed Maneuvering Point Determination for N11UT 115
Figure 4.97 – Elevator Force vs. Load Factor for N11UT 116
Figure 4.98 – Stick-Free Maneuvering Point Determination 116
Figure 4.99 – Stick-Fixed Phugoid for N22UT 117
Figure 4.100 – Stick-Free Phugoid for N22UT 117
Figure 4.101 – Short Period Frequency Sweep for N22UT 118
Figure 4.102 – Stick-Fixed Short Period for N22UT 118
Figure 4.103 – Stick-Free Short Period for N22UT 119
Figure 4.104 – Stick-Fixed Phugoid for N11UT 119
Figure 4.105 – Stick-Free Phugoid for N11UT 120
Figure 4.106 – Short Period Frequency Sweep for N11UT 120
Figure 4.107 – Stick-Fixed Short Period for N11UT 121
Figure 4.108 – Stick-Free Short Period for N11UT 121
Figure 4.109 – Lateral-Directional Static Stability for N22UT 122
Figure 4.110 – Indicated Airspeed vs. Angle of Sideslip for N22UT 123
Figure 4.111 – Lateral-Directional Static Stability for N11UT 124
Figure 4.112 – Indicated Airspeed vs. Angle of Sideslip for N11UT 125
Figure 4.113 – Stick-Fixed Spiral Mode for N22UT 126
Figure 4.114 – Stick-Free Spiral Mode for N22UT 127
Figure 4.115 – Left-to-Right Roll Mode for N22UT 128
Figure 4.116 – Right-to-Left Roll Mode for N22UT 128
Figure 4.117 – Stick-Fixed Dutch Roll Mode for N22UT 129
Figure 4.118 – Stick-Free Dutch Roll Mode for N22UT 130
Figure 4.119 – Stick-Fixed Spiral Mode for N11UT 131

Figure 4.120 – Stick-Free Spiral Mode for N11UT 132
Figure 4.121 – Left-to-Right Roll Mode for N11UT 133
Figure 4.122 – Right-to-Left Roll Mode for N11UT 133
Figure 4.123 – Stick-Fixed Dutch Roll Mode for N11UT 134
Figure 4.124 – Stick-Free Dutch Roll Mode for N11UT 135
Figure D.1 – Airspeed Deviations 141
Figure D.2 – Subsidence Ratio Plot 141
Figure D.3 – Peak-to-Peak Deviations 143
Figure D.4 – Transit Peak Ratio Plot 143
Figure D.5 – Maximum Parameter Value 145
Figure D.6 – Time Ratio Plot – Determining Damping Ratio 145
Figure D.7 – Time Ratio Plot – Determining Frequency 146
Figure D.8 – Determining X_0 and X_n 148

ABBREVIATIONS AND SYMBOLS

%MAC	Percent of mean aerodynamic chord
BHP	Brake horsepower (hp)
C.G.	Center of gravity
$\bar{c}_e$	Elevator mean aerodynamic chord (ft)
CAP	Control Anticipation Parameter ($1/g\text{-}s^2$)
CIW	Climb rate adjust for weight (ft/min)
D	Drag (lbs)
DAS	Data Acquisition System
deg (°)	Degrees
FAA	Federal Aviation Administration
FAR	Federal Aviation Regulations
F_e	Elevator stick force (lbs)
ft	Feet
g	Gravity (ft/s^2)
GPS	Global Positioning System
h_D	Density Altitude (ft)
H_i	Indicated altitude (ft)
H_o	Observed altitude (ft)
hp	Horsepower
h_p	Pressure Altitude (ft)
hr	Hour
K	Constant based on system gearing, elevator size, and horizontal tail efficiency (ft^2)

KCAS	Calibrated Airspeed (kts)
KIAS	Indicated Airspeed (kts)
kts	Knots
lbs	Pounds
l_t	Distance from wing aerodynamic center to horizontal tail aerodynamic center (ft)
MIAS	Indicated Airspeed (mph)
min	Minute
M.P.	Maneuvering Point
mph	Miles per hour
n	Load factor
nm (or nmi)	Nautical Miles
N.P.	Neutral Point
N_z	Load factor
P	Pressure at altitude (lbs/ft^2)
p	Roll rate (deg/s)
PIW	Power corrected for weight (hp)
P_s	Specific excess power (ft/s)
P_{SL}	Sea-level pressure (lbs/ft^2)
POH	Pilot's Operating Handbook
q	Dynamic pressure (lbs/ft^2)
q_c	Impact pressure (lbs/ft^2)
q_{ci}	Indicated impact pressure (lbs/ft^2)
rad	Radians

ref (subscript)	Referred value
ROC	Rate of climb (ft/min)
RPM	Revolutions Per Minute
S	Wing area (ft^2)
s	Seconds
SE	Specific Endurance (hr/lb)
S_e	Elevator area (ft^2)
SHP	Shaft horsepower
SHPSFC	Shaft Horsepower Specific Fuel Consumption
SR	Specific range (nm/lb)
T	Thrust (lbs)
test (subscript)	Test value
t_2	Time to double amplitude (s)
UTSI	University of Tennessee Space Institute
V	Velocity (ft/s)
V_C	Calibrated airspeed (kts)
V_e	Equivalent airspeed (kts)
V_i	Indicated airspeed (kts)
VIW	Airspeed corrected for weight (kts)
V_o	Observed airspeed (kts)
V_{SC}	Calibrated stall speed (kts)
$V_{SC\text{-}CG}$	Calibrated stall speed corrected for C.G. location (kts)
VSI	Vertical Speed Indicator

V_{SiW}	Indicated stall speed corrected for weight (kts)
$V_{SiW\text{-}CG}$	Indicated stall speed corrected for weight and C.G. location (kts)
V_T	True airspeed (kts, ft/s)
V_x	Best angle of climb airspeed (kts)
V_y	Best rate of climb airspeed (kts)
W	Weight (lbs)
$\dot{W}_f$	Fuel flow (lbs/hr)
α	Angle of attack (deg)
β	Angle of sideslip (deg)
γ	Heat capacity ratio
δ	Logarithmic decrement
δ_a	Aileron deflection (deg)
δ_e	Elevator deflection (deg)
ΔH_{ic}	Instrument corrected altitude (ft)
ΔH_{pc}	Altitude position error correction (kts)
Δp_{pc}	Static position error correction
δ_r	Rudder deflection (deg)
ΔV_{ic}	Instrument corrected airspeed (kts)
ΔV_{pc}	Velocity position error correction (kts)
ζ	Damping ratio
η_p	Propeller efficiency
θ	Pitch angle (deg)
ρ	Density at altitude (sl/ft^3)

ρ_{SL}	Sea-level density (sl/ft^3)
τ	Rate of change of effective angle of attack with change of elevator deflection
τ_R	Roll mode time constant
ϕ	Bank angle (deg)
ω_d	Damped natural frequency (rad/s)
ω_n	Undamped natural frequency (rad/s)
C_D	Drag coefficient
$C_{h_{\alpha_t}}$	Pitching moment coefficient due to angle of attack of horizontal tail
$C_{h_{\delta_e}}$	Elevator hinge moment coefficient due to elevator deflection
C_L	Lift coefficient
C_{l_β}	Rolling moment coefficient due to angle of sideslip or Dihedral Effect
$C_{l_{\delta_a}}$	Rolling moment coefficient due to aileron deflection or Aileron Control Power
$C_{l_{\delta_r}}$	Rolling moment coefficient due rudder deflection
C_m	Pitching moment coefficient
$C_{m_{\delta_e}}$	Pitching moment coefficient due to elevator deflection or Elevator Control Power
$C_{m_{\dot{\theta}}}$	Pitching moment coefficient due to pitch rate
C_{n_β}	Yawing moment coefficient due to sideslip or Weathercock Stability
$C_{n_{\delta_a}}$	Yawing moment coefficient due to aileron deflection
$C_{n_{\delta_r}}$	Yawing moment coefficient due to rudder deflection or Rudder Control Power
C_{Y_β}	Side force coefficient due to sideslip
$C_{Y_{\delta_a}}$	Side force coefficient due to aileron deflection
$C_{Y_{\delta_r}}$	Side force coefficient due to rudder deflection

CHAPTER 1 INTRODUCTION

1.1 Purpose

The purpose of these flight tests was to establish baseline data for the Piper Saratoga and Navajo aircraft using the installed test equipment. Prior to this research, students were only able to compare test results with those of the published POH or with previous students' results. While results should compare relatively well with those values published, the test systems are independent from factory-installed systems. This separation in systems results in a difference of results. Additionally, each POH contains only performance data and no information on stability characteristics. As was noticed during flight testing, some test results compare well with published values while others are largely different. The focus of the tests was to provide a best-possible optimized set of data to be used in reduction to the desired plots. These plots would then be used in UTSI classes and short courses by students to compare their results with those found herein based on the test equipment.

For each flight test performed, several items were delivered to UTSI for future use. As previously discussed, a best-possible set of data was provided. These data includes copies of the original flight data cards and DAS files containing all in-flight data. Also, spreadsheets of the data reduction are provided along with all plots derived. These plots were also placed in a separate manual for use by students. A standardized set of flight data cards, reduction spreadsheets, and reduction procedures were also produced.

1.2 Flight Testing Background

Flight testing is the act of performing specific maneuvers in an aircraft to determine real-world vehicle parameters and characteristics. Fundamental equations and theories are used as the basis for the design, development, and flight testing of aircraft. While the initial design process attempts to factor in all real-world effects, many assumptions must be made that can only be verified by actually flying the

aircraft. Flight test teams, consisting of engineers, managers, pilots, mechanics, and a possible range of other positions, have developed a variety of techniques useful for determining an aircraft's characteristics. Techniques vary based on the aircraft used in testing. Since propeller-driven, general aviation aircraft are generally less maneuverable, flight test techniques are primarily focused on stabilized conditions that take a long amount of time, on the order of hours, to complete. The procedures used usually focus on classic methods for flight testing as opposed to newer, less expensive approaches. In comparison, fighter aircraft are significantly more maneuverable than most other aircraft and can, therefore, perform dynamic flight test techniques that greatly reduce time and cost. However, many techniques are applicable to a range of aircraft types. Though some techniques are not acceptable for regulation standards, they may provide excellent data for military specifications or pure research purposes.

Once the purpose for flight testing is established, a program can be planned based on the requirements. The flight test team works together to determine what each flight will specifically test, how the team will perform the test, and what safety concerns are involved. Once the testing is complete, the data will be reduced to determine the parameters in question. Testing will continue until the whole program is complete and the aircraft or system can be approved, certified, or improved.

CHAPTER 2 PROGRAM DESCRIPTION

2.1 Flight Test Plan

Two different aircraft were used for flight testing. Each of the nine flight tests were performed on both vehicles. The flight tests performed were selected based on those most commonly taught in UTSI classes and short courses. Though the selected tests do not cover the entire range of a complete flight test program, the chosen tests encompass the fundamentals for both performance parameters and stability and control characteristics. The flight tests include:

- Air Data System Calibration
- Cruise Performance
- Climb Performance
- Stalls
- Longitudinal Static Stability
- Longitudinal Maneuvering Stability
- Longitudinal Dynamic Stability
- Lateral-Directional Static Stability
- Lateral-Directional Dynamic Stability

Several of the flight tests selected include the use of multiple methods. For example, climb performance was determined by using both the sawtooth climb method and the level acceleration method. The selection of methods to perform is based on aircraft limits, industry standards, and federal regulations. Using multiple methods to complete a specific test allows students to be exposed to numerous techniques and compare the reduction methods and results.

As always, safety plays a key factor in all flight testing. Since the focus of classes at UTSI is purely for educational purposes, all tests are properly briefed and any hazards, beyond those innate to all types

of flying, are avoided. Each flight began with a pre-flight briefing discussing weight, weather, emergency procedures, and details of the test to be performed. A pre-flight aircraft inspection was performed by the pilot and maintenance personnel before all crew members boarded the aircraft. Once the engines were started, the DAS was turned on and the parameters required for testing were checked. All ground checks were performed and the flights proceeded as planned. Upon return to the airport, all test parameters were checked again for continuity before the aircraft was shut down. A post-flight briefing after each flight was done to review the events of the flight and discuss any changes to be made in future flights. All test points were completed in a stable air mass absent of turbulence. Any wind present was assumed to have a constant, horizontal component and no vertical component.

All data reduction was performed using Microsoft Excel. Though several other programs exist that provide more accurate plotting and curve fitting, Excel is the most readily available and commonly used in UTSI classes.

2.2 Aircraft Description

The first aircraft used was a 1981 Piper PA-32-301 Saratoga. It is a single-engine aircraft primarily used as a “flying classroom” for UTSI classes and short courses. It is capable of carrying one pilot and up to five students or passengers. The maximum gross weight of the aircraft is 3,600 lbs. It is powered by a single Lycoming IO-540 naturally aspirated, fuel injected engine. The Saratoga is fully instrumented for flight testing and the DAS is capable of recording key parameters for both performance and stability and control tests. Both a bent probe and a Kiel probe are located under the right wing to be used for a pitot source. However, only one source is connected to the DAS at a time. Likewise, a bent static probe under the wing and static ports on the aft fuselage are installed. Again, only one static source is connected to the DAS at a time. For testing, the Kiel probe was used as the pitot source and the bent probe was used for the static source. The aircraft has a factory-installed pitot-static system that is independent of the DAS. The aircraft features an air data system boom with an angle of attack vane and an angle of sideslip vane.

Though these vanes have been calibrated on the ground, in-flight calibrations have not been performed and results with these instruments are approximate. This boom limits the maximum allowed airspeed of the aircraft to 150 KIAS. Figure 2.1, located in Appendix A with all figures, shows the Saratoga. Figures 2.2-2.4 show the factory and test air data systems for the Saratoga.

The other aircraft used was a 1967 PA-31-310 Navajo. It is a twin-engine aircraft primarily used for flight research and as a "flying classroom". It is also capable of carrying one pilot and up to five students or passengers. The maximum gross weight of the aircraft is 6,500 lbs. It is powered by two Lycoming TIO-540 turbocharged, fuel injected engines. Like the Saratoga, the Navajo is fully instrumented for performance and stability and control flight tests. A Kiel probe and bent probe are installed on the nose for use as pitot sources. A switch on the DAS rack allows the option of which source to use. A bent static probe is also located on the nose as well as static ports on the aft fuselage. Likewise, a switch on the DAS rack allows the option of which source to use. For testing, the bent pitot source and the fuselage static source was used. The Navajo does not feature an air data system boom. Instead, it uses an angle of attack cone located on the right side of the nose to determine angle of attack. Because an in-flight calibration of the angle of attack cone has not been performed and the cone is potentially affected by its location just forward and above the wing and near the right propeller, results presented contain an additional, unknown error. The Navajo uses differential pressure sensors in the nose to determine angle of sideslip. Because of this, the angle of sideslip generally has a large bias that must be removed to approximate values. Figure 2.5 shows the Navajo. Figures 2.6-2.8 show the factory and test air data systems for the Navajo.

Table 2.1, located in Appendix B with all tables, shows a list of all parameters available on both aircraft used throughout testing, the units of each, and any notes specific to that parameter.

CHAPTER 3 FLIGHT TEST TECHNIQUES

3.1 Air Data System Calibration

Many flight test programs begin with the air data system calibration. This is done in the beginning of the program because most other flight tests depend on accurate values of air data, which includes airspeed, altitude, Mach number, temperature, vertical speed, angle of attack, and angle of sideslip. The purpose of the air data system calibration is to determine the static source position error.

As an aircraft flies through the air, the pressure field surrounding the vehicle is disturbed. Placing the static source at a location of minimal pressure disturbance, such as on a boom ahead of the nose, under the wing, or on the aft fuselage, is important to reducing errors. However, errors still occur as the pressure field changes with airspeed, Mach number, angle of attack, angle of sideslip, and Reynold's number. Once the static position error correction is determined, it can be applied to correct airspeed, Mach number, and altitude. Using the Mach number, a correction to the observed outside air temperature can be made. However, for the purpose of this document, the observed temperature was assumed accurate. Many methods exist to determine the static position error correction of an aircraft. The GPS method was selected for both of the test aircraft. In the GPS method, the pilot flies at least three legs and GPS track, GPS groundspeed, airspeed, altitude, heading, outside air temperature, manifold pressure, RPM, and fuel quantity are recorded. Using the algorithm described in Advisory Circular 23-8C [2], wind speed and direction are extracted and the result is a true airspeed. This airspeed can be converted to a calibrated airspeed to determine position error correction. The test is repeated at a number of speeds across the airspeed range of the aircraft.

Doug Gray's "Using GPS to accurately establish True Airspeed (TAS)" shows how the GPS method removes the wind vector from true airspeed [13]. The GPS 4 Leg Method was selected for both of the test aircraft. The difference from using three legs is that the true airspeed is averaged from four combinations

of three legs. This allows a standard deviation to be determined which can be used as a reference to determine the accuracy of data. A large standard deviation, usually greater than 1.0, could be a result of an unstable air mass. The algorithm can be used in flight with a computer to give an immediate result. It can then be determined if a leg(s) needs to be repeated.

To begin reducing these data, instrument error corrections discerned from ground calibrations can be applied to the observed airspeed and altitude to determine indicated values. The DAS installed in each aircraft allows instrument calibration corrections to be factored into observed values; this means instrument correction values are zero in the data reduction.

$$V_i = V_o + \Delta V_{ic} \tag{3.1}$$

$$H_i = H_o + \Delta H_{ic} \tag{3.2}$$

From the algorithm, the values for true airspeed are determined for each target airspeed tested. From the indicated and true airspeeds, dynamic pressure, q_c, and indicated dynamic pressure, q_{ci}, can be calculated.

$$q_c = P\left[\left(1 + \frac{\gamma - 1}{2\gamma}\frac{\rho}{P}V_T^2\right)^{\frac{\gamma}{\gamma-1}} - 1\right] \tag{3.3}$$

$$q_{ci} = P_{SL}\left[\left(1 + \frac{\gamma - 1}{2\gamma}\frac{\rho_{SL}}{P_{SL}}V_i^2\right)^{\frac{\gamma}{\gamma-1}} - 1\right] \tag{3.4}$$

To determine the static position error, q_{ci} is subtracted from q_c.

$$\Delta P_{pc} = q_c - q_{ci} \tag{3.5}$$

The static position error can be divided by the indicated dynamic pressure to non-dimensionalize the value, allowing all altitudes tested to be compressed to a single curve. This is known as the static position error coefficient, $\Delta p_{pc}/q_{ci}$. Next, true airspeed is multiplied by the square root of the density ratio to find equivalent airspeed. At low subsonic speeds less than Mach 0.3, calibrated airspeed is assumed approximately equal to equivalent airspeed.

$$V_e = V_T\sqrt{\sigma} \tag{3.6}$$

$$V_C \cong V_e \tag{3.7}$$

Subtracting indicated airspeed from calibrated airspeed yields the velocity position error.

$$\Delta V_{pc} = V_C - V_i \tag{3.8}$$

Altitude position error can then be determined.

$$\Delta H_{pc} = \frac{\Delta P_{pc}}{\rho g} \tag{3.9}$$

The static position error coefficient, velocity position error, and altitude position error can now all be plotted against indicated airspeed. The resulting equation of the curve can be used on future tests to determine the velocity position error correction and altitude position error correction as a function of indicated airspeed.

3.2 Cruise Performance

During cruise, the aircraft is described as being in level, unaccelerated flight. Assuming small angles of attack, zero angle of sideslip, and small incidence angles of thrust, it can be said that thrust is equal to drag and lift is equal to weight. These are good assumptions since the aircraft is in a stabilized cruise configuration. Cruise performance can be viewed as power available versus power required. Power required is primarily driven by the drag, which varies with airspeed. Power available is a function of the power plant type and, if applicable, the propeller efficiency, which also varies with airspeed. Weight, center of gravity, air temperature, air density, airspeed, altitude, and fuel flow also affect cruise performance. Ultimately, cruise performance flight testing determines the specific range and specific endurance of an aircraft in level flight.

Multiple methods exist for determining cruise performance. The first flight test technique used for the test aircraft is the Speed-Power Method, or PIW-VIW Method. This method reduces the power required curves for all weights and air densities to a single curve. Several assumptions must be made for

the PIW-VIW method. First, it is assumed that both the lift coefficient and drag coefficient are constant for a given angle of attack. This is a valid assumption since airspeed, altitude, and weight change little, if at all, during the test. Also, a constant propeller efficiency must be assumed, which is an acceptable assumption on the front side of the power required curve. With these assumptions, Eqs. 3.10 and 3.11 can be derived [8]:

$$VIW = \frac{V_e}{\sqrt{W_{test}/W_{ref}}} \tag{3.10}$$

$$PIW = \frac{BHP_{test}\sqrt{\sigma}}{\sqrt[3]{W_{test}/W_{ref}}} \tag{3.11}$$

The flight test is performed by stabilizing the aircraft at maximum level flight speed and recording airspeed, altitude, air temperature, RPM, manifold pressure, fuel quantity, and fuel flow. Once the test point is complete, the method is repeated at varying airspeeds including on the back side of the power required curve, at which point power needs to be added to maintain altitude at a slower airspeed. The test should be repeated at multiple altitudes across the aircraft's altitude range. Values for maximum manifold pressure should also be determined for multiple altitudes so a manifold pressure versus altitude plot can be created. Section 9.5 of Kimberlin's *Flight Testing of Fixed-Wing Aircraft* describes, in detail, the procedure to reduce flight data and obtain plots of density altitude versus percent of power and density altitude versus true airspeed [8]. Since fuel flow was also recorded during testing, specific range and specific endurance can also be determined.

$$SR = \frac{V_T}{\dot{W}_f} \tag{3.12}$$

$$SE = \frac{1}{\dot{W}_f} \tag{3.13}$$

Also, since the lift coefficient and the drag coefficient are assumed constant at a given angle of attack, a drag polar can be created from the normalized PIW-VIW data.

$$C_L = \frac{2W_{ref}}{\rho_{SL}(VIW)^2 S} \tag{3.14}$$

$$C_D = \frac{2(550)(PIW)\eta_p}{\rho_{SL}(VIW)^3 S} \tag{3.15}$$

Plotting C_D versus C_L^2 produces a linear plot that determines the zero-lift drag coefficient, C_{Do}. Using this data, a drag polar can be created. Note that problems arise with this plot when factoring in installed power and propeller efficiency, which does not remain constant. [8]

Another method for determining cruise performance is the Constant W/δ Method. In this technique, the altitude is varied to maintain a constant weight divided by pressure ratio. As with the PIW-VIW Method, the lift coefficient is assumed to be constant. However, the drag coefficient changes through changes in parasite drag due to Reynold's number effects. Typically, a 1% change in drag coefficient is deemed acceptable for accurate test results. Once a target value of W/δ is determined, the aircraft is flown at a range of airspeeds while maintaining a constant W/δ ±2%. Airspeed, altitude, air temperature, RPM, manifold pressure, fuel quantity, and fuel flow are recorded at each test point. The test is repeated at another altitude. Using the reduction method described in *Fixed Wing Performance* Section 4.5.4, data were normalized and values for specific range and specific endurance are determined. [6]

An important parameter for both methods is fuel flow. Fuel flow can easily be determined with a fuel flow gauge. However, a fuel flow gauge may not have a reasonable resolution or may vary little between test airspeeds. A more accurate method is to time how long it takes to burn a given amount of fuel, especially if a digital fuel gauge is available. Both methods generally take a long time to perform (on the order of minutes), so data can be hand-recorded. Because of this, it is recommended a check plot be used to verify data in flight.

3.3 Climb Performance

Flight testing for climb performance is done to determine rate of climb, angle of climb, time to climb, and fuel to climb. Two methods exist to determine climb performance and both are based on the same equation, Eq. 3.16, of specific excess power.

$$P_s = \frac{(T - D)V}{W} = \frac{dH}{dt} + \frac{V_T}{g}\frac{dV}{dt} \tag{3.16}$$

If the airspeed is held constant and the altitude is changed, a vector approach known as sawtooth climbs or steady climbs can be used. If the altitude is held constant and the airspeed is changed, an energy method known as level accelerations can be used.

Sawtooth climbs are a series of climbs performed at varying airspeeds to determine the best rate of climb airspeed and the best angle of climb airspeed. For sawtooth climbs, it is assumed that the angle of attack is small, the thrust line acts along the direction of flight, and the airplane is climbing and accelerating in the direction of flight. These are valid assumptions since the aircraft is stabilized in a climb during the test. Each airspeed is flown at reciprocal headings to remove any wind effects. The test is performed through an altitude band, usually ±500 ft around the target altitude. The time it takes to climb 1,000 ft is noted and a resulting climb rate is determined. Another technique is to note the change in altitude in a given period of time (i.e. 60 seconds). While a VSI is usually available, instrument resolution is rarely precise enough to provide accurate values. Airspeed, altitude, temperature, RPM, manifold pressure, fuel quantity, and time are all recorded for each test point. Sawtooth climbs are a slow test usually taking several minutes per test point, so data is easily hand-recorded. During the test, a check plot of rate of climb versus airspeed can be created to check recorded data. Once the best rate of climb airspeed is determined, check climbs can be performed at addition altitudes using only this airspeed. Check climbs are also performed at reciprocal headings and determine the rate of climb at numerous altitudes while minimizing test time. Section 13.4 of Kimberlin's *Flight Testing of Fixed-Wing Aircraft*

details numerous methods for reducing flight data [8]. The method selected for the data reduction was the PIW-CIW method.

Level accelerations are performed by accelerating through the whole airspeed range of the tested aircraft. This technique assumes a constant altitude, a constant configuration, a constant power setting, and a constant load factor. These are generally valid assumptions since the altitude stays within a limit, the configuration doesn't change, the power is maximum, and the load factor, though not necessarily 1, is maintained within a limit. While handheld data can be taken, the use of a DAS is highly recommended as changes in airspeed occur much too fast to be accurately hand-recorded. To reduce these data, a plot of airspeed versus time is created and the derivative of the line determined. Values of P_s are calculated and plotted against airspeed. From this plot, values of P_s are selected at the altitudes tested. A plot of altitude versus airspeed is then created containing lines of constant P_s. Converting specific excess power to rate of climb yields plots of rate of climb versus airspeed. From this, the best rate of climb airspeed and the best angle of climb airspeed can be determined. Unlike those data from sawtooth climbs which can be expanded to include non-standard conditions, P_s values apply to a given test configuration, including weight. The test must be repeated multiple times at the same configuration to include all altitudes.

3.4 Stalls

Stall testing can be done for both performance and stability and control purposes. The performance aspect focuses on determining the stall speed. Designers typically define the stall speed as the speed at which C_{Lmax} is reached. More commonly known as aerodynamic stall, this is a factor of Reynold's number, wing planform, wing sweep, aspect ratio, weight, and CG location. However, real-world configurations, systems, and regulations may cause the stall to occur at a maximum elevator deflection or when a stick shaker/pusher activates. Because several other standard conditions are built on multiples of stall speed, this testing is normally performed early in a flight test program. Also, knowing stall speed allows flight test engineers to set lower limits for test airspeeds. Because of the high angle of attack during

a stall, the pitot-static system may not provide accurate information for stall speed. For this reason, a calibrated chase aircraft may typically be used.

The stability and control side of testing reveals the stall characteristics, or how the plane reacts during approach, entry, and recovery from a stall. Regardless of how the stall is defined for the specific aircraft, it is important to determine the stability and controllability of the aircraft once stall occurs. Flight test pilots and engineers aim to determine if poor stall characteristics, such as wing drop, roll-off, deep stall, and pitch-up, exist so proper steps can be taken to fix them. These negative characteristics can be corrected with such fixes as stall strips, wing fences, drooped leading edges, tail-lets, or electromechanical fixes [8].

Safety is always an important factor in aviation, especially when dealing with extreme ends of an aircraft's capabilities. For a new aircraft, extreme care should be taken when stalls are performed because both stall speed and characteristics are unknown. Performing a controllability check at decreasing airspeeds is an excellent way of implementing the build-up method for stalls. Even for long-existing aircraft, initial stall testing should incorporate controllability checks so the pilot knows what to expect as the aircraft slows.

The stall testing for the Saratoga and Navajo contained both performance and stability and control aspects. One wing was tufted with yarn to provide a visual stall progression during each of the three configurations for each aircraft: clean, landing, and a clean 30° bank. Each configuration began with a controllability check at four decreasing airspeeds. Controls in roll, pitch, and yaw were tested for effectiveness and any stall warnings were noted. The aircraft was then continuously slowed until stall occurred. The pilot was then questioned on stall warning speeds, stall speed, altitude loss, time to recover, and characteristics for entry, stall, and recovery. Subsequent test points for each configuration contained only a stall and no controllability check. The same questions were posed to the pilot for speeds and

characteristics. The technique calls for a deceleration rate of 1 kt/s from $1.1V_S$ to V_S. The deceleration rate, along with sideslip, bank angle, and stall progression on the wing, was monitored during each stall.

Once all weight, instrument, and position error corrections are determined, the actual deceleration rate can be determined. A process exists to correct the stall speed for a deceleration rate different from 1 kt/s, however, that process was not used for the test aircraft. The process that was used corrects the stall speed for CG position. This process, though not accepted by the FAA, allows the stall speed for the most unfavorable CG location to be determined. All airspeeds for a given correction (i.e. indicated, calibrated, indicated with a CG correction, and calibrated with a CG correction) can be averaged together to determine the actual stall speed. Stability and control characteristics should be noted in the post-flight report and fixed.

3.5 Longitudinal Static Stability

Flight testing for longitudinal static stability is performed to determine the neutral points of the aircraft. Determining these neutral points helps designers decide if the vehicle demonstrates sufficient longitudinal static stability or if gimmicks, such as bobweights or downsprings, need to be installed. The further aft the neutral points are from the CG, the greater the stability. As the static margin, or distance between the CG and neutral points, decreases, stability also decreases. Two types of neutral points exist for longitudinal static stability: stick-fixed and stick-free. Stick-fixed, as the name implies, is the aircraft's initial reaction when disturbed from equilibrium with the control surface in a fixed position. Stick-free, conversely, is the aircraft's initial reaction with the control surface "floating", or allowed to freely react to changes in forces and moments. Note that this only applies to aircraft with reversible control systems. Aircraft with irreversible control systems do not, without additional augmentation in the control system, innately demonstrate stick-free characteristics. Section 4.2.1.8 of USNTPS *Fixed Wing Stability and Control* describes how an irreversible control system can have stick-free characteristics [5].

The stick-fixed stability of an aircraft can be related to the elevator position with [8]:

$$\frac{d\delta_e}{dC_L} = \frac{\left({}^{dC_m}/_{dC_L}\right)_{fixed}}{C_{m_{\delta_e}}} \tag{3.17}$$

When dC_m/dC_L is zero, $d\delta_e/dC_L$ is also zero. As the CG moves aft of the stick-fixed neutral point, the pilot will notice a reversal of control position is required to maintain an airspeed. Since physically flying an aircraft with the CG aft of limits is dangerous, a safe way to determine the stick-fixed neutral point is to measure the elevator deflection with a change in airspeed from a trim condition; this will be repeated at another CG location. The airspeeds can then be converted into lift coefficients and the elevator deflection plotted against them. The slopes of the curves, $d\delta_e/dC_L$, at selected lift coefficients can then be plotted against the CG position as a percent of mean aerodynamic chord. Plotting a line between points of the same lift coefficient and extrapolating to zero yields the stick-fixed neutral point for that lift coefficient.

The stick-free stability of an aircraft can be related to the elevator force with [8]:

$$\frac{dF_e}{dV_e} = 2K\frac{W}{S}\frac{C_{h_{\delta_e}}}{C_{m_{\delta_e}}}\left(\frac{dC_m}{dC_L}\right)_{free}\frac{V_e}{V_{e_{trim}}^2} \tag{3.18}$$

dF_e/dV_e can be seen as a function of stability and trim. Dividing elevator force by dynamic pressure removes the trim dependency and makes the derivative a function of only stability.

$$\frac{d(F_e/q)}{dC_L} = -KS_e\bar{c}_e\frac{C_{h_{\delta_e}}}{C_{m_{\delta_e}}}\left(\frac{dC_m}{dC_L}\right)_{free} \tag{3.19}$$

Likewise, when $(dC_m/dC_L)_{free}$ is zero, $d(F_e/q)/dC_L$ is also zero. As the CG moves aft of the stick-free neutral point, the pilot will notice a reversal of control force is required to maintain an airspeed. The CG could be moved to determine this point but, as previously discussed, this would compromise safety. Instead, the elevator force can be measured with changing airspeed; this can be done while simultaneously recorded elevator deflection. The method for determining the stick-free neutral point is then the same as that used for the stick-fixed neutral point. The primary difference is dividing elevator force by dynamic pressure

before plotting it against lift coefficient. Because gimmicks exist in both aircraft tested, the resulting stick-free neutral points are only a "simulated" location. Removal of the gimmicks would be required to determine the actual location of neutral points.

Two different flight test techniques were used to determine the longitudinal static stability of each aircraft. The first, known as the stabilized method, begins by establishing a trim, hands-free condition for approximately ten seconds at a specified airspeed. The pilot then pitches for another airspeed, faster or slower, and the parameters, including airspeed, elevator deflection, and elevator force, are recorded. The pilot then reverses pitch to maintain an airspeed on the opposing side of trim and the required data are again recorded. This is repeated for the entire airspeed band which is, for the aircraft tested, typically 50 kts. Once all data points are collected, the controls are slowly released to neutral and the airspeed monitored. A result of friction in the system, the "free return airspeed" should be ±10% of trim. Data can be hand recorded for this method since the aircraft is in a stabilized condition. [8]

The other method is known as the level accel/decel method. Again, the aircraft is trimmed at a specified airspeed. For the purpose of this research, the trim speed for both stabilized and level accel/decel methods was the same. Once trimmed, the pilot reduces power to idle and allows the aircraft to slow. Before stall, or at another predetermined airspeed, the pilot adds full power and allows the aircraft to accelerate to maximum level airspeed while maintaining altitude. After the maximum level airspeed is reached, power is then reduced to idle and the aircraft allowed to slow through the speed range while still maintaining altitude. This technique is less accurate than the stabilized method because true equilibrium is never reached. Power effects are also a factor since the power setting changes. Because the aircraft is changing condition so quickly, automatic recording devices are required for this technique. [5]

Friction exists in all control systems. For both techniques, it is extremely important that the pilot remain on the proper side of the friction band in order to precisely measure forces. To obtain accurate

values for forces, the pilot must maintain force in the desired direction. This means that if a pilot pushes to pitch for an airspeed, the pilot must not reduce the push force while maintaining that airspeed. Conversely, if the pilot pulls to pitch for an airspeed, that pull force must be maintained. For the stabilized method, the direction of force is only maintained for a brief period. However, the level accel/decel method requires the pilot to maintain the proper direction of force for the entire speed range of the aircraft, which can lead to fatigue throughout the test. A flight test engineer can monitor elevator force to determine if the forces are within the friction band. It should be noted that a certain amount of electronic static, or feedback, may exist in the system. Once the elevator force is plotted, it can become difficult to distinguish between scatter as a result of forces moving outside the friction band or as a result of system feedback. One way to accurately monitor the friction band is to use a real-time mean plot, which tends to average out static in the system.

The data from both flight test techniques are reduced in the manner previously discussed; it can also be found in Chapter 21 of Kimberlin's *Flight Testing of Fixed-Wing Aircraft* [8]. The main difference between reducing each technique is the sheer volume of data points from the level accel/decel method. Once data from both methods are reduced, the results can be compared to see differences between the techniques.

3.6 Longitudinal Maneuvering Stability

Longitudinal maneuvering stability deals with the stability of the aircraft with a curved flight path, meaning the CG is accelerating. Similar to determining neutral points, longitudinal maneuvering stability determines the stick-fixed and stick-free maneuvering points. Usually, maneuvering points are located aft of the neutral points. Therefore, the maneuvering margin, or the distance between the CG and the stick-fixed and stick-free maneuvering points, is typically larger than the static margin and maneuvering stability is greater than static stability. Though, it is possible for maneuvering points to be between or even ahead

of neutral points. As with static stability, maneuvering stability can be increased with gimmicks in the system.

Similar to the stick-fixed neutral point, the stick-fixed maneuvering point can be determined by measuring elevator position. However, maneuvering stability differentiates with respect to normal acceleration, or load factor, instead of airspeed. This results in an elevator deflection per g for stick-fixed. For a steady turn condition [8],

$$\frac{d\delta_e}{dn} = -\frac{1}{C_{m_{\delta_e}}} \frac{{}^{W}/_{S}}{{}^{1}/_{2}\,\rho V_e^2} \left[\left(\frac{dC_m}{dC_L} \right)_{fixed} + \frac{C_{m_{\dot{\theta}}} \rho g \bar{c}}{4\left({}^{W}/_{S}\right)} \left(1 + {}^{1}/_{n^2} \right) \right] \tag{3.20}$$

Eq. 3.20 shows that stick-fixed maneuvering stability contains a stability term and a damping term. When the CG position moves to the stick-fixed neutral point, $d\delta_e/dn$ is only dependent on the damping term, which also decreases with aft CG position due to the tail arm decreasing. If the CG moves aft of the stick-fixed maneuvering point, the pilot will experience a reversal of stick position with normal acceleration. To determine the stick-fixed maneuvering point, the elevator deflection is plotted against load factor for two test CGs. The slopes of the curves at selected load factors can then be plotted against the CG position as a percent of mean aerodynamic chord. Plotting a line between points of the same normal acceleration and extrapolating to zero yields the stick-fixed maneuvering point for that load factor.

The stick-free maneuvering point is, likewise, determined by measuring elevator force, or elevator force per g. For irreversible control systems, see UNTPS *Fixed-Wing Stability and* Control section 4.7.1.5 [5]. For a reversible control system in a steady turn condition [8],

$$\frac{dF_e}{dn} = -K \frac{W}{S} \frac{C_{h_{\delta_e}}}{C_{m_{\delta_e}}} \left(\frac{dC_m}{dC_L} \right)_{free} + K \frac{1}{2} \rho l_t g \left(1 + \frac{1}{n^2} \right) \left(C_{h_{\alpha_t}} - \frac{C_{h_{\delta_e}}}{\tau} \right) \tag{3.21}$$

Again, Eq. 3.21 shows a stability term and a damping term. When the CG position moves to the stick-free neutral point, dF_e/dn is only dependent on the decreasing damping term. This follows the same trend as the stick-fixed maneuvering point. If the CG moves aft of the stick-free maneuvering point, the pilot will

experience a reversal of stick force with normal acceleration. To determine the location of the stick-free maneuvering point, elevator force is plotted against load factor for at least two test CGs. The slopes of the curves at selected load factors can then be plotted against the CG position as a percent of mean aerodynamic chord. Extrapolating a line from points of the same load factor to zero will provide the stick-free maneuvering point.

The flight test technique selected was the stabilized load factor method. This method begins with the aircraft in a trim shot. The pilot then climbs to the top of the data band and places the aircraft in a 15° bank to one direction. The bank angle and trim airspeed are maintained which stabilizes the normal acceleration. Data, including load factor, elevator deflection, and elevator force, is then recorded. Data is also taken at 30°, 45°, and 60°. The pilot then repeats the process to the opposite direction. The entire test is repeated at a different CG location. Because this is a stabilized method, data can be hand-recorded and a check plot used in flight to determine accuracy.

As previously discussed, parameters should be closely monitored to ensure the controls remain on the proper side of the friction band. As a function of the aircraft, slight changes in airspeed can have a large impact on elevator forces [5]. Note that the normal acceleration will show little change between trim and small bank angles because load factor is directly related to bank angle.

$$n = \frac{1}{\cos \phi} \tag{3.22}$$

As long as the airspeed and bank angle are maintained within tolerances, an increasing load factor will be seen with increasing bank angle. Because of the increasing horizontal component of lift with increasing bank angle, data points above 45° may be difficult to obtain.

3.7 Longitudinal Dynamic Stability

The study of aircraft dynamics is to determine how an aircraft responds to a disturbance over a period of time. Much like longitudinal static stability, longitudinal dynamic stability is generally not coupled with other axes. Positive dynamic stability is defined as the aircraft's tendency to return to the trim state, negative dynamic stability is the aircraft's tendency to diverge, and neutral dynamic stability is the aircraft's tendency to remain at the disturbed state over time. Two modes of motion defined by longitudinal dynamic testing are the phugoid, or long period, mode and the short period mode. Because both modes are second order, oscillatory systems, their behavior is similar to a spring-mass-damper system. An in-depth explanation of longitudinal dynamic theory is covered in Chapter 22 of Kimberlin's *Flight Testing of Fixed-Wing Aircraft* and Chapter 4 of the U.S. Navy's *Fixed Wing Stability and Control* [5, 8].

The phugoid has a long period with light damping. Airspeed, altitude, and pitch angle change while angle of attack and load factor remain near constant. Once disturbed from trim, the aircraft will successively climb and dive. As altitude and pitch increase, speed decreases, and vice versa. Flight testing the phugoid is relatively simple. Once established in a trim condition at the desired airspeed and configuration, the pitch is adjusted to alter the airspeed approximately 10 kts. The controls are slowly returned to trim position and either held or released; a difference usually exists between stick-fixed and stick-free conditions. Airspeed, altitude, pitch angle, and time are recorded. Since parameters change slowly, data can be collected by hand or by use of a DAS. Once data are collected, the damped natural frequency, $\omega_{d\text{-}ph}$, is determined by:

$$\omega_d = 2\pi\left(\frac{\Delta cycles}{\Delta time}\right) \tag{3.23}$$

Using either the subsidence ratio method ($0.0 < \zeta < 0.3$) or the transient peak ratio method ($0.01 < \zeta < 1.00$), the damping frequency, ζ_{ph}, is determined. Appendix D shows the procedure for multiple methods

of determining damping ratio. Both the damped natural frequency and the damping ratio can now be used to find the undamped natural frequency, $\omega_{n\text{-}ph}$, of the phugoid.

$$\omega_n = \frac{\omega_{d_{ph}}}{\sqrt{1-\zeta^2}} \tag{3.24}$$

If the phugoid is divergent, the time to double amplitude can be found with:

$$t_2 = \frac{0.693}{\zeta \omega_n} \tag{3.25}$$

The short period, conversely to the phugoid, is a quick motion that is usually heavily damped. While angle of attack, pitch, and load factor change, airspeed and altitude remain near constant. The technique used for testing the short period is the doublet input. This technique excites the short period while suppressing the phugoid. Once trimmed, the pilot performs a frequency sweep of the flight controls to determine the short period frequency of the aircraft. The pilot then inputs a doublet at this short period frequency and angle of attack, pitch, elevator deflection, load factor, and time are recorded. Because the short period occurs quickly, a DAS is required to collect data. The test should be repeated for both stick-fixed and stick-free conditions. From the collected data, the damped natural frequency is determined as described in Eq. 3.23. The damping ratio can be found using the subsidence ratio method ($0.0 < \zeta < 0.3$), the transient peak ratio method ($0.3 < \zeta < 0.5$), the time ratio method ($0.5 < \zeta < 2.0$), or the log decrement equation method. From these values, the undamped natural frequency can be determined using Eq. 3.24. If the short period is divergent, the time to double amplitude can be calculated using Eq. 3.25. To further describe the short period, the ratio of load factor to angle of attack, n_z/α, and the Control Anticipation Parameter, CAP, can be found. From the frequency sweep, n_{zmax}/α_{max}, which occurs at $\omega_{n\text{-}sp}$, can be determined. Using this, the CAP can be calculated by:

$$CAP = \frac{\omega_n^2}{\left({}^{n_z}/_{\alpha}\right)} \tag{3.26}$$

3.8 Lateral-Directional Static Stability

Lateral-directional static stability deals with the characteristics of the aircraft when the relative wind diverges from the plane of symmetry. This angle is known as the angle of sideslip. Positive sideslip is generally considered the nose pointed left or "wind in the right ear". While angle of attack is useful to the pilot to change lift coefficient, airspeed, or other aspects, angle of sideslip is primarily only helpful during landing. During normal flying conditions, maintaining zero sideslip helps reduce drag. Unlike longitudinal stability which is assumed uncoupled from the other axes, lateral and directional stability are cross-coupled. This means that a yaw input also produces a roll and a roll input also produces a yaw.

Focusing just on lateral stability, Eq. 3.27 shows the rolling moment [8].

$$C_{l_\beta}\beta + C_{l_{\delta_r}}\delta_r + C_{l_{\delta_a}}\delta_a = 0 \tag{3.27}$$

C_{l_β} is the rolling moment as a result of sideslip. This is also known as the dihedral effect. The wing is the main contributor to lateral stability. Increasing the wing dihedral angle, or the vertical displacement of the wing from level, increases lateral stability. Conversely, an aircraft with negative dihedral, or anhedral, has less lateral stability. $C_{l_{\delta_r}}$ is the rolling moment due to rudder deflection. This is a result of the vertical tail being some distance, usually above, the longitudinal axis. $C_{l_{\delta_a}}$ is the rolling moment as a result of aileron deflection, or the aileron power. This is how much control the ailerons have to provide a rolling moment. Other derivatives may exist depending on the aircraft being tested.

Focusing just on directional stability, Eq. 3.28 shows the yawing moment. [8]

$$C_{n_\beta}\beta + C_{n_{\delta_r}}\delta_r + C_{n_{\delta_a}}\delta_a = 0 \tag{3.28}$$

C_{n_β} is the yawing moment as a result of sideslip. This is also known as "weathercock" stability. It is the tendency for the aircraft to return to zero sideslip once disturbed. $C_{n_{\delta_r}}$ is the yawing moment as a result

of rudder deflection. This is also known as the rudder power, or how much control the rudder provides when deflected. $C_{n_{\delta_a}}$ is the yawing moment as a result of aileron deflection. An aileron deflected downward produces parasite and induced drag while the upward aileron only produces parasite drag. This results in a yawing moment known as adverse yaw. For aircraft that use spoilers, only parasite drag is present on the deflected surface; this is, in contrast, known as proverse yaw.

Because lateral and directional stability are coupled, Eq. 3.29 shows the resulting side-forces. [8]

$$C_{Y_\beta}\beta + C_{Y_{\delta_r}}\delta_r + C_{Y_{\delta_a}}\delta_a + C_L\phi = 0 \tag{3.29}$$

The first three parameters are a resultant side-force of sideslip, rudder deflection, and aileron deflection, respectively. However, the fourth parameter shows the effect of lift coefficient with bank angle.

To determine the lateral-directional static stability of the test aircraft, the steady heading sideslip method was used. For this method, each test point started with a trim shot. Once stabilized, data for rudder position and force, aileron position and force, bank angle, elevator force, and airspeed were taken. The aircraft were placed in a sideslip by inputting a rudder deflection and countering with aileron deflection to maintain a heading. Rudder deflection is then increased and aileron deflection is added to maintain the heading. This was repeated for several rudder deflections to both the left and the right. Since this is a stabilized method, data is hand-recorded. However, because so many parameters are recorded, the use of a DAS can reduce FTE workload. Two methods of rudder deflection can be used. The first is ball deflection. This method is easier for the pilot to maintain as he/she is directly looking at how much the ball is deflected from center. The other method is rudder pedal deflection. This method is more dependent on the FTE to monitor. For the purposes of this document, the ball deflection method was used.

Once the flight test is complete, data reduction is relatively simple. Any biases in forces are removed. Also, due to the systems installed on the test aircraft, biases in sideslip must also be removed. Plots are then created for rudder deflection, rudder force, aileron deflection, aileron force, bank angle,

and elevator force versus angle of sideslip. An increasing sideslip should result in increasing deflections, forces, and bank angle. Generally, it should be seen that rudder deflection and force shows an opposite slope to aileron deflection and force. Also, the bank angle direction tends to follow aileron deflection. Elevator forces can determine the pitch tendency of the aircraft while in a sideslip. The propeller slipstream also plays a significant role in lateral-directional static stability. For this reason, lateral-directional stability is usually not symmetric for both left and right sideslips.

3.9 Lateral-Directional Dynamic Stability

Lateral-directional dynamic stability, much like lateral-directional static stability, involves a coupling of two axes. Three modes of motion are the primary focus of lateral-directional dynamic testing. Two of these modes, the spiral mode and the roll mode, are first order, non-oscillatory motions. The remaining mode, the Dutch roll mode, is a second order, oscillatory motion. An in-depth explanation of lateral-directional dynamic theory is covered in Chapter 29 of Kimberlin's *Flight Testing of Fixed-Wing Aircraft* and Chapter 5 of the U.S. Navy's *Fixed Wing Stability and Control* [5, 8].

The spiral mode is described as a convergence, divergence, or neutral displacement in bank angle as a result from a wings level disturbance. The motion requires no input to be excited and is, even if slowly divergent, easily controlled by the pilot. The objective of the flight test is to determine the time to half or the time to double amplitude. Testing is performed by using only rudder to place the aircraft in a 10° bank. Rudder controls are then held or released and the resulting motion monitored. The test is repeated for both left and right bank angles. The spiral mode generally has a long period and data is hand-recorded. Data reduction is simple with bank angle plotted against time and the time to half or double amplitude determined for both left and right. Because of the gentle nature of the spiral mode, propeller effects of single-engine aircraft and asymmetric thrust of multi-engine aircraft may mask the mode.

The roll mode is a heavily damped mode excited by a roll input. The objective of the flight test is to determine the roll mode time constant, τ_R. The roll mode time constant is defined as 63.2% of the

steady state roll rate [5]. The test is performed by stabilizing the aircraft in a 30° bank to either direction. The pilot, using only aileron, applies an aileron step input and rolls through the opposite 30°. The test is repeated for both directions and aileron deflection, bank angle, roll rate, and time are recorded. While handheld data can be used, using a DAS can provide more precise results. To reduce the data, roll rate is plotted against time and the roll mode time constant is determined for both left and right rolls.

The Dutch roll mode, or lateral-directional oscillation mode, is a generally heavily damped motion that, while sometimes considered a nuisance, can be used by the pilot for sideslip corrections. It is the mode that allows bank angle to be controlled by rudder input. Dutch roll testing is performed to determine the natural frequency, the damping ratio, and the roll-to-sideslip ratio, ϕ/β, of the aircraft. Because the Dutch roll mode is a coupled motion, accurately determining the frequency and damping ratio is difficult. From a level trim condition, the pilot performs a frequency sweep of the rudder pedals to determine the Dutch roll mode frequency. The pilot then inputs a rudder doublet at this frequency and either holds or releases the controls. Symmetry of the doublet is important to avoid exciting the spiral and roll modes. Bank angle, sideslip angle, yaw angle, roll rate, rudder deflection, aileron deflection, and time are all recorded. Because the period may be short, a DAS should be used to record the parameters. Once data is collected, the damped natural frequency and the damping ratio can be determined. Plots of roll angle and sideslip angle versus time should be made and ϕ/β ratio determined. If the mode is divergent, the time to double amplitude should be calculated.

CHAPTER 4 RESULTS AND DISCUSSION

4.1 Air Data System Calibration

4.1.1 Saratoga – GPS 4 Leg Method

The results of the air data system calibration for the Saratoga can be seen in Figures 4.1-4.3. Figure 4.1 shows the position error correction versus indicated airspeed. The plot is non-linear with zero correction error at approximately 94 kts. Values range from 0.2010 to -0.1359. Figure 4.2 shows the velocity position error correction versus indicated airspeed. Corrections vary from 6.6 kts to -9.6 kts. Comparing these values with FAR 23.1323, only ΔV_{pc} for target airspeeds of 100 and 110 fall within regulations. The POH shows a linear trend, except at speeds less than 80 KIAS, that does not exceed approximately 2.5 kts for the speed range published. The altitude position error correction versus indicated airspeed is shown in Figure 4.3. This plot is also non-linear. Comparing this to FAR 23.1325, only the ΔH_{pc} at a target airspeed of 100 is within regulations. The Saratoga POH used does not contain an altitude position error correction plot. [1, 12]

4.1.2 Navajo – GPS 4 Leg Method

Figures 4.4-4.6 show the results for the air data system calibration for the Navajo. Figure 4.4 shows the position error correction coefficient versus indicated airspeed. The plot shows that $\Delta p_{pc}/q_{ci}$ is non-linear for the test system. For the airspeeds tested, $\Delta p_{pc}/q_{ci}$ varies from -0.0664 to -0.0936. Figure 4.5 shows the velocity position error correction versus indicated airspeed. Again, the plot is non-linear and can be seen to have a minimum correction of -3.9 kts and a maximum of -7.0 kts. According to FAR 23.1323, ΔV_{pc} must remain within three percent of the calibrated airspeed or five knots, whichever is greater. For the two slowest airspeeds tested, ΔV_{pc} falls within regulations. However, the other four airspeeds tested exceed FAA regulations. Comparing the test system with the factory system, which also shows a non-linear trend, the test system shows a much larger correction. The factory system indicates

zero correction error at approximately 155 kts while the test system indicates the greatest correction at nearly the same airspeed. Figure 4.6 shows the altitude position error correction versus indicated airspeed. The plot is non-linear with corrections ranging from -41.9 ft to -133.7 ft. Comparing these results with FAR 23.1325, the limits of ±30 ft per 100 kts are exceeded at all target airspeeds. According to the POH, the factory system does not exceed ±30 ft per 100 kts across the whole speed range. [1, 10]

4.2 Cruise Performance

4.2.1 Saratoga – PIW-VIW Method

The results of the PIW-VIW method for cruise performance flight testing for the Saratoga can be seen in Figures 4.7-4.14. Figure 4.7 shows the plot of PIW versus VIW. This curve follows the expected trend; slowing down or speeding up from the minimum power required airspeed, while maintaining altitude, requires more power. Using Figure 4.8, the raw data is normalized for all altitudes and a single curve is created. Figure 4.9 shows the data of pressure altitude versus maximum manifold pressure. As expected for a normally aspirated engine, the manifold pressure decreases with altitude. Using Figures 4.7 and 4.9, a plot of density altitude versus true airspeed, Figure 4.10, was created. This plot is used by pilots to determine the expected true airspeed for a given power setting at altitude. The plot shows curves for full throttle and 75% power. The full throttle curve shows, as expected based on the results in Figure 4.9, that the true airspeed at max power decreases as altitude increases. This trend matches that shown in the Saratoga POH. However, the POH uses a higher RPM setting so the values shown in Figure 4.9 are less than those published. Conversely, the 75% curve shows that the true airspeed will increase with altitude at the specified power setting. This curve crosses the full throttle curve between 7,500ft and 8,000ft; above this altitude is where the Saratoga is no longer able to produce 75% power. This coincides with the POH. The PIW-VIW method also allows for the creation of a drag polar for the aircraft. Figure 4.11 shows a plot of drag coefficient versus lift coefficient squared. The y-intercept of the line shows a value of 0.0428. This is the determined zero-lift drag coefficient of the Saratoga. Using this value, along

with other lift and drag coefficient values determined from data expansion, Figure 4.12 was created. The shape of the curve is that expected for a subsonic aircraft from stall speed to maximum level flight speed. Figure 4.13 shows a plot of specific range versus calibrated airspeed for both altitudes tested. The plot shows that the Saratoga has a higher specific range at 10,000 ft than at 5,000 ft. The best specific range at 10,000 ft is slightly more than 1.80 nmi/lb at approximately 92 KCAS and at 5,000 ft is slightly more than 1.35 nmi/lb at approximately 110 KCAS. Figure 4.14 shows the plot of specific endurance versus calibrated airspeed. The Saratoga is shown to have a higher specific endurance at 10,000 ft than at 5,000 ft. The best specific endurance is roughly 0.0175 hr/lb at approximately 85 KCAS at 10,000 ft and approximately 0.0138 hr/lb at 72 KCAS at 5,000 ft. These values of specific range and specific endurance match well with the published results in the POH. [12]

4.2.2 Saratoga – W/δ Method

Figures 4.15-4.21 show the results of the W/δ method for cruise performance testing. A plot of equivalent shaft horsepower versus equivalent airspeed is shown in Figure 4.15. The plot contains both raw and normalized data for 10,000 ft and 5,000 ft. As expected, it can be seen that less power is needed to maintain the same airspeed at a higher altitude. Also, an airspeed pertaining to a minimum power required can be seen for each altitude. For the Saratoga, it appears the airspeed for minimum equivalent shaft horsepower is between 70 and 75 kts for both altitudes flown. Figure 4.16 shows a plot of the normalized equivalent shaft horsepower versus the normalized equivalent airspeed. The normalized values of Figure 4.16 are those plotted with curves in Figure 4.15. A plot of fuel flow versus calibrated airspeed is shown in Figure 4.17. The trend shows that as altitude increases, fuel flow decreases. The airspeed for minimum fuel flow at 10,000 ft is approximately 82 KCAS and at 5,000 ft is approximately 72 KCAS. It is seen and expected that the airspeed for minimum fuel flow increases with altitude. Also, the test at 10,000 ft was conducted at a lower weight than at 5,000 ft. The difference of shape and location of each curve represents the changes to altitude and weight. Figure 4.18 shows a plot of referred fuel flow

versus referred shaft horsepower. For 10,000 ft, the minimum referred fuel flow is around 76 lbs/hr at approximately 120 hp; for 5,000 ft, the minimum referred fuel flow is around 86 lbs/hr at approximately 160 hp. Figure 4.18 follows the same trend as Figure 4.17 in relation to changes in altitude and weight. A plot of shaft horsepower specific fuel consumption versus referred shaft horsepower is shown in Figure 4.19. At 10,000 ft, the Saratoga has a SHPSFC between 0.475 and 0.500 lb/hr/hp at approximately 195 hp. At 5,000 ft, the SHPSFC is slightly less than 0.425 lb/hr/hp at approximately 235 hp. Figure 4.20 shows the specific range versus calibrated airspeed using the W/δ method. These results match with those from the PIW-VIW method. Specific endurance versus calibrated airspeed is shown in Figure 4.21. Like specific range, the values of specific endurance match with those found using the PIW-VIW method. [12]

4.2.3 Navajo – PIW-VIW Method

The results of the PIW-VIW method for Navajo cruise performance are shown in Figures 4.22-4.29. Figure 4.22 shows the plot of PIW versus VIW, containing both raw and normalized values for all altitudes tested. Figure 4.23 shows the normalized PIW versus the normalized VIW; these normalized values are those plotted in Figure 4.22. The airspeed for minimum power required to maintain level flight is between 95 and 100 kts. Figure 4.24 shows a plot of pressure altitude versus manifold pressure. The manifold pressure is seen to increase with altitude; since the Navajo has turbocharged engines, this trend is expected up to the engines' critical altitude. A plot of density altitude versus true airspeed is seen in Figure 4.25 for two different power settings. For full throttle, the Navajo shows the opposite trend that the Saratoga does in Figure 4.10. Because the Navajo is turbocharged and the Saratoga is naturally aspirated, the Navajo is able to reach higher true airspeeds at full throttle with increasing altitude. This is also only true up to the Navajo's engines' critical altitude. The results in Figure 4.25 compare very well with those published in the Navajo POH; any differences appear to be from a difference in power setting. Figure 4.26 shows a plot of drag coefficient versus lift coefficient squared. From this plot, the zero-lift drag coefficient of the Navajo is 0.0353. A drag polar, Figure 4.27, was created using lift and drag coefficients

determined from data expansion. The trend follows that expected for a subsonic aircraft across its airspeed range. The specific range versus calibrated airspeed can be seen in Figure 4.28. At 10,000 ft, a maximum specific range between 1.05 and 1.10 nmi/lb is found at approximately 125 KCAS; at 5,000 ft, a maximum specific range of roughly 0.80 nmi/lb is found at approximately 120 KCAS. It is expected to have a greater max specific range at a higher altitude and this trend is seen. Figure 4.29 shows a plot of specific endurance versus calibrated airspeed. The max specific endurance at 10,000 ft is roughly 0.00875 hr/lb at approximately 70 KCAS; at 5,000 ft, the max specific endurance is roughly 0.00825 hr/lb at approximately 35 KCAS. Comparing these values to the POH, the specific range and specific endurance match well with published values. The maximum specific endurance airspeeds, however, are significantly lower than those published. [10]

4.2.4 Navajo – W/δ Method

Figures 4.30-4.36 show the results of the W/δ method for the Navajo. Equivalent shaft horsepower versus equivalent airspeed is shown in Figure 4.30. The raw data is normalized, as seen in Figure 4.31, and plotted with a fitted curve. The airspeed for minimum power required to maintain level flight is between 90 and 95 kts for both altitudes. Figure 4.32 shows a plot of fuel flow versus calibrated airspeed. As expected, the Navajo exhibits lower fuel flow at a higher altitude. At 10,000 ft, approximately 97 KCAS is the airspeed for minimum fuel flow; at 5,000 ft, approximately 90 KCAS is the airspeed for minimum fuel flow. A higher minimum fuel flow airspeed is expected with increasing altitude. A plot of referred fuel flow versus referred shaft horsepower is shown in Figure 4.33. It can be seen that a higher altitude produces a lower fuel flow for the same amount of horsepower. This trend coincides with what is expected. Figure 4.34 shows a plot of shaft horsepower specific fuel consumption versus referred shaft horsepower. As expected, the Navajo exhibits lower SHPSFC at a higher altitude. The minimum SHPSFC at 10,000 ft is slightly more than 0.45 lb/hr/hp while at 5,000 ft it is approximately 0.65 lb/hr/hp. Specific range versus calibrated airspeed is shown in Figure 4.35. The Navajo has a greater specific range at a

higher altitude. These values are slightly less than those seen in Figure 4.28 using the PIW-VIW method. Figure 4.36 shows the specific endurance versus calibrated airspeed. They are similar to those seen in Figure 4.29 using the PIW-VIW including the significantly lower maximum specific endurance airspeeds. [10]

4.3 Climb Performance

4.3.1 Saratoga – Sawtooth Climb Method

Figures 4.37-4.39 show the results of the sawtooth climb method of the Saratoga. Rate of climb versus calibrated airspeed is shown in Figure 4.37. The rate of climb plotted is that directly calculated in-flight. At 5,000 ft, the maximum rate of climb is around 625 ft/min at approximately 81 KCAS and the best angle of climb airspeed is approximately 73 KCAS. At 10,000 ft, the maximum rate of climb is just below 400 ft/min at approximately 80 KCAS and the best angle of climb airspeed is approximately 75 KCAS. As expected for a normally aspirated engine, the Saratoga exhibits better climb performance at a lower altitude. Also, the best rate of climb speed decreases while the best angle of climb airspeed increases with altitude. PIW versus CIW is plotted in Figure 4.38. This plot is used to expand the data to nonstandard conditions. Figure 4.39 shows a plot of density altitude versus rate of climb. When compared with the Saratoga POH, the results are similar. A higher RPM was used in the POH which could be a cause for lower values from this testing. These values also meet the requirements of FAR 23.63 and 23.65. [1, 12]

4.3.2 Saratoga – Level Accel Method

The results of the level accel method are shown in Figures 4.40-4.44. Figure 4.40 shows a plot of true airspeed versus time. As expected with a normally aspirated engine, the Saratoga was able to reach a higher true airspeed in a shorter amount of time at a lower altitude. A trendline was fit to the data and the derivative of the equation was taken. This derivative was used to calculated values of P_s that are plotted versus true airspeed in Figure 4.41. For safety purposes, the aircraft was not slowed to stall speed during the test, so the entire range of airspeeds is not included. However, trendlines were fit to determine

extrapolated values. From this plot, values of P_s were selected and the corresponding true airspeeds for each altitude was determined. Figure 4.42 shows a plot of pressure altitude versus indicated airspeed. To accurately fit a curve, test points at higher altitudes would need to be completed. However, the expected trend can still be seen. The outermost data points follow a constant line of P_s=0; as the contours move inward, the Saratoga exhibits increasing specific excess power. For the altitudes tested, a maximum value of P_s was determined to be 11.6 ft/s at 2,500 ft. Figure 4.43 shows another plot of rate of climb versus calibrated airspeed. Comparing this plot with Figure 4.37, it can be seen that both techniques produce similar results. The level accel method appears to produce slightly higher values of V_y. This can easily be seen in the maximum rate of climb data at 10,000 ft. Figure 4.44 shows another plot of density altitude versus rate of climb. Comparing this plot with Figure 4.39, the level accel method appears to produce a greater absolute ceiling for the Saratoga. Also, the maximum rate of climb at sea level is similar to that shown in Table 4.1 even though the average test weight is 200 lbs less than that used for the PIW-CIW expansion. The level accel method appears to show a slower decrease in performance as altitude increases for the Saratoga. Further tests would need to be performed in order to create more lines at other weights. Error in the level accel method could be a result of restrictions in airspeed range and the limited curve fitting capability of Excel. Again, these values meet the requirements of FAR 23.63 and 23.65. [1, 12]

4.3.3 Navajo – Sawtooth Climb Method

Figures 4.45-4.47 show the results of the sawtooth climb method on the Navajo. Rate of climb versus calibrated airspeed is shown in Figure 4.45. Since the Navajo is turbocharged, similar maximum climb rates are seen for 5,000 ft and 10,000 ft, 1,225 ft/min and 1,200 ft/min respectively. The values of V_y compare very well with those published in the Navajo POH of around 90 kts. As expected, the value of the best angle of climb airspeed increases with altitude. However, Figure 4.45 shows that the Navajo has a better climb rate at this airspeed at 10,000 ft; this could be a result of the turbocharged engines. Figure

4.46 shows a plot of PIW-CIW. As previously mentioned, this plot is used to expand the data to create Figure 4.47, density altitude versus rate of climb. Unlike the Saratoga, the Navajo exhibits less decrease to climb performance with altitude. Figure 4.47 does not include the decrease in performance above the turbocharger critical altitude. Though the POH uses a higher manifold pressure setting, the calculated results compare well. These values also meet the requirements of FAR 23.63 and 23.65. [1, 10]

4.3.4 Navajo – Level Accel Method

The results of the level accel method are shown in Figures 4.48-4.52. Figure 4.48 shows a plot of true airspeed versus time. Again, a curve was fit to each data set and the derivative of the line taken to determine values of P_s. Figure 4.49 shows these values of specific excess power versus true airspeed. Again, the aircraft was not slowed to stall speed for safety reasons, so curves were fit to extrapolate points on the slow end of the speed range. For this reason, values on the slow end are purely estimates. Using values of P_s selected from this plot, a plot of pressure altitude versus indicated airspeed can be seen in Figure 4.50. The outermost points correspond to a P_s=0 with increasing values occurring with smaller contours. The maximum value of specific excess power determined was 22.5 ft/s at 2,500 ft. Figure 4.51 shows a plot of rate of climb versus calibrated airspeed. The maximum rates of climb vary significantly more than in Figure 4.45, though the corresponding airspeeds are similar, while the best angle of climb airspeeds change significantly less than in Figure 4.45. These values are still similar to those in the POH. Curves were not fit to this data due to excessive over estimation of Excel. Finally, a plot of density altitude versus rate of climb is shown in Figure 4.52. It compares well against the results of Figure 4.47. The average test weight was between 5,500 lbs and 6,000 lbs; the maximum rate of climb at sea level falls between the respective maximums seen in Figure 4.47. The level accel method appears to show an increased loss of performance with altitude compared to Figure 4.47. The results still compare well with the POH and meet the requirements of FAR 23.63 and 23.65. [1, 10]

4.4 Stalls

4.4.1 Saratoga – Stalls

Three configurations were selected to test: clean, landing, and 30° bank clean. Each configuration consisted of a controllability check followed by multiple stalls. All deceleration rates were measured from $1.1V_S$ as required by FAR 23.49. Airspeeds described by the pilot were read from the pilot's airspeed indicator while tables and figures use DAS data.

Stall A was the clean configuration: flaps up. During the controllability check, controls were deemed effective by the pilot down to 70 KIAS on the pilot's airspeed indicator, at which point they became sluggish. The controllability check proceeded into a stall. All stalls exhibited similar characteristics. The stall warnings, a horn and buffet, were deemed adequately early, continuous, distinctive, perceptible, and not overlooked. The warnings met the requirements of FAR 23.207, occurring no less than 5 kts before stall. The stall itself was described as obvious with a g-break leading to a nose drop; no wing rocking or intolerable buffeting occurred. This meets the requirements of FAR 23.201. The recovery was considered simple and immediate with an approximate recovery time of 2 seconds and height loss of 300 ft. The stall progression began at the trailing edge at the wing root and proceeded outward and forward simultaneously. Table 4.3 shows the stall speeds according to the DAS. Though not allowed by the FAA, a correction to stall speed for CG position is included. Figure 4.53 shows plots of indicated airspeed versus time for each stall in the clean configuration. [1]

Stall B was the landing configuration: full flaps. According to the pilot, control in all axes were considered effective down to 65 KIAS on the pilot's airspeed indicator. Once again, the controllability check concluded with a stall. All stalls in this configuration shared similar characteristics. The stall warnings, a horn and buffet, were again considered adequately early, distinctive, continuous, perceptible, and not overlooked. Though an occasional early horn chirp would occur, the warning indications meet the requirements of FAR 23.207. The stall was again defined by a g-break leading to a nose drop, meeting the

requirements of FAR 23.201. The stall was obvious with no wing rocking or intolerable buffeting. The recovery was described as simple and immediate, losing 300 ft and recovering in approximately 2 seconds. The stall progression began at the trailing edge at the wing root and proceeded forward first before moving outward. Table 4.4 shows the stall speeds for the landing configuration. The Saratoga meets the requirements of FAR 23.49 by having a stall speed of less than 61 KCAS for a maximum landing flap configuration. However, the Saratoga does not meet this requirement based on the C.G. corrected stall speed. Figure 4.54 shows plots of indicated airspeed versus time in the power approach configuration. [1]

Stall C was a clean configuration while in a 30° bank to the left: flaps up. During the controllability check, controls in all axes were deemed effective down to 80 KIAS on the pilot's airspeed indicator. The controllability check ended in a stall before repeating the configuration three more times. The stall warning continued to activate adequately early and was distinctive, continues, perceptible, and not overlooked. The stall warning occurred well above the stall and meets the requirements of FAR 23.207. The stalls were defined by an obvious g-break leading to a nose down pitch. No wing rocking or intolerable buffeting was noticed. The stall recovery was considered immediate and simple; the height lost was no more than 350 ft and the recovery time was approximately 2 seconds. All stall characteristics meet the requirements of FAR 23.201 and 23.203. The stall progression was seen to start at the trailing edge at the wing root and proceed outward first before moving forward. Table 4.5 shows the determined stall speeds. Figure 4.55 shows the plots of indicated airspeed versus time for the banked stalls. [1]

4.4.2 Navajo – Stalls

The same three configurations selected for the Saratoga were tested on the Navajo: clean, landing, and 30° bank clean. Also, each configuration test consisted of a controllability check followed by stalls. All deceleration rates were measured from $1.1V_S$ as required by FAR 23.49 [1]. Airspeeds described by the pilot were read from the pilot's airspeed indicator while tables and figures use DAS data.

Stall A was again the clean configuration: landing gear up, flaps up, cowl flaps closed. During the controllability check, controls in all axes were described as effective down to 110 MIAS on the pilot's airspeed indicator. At 105 MIAS, the controls were considered sluggish and at 110 MIAS they were described as more sluggish. Stall warning for the Navajo is a light and buffet, both occurring sufficiently early and meeting the requirements of FAR 23.207. The warnings were described as distinctive, continuous, perceptible, and not overlooked. The stall was defined by a g-break leading to a nose down pitch and a slight roll to the right, meeting the requirements of FAR 23.201. The pilot described the motion as obvious and no wing rocking or intolerable buffeting was noticed. The recovery was considered simple and immediate, losing no more than 300 ft and occurring in approximately 3 seconds. The stall progression began on the trailing edge at the wing root and moved to the leading edge before moving outward. Table 4.6 shows the stall results. Again, though not allowed by the FAA, a C.G. correction was applied to the stall speeds. Figure 4.56 shows the results in plots of indicated airspeed versus time in the clean configuration. [1]

Stall B was the landing configuration: landing gear down, full flaps, and cowl flaps closed. The controllability check showed effective controls down to 100 MIAS on the pilot's airspeed indicator. Roll became sluggish while pitch and yaw became mildly sluggish at 95 MIAS. Controls in all axes were considered more sluggish at 90 MIAS. Stall warnings met the requirements of FAR 23.207 with the light and buffet being described as distinctive, continuous, perceptive, and not overlooked. The stall was defined by a g-break with a nose down pitch and slight roll to the right and meets the requirements of FAR 23.201. Since the Navajo is a multiengine airplane with a maximum gross weight of more than 6,000 lbs, it does not have to meet the maximum stall speed in a landing configuration of 61 KIAS requirement of FAR 23.49. No wing rocking or intolerable buffeting were noticed. The stall recovery was immediate and simple, taking approximately 3 seconds to recover and losing around 300 ft. The stall progression began on the trailing edge at the wing root and moved forward before moving outward. Table 4.7 shows

the stall speed results and Figure 4.57 shows the corresponding plots of indicated airspeed versus time in the power approach configuration. [1]

Stall C was a clean configuration in a 30° left bank: landing gear up, flaps up, cowl flaps closed. Controls were considered effective down to 105 MIAS with roll becoming sluggish at that point. Stall warnings, the light and buffet, were adequately early, meeting the requirements of FAR 23.207 and were described as distinctive, perceptible, continuous, and not overlooked. The stall was defined by a g-break with a nose down pitch and a roll to the right. The aircraft exhibited no wing rocking or intolerable buffet and meets the requirements of FAR 23.201. The recovery was considered simple and immediate taking approximately 3 seconds and losing no more than 300 ft. The stall progression began on the trailing edge at the wing root and moved forward before moving outward. Table 4.8 shows the results of the banking stalls and Figure 4.58 shows the corresponding plots of indicated airspeed versus time for a turning stall. [1]

4.5 Longitudinal Static Stability

4.5.1 Saratoga – Stabilized Method

Figures 4.59-4.62 show the determination of the stick-fixed neutral points using the stabilized method for the Saratoga. Elevator deflection versus calibrated airspeed is plotted in Figure 4.59. As can be seen, since the power and trim settings remained constant throughout the test, a pull was required to reach speeds below the trim airspeed and a push was required to reach speeds above trim. Also, the plot shows that having a forward C.G. results in greater elevator deflections compared to an aft C.G. to maintain the same airspeed. This trend is expected since a farther forward C.G. yields a greater static margin and, therefore, greater static stability. Figure 4.60 shows a plot of elevator deflection versus lift coefficient. This plot shows the same trend as Figure 4.59: to reach a greater lift coefficient (i.e. slower speed) from trim, a pull is required; to reach a lower lift coefficient (i.e. faster speed) from trim, a push is required. Again, a forward C.G. requires more deflection than an aft C.G. to maintain the same airspeed.

Figure 4.61 shows the determination of stick-fixed neutral point by extrapolating each line of constant lift coefficient to zero. The neutral points are seen to be located behind the aft C.G. limit of the aircraft. Figure 4.62 shows the stick-fixed neutral point versus lift coefficient. This plot shows that as the lift coefficient increases, the stick-fixed neutral point moves closer to the aft C.G. limit. The neutral points for the lift coefficients at trim are seen to be aft of the C.G. limit, which is desired.

Figures 4.63-4.66 show the determination of the stick-free neutral points using the stabilized method. Elevator force versus calibrated airspeed is plotted in Figure 4.63 Since the power and trim settings remain constant throughout the test, it can be seen that a pull was required to obtain speeds less than trim and a push was required to obtain speeds greater than trim. As expected, a forward C.G. requires more force compared to an aft C.G. to obtain the same airspeed. After all test points, the controls were released and the airspeed returned to within plus or minus 10% of the trim airspeed. With that information and the use of Figure 4.63, it can be seen that the Saratoga meets the requirements of FAR 23.173 for the trim condition tested [1]. Figure 4.64 shows a plot of elevator force versus lift coefficient. As discussed in Section 3.5, elevator force is divided by dynamic pressure to remove the derivative dependence on the trim condition. Again, the line for the forward C.G. has a higher gradient than that of the aft C.G., which is desired and shows greater stability at a forward C.G. Figure 4.65 shows the determination of the stick-free neutral points. The lift coefficients selected are the same as those used in Figure 4.61. Although stick-free neutral points are generally located ahead of stick-fixed neutral points, Figure 4.65, when compared to Figure 4.61, shows that the stick-free neutral points are actually aft of the stick-fixed neutral points. Due to a unique design in the Saratoga stabilator in which the hinge line is ahead of the center of pressure, it is expected to see the stick-free condition have greater stability than the stick-fixed condition. Also, the Saratoga contains a bobweight; this means the stick-free neutral points seen in Figure 4.65 are only apparent locations and not the true positions of these neutral points. Figure 4.66 shows a plot of the stick-free neutral points versus lift coefficient. Again, though much more exaggerated

than for the stick-fixed neutral points, it can be seen that as the lift coefficient decreases, the location of the stick-free neutral points moves aft. The trim lift coefficients are apparently located significantly aft of the C.G limit.

4.5.2 Saratoga – Level Accel/Decel Method

The determination of the stick-fixed neutral points using the level accel/decel method are shown in Figures 4.67-4.70. Figure 4.67 shows a plot of elevator deflection versus calibrate airspeed using data collected by the DAS. A single line is faired through both the acceleration and deceleration values for each test point; this helps remove any power effects as discussed in Section 3.5. The plot shows that to obtain an airspeed below trim, a pull is required and to obtain an airspeed above trim, a push is required. Also, greater deflection is required with a forward C.G. Comparing this plot to Figure 4.59, it can be seen that both plots show similar results using two different methods. Figure 4.68 shows a plot of elevator deflection versus lift coefficient. As expected based on the results of Figure 4.67, a pull is required to achieve lift coefficients higher than trim and a push is required to achieve lift coefficients lower than trim; a forward C.G. also requires more deflection than an aft C.G. to maintain the same airspeed. Comparing this plot with Figure 4.60, both plots show similar results. The higher gradient of the curves in Figure 4.68 could be a result of the larger airspeed range tested. Figure 4.69 shows the stick-fixed neutral point determination. As expected, as the lift coefficient increases, the neutral point moves forward. Comparing this plot with Figure 4.61, it can be seen that the level accel/decel method produces a neutral point 0.5 inches ahead of the aft C.G. limit for a lift coefficient of 0.7 while the stabilized method shows the neutral point for the same lift coefficient 11 inches aft of the C.G. limit. These differences are most likely a result of one method providing stabilized test points and the other never reaching a stabilized condition. However, Figure 4.70, a plot of stick-fixed neutral points versus lift coefficient, shows that the neutral point at trim, which is the most important, is aft of the C.G. limit; this is the desired location. Comparing

this plot with Figure 4.62, it can be seen that the level accel/decel method produces neutral points more forward than those found using the stabilized method.

Figures 4.71-4.74 show the determination of the stick-free neutral points using the level accel/decel method. A plot of elevator force versus calibrated airspeed is shown in Figure 4.71. The data shows that a pull is required to obtain airspeeds less than trim and a push is required to obtain airspeeds greater than trim. Also, the curve for a forward C.G. has a higher gradient than that of an aft C.G., which is expected. This plot, showing similar results to Figure 4.63, meets the requirements of FAR 23.173 [1]. Both the stabilized and level accel/decel methods show that the Saratoga meets the certification requirements for the trim condition tested. Figure 4.72 shows a plot of elevator force versus lift coefficient. Again, the expected trend is shown and the results are similar to the stabilized method shown in Figure 4.64. Figure 4.73 shows the determination of the stick-free neutral points. Again, since the Saratoga uses a bobweight in the control system, these neutral points are only apparent and not the actual locations. All gimmicks in the system would have to be removed to determine the actual neutral points. The plot shows that as lift coefficient increases, the stick-free neutral point moves aft; this is the opposite trend from what is expected, is not seen in Figure 4.69, and could be a result of gimmicks in the control system and the technique used. Figure 4.74 shows the stick-free neutral points plotted against lift coefficient. As opposed to the stabilized method, the stick-free neutral points move aft as lift coefficient increases. The level accel/decel method shows the stick-free neutral points located much closer to one another in comparison to those found using the stabilized method. The stick-free neutral point at trim is seen to be behind the aft C.G. limit, which is desired.

4.5.3 Navajo – Stabilized Method

Figures 4.75-4.78 show the results of the Navajo's longitudinal static stability using the stabilized method. All plots are scaled to provide easy comparison between methods. A plot of elevator deflection versus calibrated airspeed is shown in Figure 4.75. Since power and trim setting do not change during the

test, the plot shows that elevator up (from trim position) is required to obtain speeds below trim and elevator down (from trim position) is required to obtain speeds above trim. Also, the plot shows a forward C.G. requires more deflection than an aft C.G. to maintain the same airspeeds; this shows that a forward C.G. provides more static stability than an aft C.G. Figure 4.76 shows a plot of elevator deflection versus lift coefficient. Since lift coefficient is a function of airspeed, this plot reflects the same trend as that seen in Figure 4.75; a lower lift coefficient correlates to a higher airspeed and, therefore, elevator trailing edge down (from trim position) and vice versa for a higher lift coefficient. Also, a forward C.G. is shown to require more elevator deflection compared to an aft C.G. to obtain the same lift coefficients. The stick-fixed neutral point determination is shown in Figure 4.77. The plot shows, as expected, that as the lift coefficient increase, the stick-fixed neutral point moves forward. Figure 4.78 shows the stick-fixed neutral points plotted against lift coefficient. This plot also shows the trend of the stick-fixed neutral point moving forward as lift coefficient increases. As can be seen, the stick-fixed neutral point at the trim condition at located aft of the C.G. limit, which is desired.

Figures 4.79-4.82 show the stick-free neutral point determination using the stabilized method. Elevator force versus calibrated airspeed is plotted in Figure 4.79. This plot shows that a pull is required to reach airspeed below trim and a push is required to reach speeds above trim. After all test points, the controls were released and the airspeed returned to within plus or minus 10% of the trim airspeed. This information, along with the plot, meets the requirements of FAR 23.173 to show the longitudinal static stability of the Navajo [1]. The gradients of each curve are similar. This could be a result of the downspring located in the elevator control system. Figure 4.80 shows a plot of elevator force versus lift coefficient. This plot shows the same trend as Figure 4.79; a lower lift coefficient correlates to a higher airspeed and, therefore, a push and vice versa for a higher lift coefficient. This plot also shows similar gradients between C.G. positions. Figure 4.81 shows the determination of the stick-free neutral points. Since the Navajo incorporates a downspring in the elevator control system, these neutral points are apparent and not the

actual locations. The trend seen is expected; the stick-free neutral points move forward as lift coefficient increases and vice versa. Comparing this plot with Figure 4.77, it can be seen that the stick-free neutral points are located behind the stick-fixed neutral points for each lift coefficient plotted. As previously discussed, stick-fixed neutral points are generally located behind stick-free neutral points. However, the purpose of the downspring is to increase the force felt by the pilot when deviating from trim which creates the feeling of increased stability. Because of this, the apparent stick-free neutral points are shown to be located aft of the stick-fixed neutral points. Figure 4.82 shows the stick-free neutral points plotted against lift coefficient. As expected, the stick-free neutral points move aft as lift coefficient decreases. Also, the trim condition is located well-aft of the C.G. limit.

4.5.4 Navajo – Level Accel/Decel Method

The results of the stick-fixed neutral point determination using level accel/decel method are shown in Figures 4.83-4.86. Figure 4.83 shows a plot of elevator deflection versus calibrated airspeed. The expected trend is seen: elevator trailing edge up (from trim position) is required to obtain speeds below trim and elevator trailing edge down (from trim position) is required to obtain speeds above trim. Also, a forward C.G. requires greater deflections than an aft C.G. to maintain the same airspeeds. The values plotted are similar to those seen in Figure 4.75 using the stabilized method except that the level accel/decel method encompasses a much wider range of airspeeds. Figure 4.84 shows a plot of elevator deflection versus lift coefficient. This plot reflects the same trend as Figure 4.83 for a forward C.G. requiring more elevator deflection than an aft C.G. for a given lift coefficient. Comparing Figure 4.84 with Figure 4.76, it can be seen that the results are similar for each method. Figure 4.85 shows the determination of stick-fixed neutral points. This plot shows that the stick-fixed neutral points selected are located behind the aft C.G. limit, which is desired. Comparing this with Figure 4.77, the level accel/decel method produces stick-fixed neutral points located much closer to one another than the stabilized

method. Figure 4.86, which shows the stick-fixed neutral points versus lift coefficient, shows that the stick-fixed neutral point at the trim condition is located aft of the C.G. limit, which is desired.

The stick-free neutral point determination using the level accel/decel method is seen in Figures 4.87-4.90. Figure 4.87 shows a plot of elevator force versus calibrated airspeed. The plot shows that a pull is required to obtain airspeeds below trim and a push is required to obtain airspeeds above trim. However, the faired lines of each set of data show a unique trend which may be a result of data scatter seen in the plot. Comparing this plot with Figure 4.79, the forces required at airspeeds common to both techniques are similar. This plot shows that the Navajo meets the requirements of FAR 23.173 for longitudinal static stability [1]. Figure 4.88 shows a plot of elevator force versus lift coefficient. This plot shows that an increasing deviation from trim requires increasing force, mirroring the results of Figure 4.87. Figure 4.88 also shows that a forward C.G. requires greater force than an aft C.G. to reach a given airspeed. Comparing this plot with Figure 4.80, it can be seen that each plot shows similar forces requires for given lift coefficients at each C.G. Figure 4.89 shows the plot used to determine the stick-free neutral point. The plot shows that as lift coefficient increases, the stick-free neutral point moves aft; this is the opposite trend from what is expected, is not seen in Figure 4.85, and could be a result of gimmicks in the control system and the technique used. The same trend was seen in Figure 4.63 for the Saratoga stick-free neutral point using the same technique. Comparing this plot with Figure 4.85, it can be seen that the stick-free neutral points are located aft of the stick-fixed neutral points. As previously explained in Section 4.5.3, the purpose of the downspring is to provide the pilot with a sense of increases stability. Because of this, these stick-free neutral points are only apparent locations. Figure 4.90 shows a plot of each stick-free neutral point versus lift coefficient. Though the forward movement of neutral point with decreasing lift coefficient is undesired, the trim condition is still seen to be behind the aft CG limit, which is desired.

4.6 Longitudinal Maneuvering Stability

4.6.1 Saratoga – Stabilized Load Factor Method

Figures 4.91-4.94 show the results of longitudinal maneuvering stability for the Saratoga. Figure 4.91 shows a plots of elevator deflection versus load factor. Since airspeed and trim setting are constant, it can be seen that an increase in trailing edge up deflection is required as load factor increases. Also, a forward C.G. requires more deflection than an aft C.G. to maintain a given load factor. This is the expected trend since a forward C.G. provides a greater maneuvering margin and, therefore, greater stability. Data points at 60° bank were not obtained; further testing would be required to determine the trend of elevator deflection at higher bank angles. Figure 4.92 shows the determination of the stick-fixed maneuvering points. Extrapolating each line shows that the stick-fixed maneuvering points are located within 2 %MAC of each other for load factors of 1.0, 1.2, and 1.4. Also, the stick-fixed maneuvering point moves forward as load factor increases, which is expected. Figure 4.93 shows a plot of elevator force versus load factor. It can be seen that as load factor increases, more pull force is required since airspeed and trim setting are constant. Also, though the results for each C.G. are similar for small increases of load factor, a forward C.G. requires more force than an aft C.G. to maintain a higher load factor. Further testing would be required to determine the force required at a load factor of 3.8, the maximum for the Saratoga [12]. This would show if the Saratoga meets the requirements of FAR 23.155 [1]. For the purpose of safety in a classroom environment at UTSI, the maximum load factor does not exceed 2.0. Though the results show the proper trend to meet the requirements, data at a load factor of 3.8 is needed to fully meet the requirements. Figure 4.94 shows the determination of stick-free maneuvering points. The stick-free maneuvering points are seen to be located aft of the stick-fixed maneuvering points seen in Figure 4.92 except at a load factor of 1.4. The stick-free maneuvering point is located 1 %MAC ahead of the stick-fixed maneuvering point for a load factor of 1.4. Since the Saratoga incorporates a bobweight, the values of stick-free maneuvering point are apparent and not the exact locations.

4.6.2 Navajo – Stabilized Load Factor Method

Figures 4.95-4.98 show the results of longitudinal maneuvering stability for the Navajo. Figure 4.95 shows a plot of elevator deflection versus load factor. It can be seen that, since airspeed and trim setting are constant, an increase in load factor requires increased trailing edge up deflection. Also, a forward C.G. requires greater deflection than an aft C.G. to obtain a given load factor. Further testing would need to be performed in order to obtain data at a load factor of 2.0. Figure 4.96 shows the determination of stick-fixed maneuvering points. As expected, as load factor increase, the stick-fixed maneuvering point moves forward. The plot shows that a load factor of 1.6 results in a maneuvering point located approximately 0.5 %MAC ahead of the aft C.G. limit while load factors of 1.3 and 1.0 are located aft of the limit. Figure 4.97 shows a plot of elevator force versus load factor. The plot shows that as load factor increases, increased pull force is required since airspeed and trim setting are constant. Also, a forward C.G. requires greater force than an aft C.G. to maintain a given load factor. Though this plot shows the proper trend to meet the requirements of FAR 23.155, further testing would be required to determine the force required at a maximum load factor of 3.6 for the Navajo [1, 10]. Figure 4.98 shows the determination of the stick-free maneuvering points. It can be seen that as load factor increases, the stick-free maneuvering points move forward, which is expected. These maneuvering points are all located within 1 %MAC of each other and are ahead of the stick-fixed maneuvering point for load factors of 1.0 and 1.3. These are apparent stick-free maneuvering points since the Navajo control system incorporates a downspring.

4.7 Longitudinal Dynamic Stability

4.7.1 Saratoga – Phugoid

Figure 4.99 shows the results for the stick-fixed phugoid in the Saratoga. As can be seen, once the controls were returned to the trim position, the phugoid motion was oscillatory and lightly damped. The period was determined to be 33.9 seconds with the damped natural frequency being 0.185 rad/s. The

subsidence ratio method, which is described in Appendix D with all other methods of determining damping ratio, was used to determine the damping ratio. The damping ratio was determined to be 0.0917 which produced an undamped natural frequency of 0.186 rad/s. These plots show that the Saratoga meets the requirement of FAR 23.181 for a long period motion [1]. Also, the Saratoga meets Level 1 requirements of MIL-HDBK-1797 for a damping ratio greater than 0.040 [4].

Figure 4.100 shows the results for the stick-free phugoid in the Saratoga. Again, the motion was oscillator and lightly damped. The period was found to be 31.1 seconds with a damped natural frequency of 0.202 rad/s. The subsidence ratio method was used to determine a damping ratio of 0.100 producing an undamped natural frequency of 0.203 rad/s. These plots also show that the Saratoga meets the requirements established in FAR 23.181 for a long period motion [1]. The stick-free phugoid motion also meets the Level 1 requirements of MIL-HDBK-1797 for a damping ratio greater than 0.040 [4].

4.7.2 Saratoga – Short Period

Figure 4.101 shows the frequency sweep performed by the pilot to determine the approximate short period frequency. As can be seen, the plane follows slow inputs, becomes 180° out of phase at the short period frequency, and reacts minimally to rapid inputs. This shows how the aircraft acts like a spring-mass-damper system and can also show the value of n_{zmax}/α_{max}, which was determined to be 11.7 g/rad.

Figure 4.102 shows the stick-fixed short period. The motion was oscillatory and heavily damped with a period of 1.6 seconds and a damped natural frequency of 3.93 rad/s. Using the log decrement equation method, the damping ratio was found to be 0.188 producing an undamped natural frequency of 3.99 rad/s. The Saratoga meets the requirements of FAR 23.181 for a heavily damped stick-fixed short period [1]. N_{zmax}/α_{max} was found to be 12.9 g/rad for the test which produced a CAP of 1.24 1/g-s^2. It also meets the Level 3 requirements for all Categories of MIL-HDBK-1797 [4].

Figure 4.103 shows the stick-free short period. The motion was also oscillatory and heavily damped with a period of 1.1 seconds and a damped natural frequency of 5.71 rad/s. The log decrement

equation method, was used to determine a damping ratio of 0.202 and an undamped natural frequency of 5.83 rad/s. This meets the requirements of FAR 23.181 for a heavily damped stick-free short period [1]. N_{zmax}/α_{max} was determined to be 12.6 g/rad producing a CAP of 2.71 1/g-s^2. This meets the Level 3 requirements for Categories A and C and Level 2 requirements for Category B of MIL-HDBK-1797 [4].

4.7.3 Navajo – Phugoid

Figure 4.104 shows the stick-fixed phugoid in the Navajo. The motion is seen to be oscillatory and lightly damped with a period of 42.6 seconds giving a damped natural frequency of 0.148 rad/s. The transient peak method was used to determine a damping ratio of 0.0600 producing an undamped natural frequency of 0.148 rad/s. This meets the requirements of FAR 23.181 for a long period oscillation [1]. It also meets the Level 1 requirements of MIL-HDBK-1797 [4].

Figure 4.105 shows the stick-free phugoid. This motion was also oscillatory and lightly damped with a period of 39.0 seconds and a damped natural frequency of 0.161 rad/s. The subsidence ratio method was used to determine a damping ratio of 0.0500 producing an undamped natural frequency of 0.161 rad/s. This motion also meets the requirements of FAR 23.181 and the Level 1 requirements of MIL-HDBK-1797 [1, 4].

4.7.4 Navajo – Short Period

Figure 4.106 shows the frequency sweep performed by the pilot to determine the approximate short period frequency in-flight. It can be seen that the plane reacts with the motion during slow inputs, reacts 180° out of phase at the short period frequency, and reacts minimally at rapid inputs. N_{zmax}/α_{max} was determined to be -154.1 g/rad. The negative sign of this value is most likely due to the errors discussed in Section 2.2 of the angle of attack cone location.

Figure 4.107 shows the stick-fixed short period. The motion is seen to be oscillatory and heavily damped. The period is 2.8 seconds with a damped natural frequency of 2.24 rad/s. The log decrement equation method, was used to determine a damping ratio of 0.233 producing an undamped natural

frequency of 2.31 rad/s. This meets the requirements of FAR 23.181 for a heavily damped stick-fixed short period oscillation [1]. N_{zmax}/α_{max} was determined to be -26.6 g/rad producing a CAP of -0.199 1/g-s^2. The Navajo meets the requirements of Level 3 for Categories A and C and Level 2 for Category B of MIL-HDBK-1797 [4]. An in-flight calibration of the angle of attack cone would be required to provide accurate values of n_{zmax}/α_{max} and CAP.

Figure 4.108 shows the stick-free short period. The motion is also seen to be oscillatory and heavily damped. The period was determined to be 2.1 seconds with a damped natural frequency of 2.99 rad/s. Using the log decrement equation method, the damping ratio was found to be 0.215 producing an undamped natural frequency of 3.06 rad/s. This meets the requirements of FAR 23.181 for a heavily damped stick-free short period oscillation [1]. N_{zmax}/α_{max} was found to be -21.7 g/rad with a CAP of -0.432 1/g-s^2. The stick-free short period also meets the requirements of Level 3 for Categories A and C and Level 2 for Category B of MIL-HDBK-1797 [4]. Again, an in-flight calibration of the angle of attack cone would be required to provide accurate values of n_{zmax}/α_{max} and CAP.

4.8 Lateral-Directional Static Stability

4.8.1 Saratoga – Steady Heading Sideslip Method

Figures 4.109-4.110 show the results of the lateral-directional static stability on the Saratoga. Figure 4.109 show a composite of six plots; rudder deflection, rudder force, aileron deflection, aileron force, angle of bank, and elevator force are all plotted against angle of sideslip. Each plot contains a curve for a cruise configuration and a power approach configuration. Using the conventions described in Table 2.1, it can be seen that right rudder produces a negative angle of sideslip and left rudder produces a positive angle of sideslip. Also, greater rudder deflections produce a greater sideslip. This plot, along with the others, show greater sideslip angles were achieved in the power approach configuration; this could be a result of the lower power setting while the plane was in a descent. The rudder forces mirror the rudder deflections: greater deflections require greater forces. The aileron deflections show the expected

trend when compared to rudder deflection. As rudder input increases, aileron deflection in the opposite direction is required to maintain heading. The cruise configuration shows that the aileron deflection required begins to taper and reverse at higher angles of sideslip. The aileron forces reflect what the aileron deflections show. For the cruise configuration, negative sideslip (i.e. right rudder) requires little left aileron and little force whereas positive sideslip (i.e. left rudder) requires a greater amount of right aileron and much greater force. For the power approach configuration; both positive and negative sideslip require approximately the same amount of deflection but right aileron requires nearly zero force while left aileron requires several pounds. Angle of bank shows that a greater sideslip requires more bank for each configuration. This is expected since, to maintain a steady heading with the rudder deflected, opposite aileron is needed which produces a bank in the same direction as the aileron deflection. The final plot shows how sideslip affects elevator force. Traditionally, this technique requires the pilot to maintain the same pitch attitude determined at trim for all test points since the indicated airspeed is affected by sideslip. However, since these tests are performed in an educational environment rather than for certification purposes and a calibration has not been performed to demonstrate the exact effect of sideslip on indicated airspeed, the pilot used the indicated airspeed as a simpler reference. It can be seen, for the cruise configuration, that increased elevator down force was required for increasing negative sideslip while little elevator down force was required for positive sideslip angles. For the power approach configuration, little elevator force was required for all sideslip angles and it reverses at higher angles. Based on FAR 23.177, further testing would be required to determine if the Saratoga meets the full requirements for certification [1]. Larger angles of sideslip would need to be obtained to show the full range of lateral-directional static stability. This would help determine if any reversal of deflections or forces seen in Figure 4.107 are part of the Saratoga's stability or a result of data points simply being close together. Overall, the Saratoga demonstrates positive lateral-directional stability for the data points tested.

Figure 4.110 shows a plot of indicated airspeed versus angle of sideslip. As previously mentioned, this plot would normally show how airspeed changes with angle of sideslip. However, since the pilot used indicated airspeed rather than pitch angle to stabilize during a test point, this plot is used only to demonstrate all aspects of data reduction for the technique.

4.8.2 Navajo – Steady Heading Sideslip Method

Figures 4.111-4.112 show the results of the lateral-directional static stability for the Navajo. Figure 4.111 shows a composite of six plots; rudder deflection, rudder force, aileron deflection, aileron force, angle of bank, and elevator force are all plotted against angle of sideslip. Each plot contains a curve for a cruise configuration and a power approach configuration. Unlike the Saratoga, the power approach configuration in the Navajo was performed while maintaining altitude rather than in a descent. This resulted in a higher power setting than would normally be required in this configuration. The rudder deflection can be seen to increase with increasing angle of sideslip. Though the rudder deflection appears greater for the power approach configuration, the rudder forces for both configurations are very similar. The aileron deflection for the cruise configuration is, as desired, opposite the rudder deflection. The aileron deflection for the power approach configuration changes very little, less than 1°, for all angles of sideslip. Much like the rudder forces, the aileron forces are similar for both configurations, showing an increase in force with an increase in angle of sideslip. The angle of bank is seen to increase with angle of sideslip for both configurations as well. The elevator force is shown in the final plot. Like the technique described for the Saratoga, the pilot used indicated airspeed as a reference rather than pitch angle. Increased elevator up force is shown for increasing sideslip in the cruise configuration. The power approach configuration shows that positive sideslip requires elevator force up while negative sideslip requires elevator force down. Although further testing would need to be performed to meet all of the requirements of FAR 23.177, the Navajo exhibits positive lateral-directional static stability for the data points tested [1].

Figure 4.112 shows a plot of indicated airspeed versus angle of sideslip. For the same reasons discussed for Figure 4.110, this plot is used to solely to demonstrate the full reduction process.

4.9 Lateral-Directional Dynamic Stability

4.9.1 Saratoga – Spiral Mode

Figure 4.113 shows the results of the stick-fixed spiral mode for both left and right directions. Rudder deflection and bank angle are plotted against time for both directions. The left bank was found to be convergent with a time to half amplitude of 3.7 s. The right bank was also convergent with a time to half amplitude of 5.4 s.

Figure 4.114 shows the stick-free spiral mode for both left and right directions. Rudder deflection and bank angle are plotted against time for both directions. The left bank was found to be divergent with a time to double amplitude of 9.6 s. This meets the Level 3 requirements for all categories in MIL-HDBK-1797 [4]. It is possible that this divergence is a result of propeller effects masking the spiral mode. The right bank was found to be convergent with a time to half of 3.7 s.

4.9.2 Saratoga – Roll Mode

Figure 4.115 shows the results of the roll mode banking to the right. The figure shows aileron deflection, roll rate, and bank angle versus time. The maximum roll rate was found to be 63.5 deg/s. 63.2% of the maximum roll rate was 40.1 deg/s giving a roll mode time constant 0.35 s. This meets the Level 1 requirements for all categories of MIL-HDBK-1797 [4].

Figure 4.116 shows the results of the roll mode banking to the left. The figure shows aileron deflection, roll rate, and bank angle versus time. The maximum roll rate was found to be 59.5 deg/s. 63.2% of the maximum roll rate was 37.6 deg/s giving a roll mode time constant of 0.22 s. This meets the Level 1 requirements for all categories of MIL-HDBK-1797 [4].

4.9.3 Saratoga – Dutch Roll Mode

Figure 4.117 shows the stick-fixed Dutch roll mode. The figure shows rudder deflection, bank angle, and angle of sideslip versus time. The ϕ/β ratio was found to be 1.1 showing that the Saratoga is slightly roll dominated. The period was 2.7 s giving a damped natural frequency of 2.33 rad/s. Using the log decrement equation method, the damping ratio was found to be 0.15 and the undamped natural frequency was 2.35 rad/s. These values meet the Level 1 requirements for Categories B and C and the Level 2 requirements for all categories of MIL-HDBK-1797 [4]. The Saratoga also meets the requirements of FAR 23.181 for the stick-fixed Dutch roll mode [1].

Figure 4.118 shows the stick-free Dutch roll mode. The figure shows rudder deflection, bank angle, and angle of sideslip versus time. The ϕ/β ratio was found to be 1.2 showing that the Saratoga is slightly roll dominated. The period was 2.9 s giving a damped natural frequency of 2.17 rad/s. The log decrement equation method, was used to determine a damping ratio of 0.141 and an undamped natural frequency of 2.19 rad/s. This meets the Level 1 requirements for Categories B and C and the Level 2 requirements for all categories of MIL-HDBK-1797 [4]. The Saratoga also meets the requirements of FAR 23.181 for the stick-free Dutch roll mode [1]. From the bank angle plot, it appears that the spiral mode was excited during the test.

4.9.4 Navajo – Spiral Mode

Figure 4.119 shows the stick-fixed spiral mode for both left and right directions. Rudder deflection and bank angle are plotted against time for both directions. The left bank was found to be divergent with a time to double amplitude of 39.7 s. This meets the Level 1 requirements for all categories of MIL-HDBK-1797 [4]. The right bank was found to be divergent with a time to double amplitude of 13.4 s. This meets the Level 1 requirements for Category A and the Level 2 requirements for Categories B and C of MIL-HDBK-1797 [4].

Figure 4.120 shows the stick-free spiral mode for both left and right directions. Rudder deflection and bank angle are plotted against time for both directions. The left bank was found to be divergent with a time to double amplitude of 70.8 s. This meets the Level 1 requirements for all categories of MIL-HDBK-1797 [4]. The right bank was found to be divergent with a time to double amplitude of 21.3 s. This meets the Level 1 requirements for all categories of MIL-HDBK-1797 [4].

4.9.5 Navajo – Roll Mode

Figure 4.121 shows the roll mode banking left to right. Aileron deflection, roll rate, and bank angle are plotted against time. The maximum roll rate was found to be 34.0 deg/s. 63.2% of the maximum roll rate is 21.5 deg/s giving a roll mode time constant of 0.45 s. This meets the Level 1 requirements for all categories of MIL-HDBK-1797 [4].

Figure 4.122 shows the roll mode banking right to left. Aileron deflection, roll rate, and bank angle are plotted against time. The maximum roll rate was found to be 30.0 deg/s. 63.2% of the maximum roll rate is 18.9 deg/s giving a roll mode time constant 0.55 s. This meets the Level 1 requirements for all categories of MIL-HDBK-1797 [4].

4.9.6 Navajo – Dutch Roll Mode

Figure 4.123 shows the stick-fixed Dutch roll mode. Rudder deflection, bank angle, and angle of sideslip are plotted against time. The ϕ/β ratio was found to be 0.3 showing that the Navajo is very yaw dominated. The period was 2.3 s giving a damped natural frequency of 2.73 rad/s. The log decrement equation method, was used to determine a damping ratio of 0.117 and an undamped natural frequency of 2.75 rad/s. These values meet the Level 1 requirements for Categories B and C and the Level 2 requirements for all categories of MIL-HDBK-1797 [4]. The Navajo also meets the requirements of FAR 23.181 for the stick-fixed Dutch roll mode [1]. From the bank angle plot, it appears that the spiral mode was excited during the test.

Figure 4.124 shows the stick-free Dutch roll mode. Rudder deflection, bank angle, and angle of sideslip are plotted against time. The ϕ/β ratio was found to be 0.3 showing that the Navajo is very yaw dominated. The period was 2.4 s giving a damped natural frequency of 2.62 rad/s. The log decrement equation method, was used to determine a damping ratio of 0.108 and an undamped natural frequency of 2.63 rad/s. These values meet the Level 1 requirements for Categories B and C and the Level 2 requirements for all categories of MIL-HDBK-1797 [4]. The Navajo also meets the requirements of FAR 23.181 for the stick-free Dutch roll mode [1]. From the bank angle plot, it appears that the spiral mode was excited during the test.

CHAPTER 5 CONCLUSION

5.1 Overview

The purpose of this thesis was to determine baseline data for the test instruments installed on the UTSI Piper Saratoga and Navajo. Because the test systems are independent from the factory systems, differences arise in flight data. Though the indicated values for each DAS are noticeably different, the air data system calibrations provided accurate calibrated values when compared to the factory systems. Performance parameters, such as range, endurance, climb rates, and stall speeds, largely compare well with the published values. In general, both aircraft showed acceptable static and dynamic stability characteristics. Since gimmicks exist in each system, the values presented are only apparent. However, the data obtained meets the purpose of this thesis for multiple reasons: (1) it shows the implementation of flight test techniques in order to determine aircraft characteristics and, in some cases, to compare multiple techniques to one another; (2) the plots created are to be used by students as references to compare their own values; and (3) performing each test allowed all involved valuable experience in flight planning, test execution, and data reduction.

5.2 Recommendations

While testing for certification or research would include repeated testing of each subject, only a single flight was allotted for each aircraft for each topic due to the volume of data presented and the time involved for each test. Further testing would be required to determine to most accurate values for these parameters using the test systems. It is recommended that future testing for the purpose of providing baseline data focus on a single or a select few topics. This would allow the flight test engineers to concentrate on a single concept (performance, stability and control, cruise performance, longitudinal dynamics, etc.) and provide a much more in-depth discussion of each. Also, as previously mentioned,

Microsoft Excel was used for data reduction due to its wide availability and popularity. The use of more capable plotting software could produce results more accurate to actual parameters.

BIBLIOGRAPHY

1. eCFR - Code of Federal Regulations. (2014). *eCFR - Code of Federal Regulations*. Retrieved October 27, 2014, from http://www.ecfr.gov/cgi-bin/text-idx?SID=1b5403d4053c0fcde4f1f2f3036320a5&tpl =/ecfrbrowse/Title14/14cfr23_main_02.tpl

2. Flight Test Guide for Certification of Part 23 Airplanes. (n.d.). *Federal Aviation Administration*. Retrieved October 27, 2014, from http://www.faa.gov/documentLibrary/media/Advisory_Circular/AC%2023-8C.pdf

3. *Flight Testing Newton's Laws*. (1999). Lancaster, CA: NASA Dryden Educator Resource Center.

4. *Flying Qualities of Piloted Aircraft*. (1997). Washington, D.C.: U.S. Dept. of Defense.

5. *Fixed Wing Stability and Control*. (1997). Patuxent River, MD: U.S. Naval Test Pilot School.

6. Gallagher, G. L., Higgins, L. B., Khinoo, L. A., & Pierce, P. W. (1992). *Fixed Wing Performance*. Patuxent River, MD: U.S. Naval Test Pilot School.

7. Herrington, R., Shoemacher, P., Bartlett, E., & Dunlap, E. (1966). *Flight Test Engineering Handbook*. Edwards Air Force Base, Calif.: United States Air Force, Air Force Systems Command, Air Force Flight Test Center.

8. Kimberlin, R. D. (2003). *Flight Testing of Fixed-Wing Aircraft*. Reston, VA: American Institute of Aeronautics and Astronautics.

9. Martos, Borja. (2013). *Longitudinal Dynamic Stability Flight Test Techniques* [PowerPoint slides].

10. *Navajo Pilot's Operating Handbook*. (2002). Vero Beach, FL: Piper Aircraft Corporation Publication Department.

11. Nelson, R. (1998). *Flight Stability and Automatic Control* (2nd ed.). New York: McGraw-Hill.

12. *Saratoga Pilot's Operating Handbook*. (1980). Vero Beach, FL: Piper Aircraft Corporation Publication Department.

13. "Using GPS to Accurately Establish True Airspeed", David Gray, unpublished paper available at www.ntps.edu/downloads.htm, June 1998.

APPENDICES

APPENDIX A FIGURES



Figure 2.1 – Piper PA-32 Saratoga



Figure 2.2 – Saratoga Factory Pitot-Static Mast



Figure 2.3 – Saratoga Test Air Data System
Total Temperature Probe (Left), Bent Static Probe (Top Center), Kiel Pitot Probe (Bottom Center), Bent Pitot Probe (Right)



Figure 2.4 – Saratoga Test Fuselage Static Port



Figure 2.5 – Piper PA-31 Navajo



Figure 2.6 – Navajo Factory Pitot Tube



Figure 2.7 – Navajo Static Ports
Factory Static Port (Top) and Test Fuselage Static Port (Bottom)



Figure 2.8 – Navajo Test Air Data System
Kiel Pitot Probe (Top), Bent Pitot Probe (Top Center), Bent Static Probe (Bottom Center), Total Temperature Probe (Bottom)

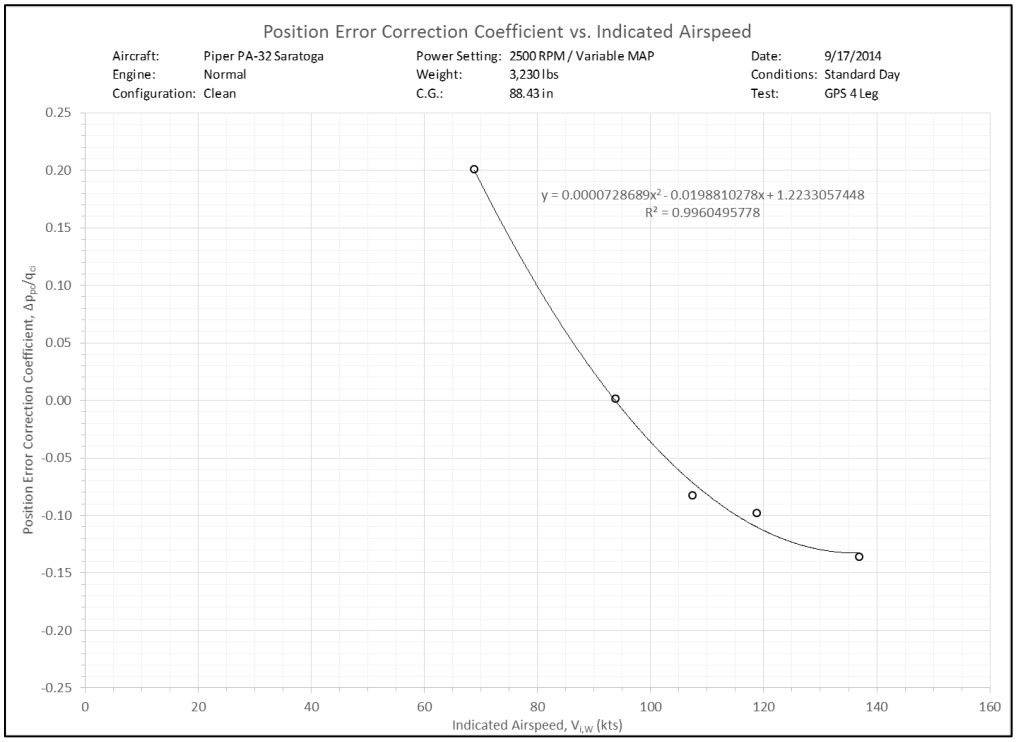


Figure 4.1 – Position Error Correction Coefficient vs. Indicated Airspeed for N22UT

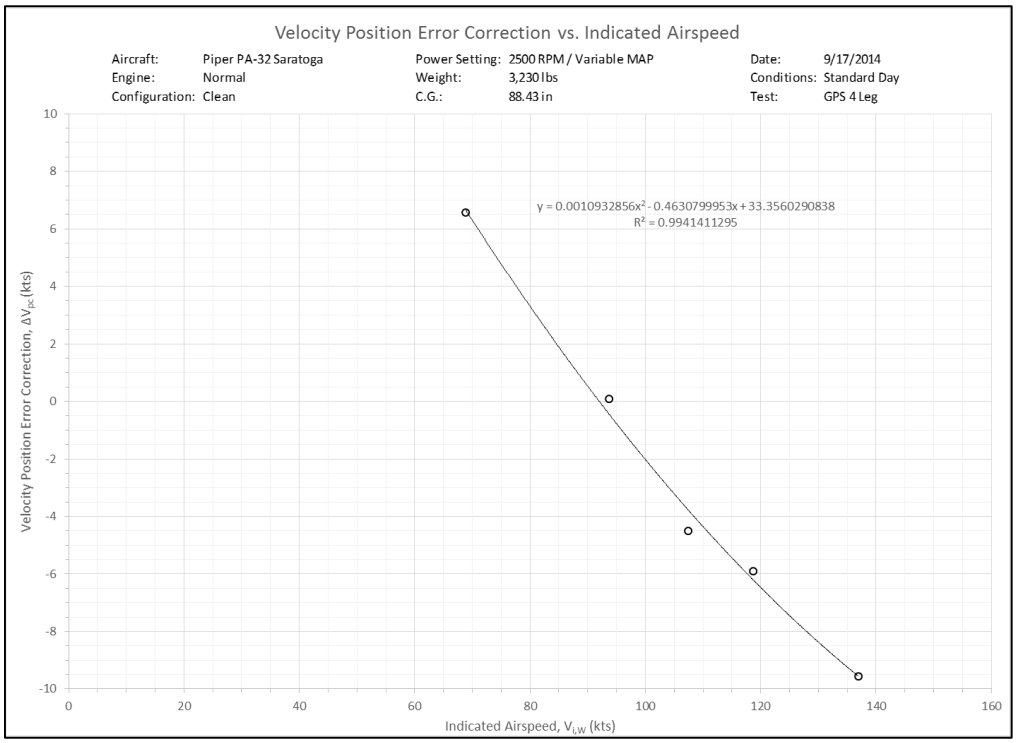


Figure 4.2 – Velocity Position Error Correction vs. Indicated Airspeed for N22UT

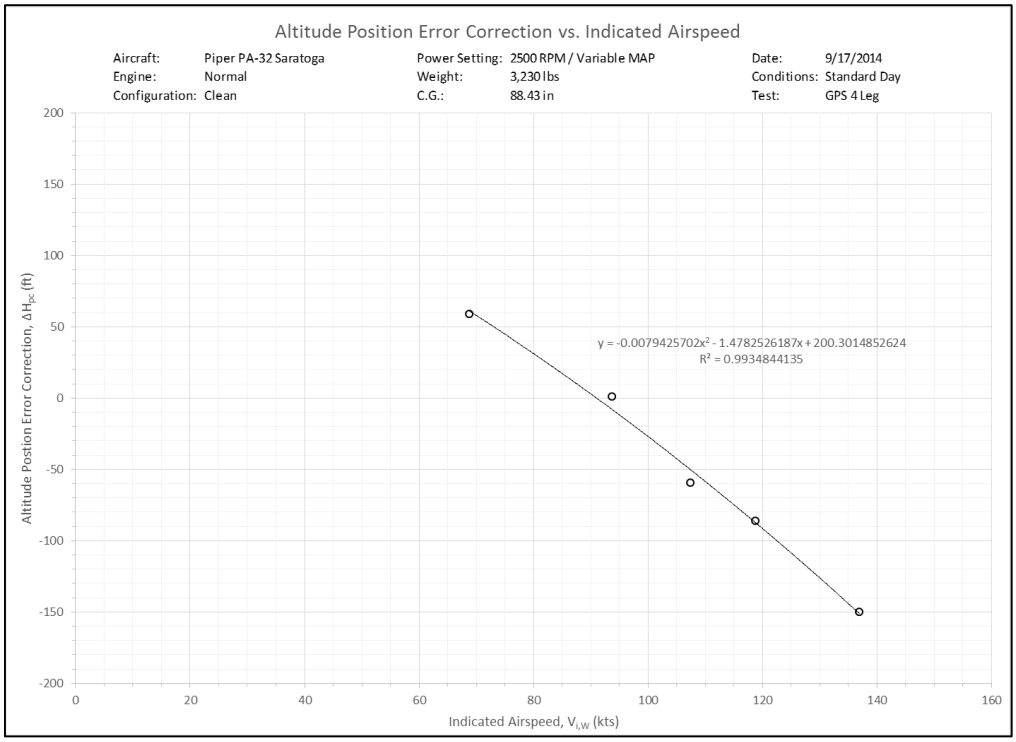


Figure 4.3 – Altitude Position Error Correction vs. Indicated Airspeed for N22UT

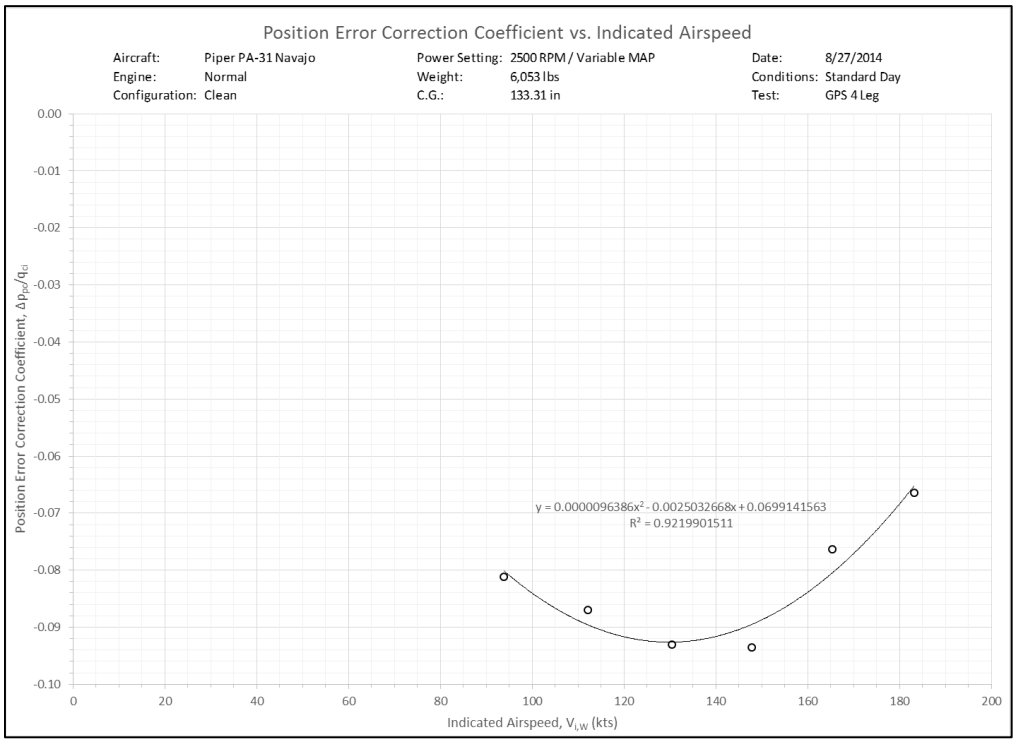


Figure 4.4 – Position Error Correction Coefficient vs. Indicated Airspeed for N11UT

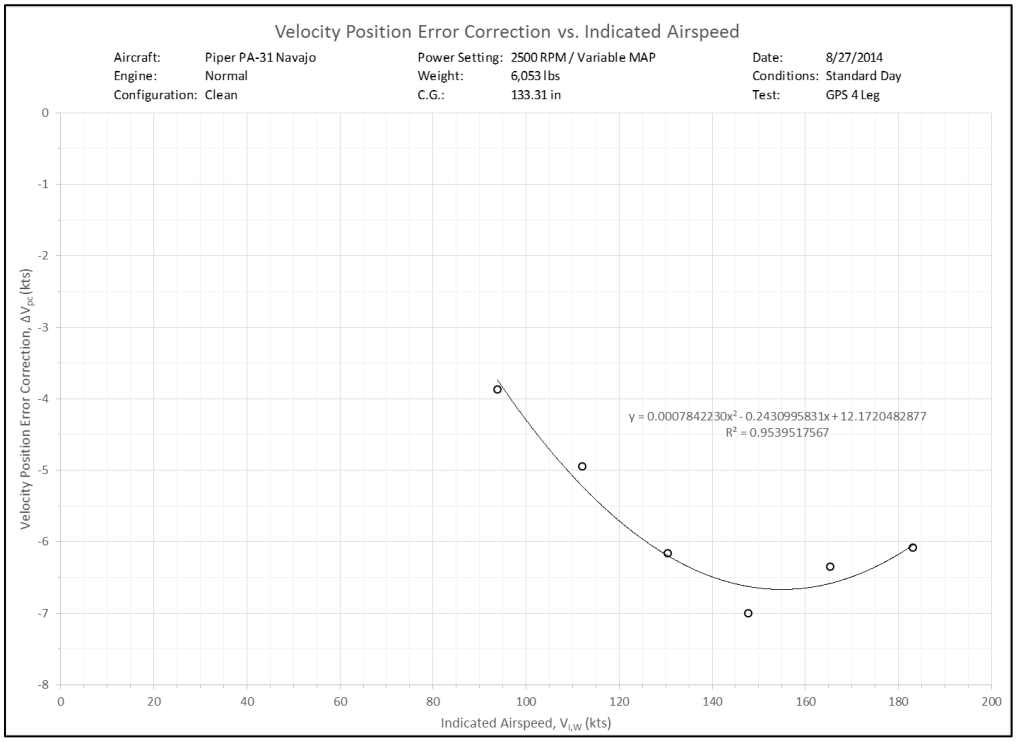


Figure 4.5 – Velocity Position Error Correction vs. Indicated Airspeed for N11UT

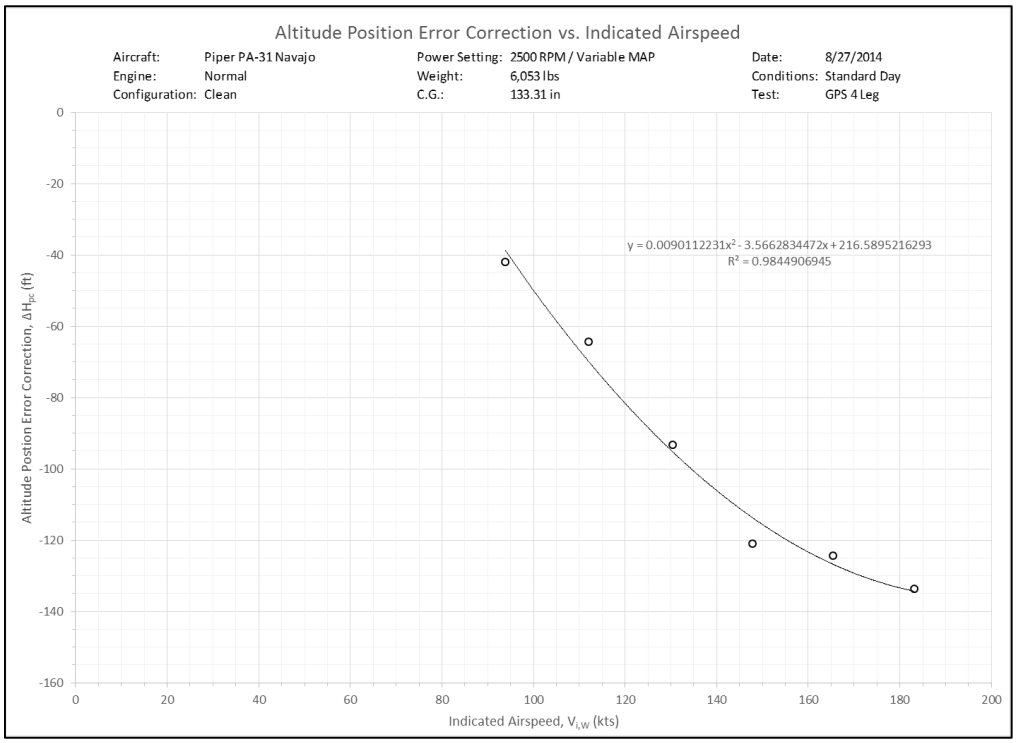


Figure 4.6 – Altitude Position Error Correction vs. Indicated Airspeed for N11UT

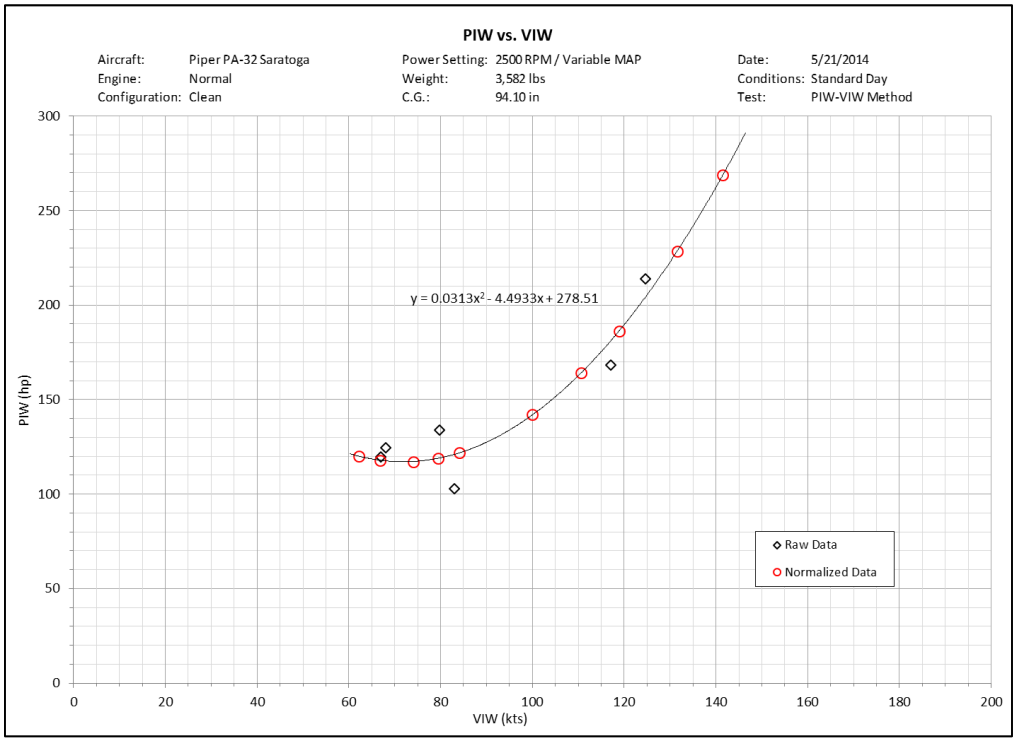


Figure 4.7 – PIW vs. VIW for N22UT

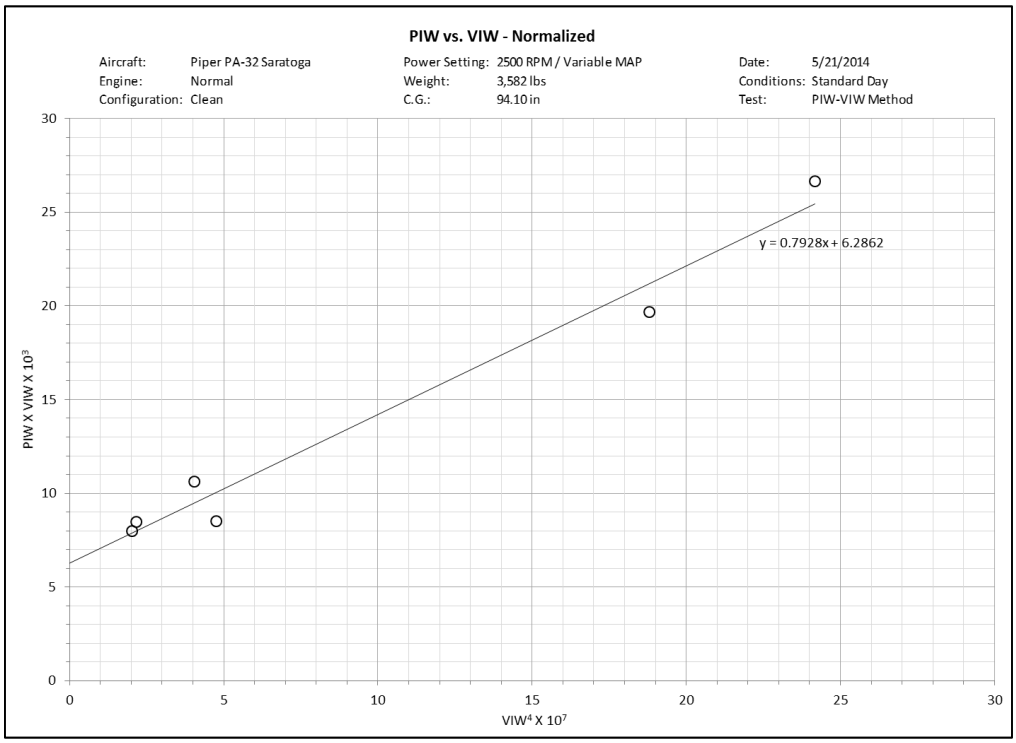


Figure 4.8 – Normalized PIW vs. VIW for N22UT

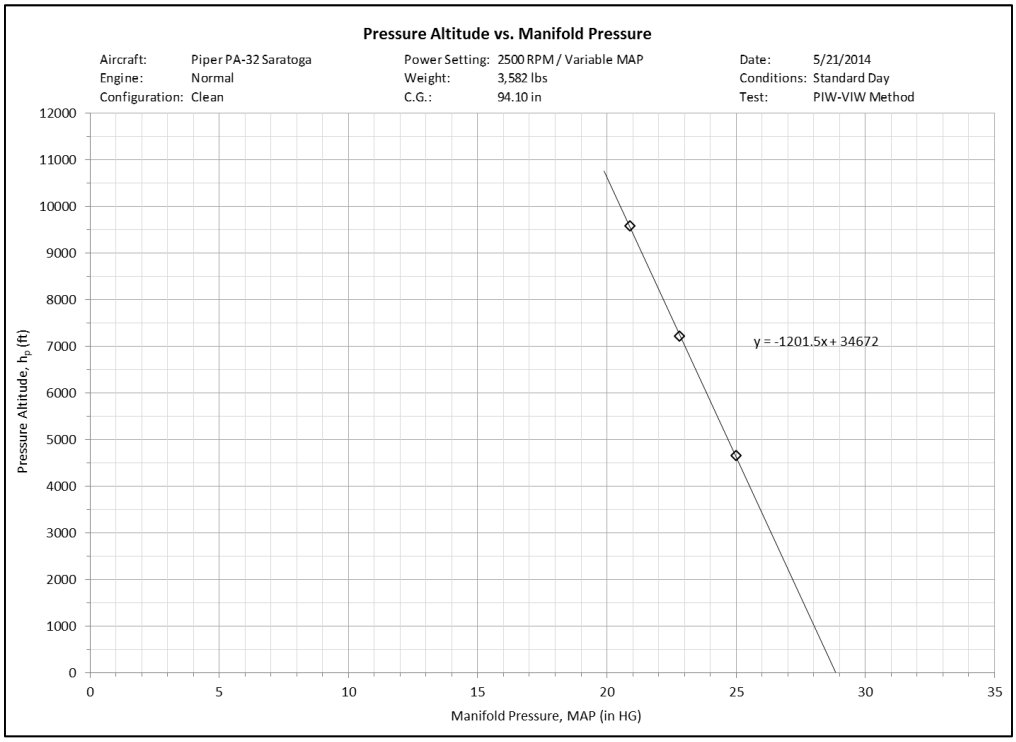


Figure 4.9 – Pressure Altitude vs. Manifold Pressure for N22UT

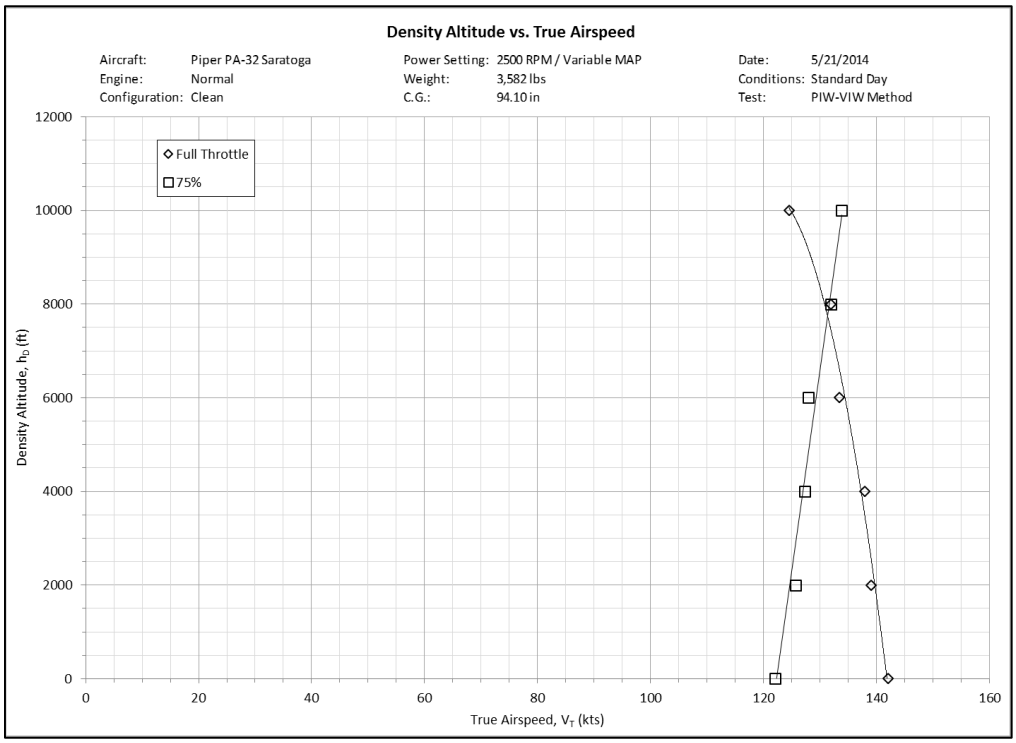


Figure 4.10 – Density Altitude vs. True Airspeed for N22UT

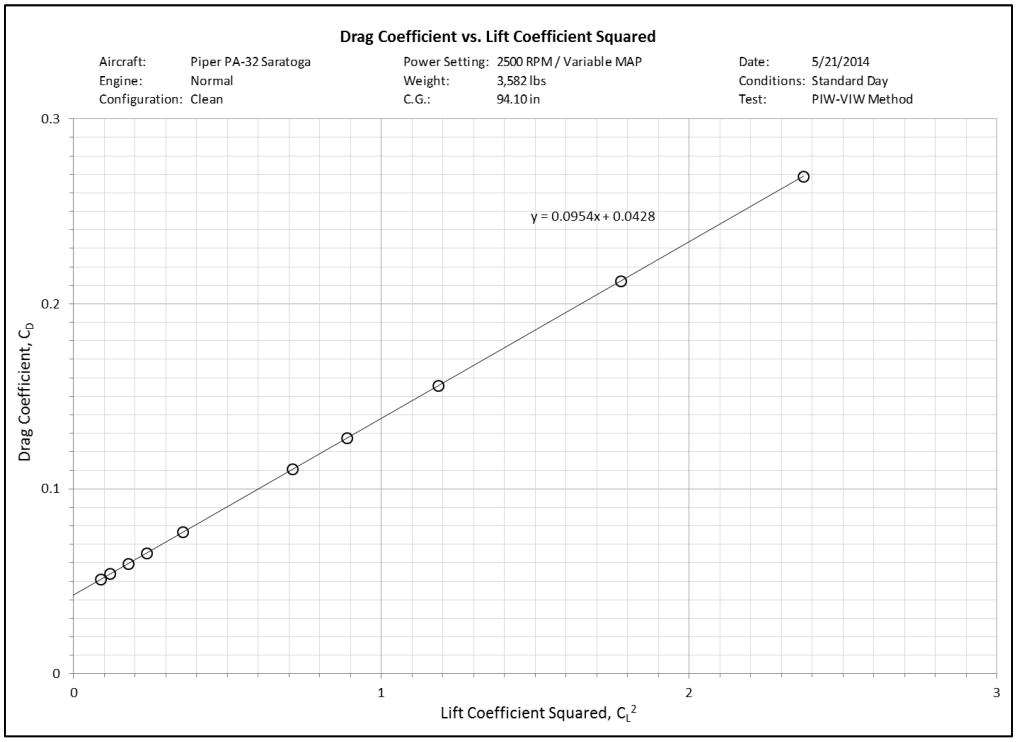


Figure 4.11 – Drag Coefficient vs. Lift Coefficient Squared for N22UT

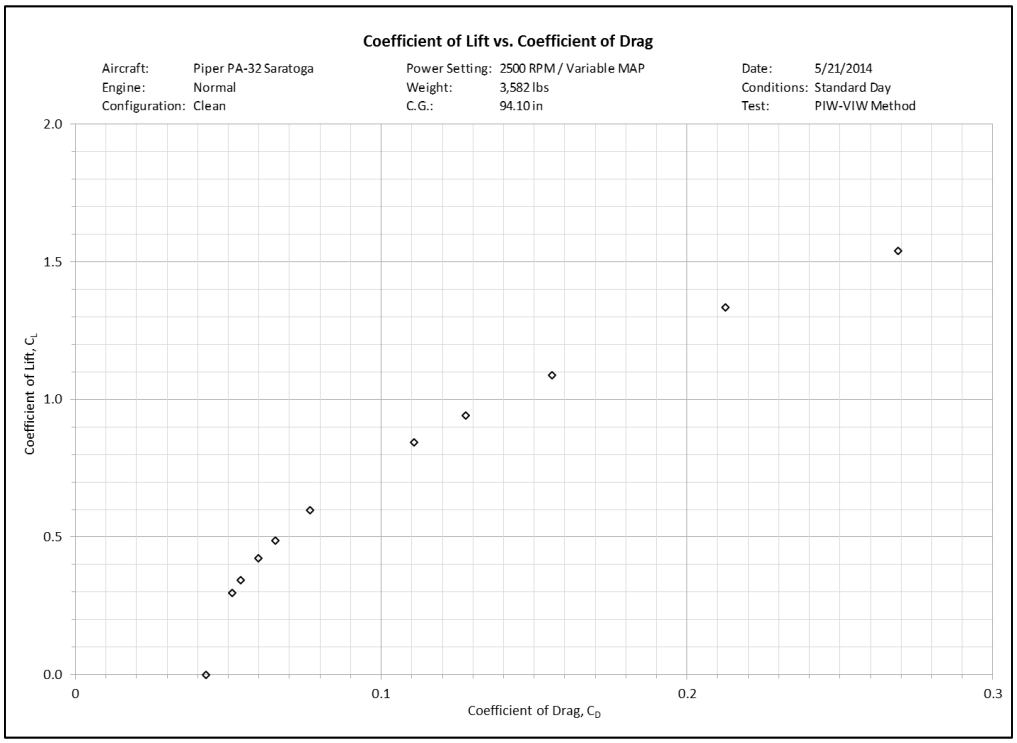


Figure 4.12 – Drag Polar for N22UT

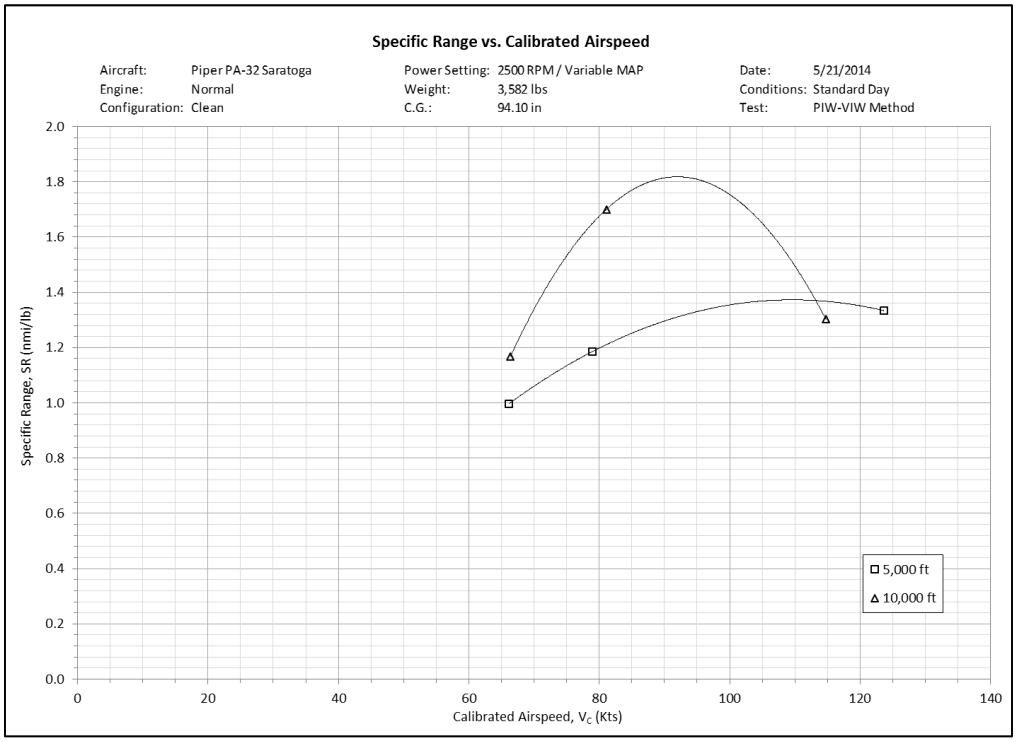


Figure 4.13 – Specific Range Using the PIW-VIW Method for N22UT

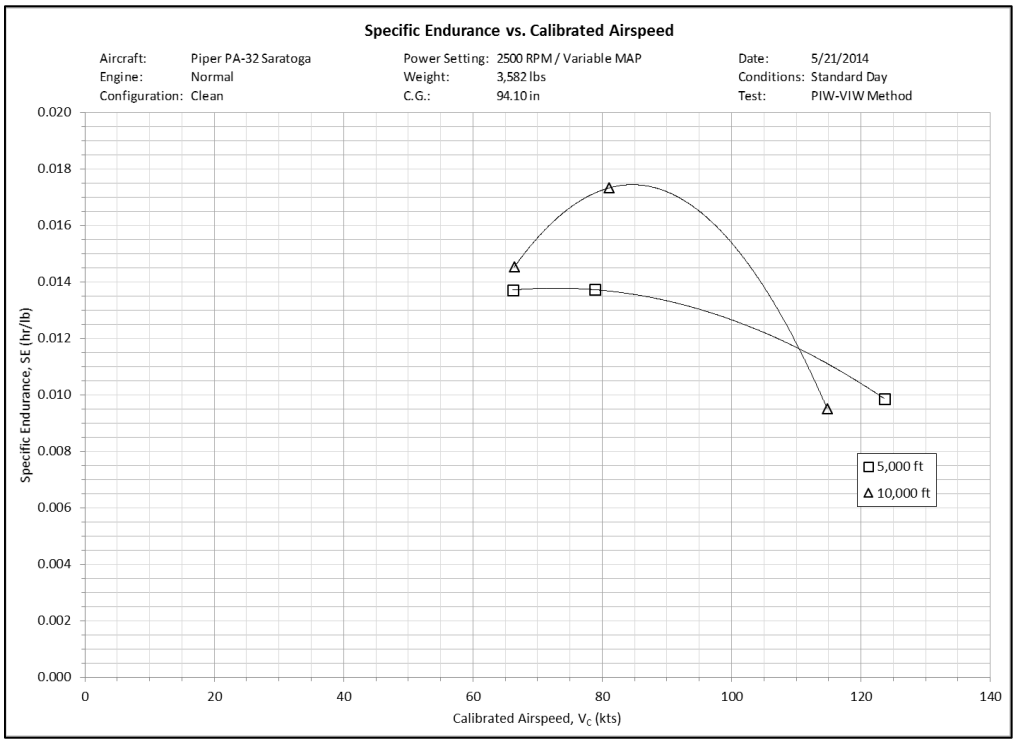


Figure 4.14 – Specific Endurance Using the PIW-VIW Method for N22UT

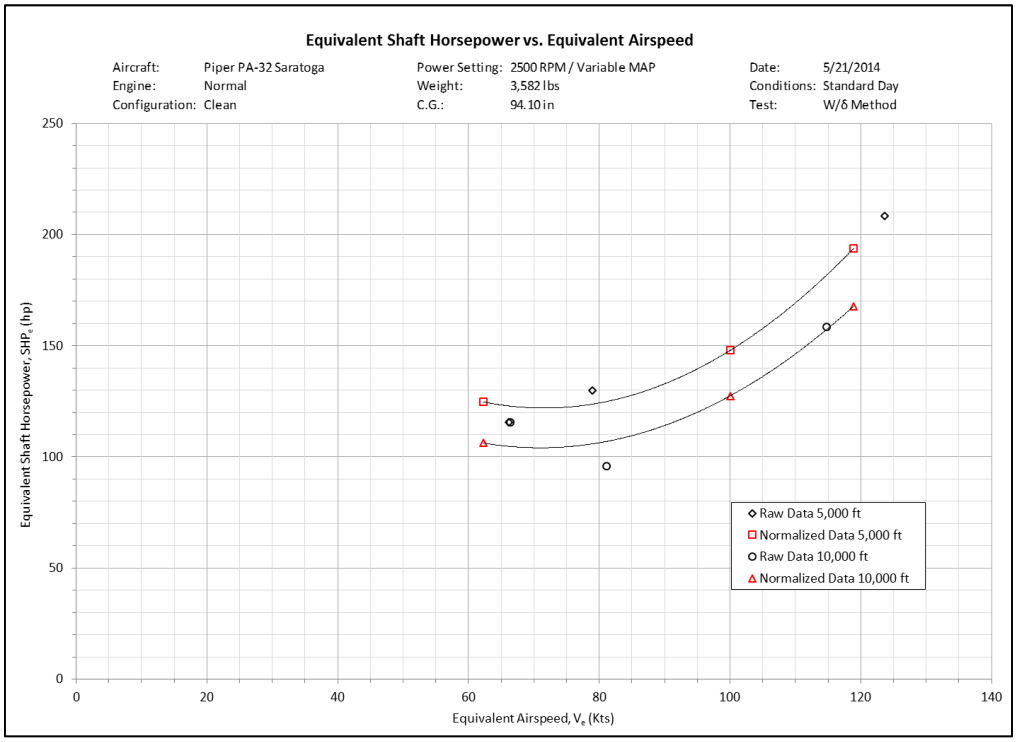


Figure 4.15 – Equivalent Shaft Horsepower vs. Equivalent Airspeed for N22UT

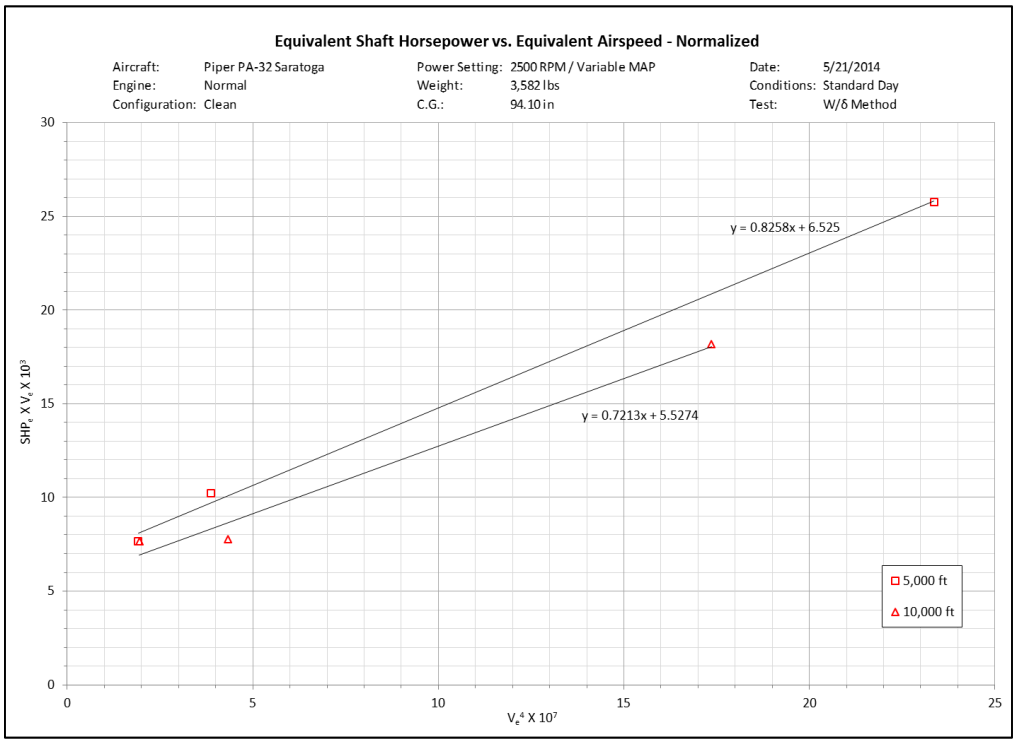


Figure 4.16 – Normalized Equivalent Shaft Horsepower vs. Equivalent Airspeed for N22UT

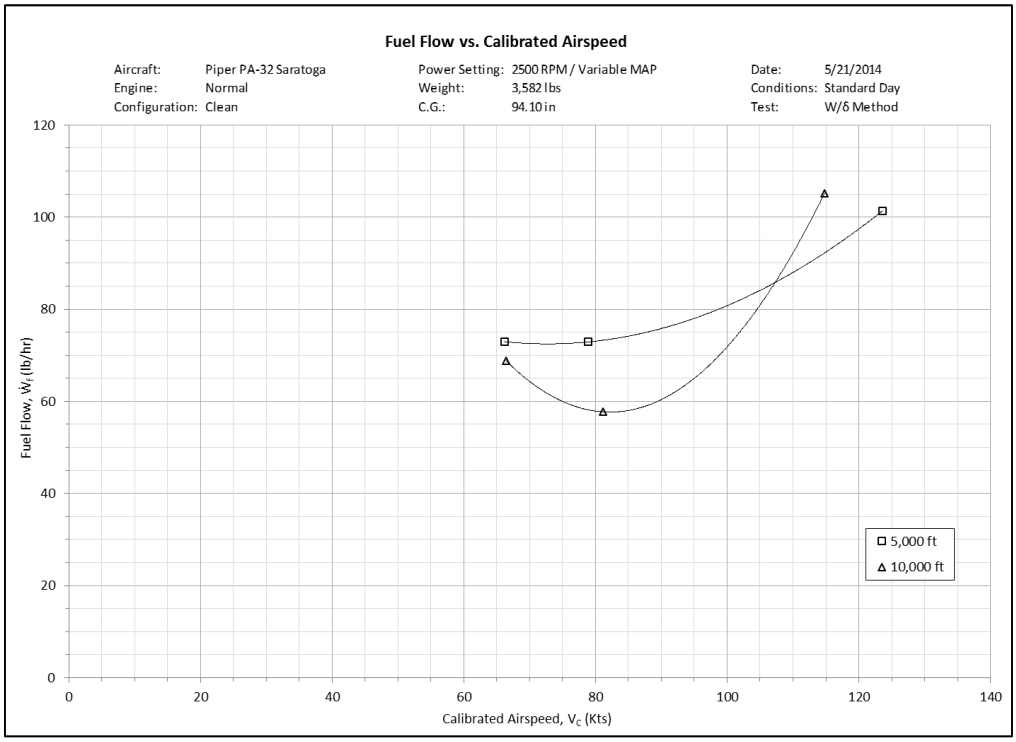


Figure 4.17 – Fuel Flow vs. Calibrated Airspeed for N22UT

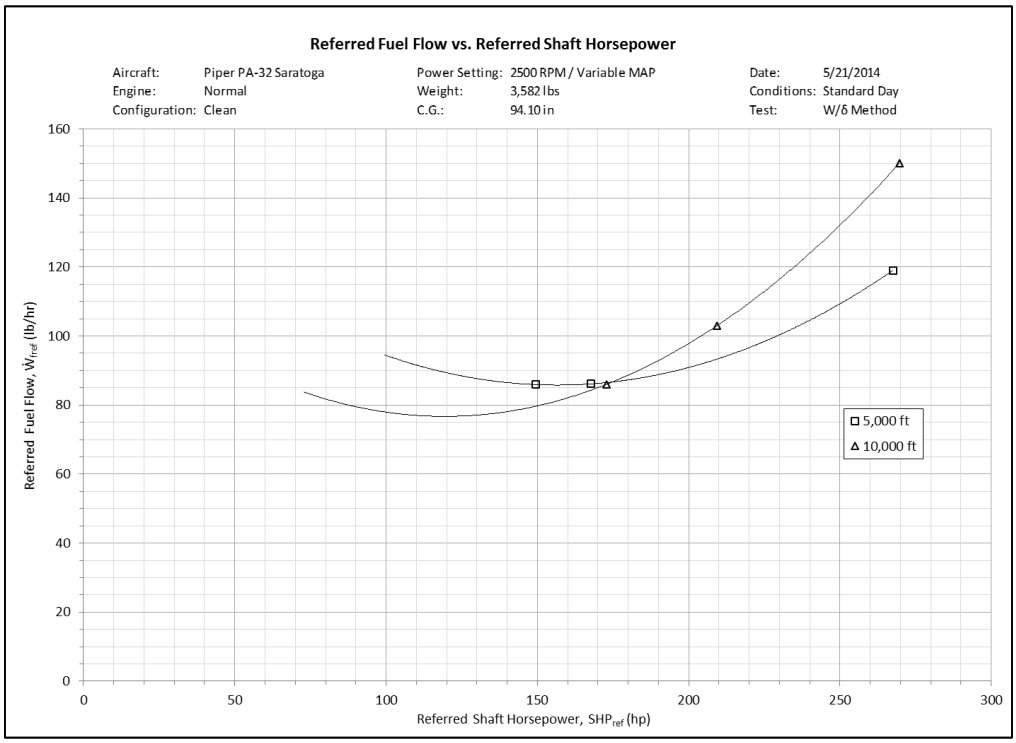


Figure 4.18 – Referred Fuel Flow vs. Referred Shaft Horsepower for N22UT

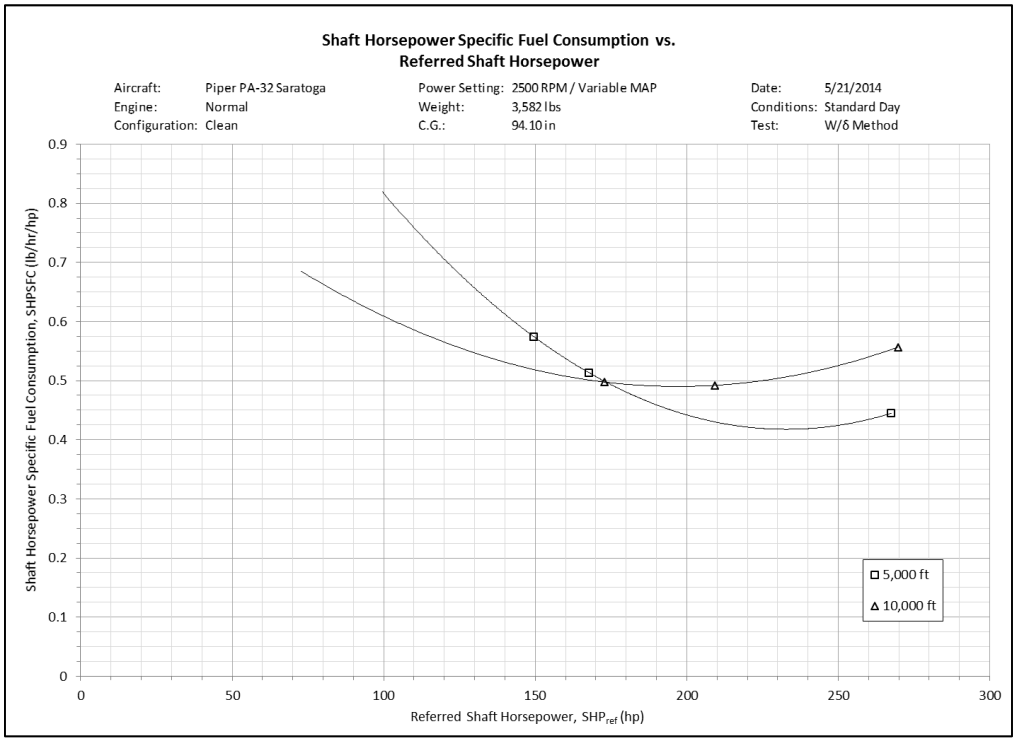


Figure 4.19 – Shaft Horsepower Specific Fuel Consumption vs. Referred Shaft Horsepower for N22UT

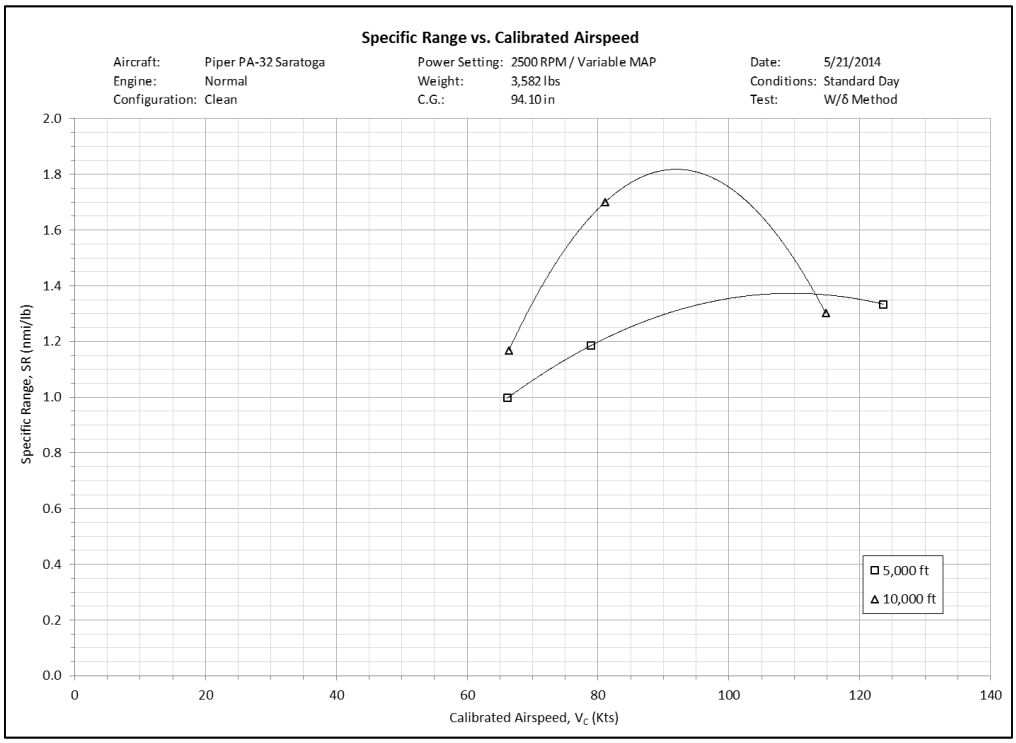


Figure 4.20 – Specific Range Using W/δ Method for N22UT

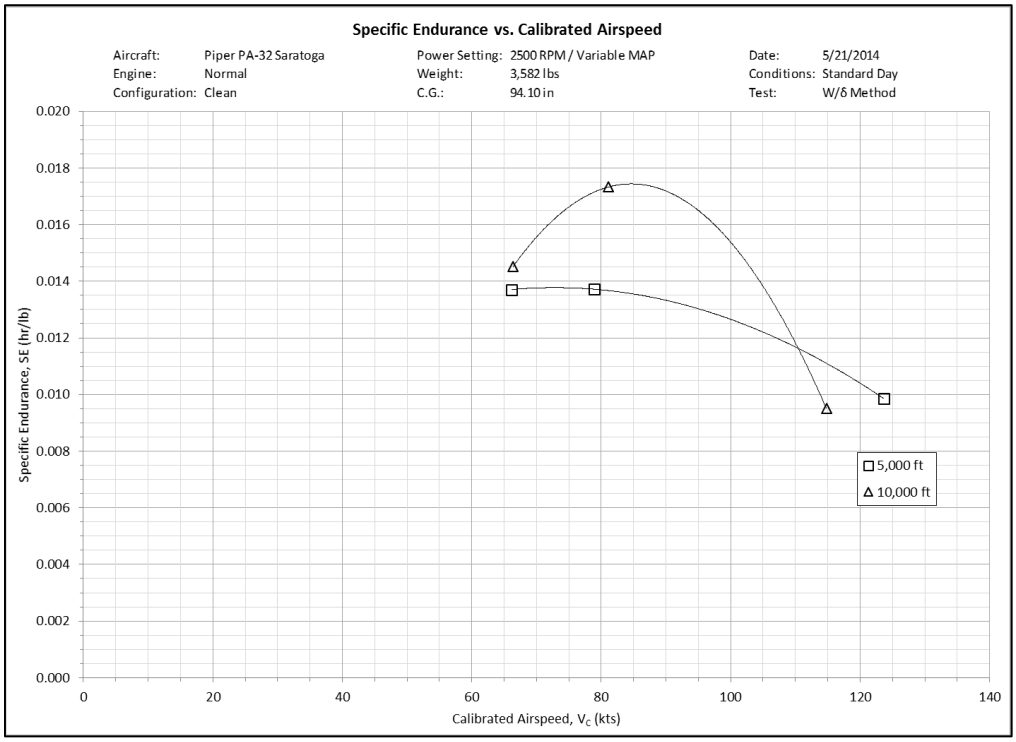


Figure 4.21 – Specific Endurance Using W/δ Method for N22UT

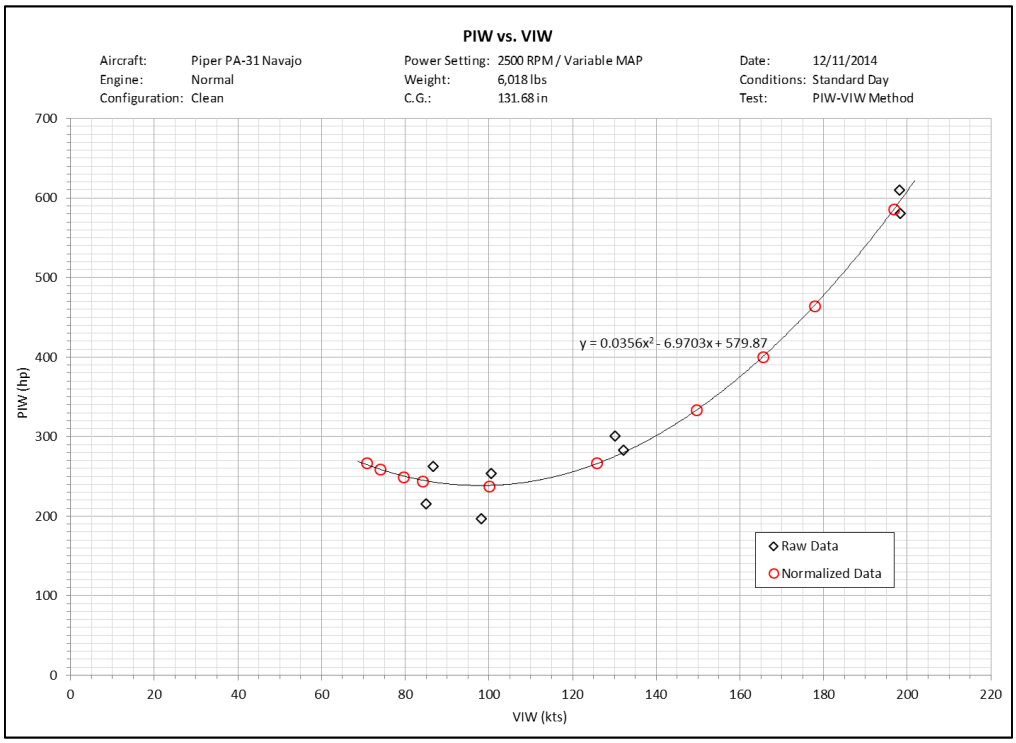


Figure 4.22 – PIW vs. VIW for N11UT

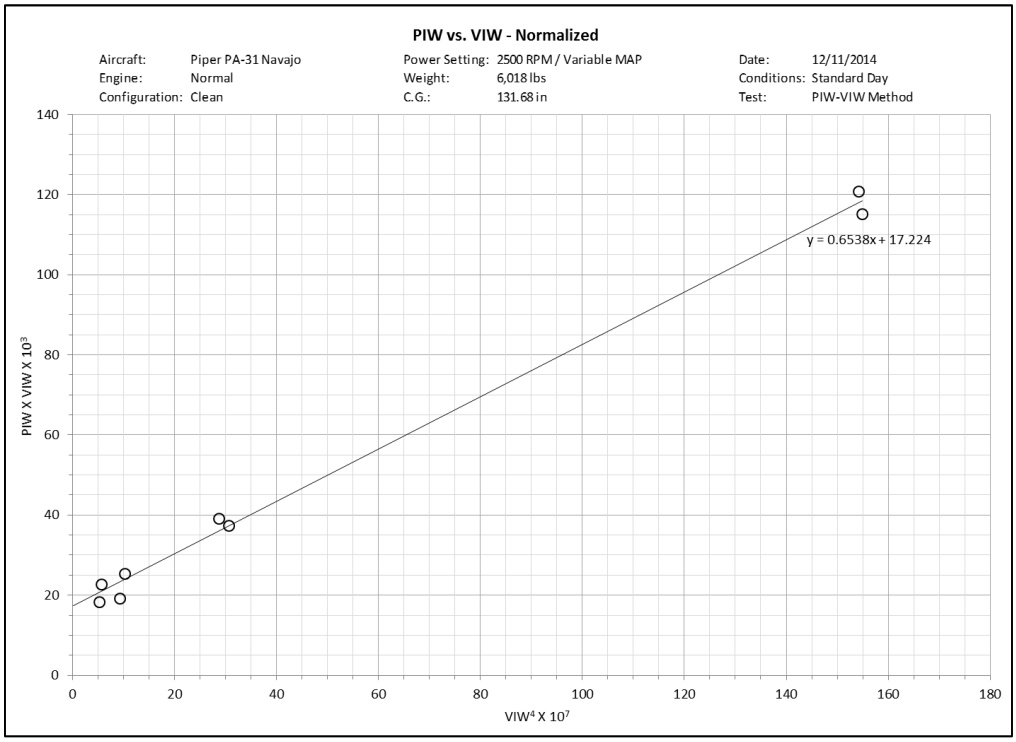


Figure 4.23 – Normalized PIW vs. VIW for N11UT

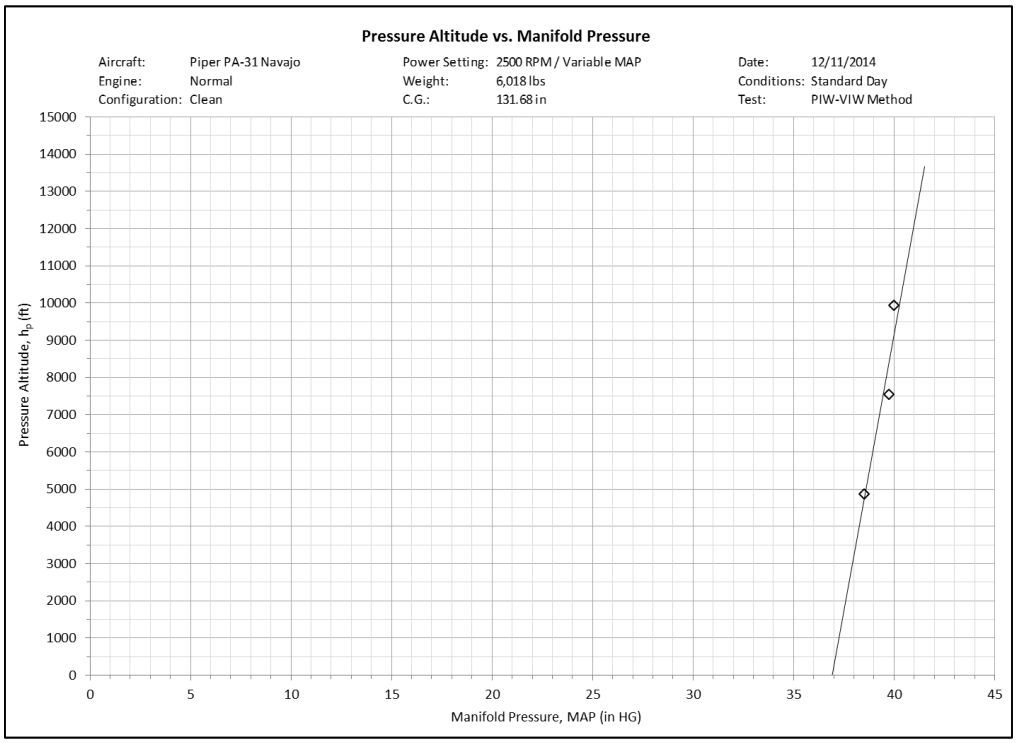


Figure 4.24 – Pressure Altitude vs. Manifold Pressure for N11UT

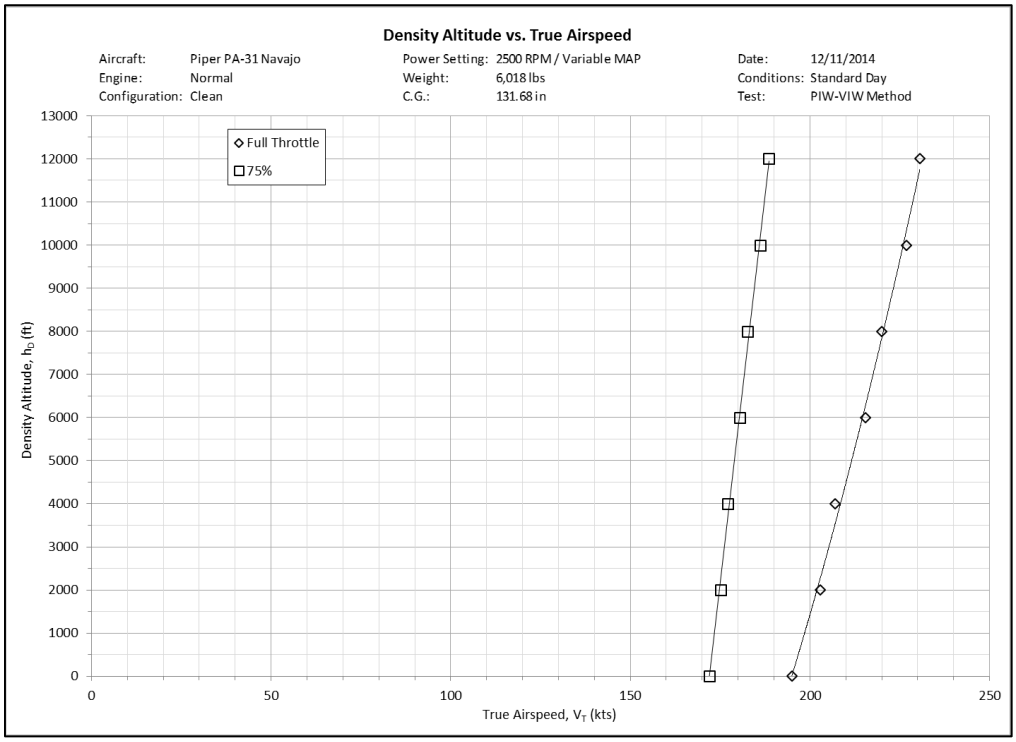


Figure 4.25 – Density Altitude vs. True Airspeed for N11UT

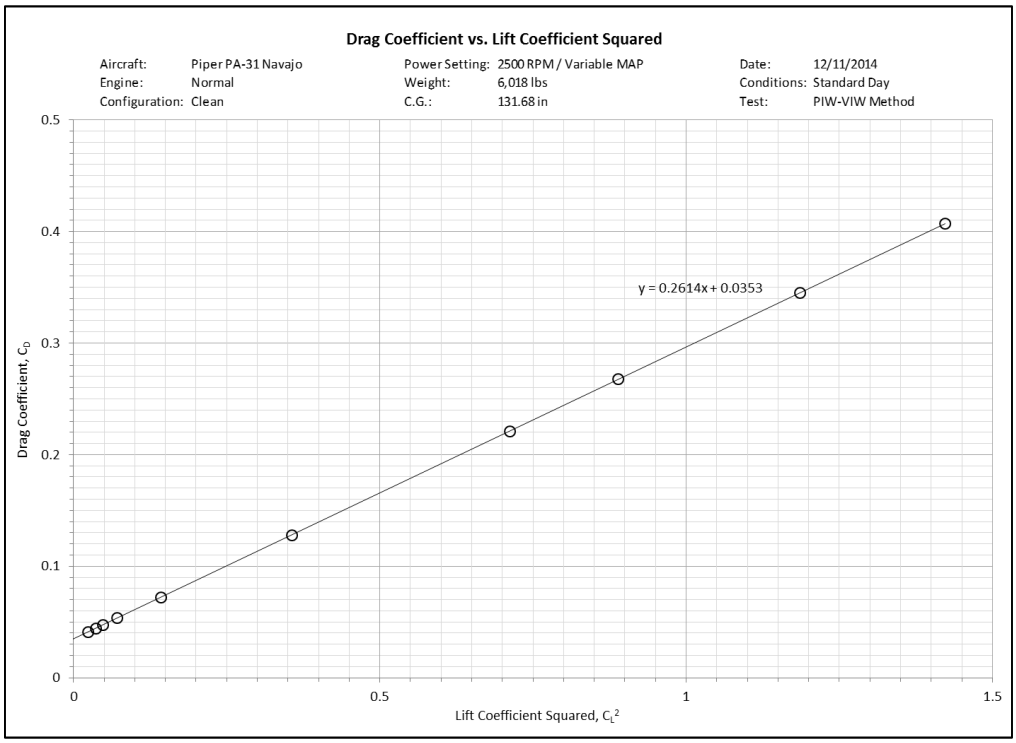


Figure 4.26 – Drag Coefficient vs. Lift Coefficient Squared for N11UT

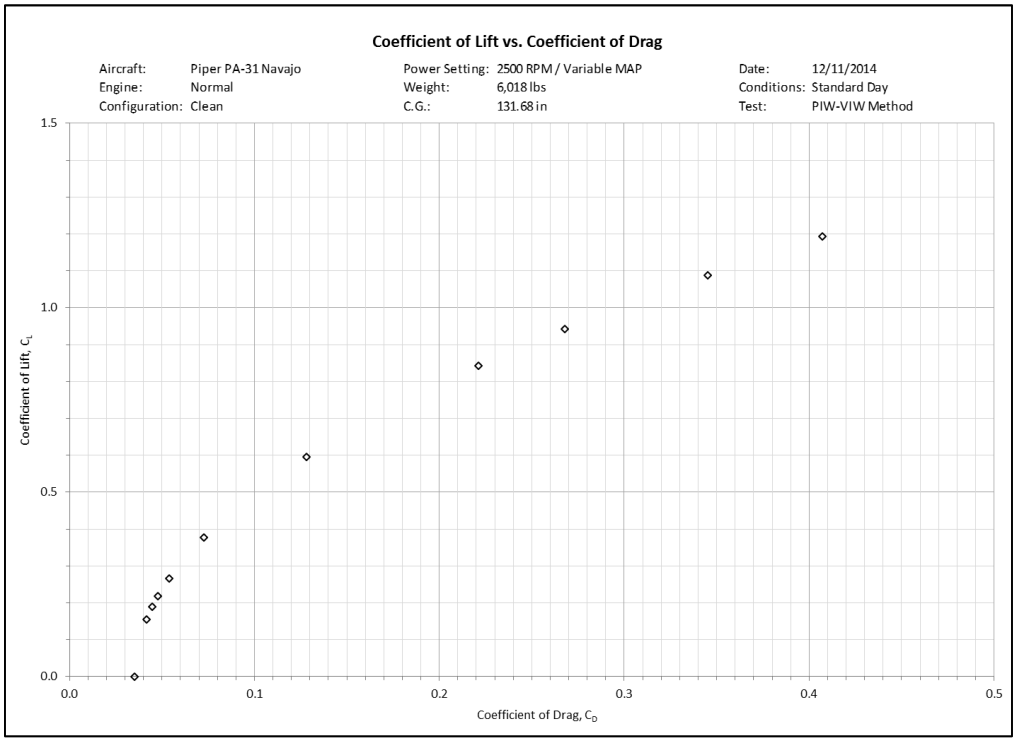


Figure 4.27 – Drag Polar for N11UT

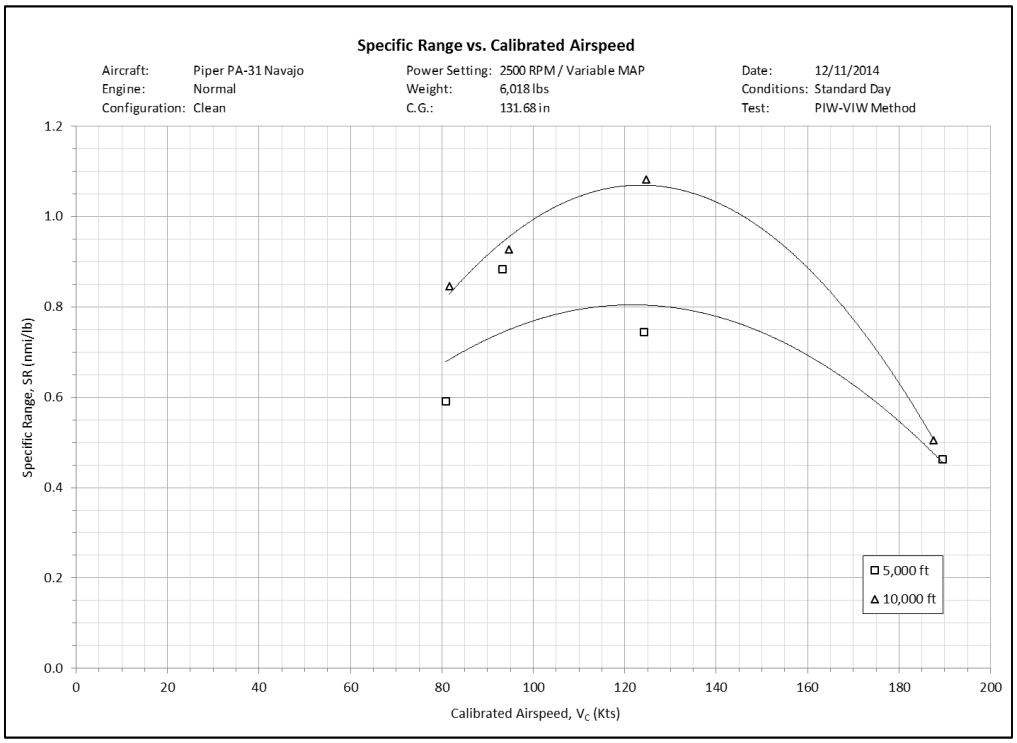


Figure 4.28 – Specific Range Using PIW-VIW Method for N11UT

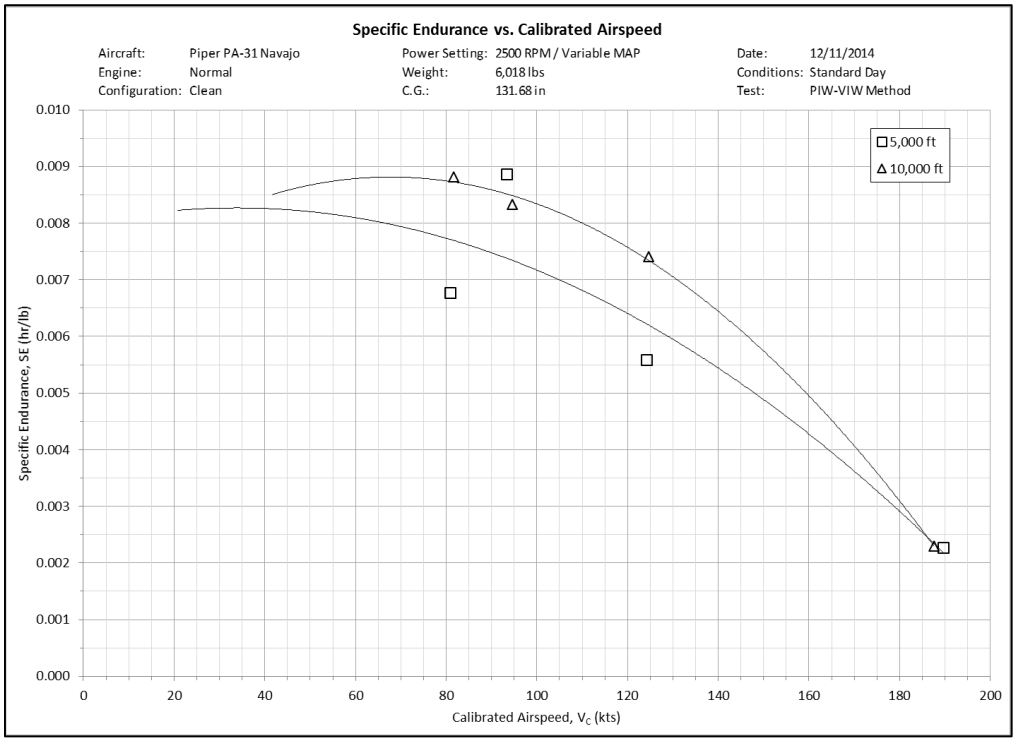


Figure 4.29 – Specific Endurance Using PIW-VIW Method for N11UT

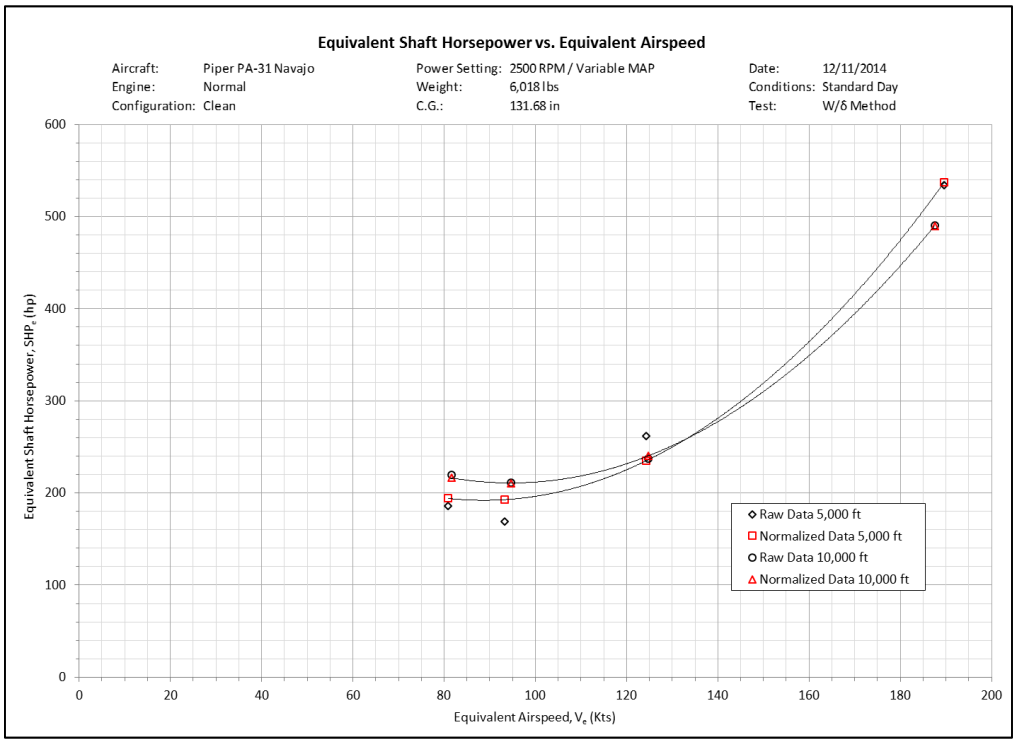


Figure 4.30 – Equivalent Shaft Horsepower vs. Equivalent Airspeed for N11UT

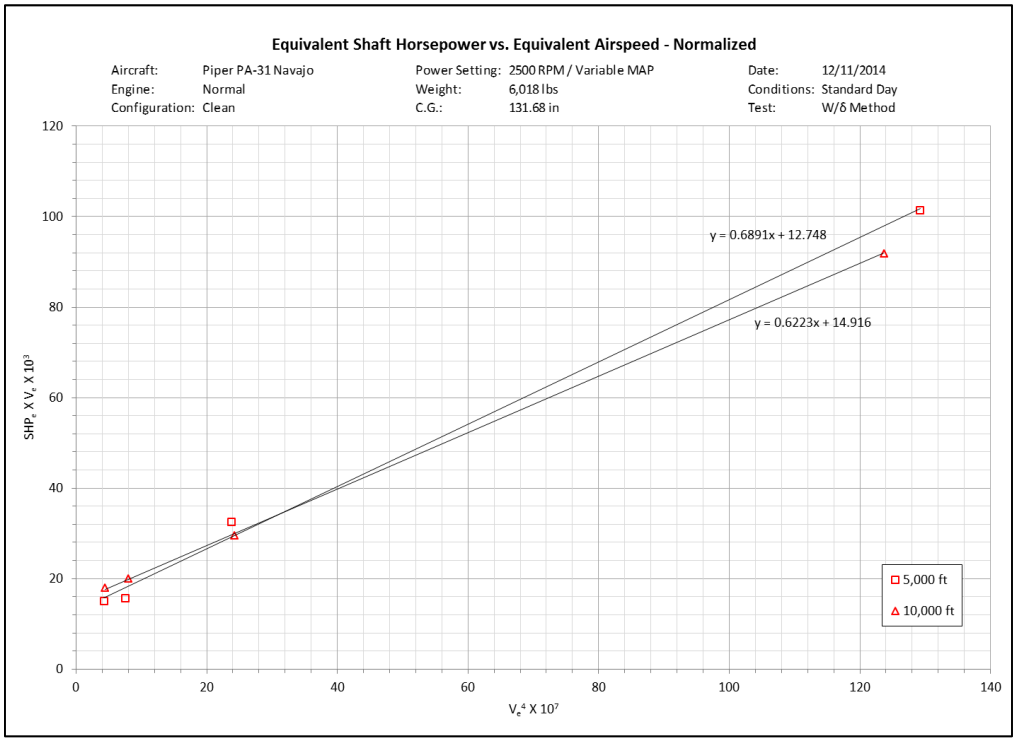


Figure 4.31 – Normalized Equivalent Shaft Horsepower vs. Equivalent Airspeed for N11UT

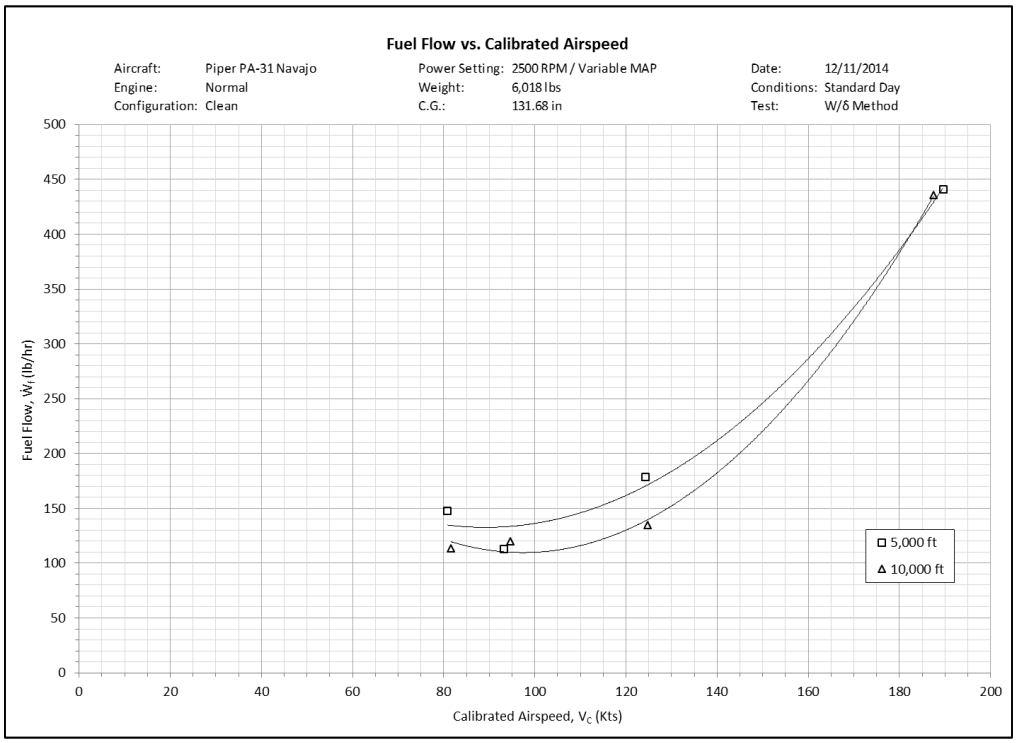


Figure 4.32 – Fuel Flow vs. Calibrated Airspeed for N11UT

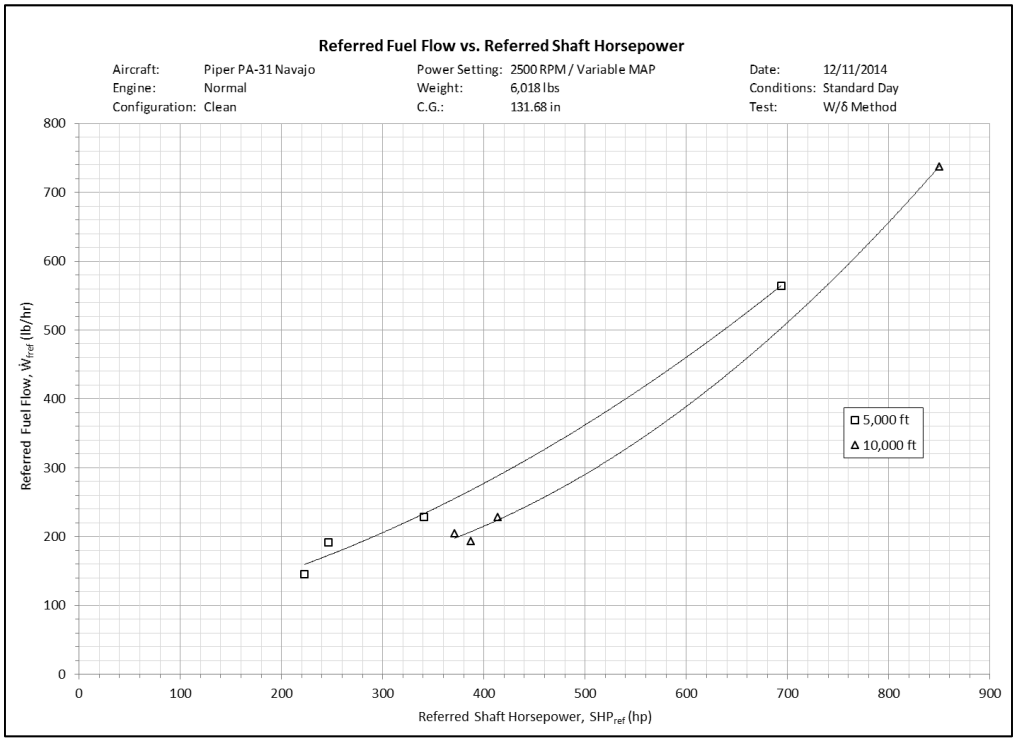


Figure 4.33 – Referred Fuel Flow vs. Referred Shaft Horsepower for N11UT

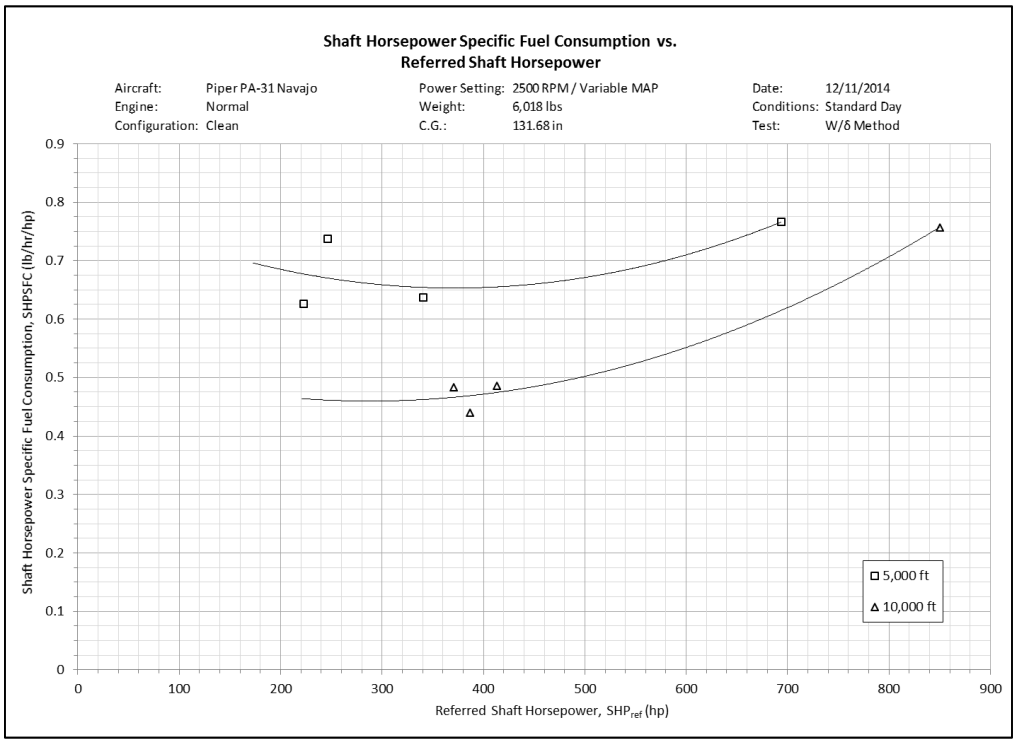


Figure 4.34 – Shaft Horsepower Specific Fuel Consumption vs. Referred Shaft Horsepower for N11UT

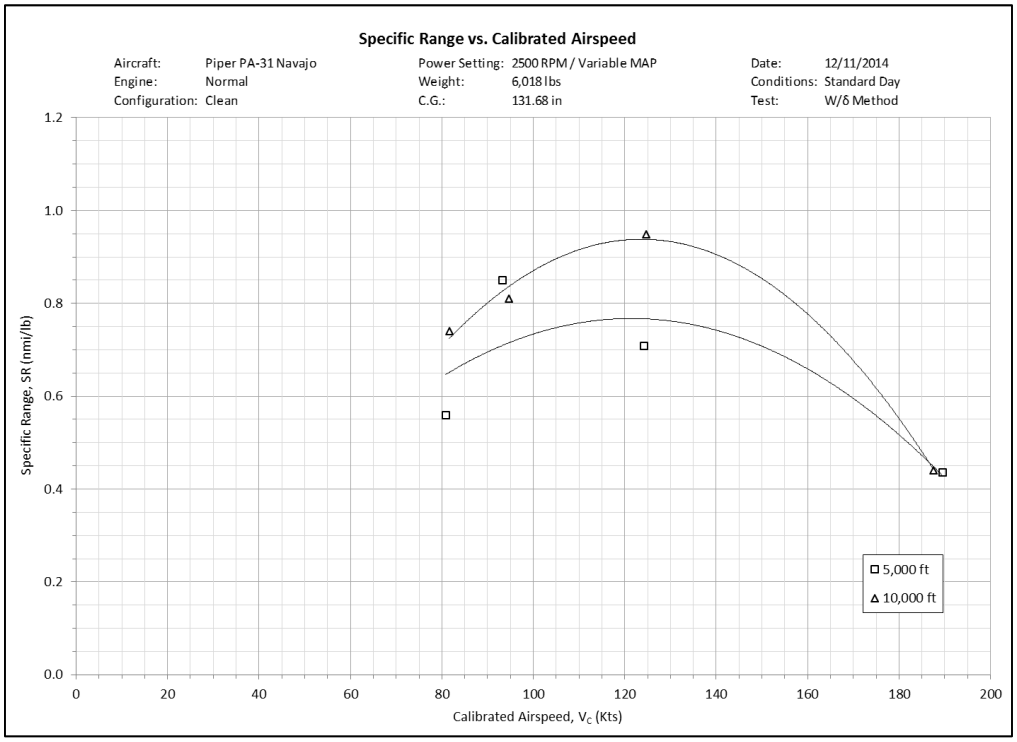


Figure 4.35 – Specific Range Using W/δ Method for N11UT

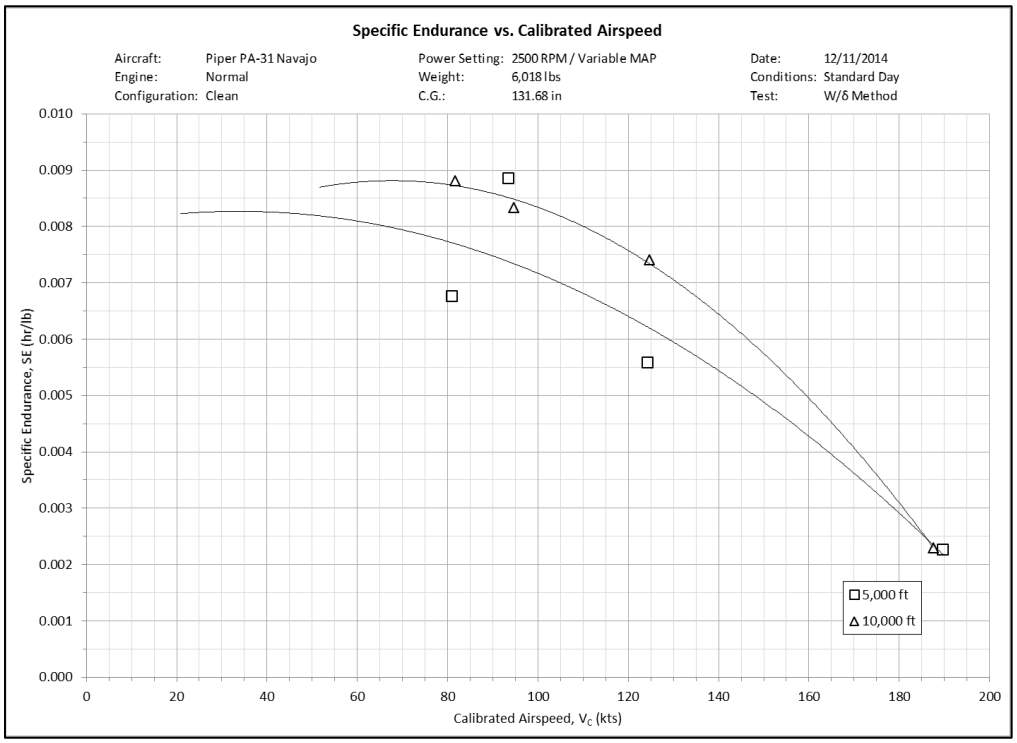


Figure 4.36 – Specific Endurance Using W/δ Method for N11UT

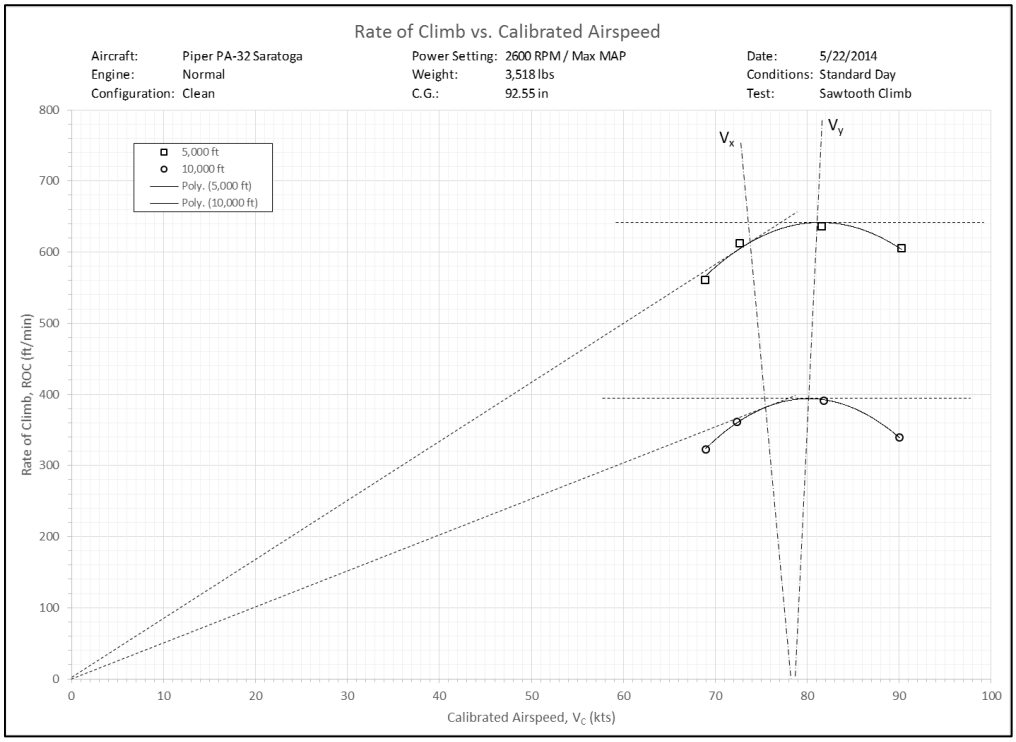


Figure 4.37 – Rate of Climb vs. Calibrated Airspeed Using Sawtooth Climbs for N22UT

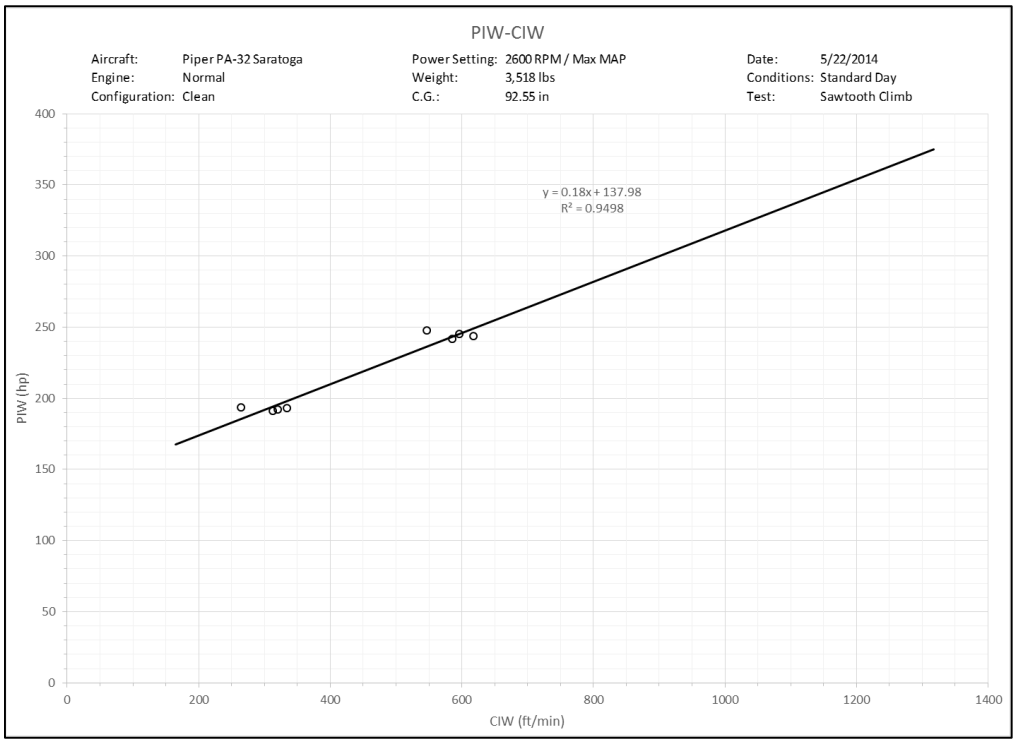


Figure 4.38 – PIW vs. CIW for N22UT

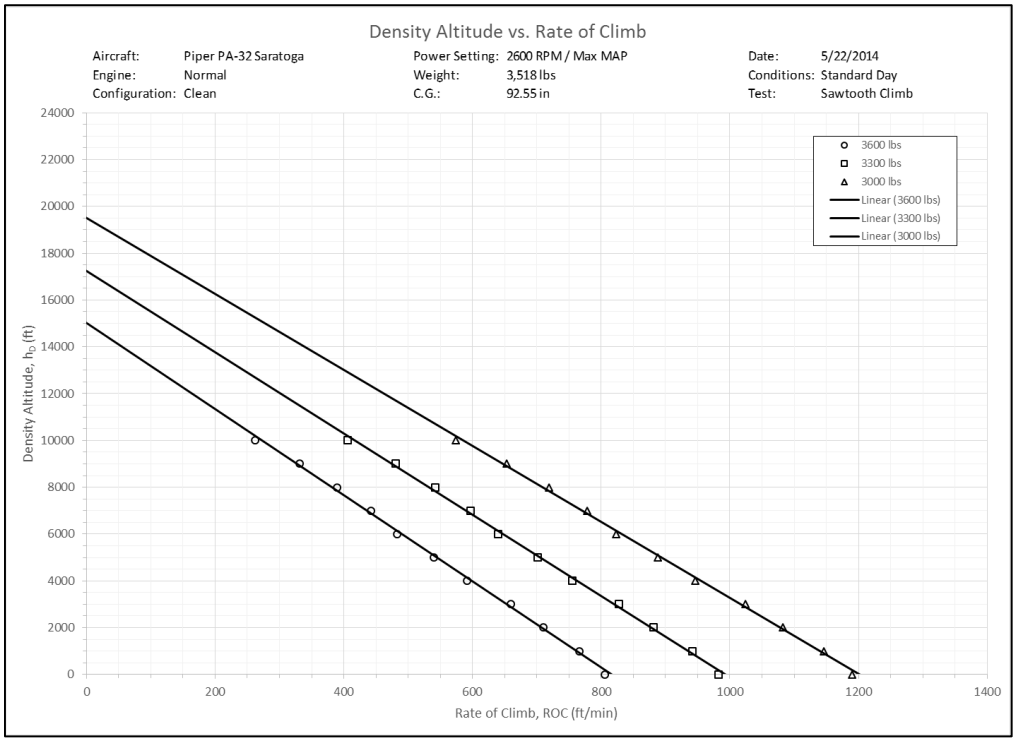


Figure 4.39 – Density Altitude vs. Rate of Climb Using Sawtooth Climb for N22UT

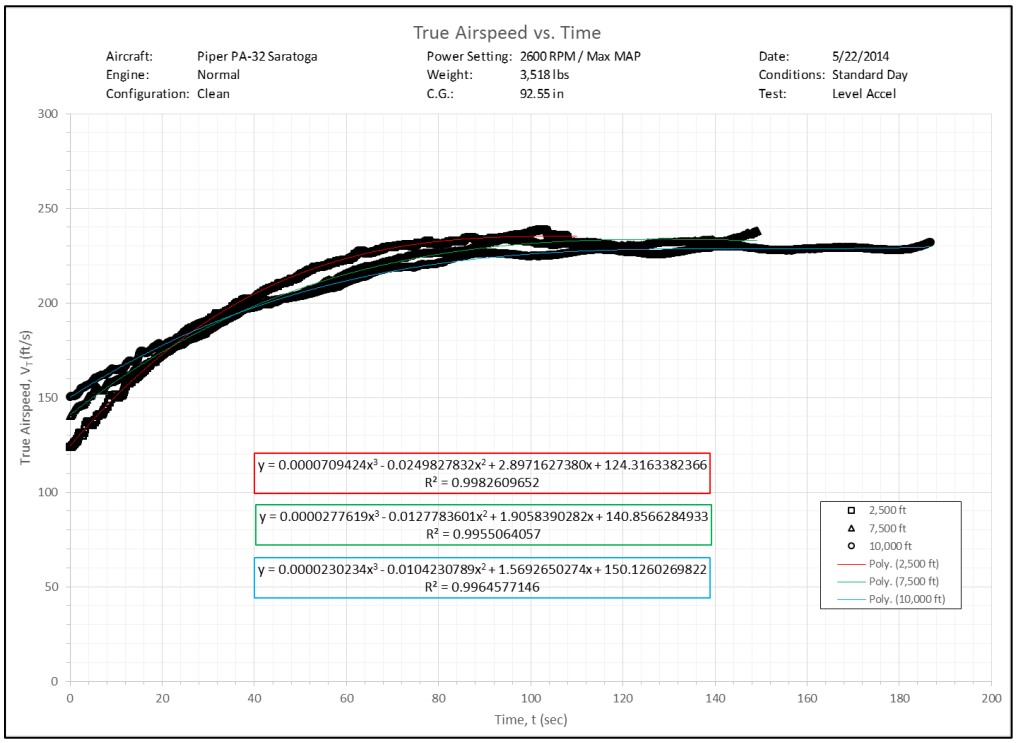


Figure 4.40 – True Airspeed vs. Time for N22UT

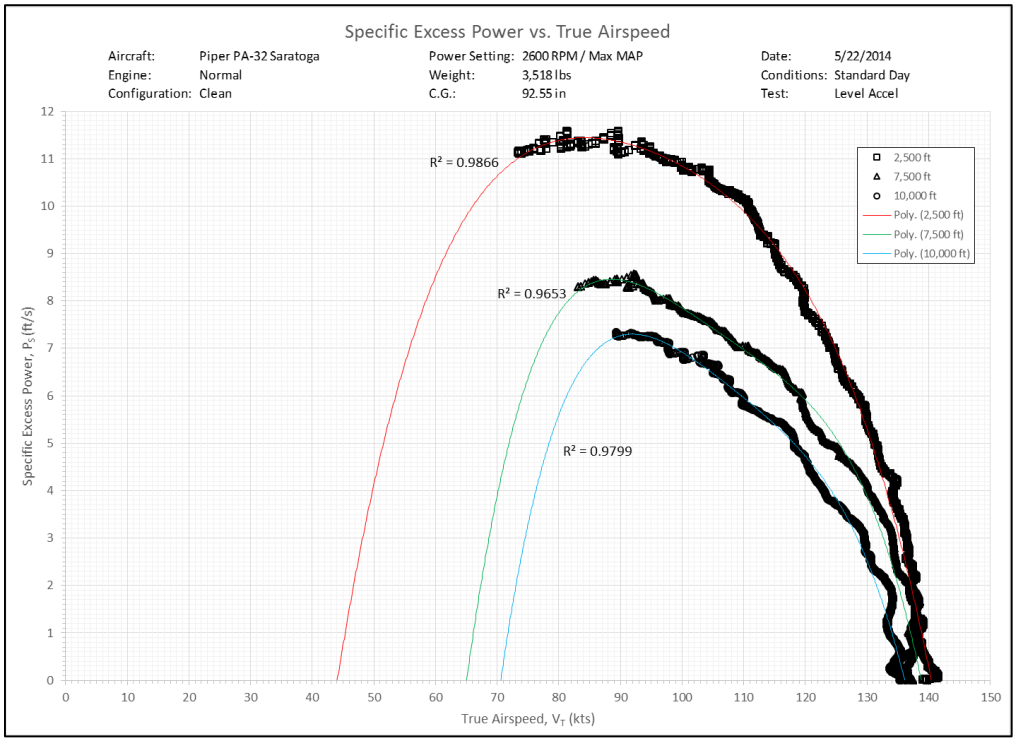


Figure 4.41 – Specific Excess Power vs. True Airspeed for N22UT

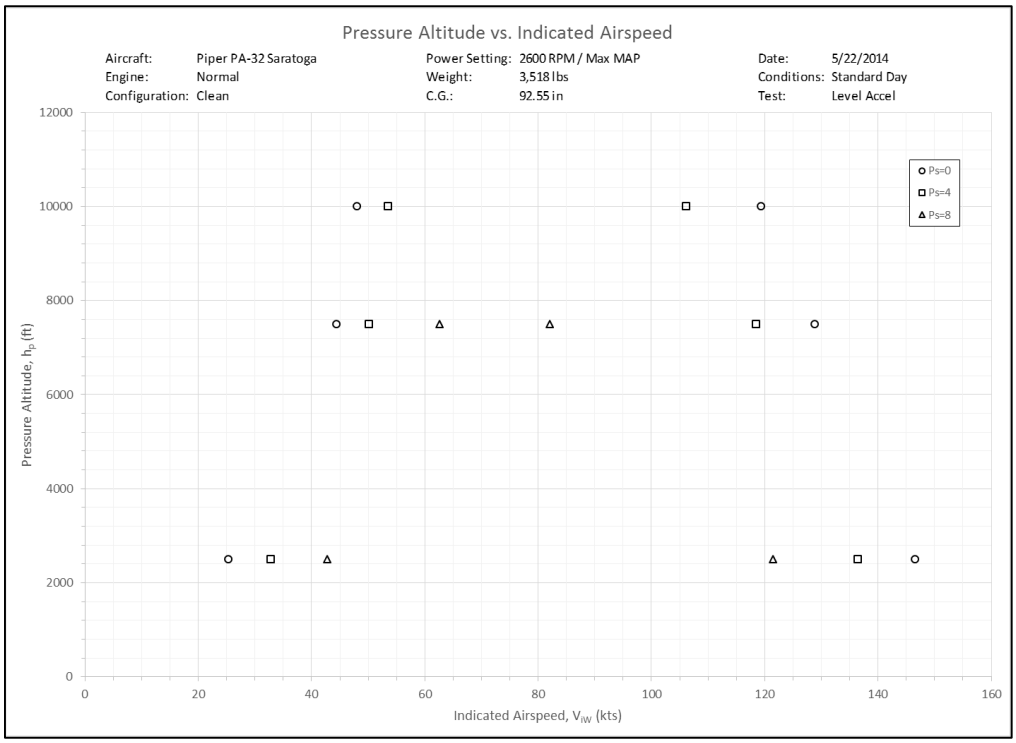


Figure 4.42 – Pressure Altitude vs. Indicated Airspeed for N22UT

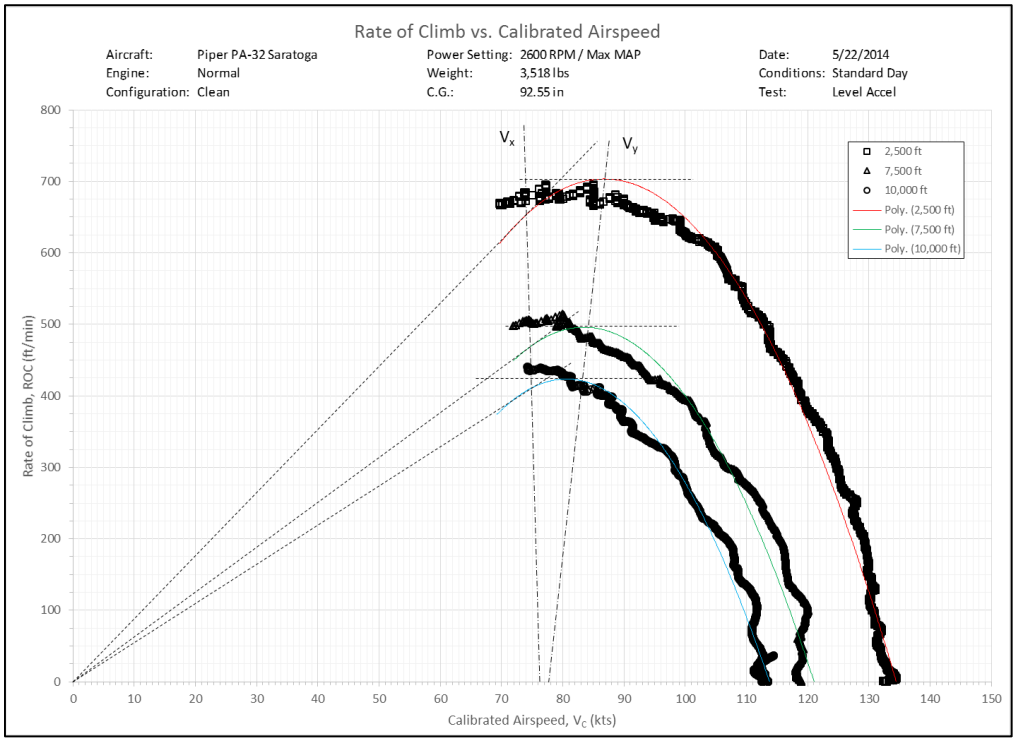


Figure 4.43 – Rate of Climb vs. Calibrated Airspeed Using Level Accel for N22UT

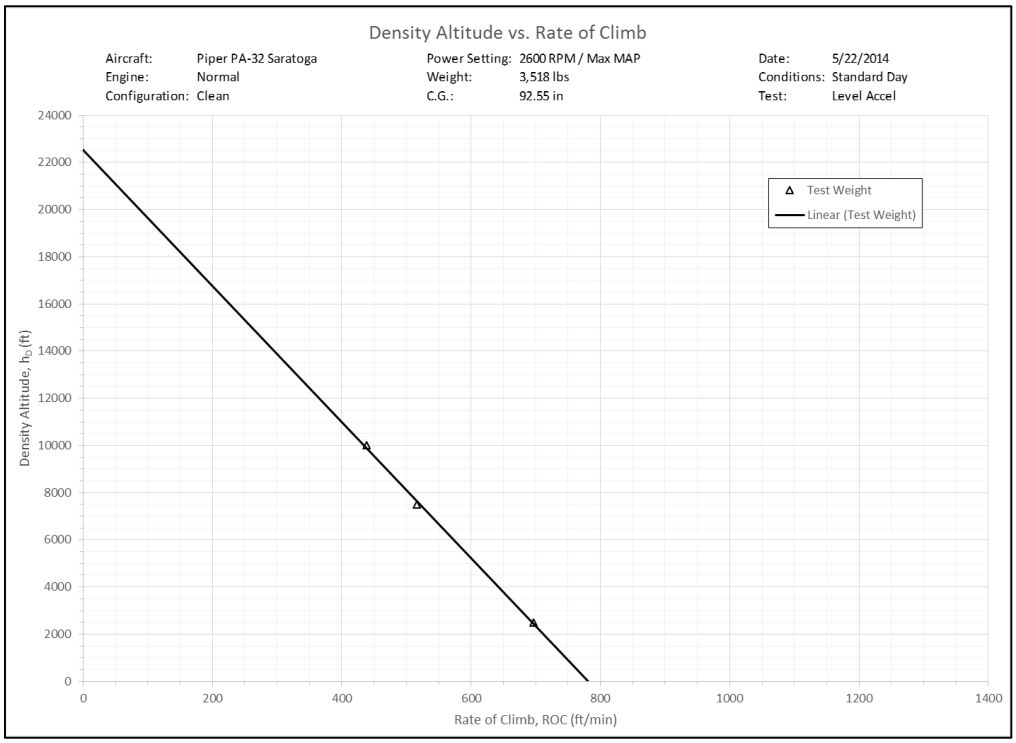


Figure 4.44 – Density Altitude vs. Rate of Climb Using Level Accel for N22UT

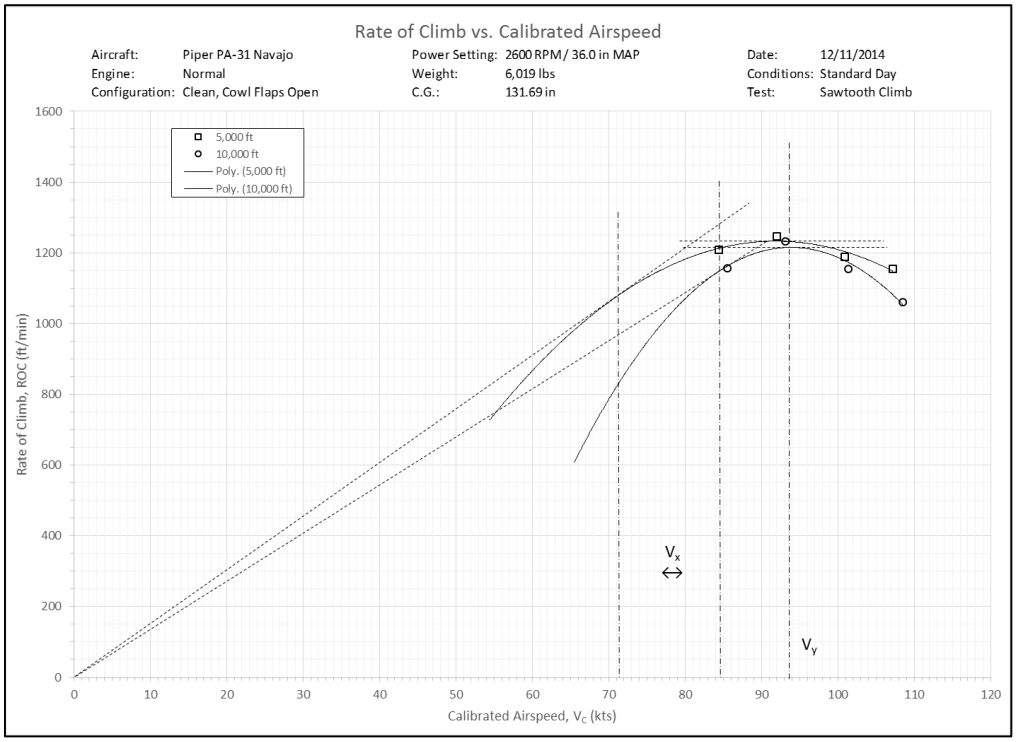


Figure 4.45 – Rate of Climb vs. Calibrated Airspeed Using Sawtooth Climb for N11UT

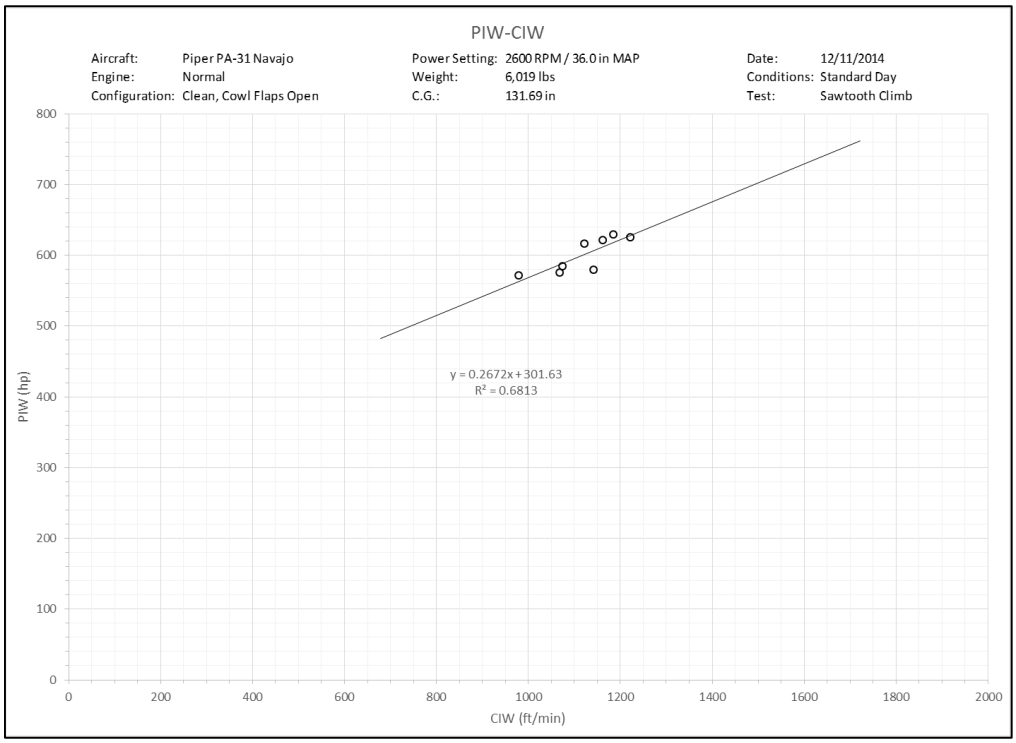


Figure 4.46 – PIW vs. CIW for N11UT

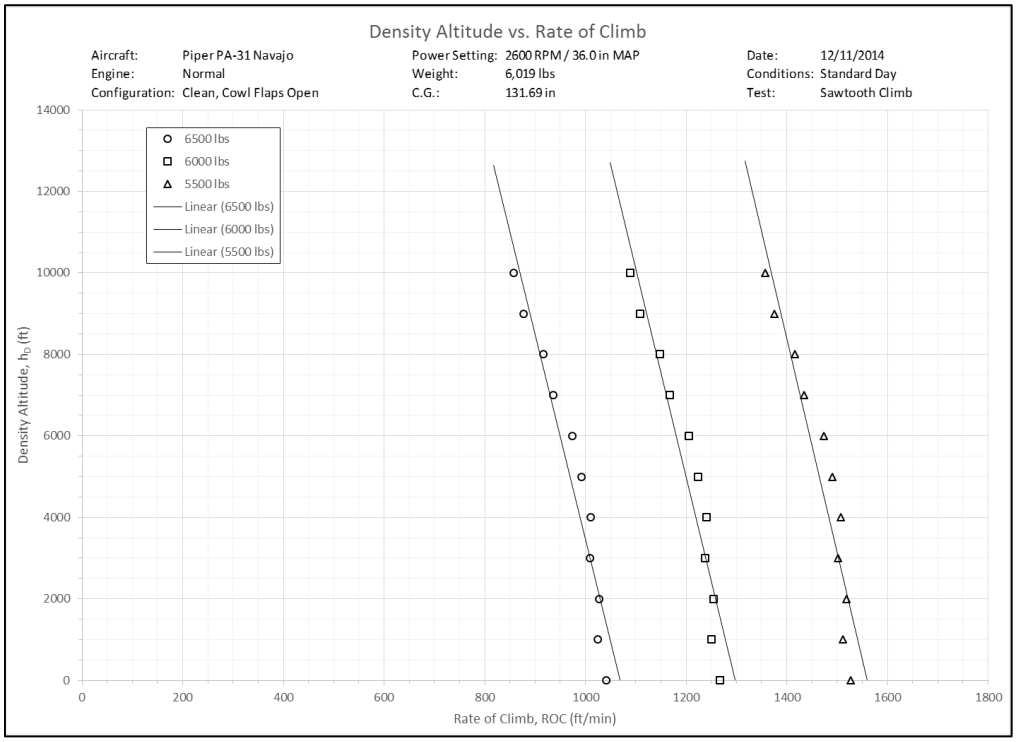


Figure 4.47 – Density Altitude vs. Rate of Climb Using Sawtooth Climb for N11UT

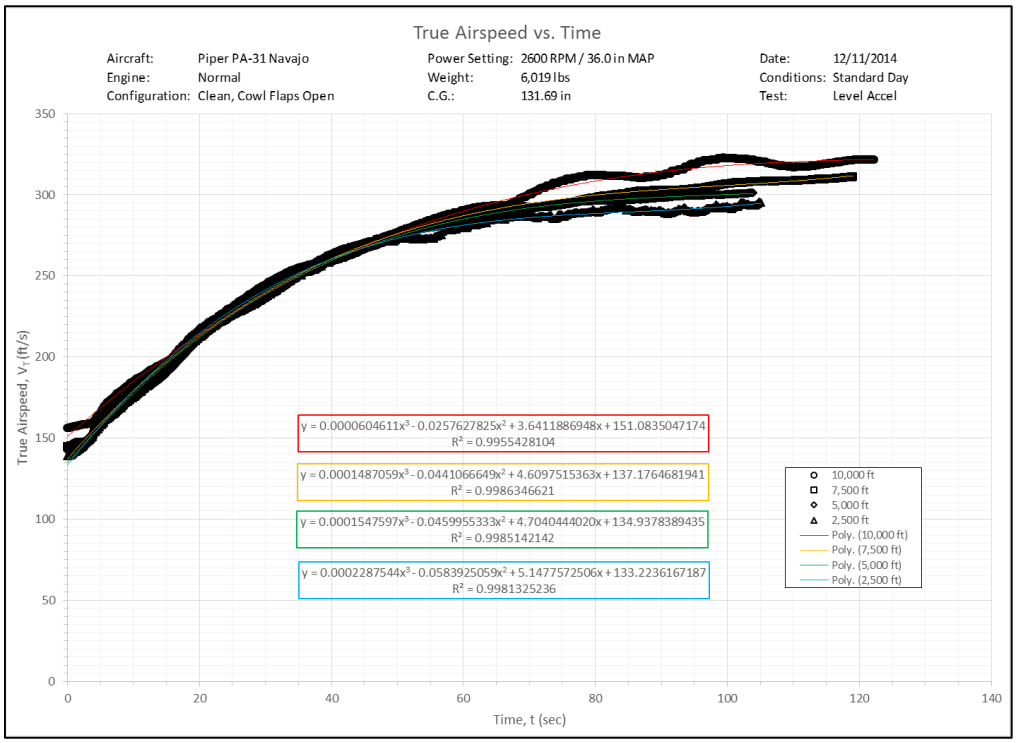


Figure 4.48 – True Airspeed vs. Time for N11UT

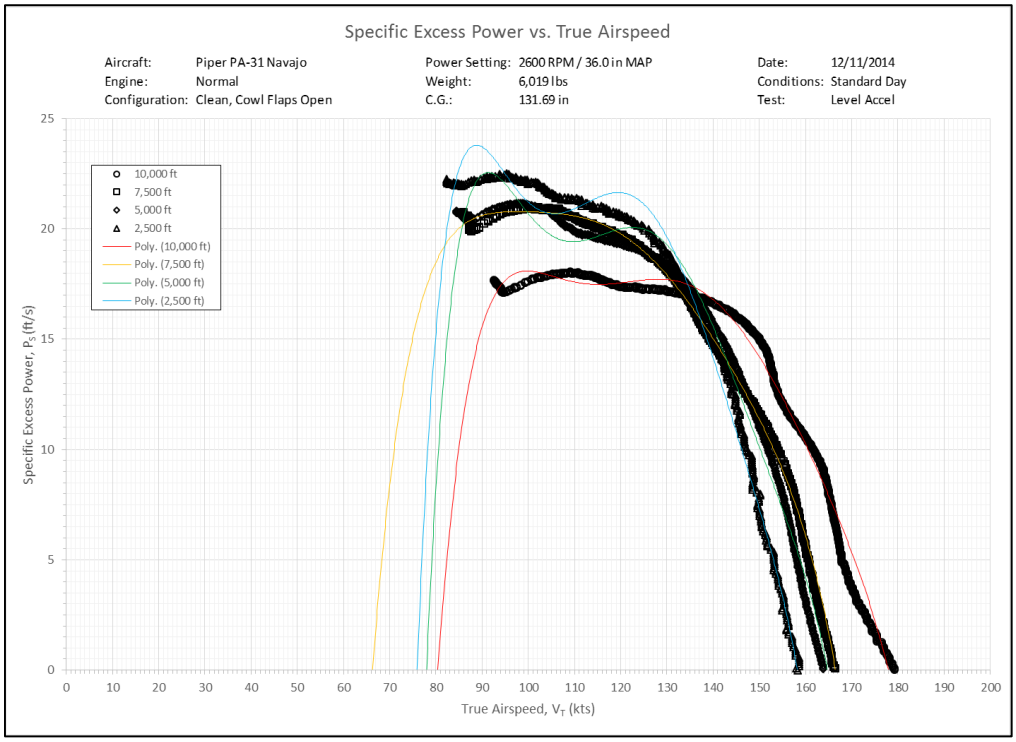


Figure 4.49 – Specific Excess Power vs. True Airspeed for N11UT

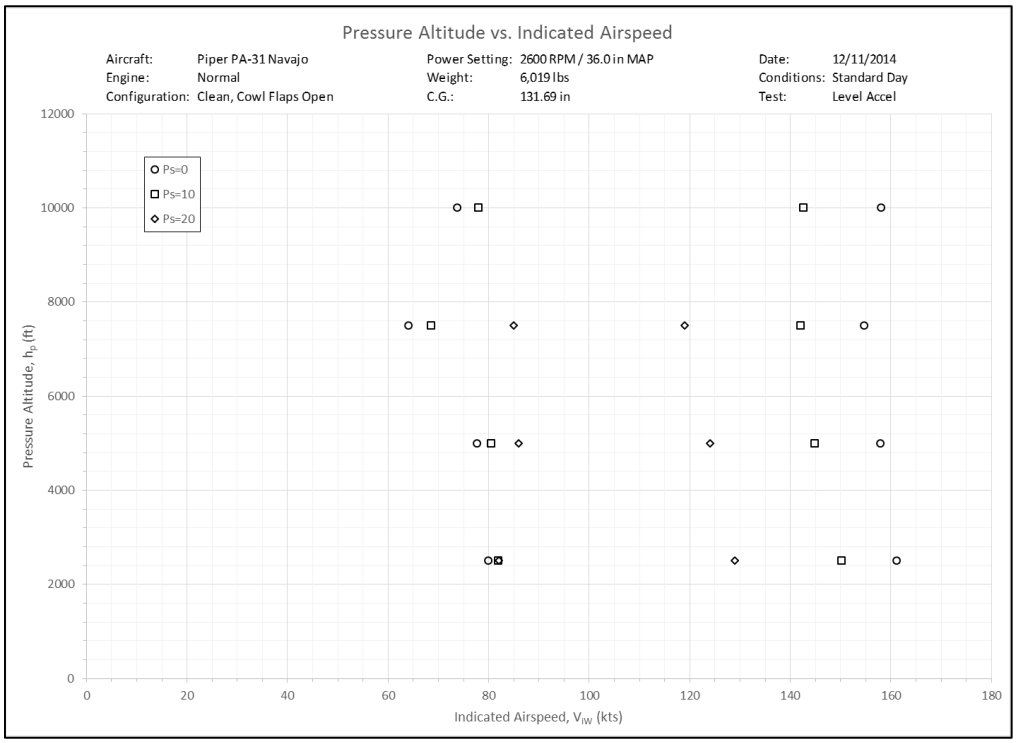


Figure 4.50 – Pressure Altitude vs. Indicated Airspeed for N11UT

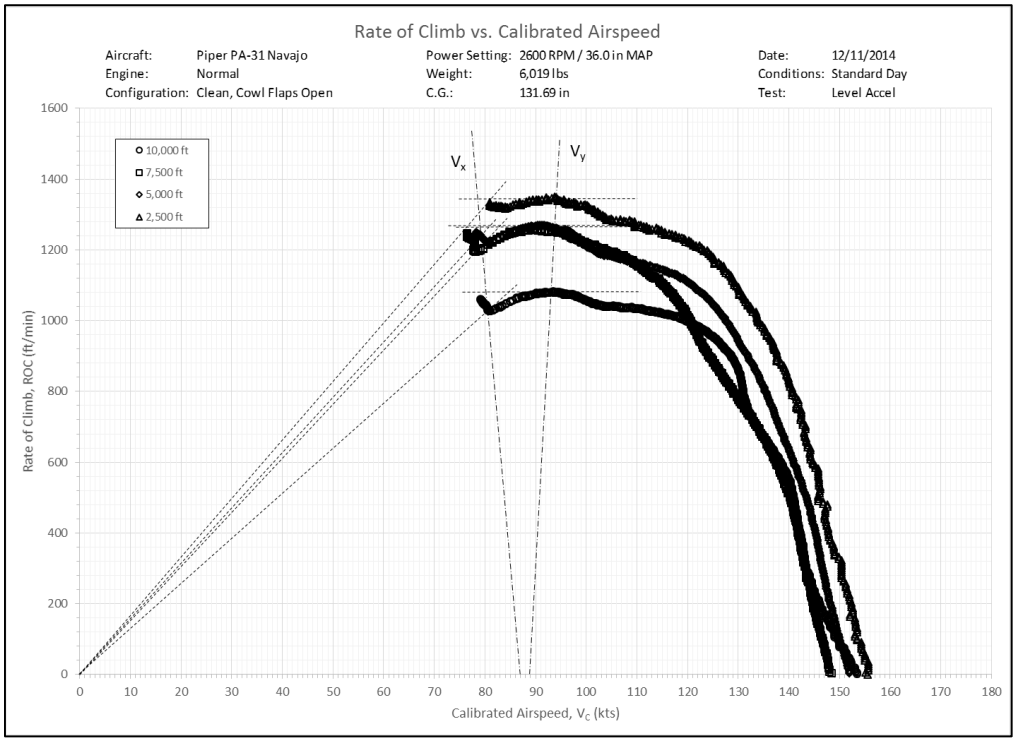


Figure 4.51 – Rate of Climb vs. Calibrated Airspeed Using Level Accel for N11UT

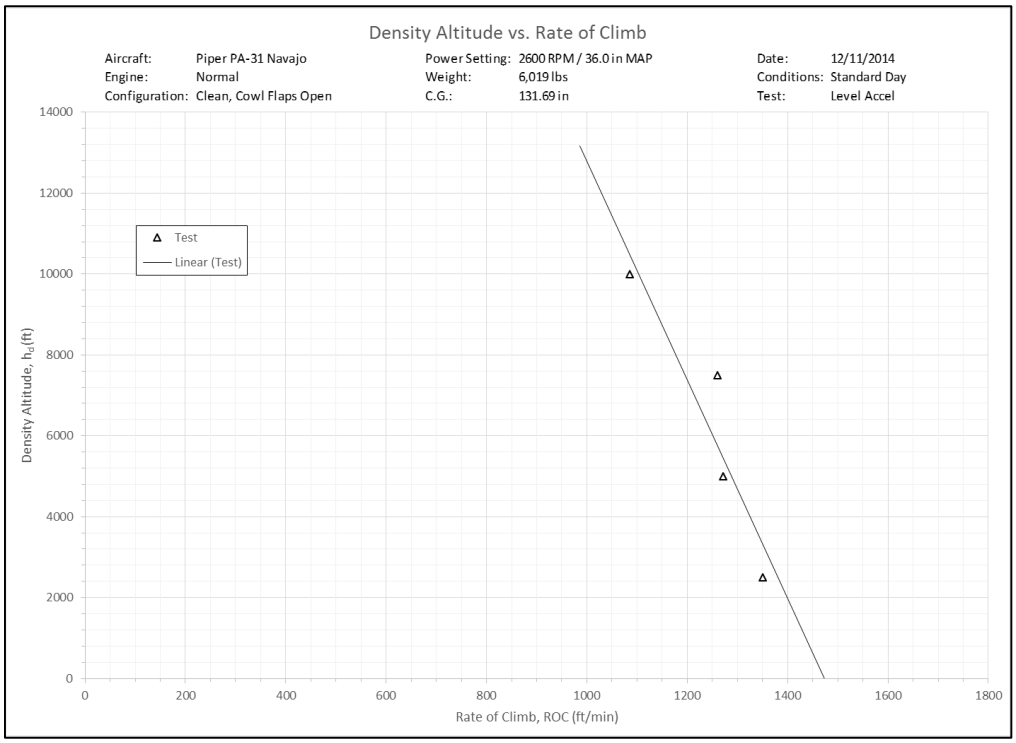


Figure 4.52 – Density Altitude vs. Rate of Climb Using Level Accel for N11UT

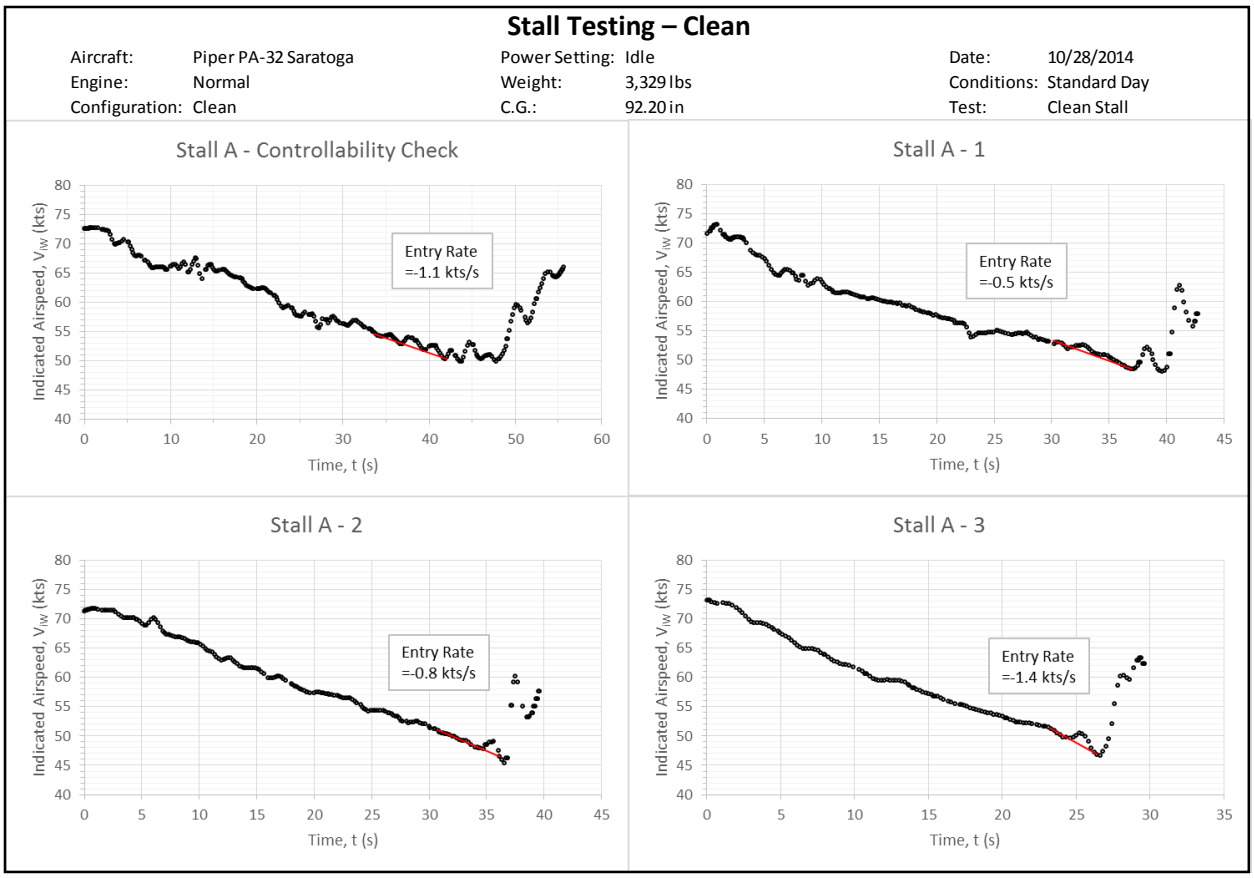


Figure 4.53 – Stall Testing in a Clean Configuration for N22UT

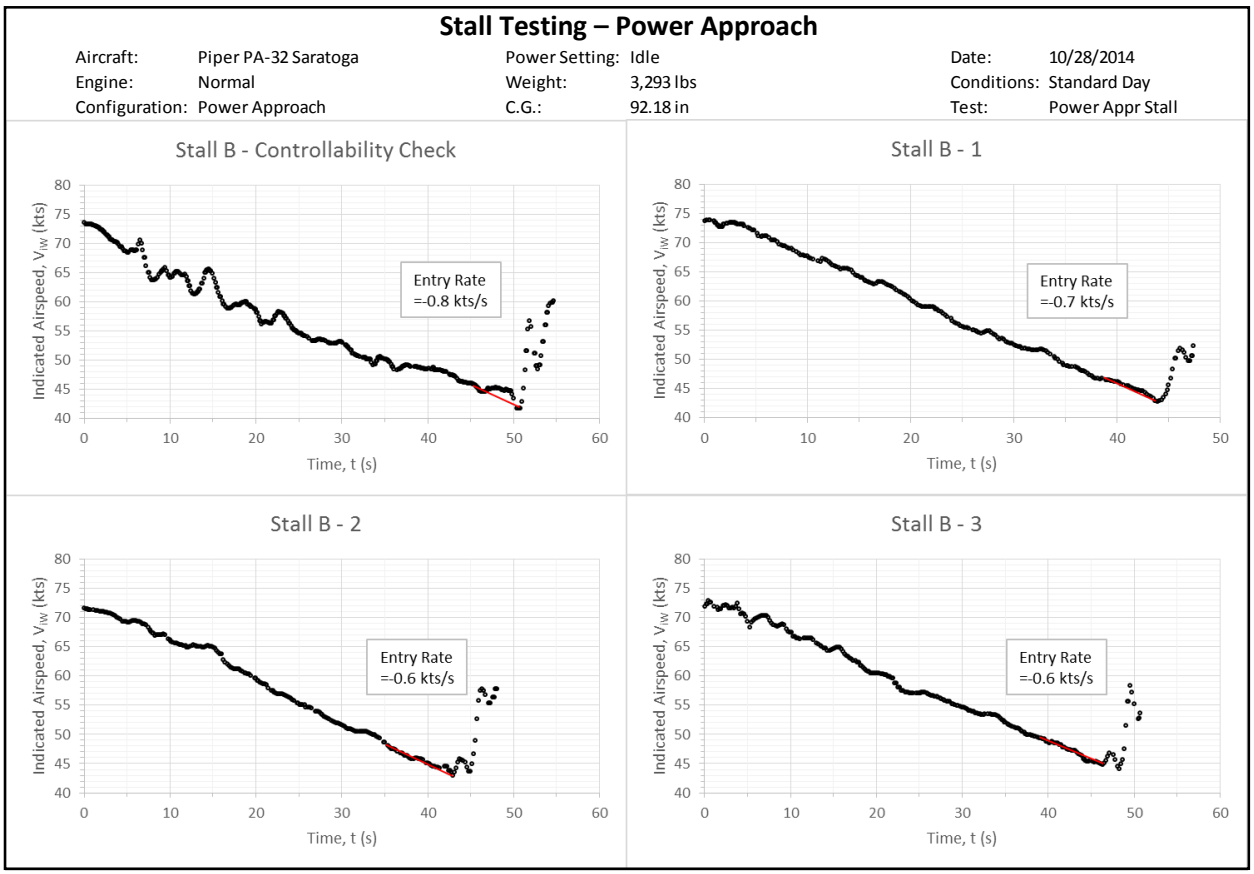


Figure 4.54 – Stall Testing in a Power Approach Configuration for N22UT

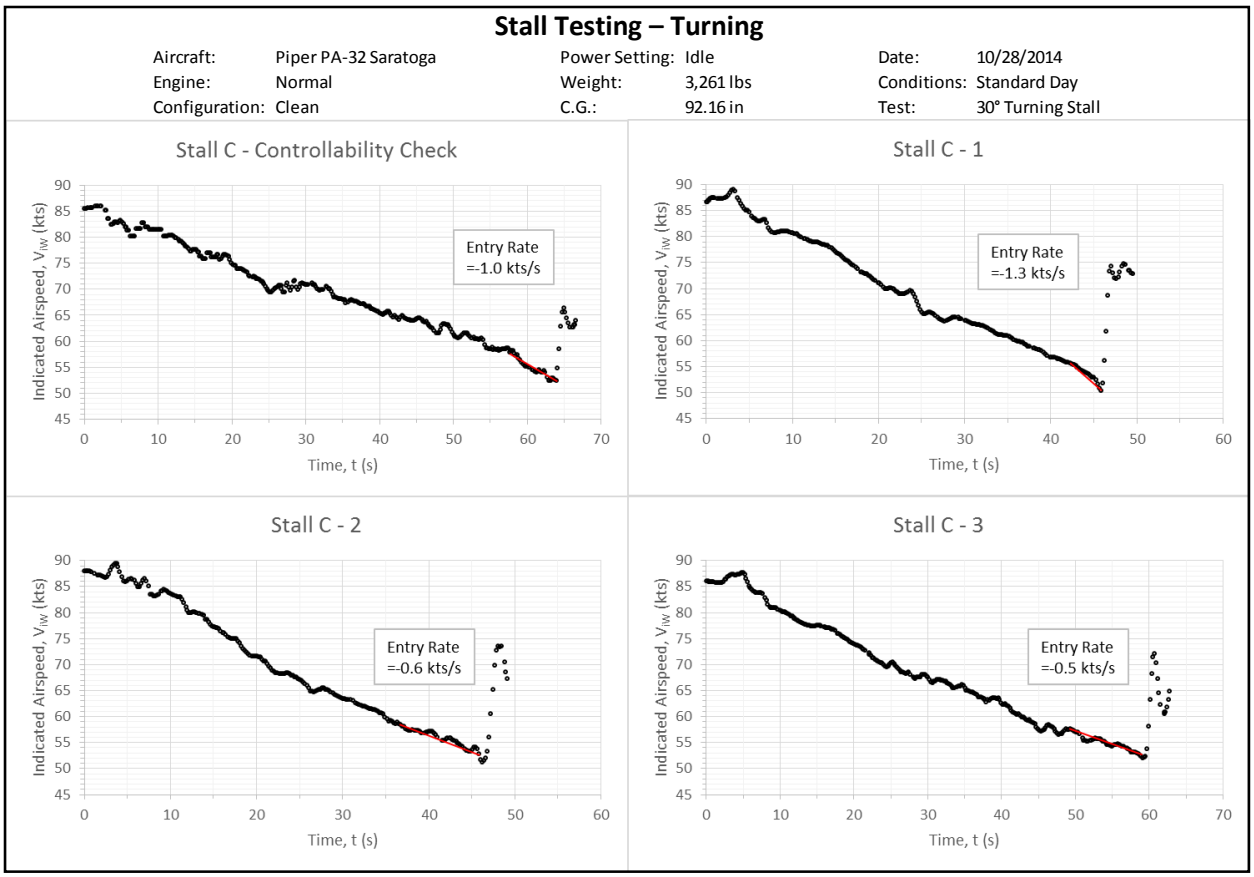


Figure 4.55 – Stall Testing in a 30° Turn for N22UT

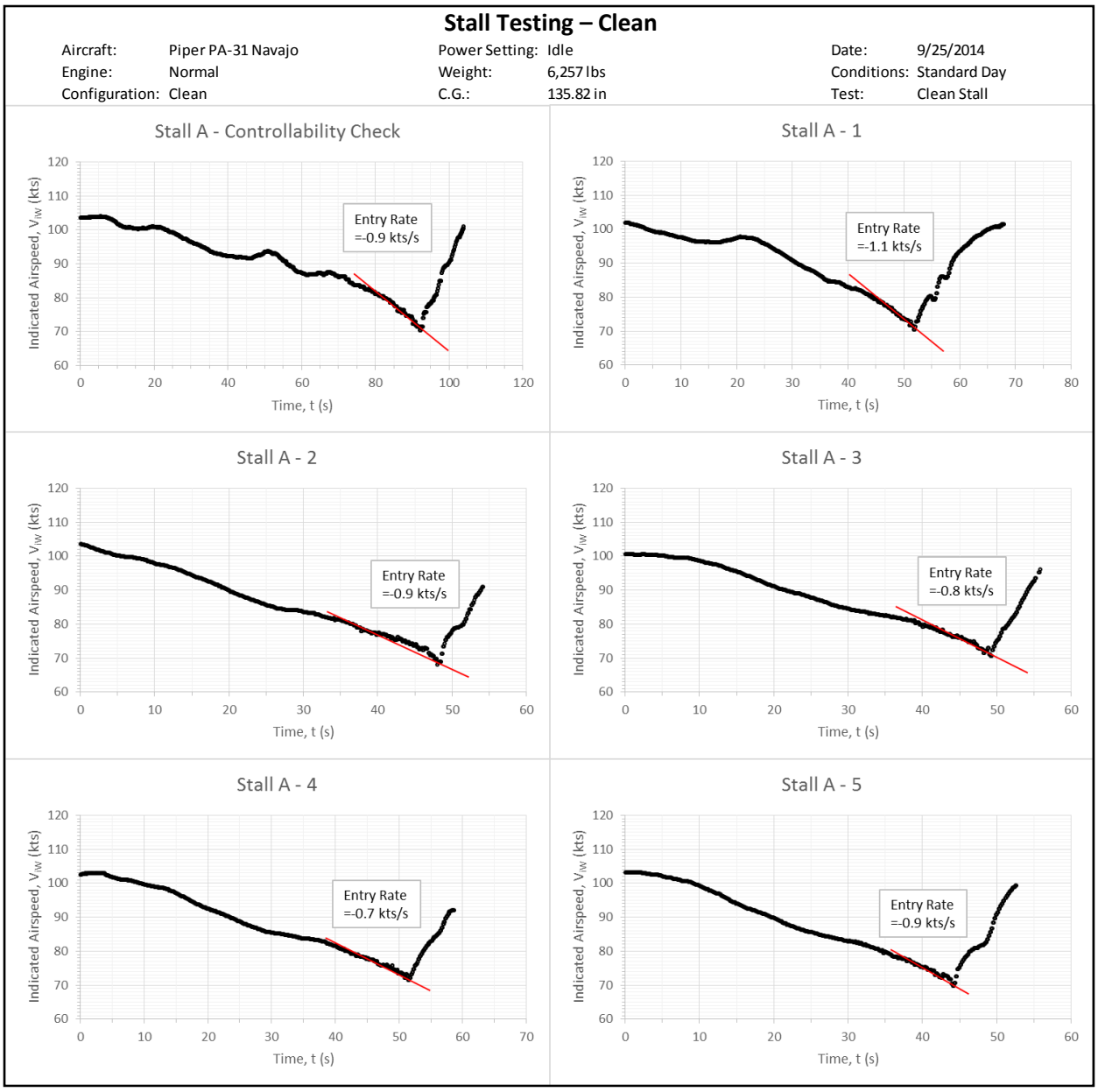


Figure 4.56 – Stall Testing in a Clean Configuration for N11UT

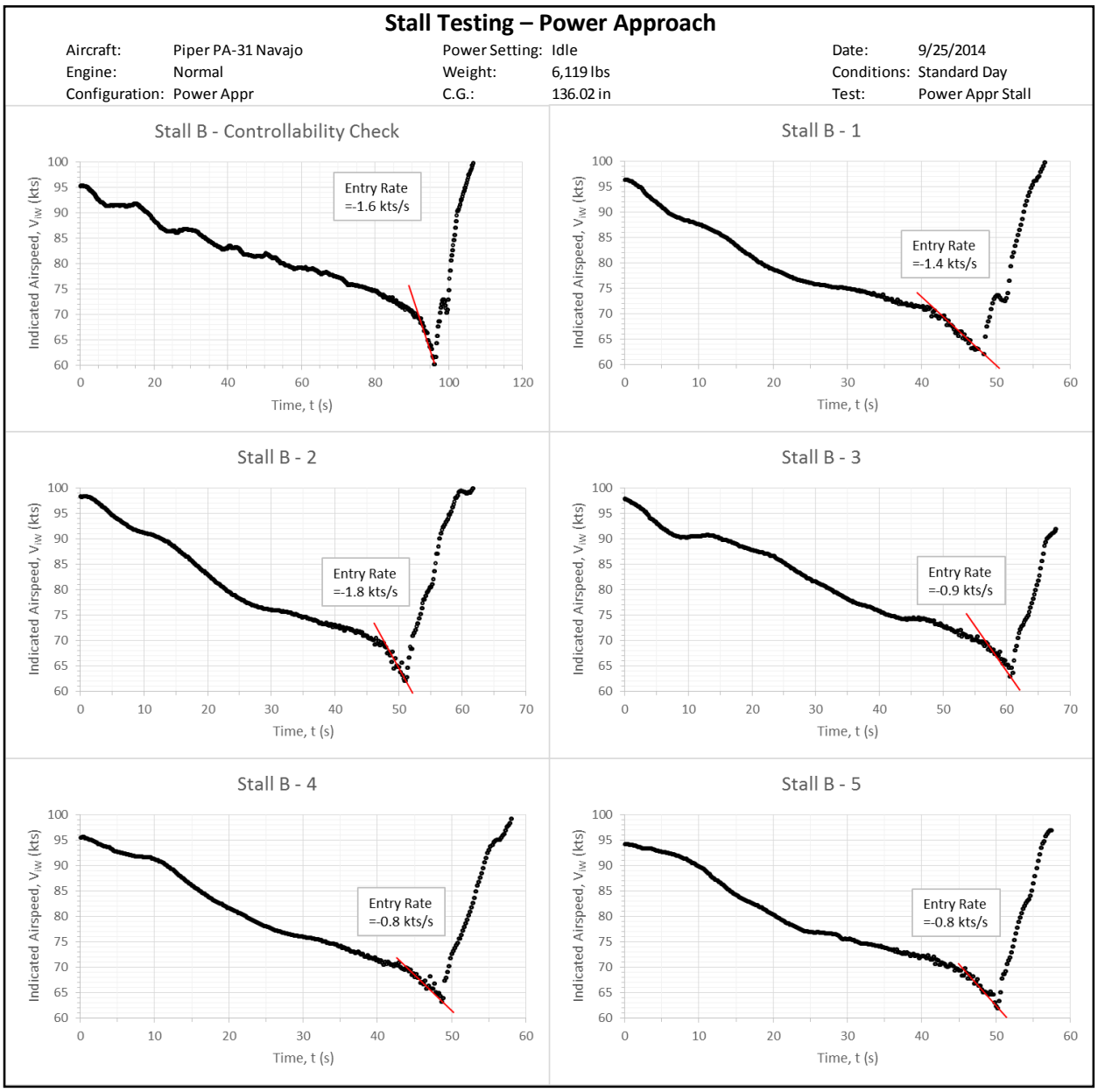


Figure 4.57 – Stall Testing in a Power Approach Configuration for N11UT

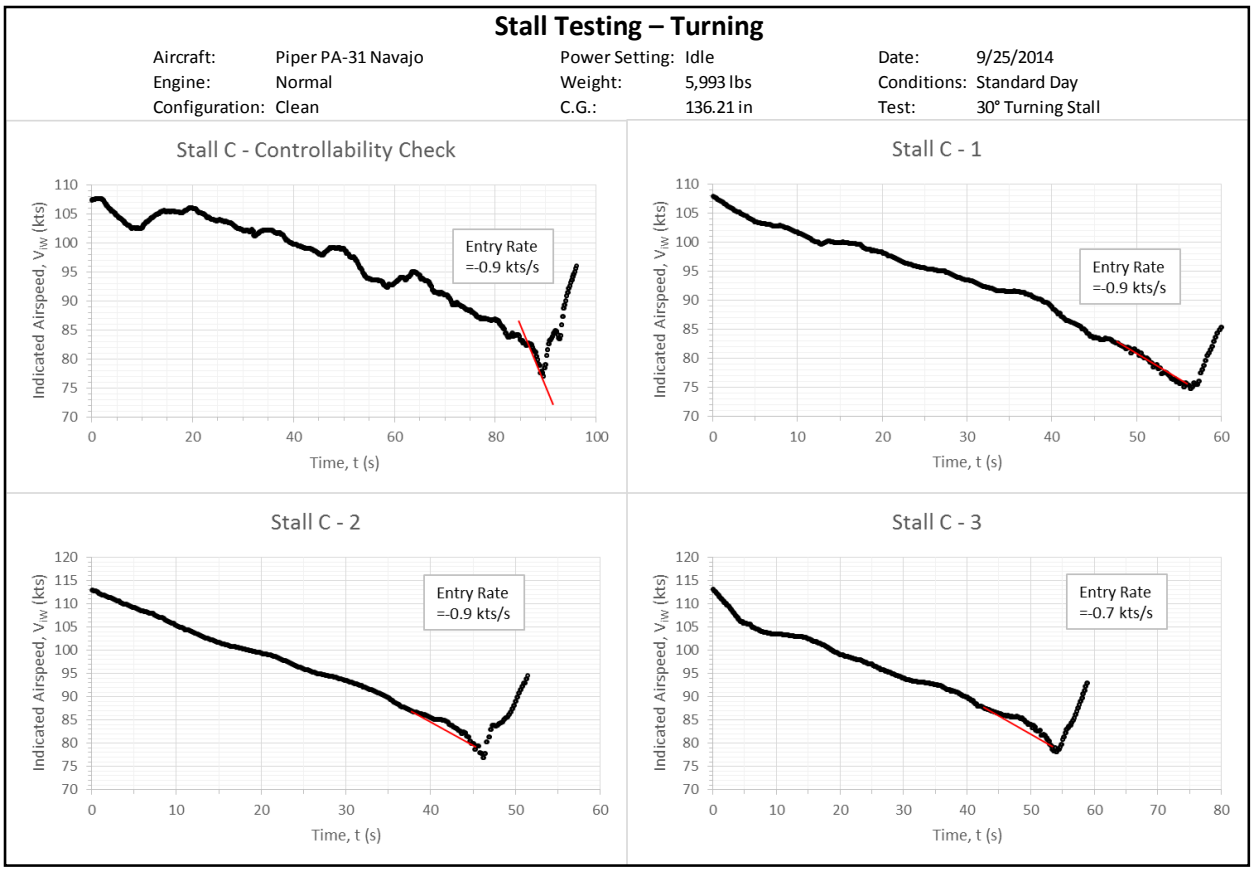


Figure 4.58 – Stall Testing in a 30° Turn for N11UT

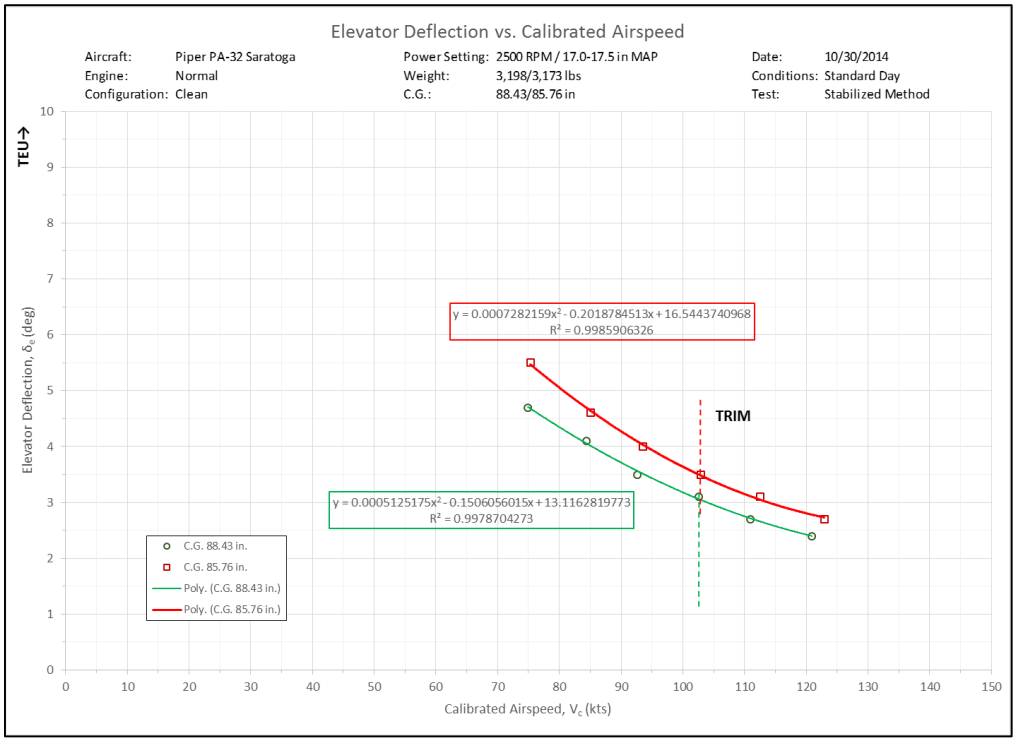


Figure 4.59 – Elevator Deflection vs. Calibrated Airspeed Using Stabilized Method for N22UT

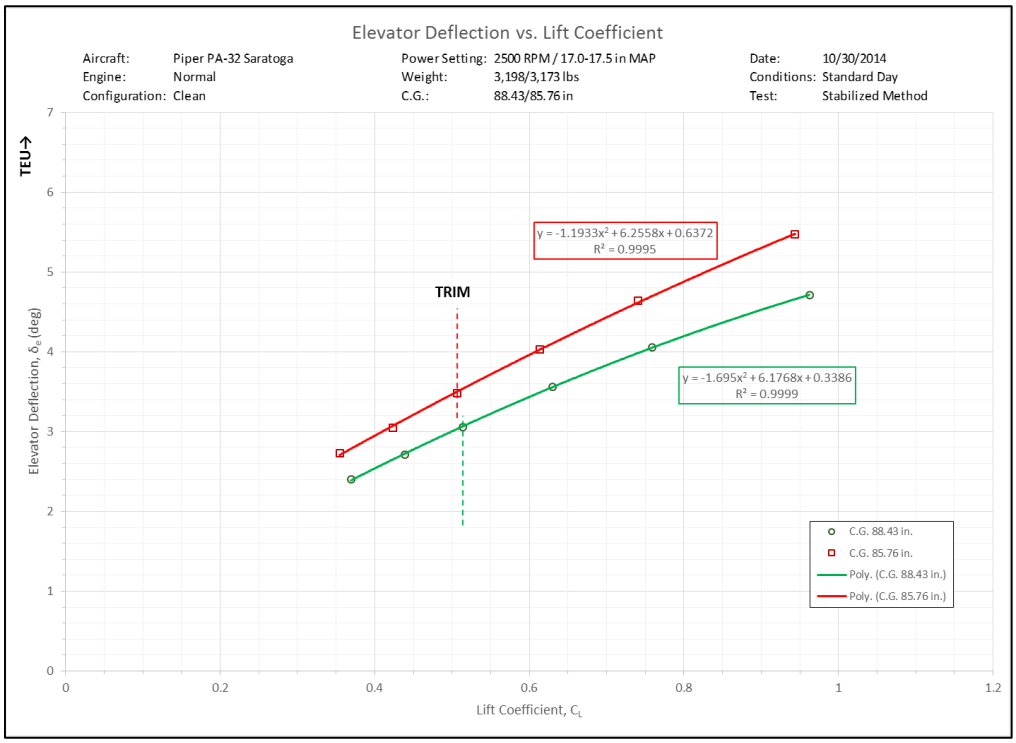


Figure 4.60 – Elevator Deflection vs. Lift Coefficient Using Stabilized Method for N22UT

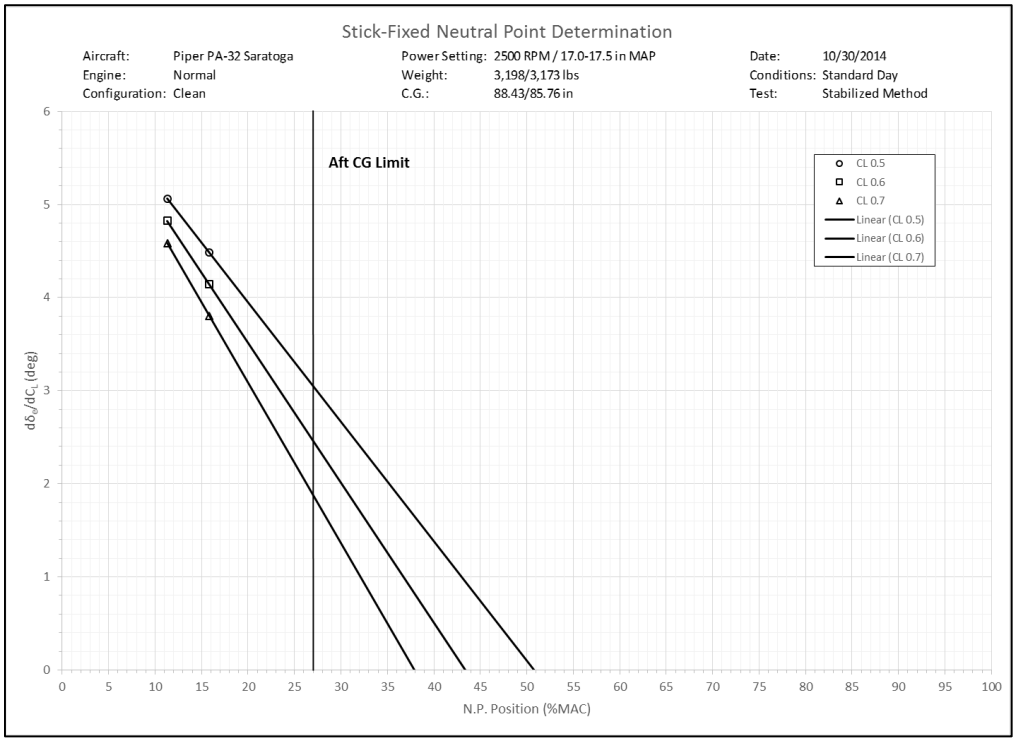


Figure 4.61 – Stick-Fixed Neutral Point Determination Using Stabilized Method for N22UT

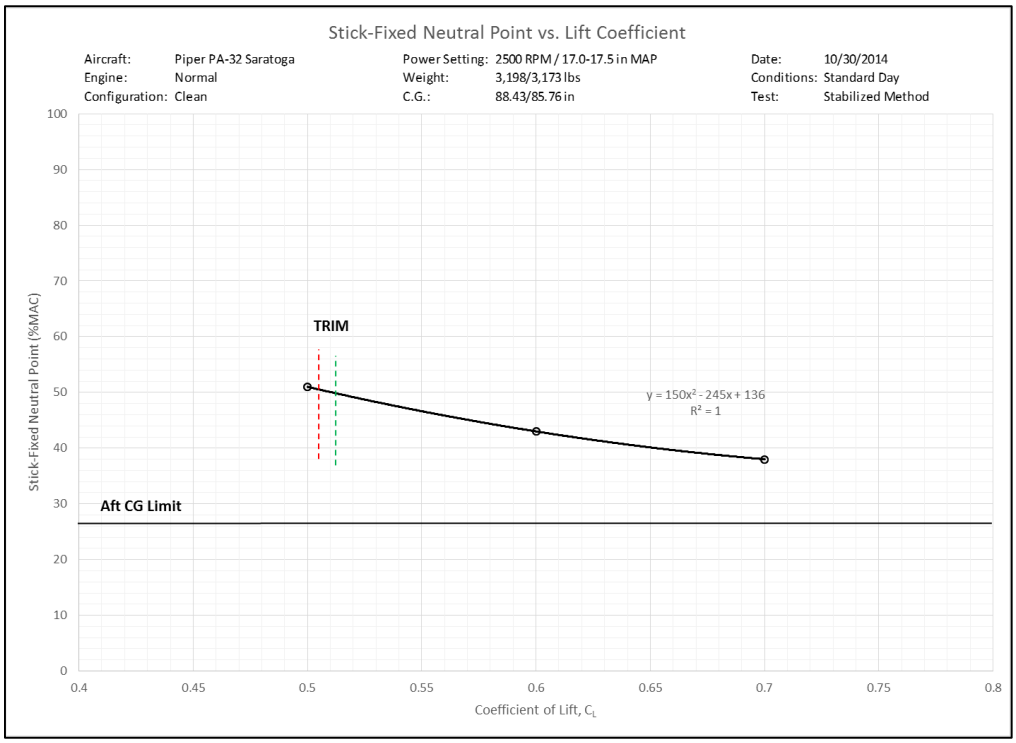


Figure 4.62 – Stick-Fixed Neutral Point vs. Lift Coefficient Using Stabilized Method for N22UT

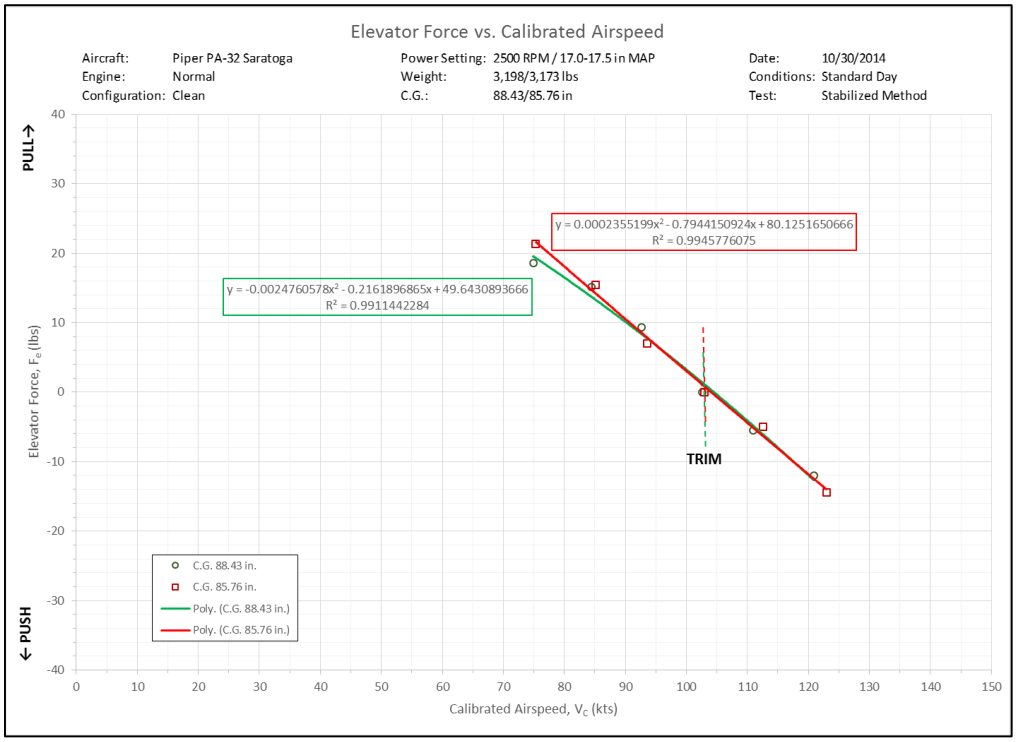


Figure 4.63 – Elevator Force vs. Calibrated Airspeed Using Stabilized Method for N22UT

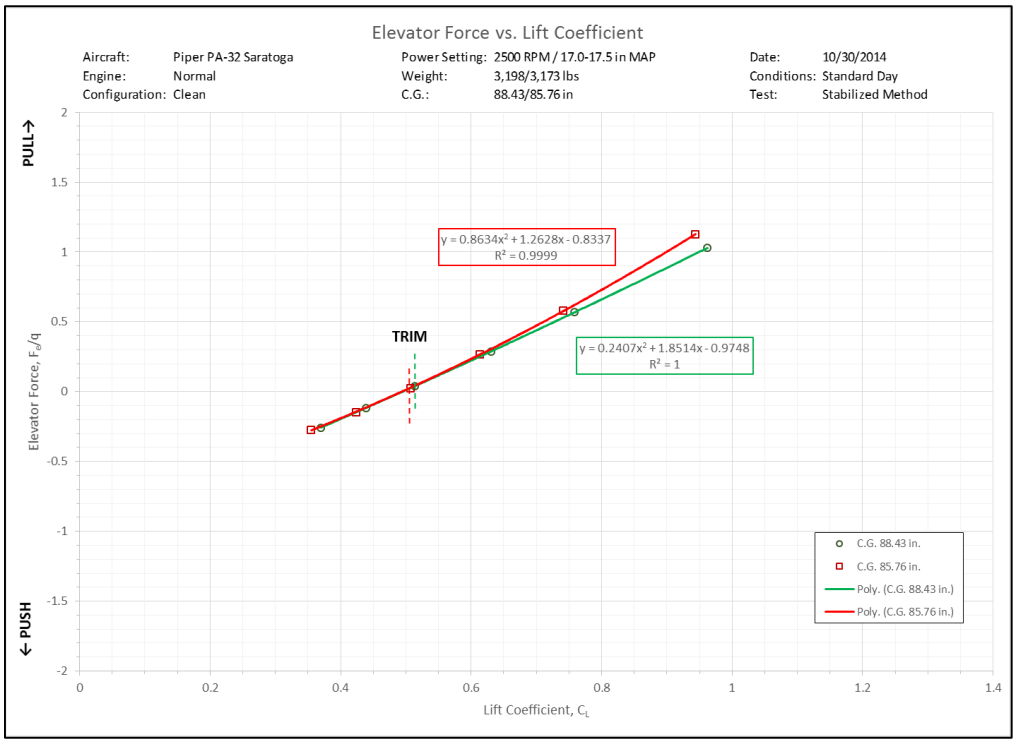


Figure 4.64 – Elevator Force vs. Lift Coefficient Using Stabilized Method for N22UT

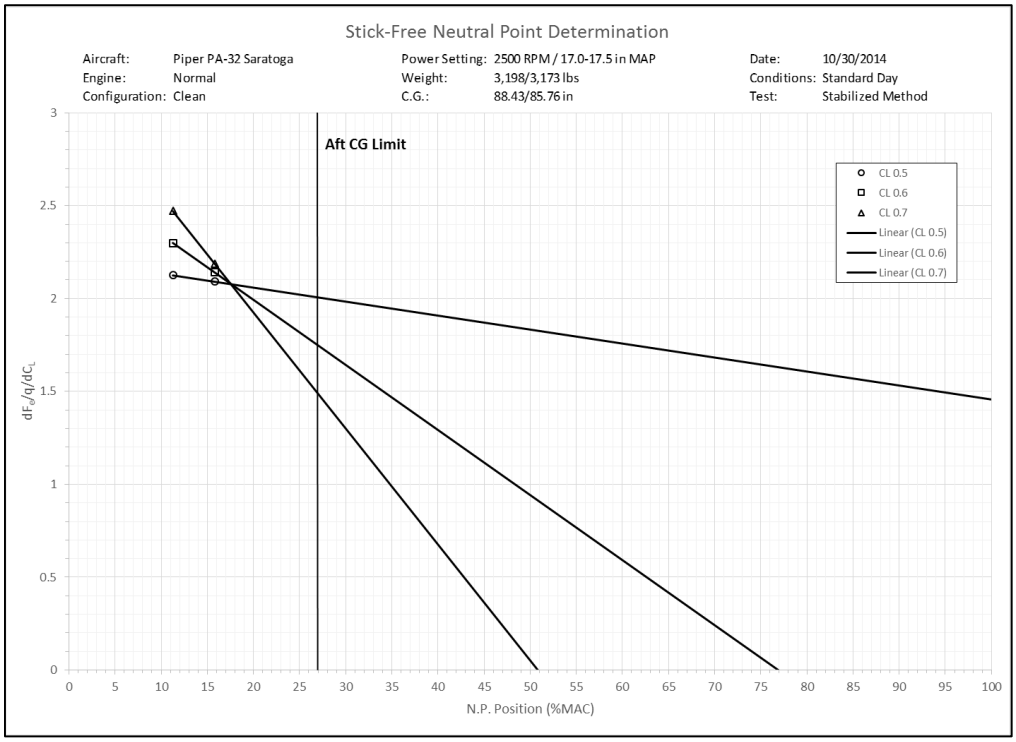


Figure 4.65 – Stick-Free Neutral Point Determination Using Stabilized Method for N22UT

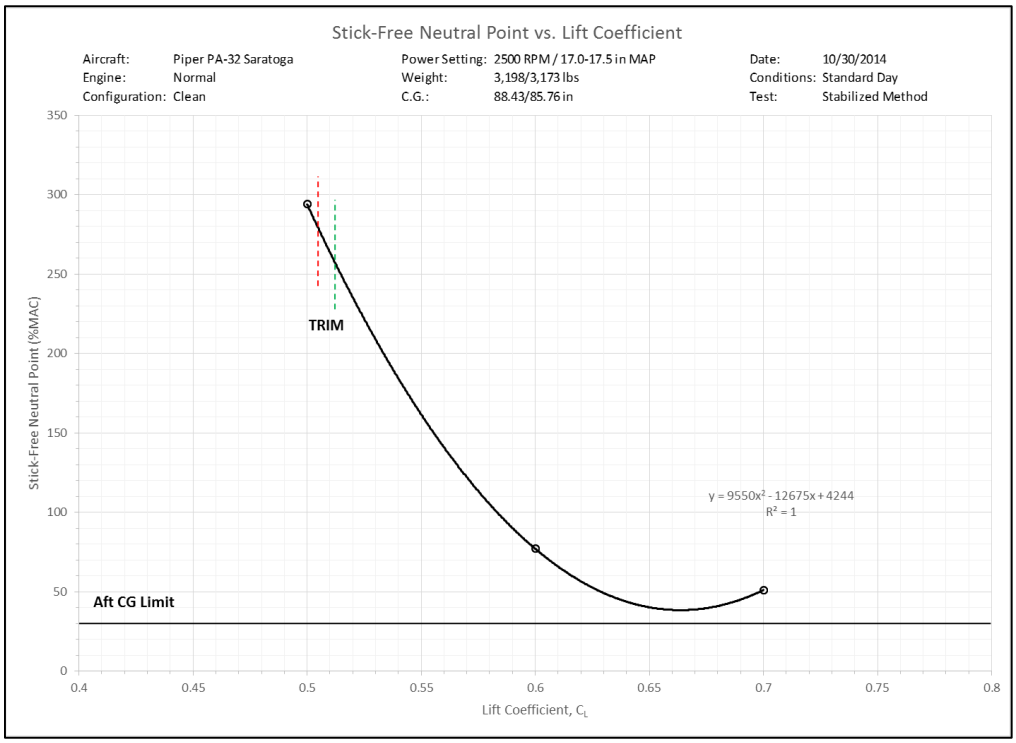


Figure 4.66 – Stick-Free Neutral Point vs. Lift Coefficient Using Stabilized Method for N22UT

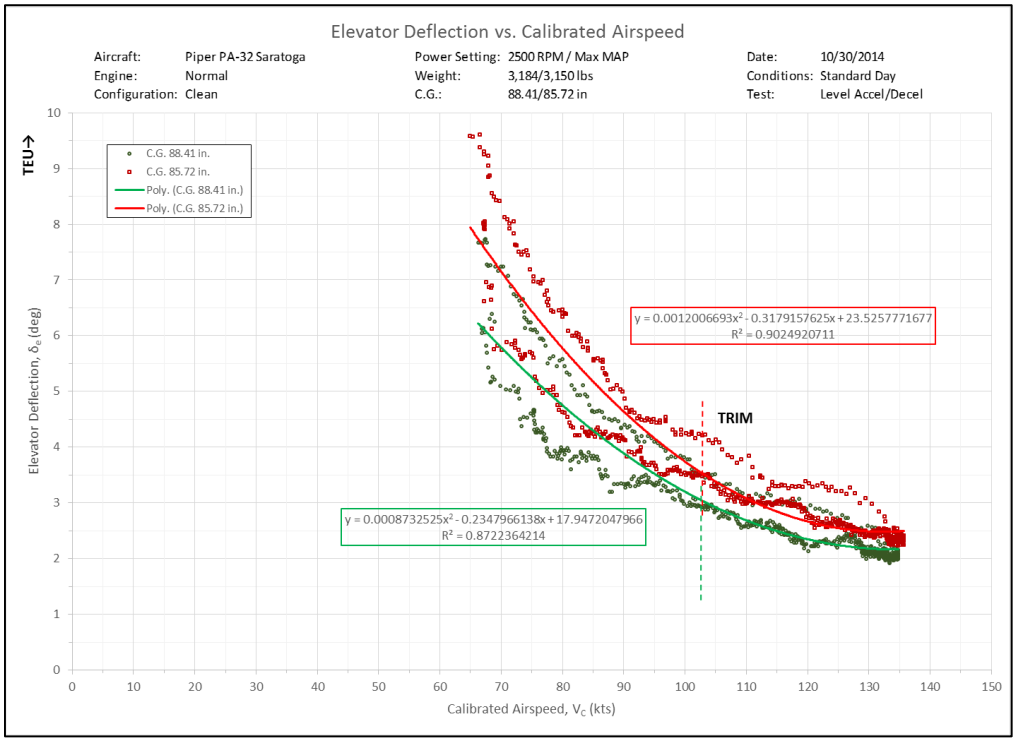


Figure 4.67 – Elevator Deflection vs. Calibrated Airspeed Using Level Accel/Decel for N22UT

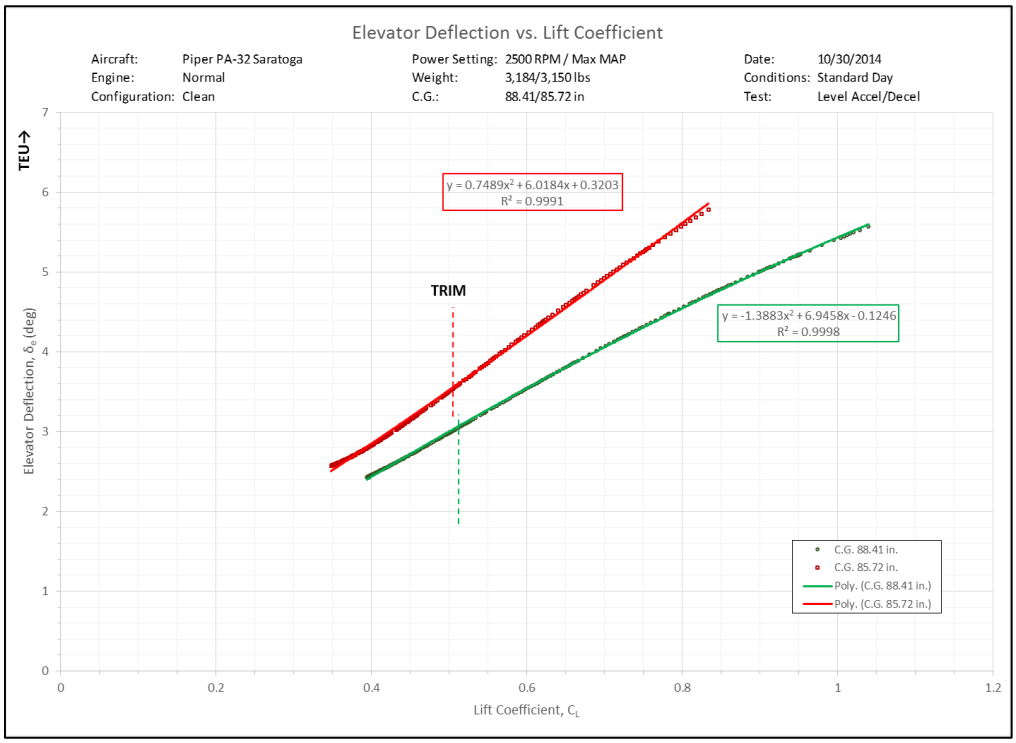


Figure 4.68 – Elevator Deflection vs. Lift Coefficient Using Level Accel/Decel for N22UT

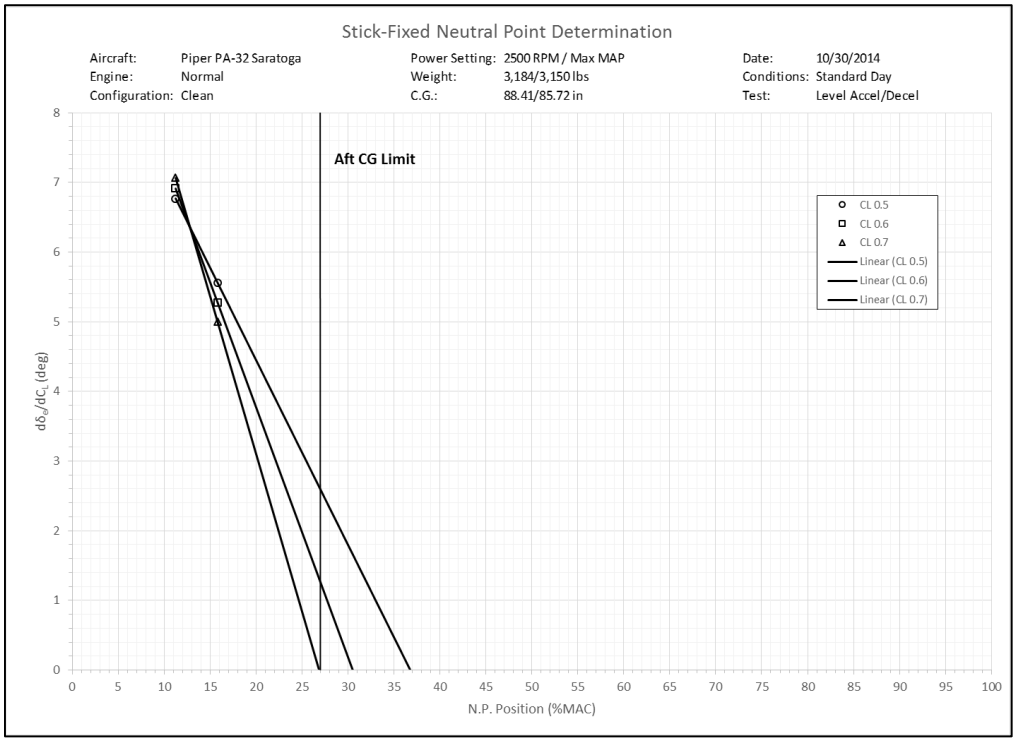


Figure 4.69 – Stick-Fixed Neutral Point Determination Using Level Accel/Decel for N22UT

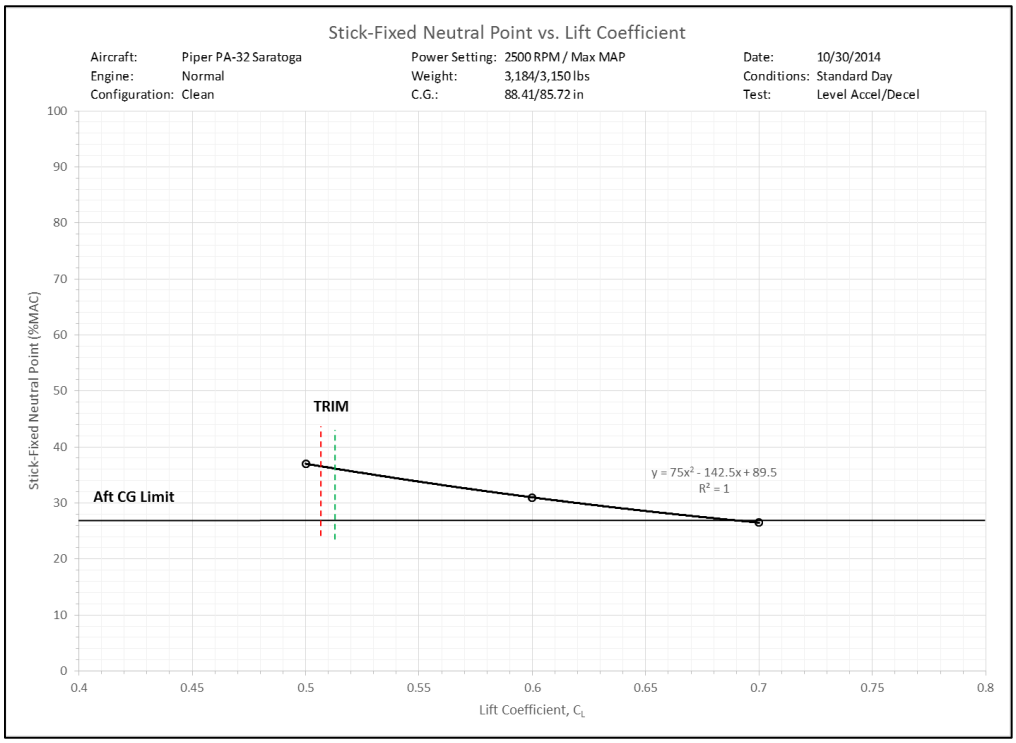


Figure 4.70 – Stick-Fixed Neutral Point vs. Lift Coefficient Using Level Accel/Decel for N22UT

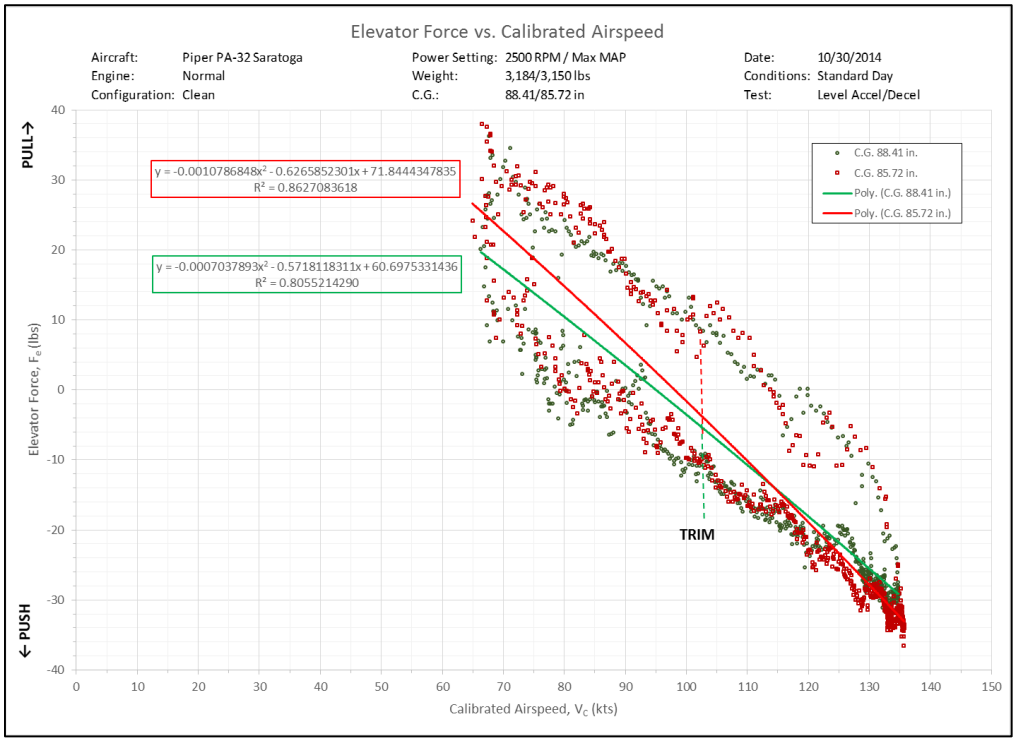


Figure 4.71 – Elevator Force vs. Calibrated Airspeed Using Level Accel/Decel for N22UT

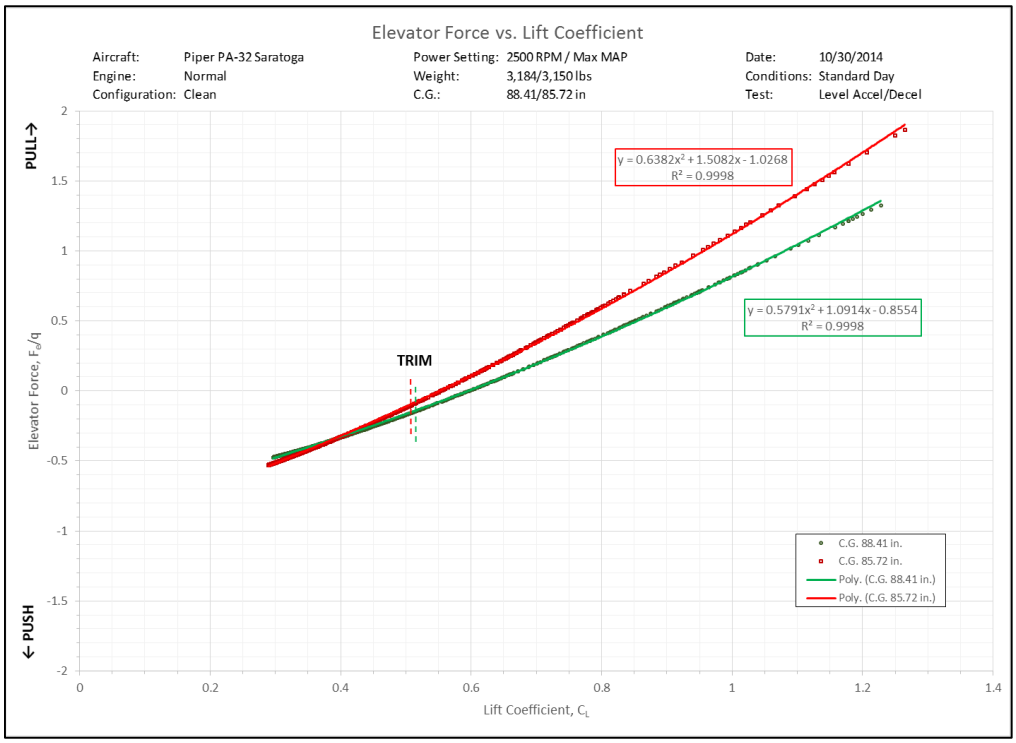


Figure 4.72 – Elevator Force vs. Lift Coefficient Using Level Accel/Decel for N22UT

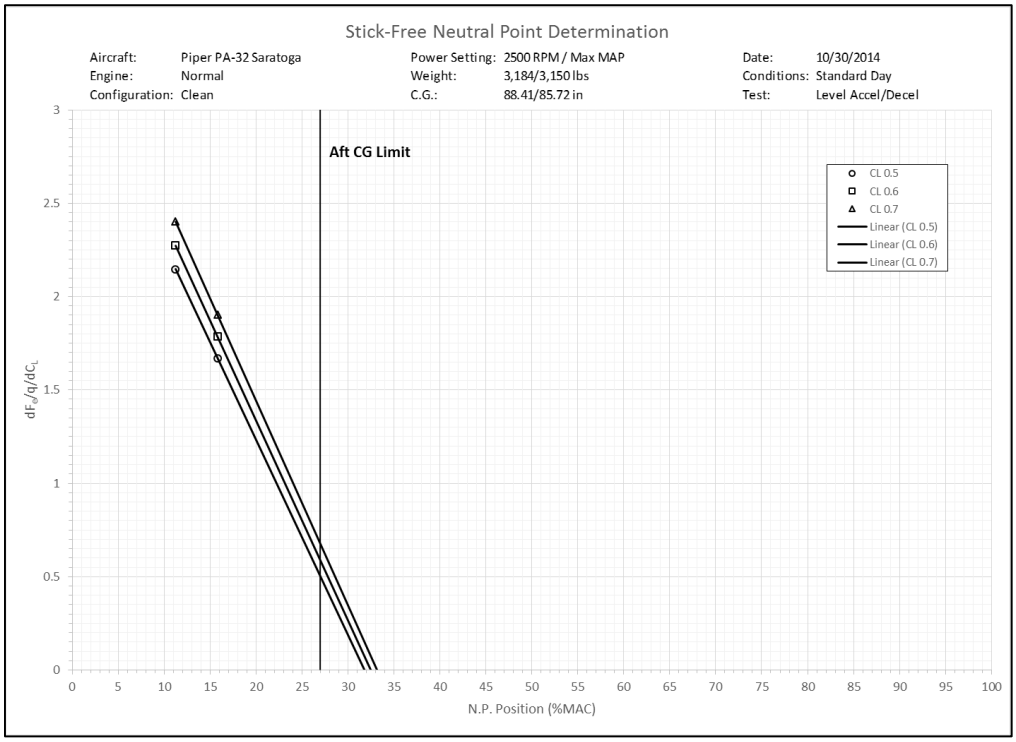


Figure 4.73 – Stick-Free Neutral Point Determination Using Level Accel/Decel for N22UT

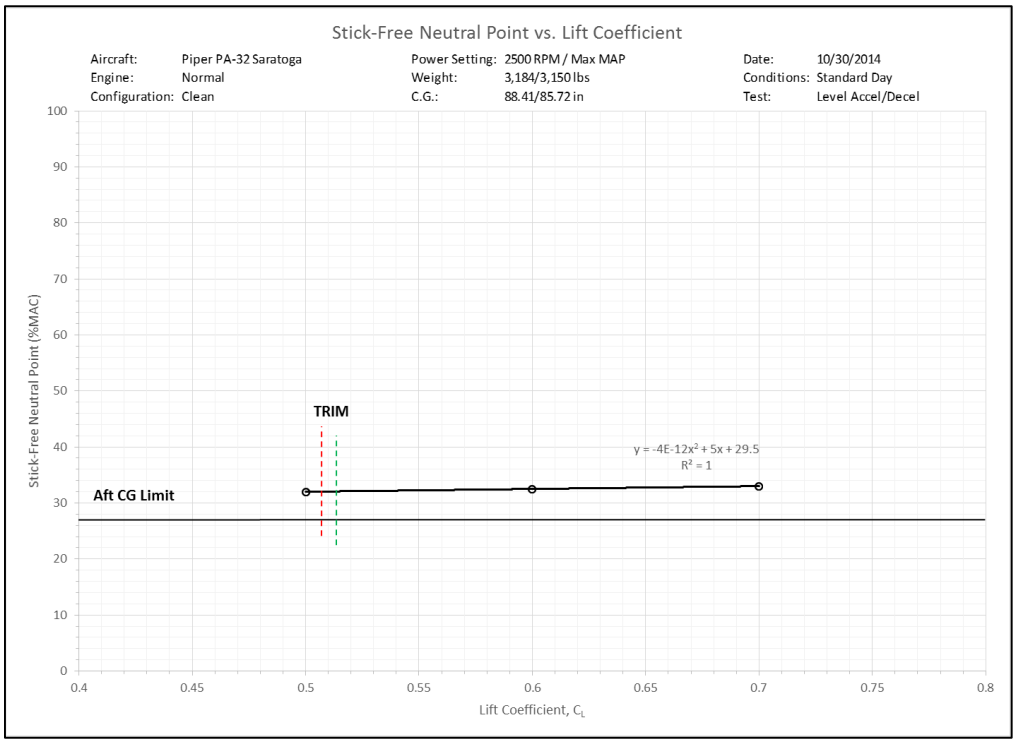


Figure 4.74 – Stick-Free Neutral Point vs. Lift Coefficient Using Level Accel/Decel for N22UT

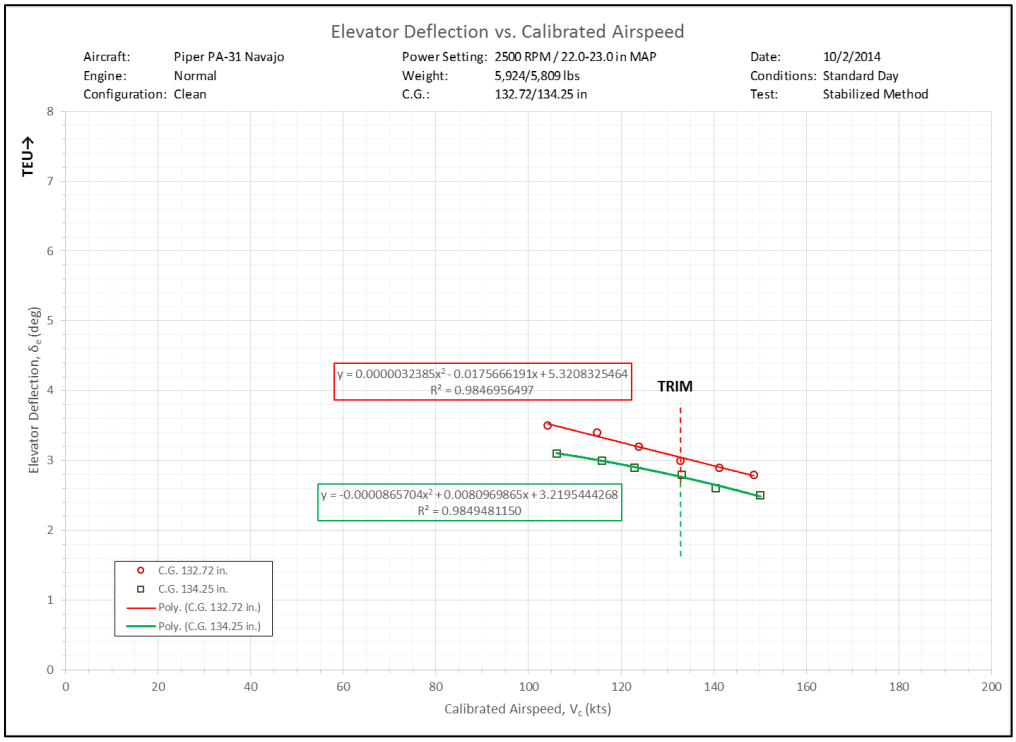


Figure 4.75 – Elevator Deflection vs. Calibrated Airspeed Using Stabilized Method for N11UT

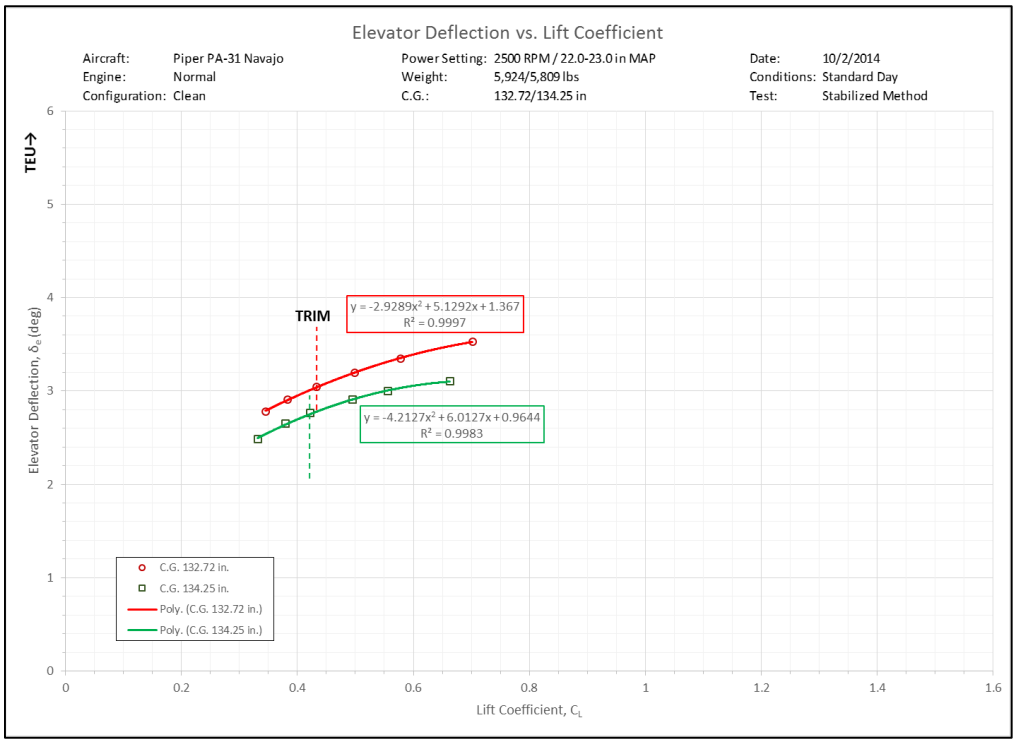


Figure 4.76 – Elevator Deflection vs. Lift Coefficient Using Stabilized Method for N11UT

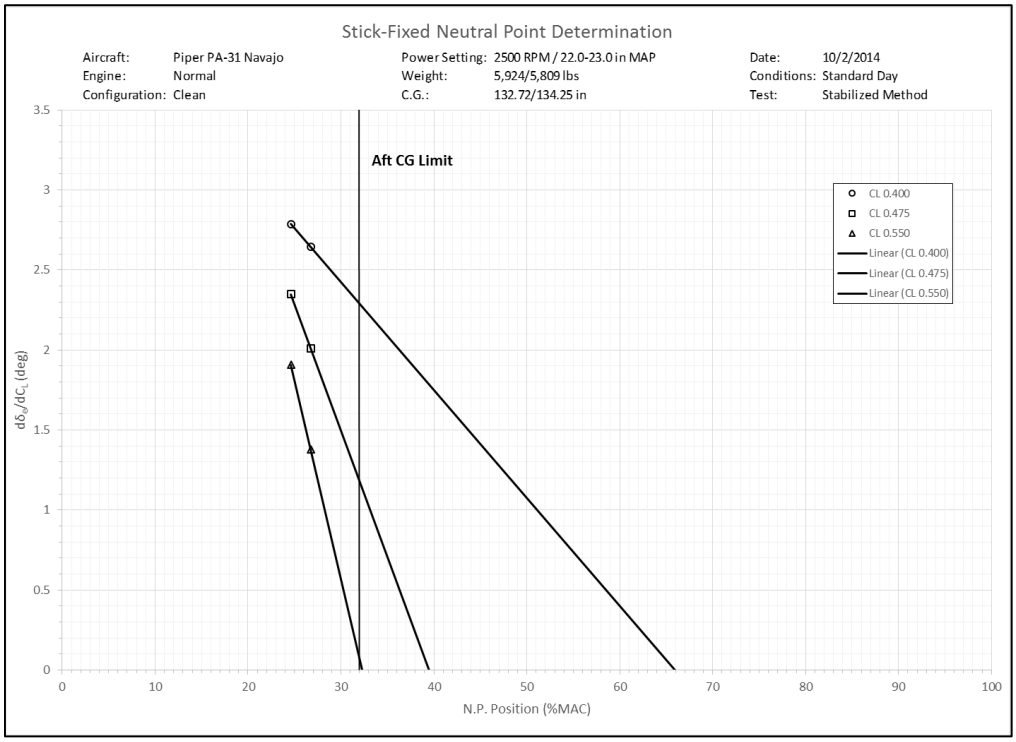


Figure 4.77 – Stick-Fixed Neutral Point Determination Using Stabilized Method for N11UT

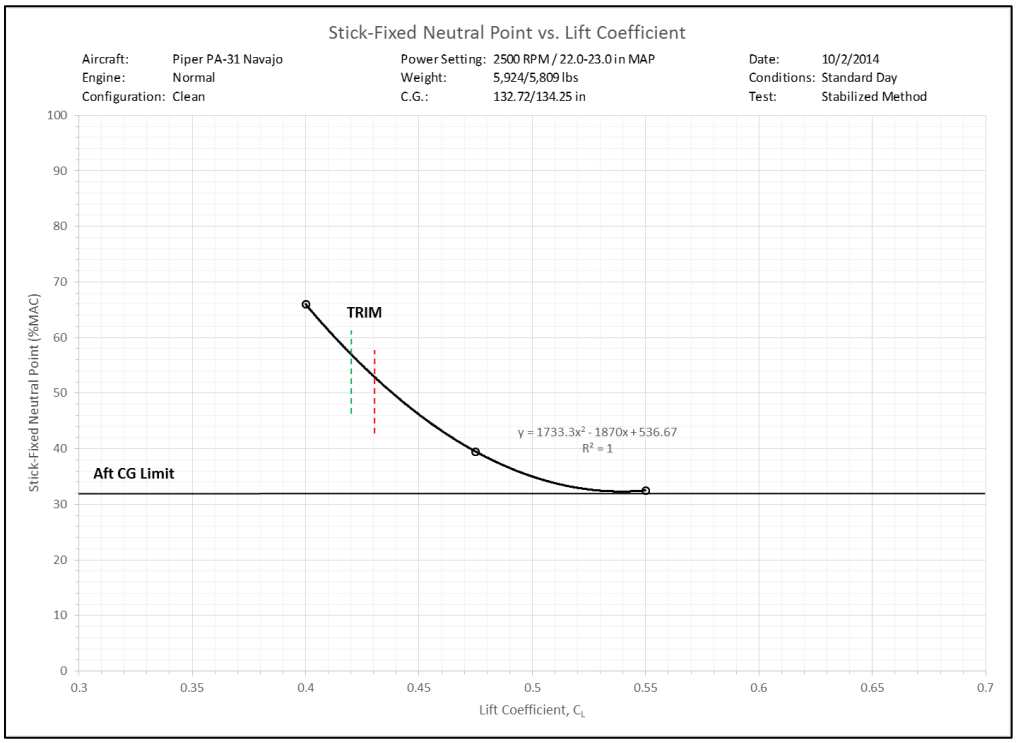


Figure 4.78 – Stick-Fixed Neutral Point vs. Lift Coefficient Using Stabilized Method for N11UT

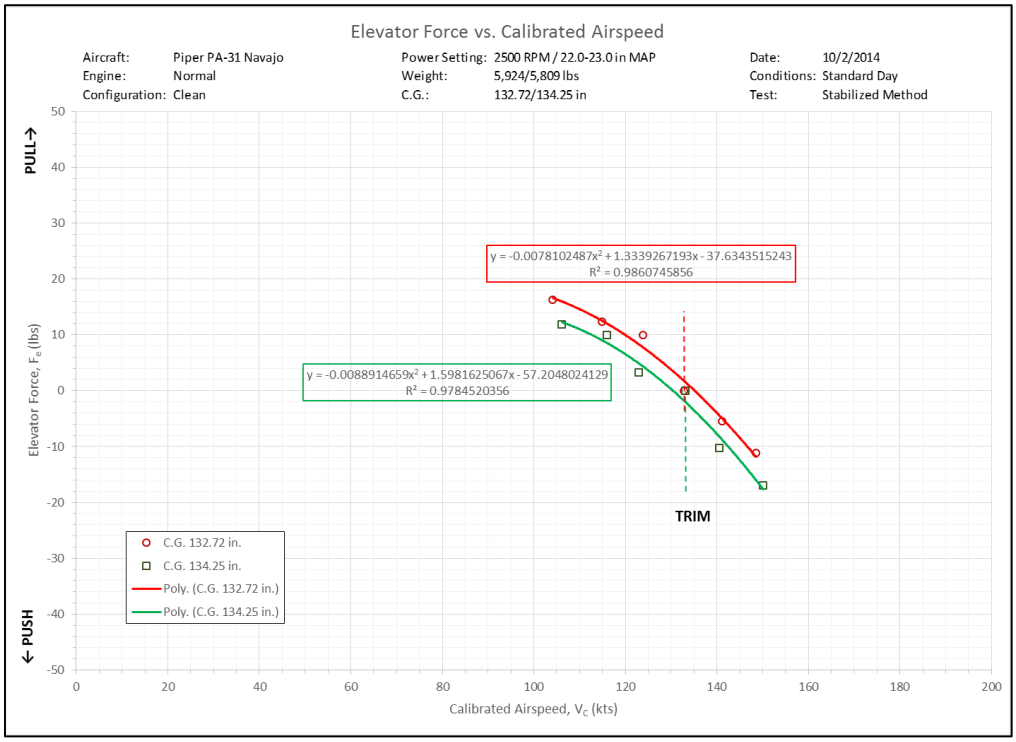


Figure 4.79 – Elevator Force vs. Calibrated Airspeed Using Stabilized Method for N11UT

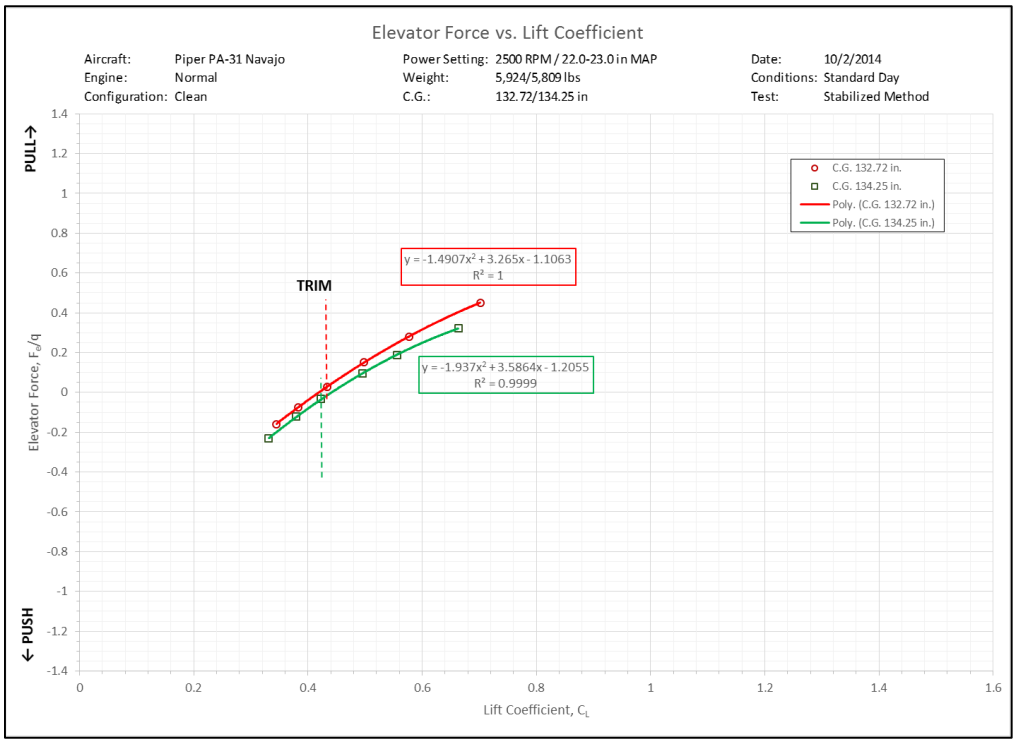


Figure 4.80 – Elevator Force vs. Lift Coefficient Using Stabilized Method for N11UT

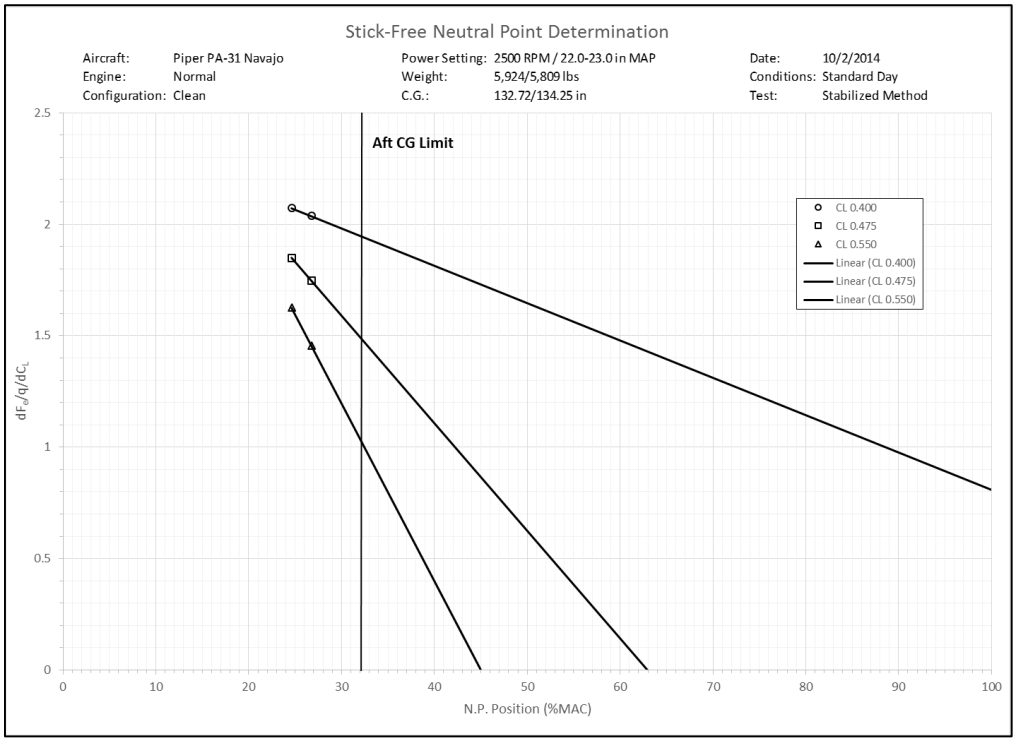


Figure 4.81 – Stick-Free Neutral Point Determination Using Stabilized Method for N11UT

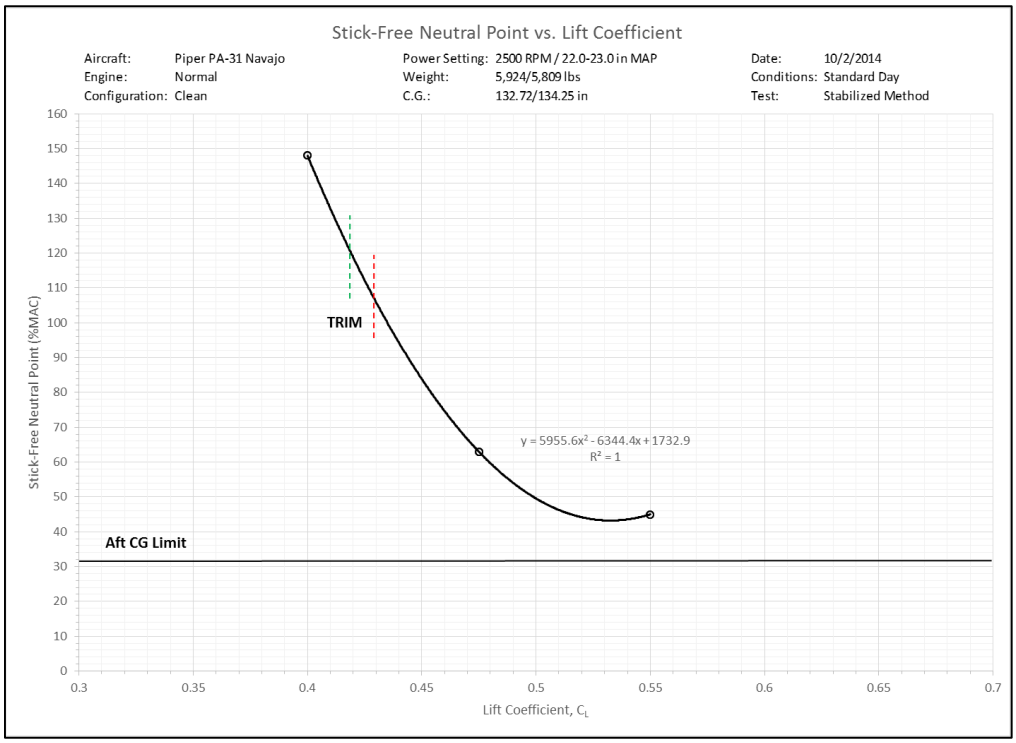


Figure 4.82 – Stick-Free Neutral Point vs. Lift Coefficient Using Stabilized Method for N11UT

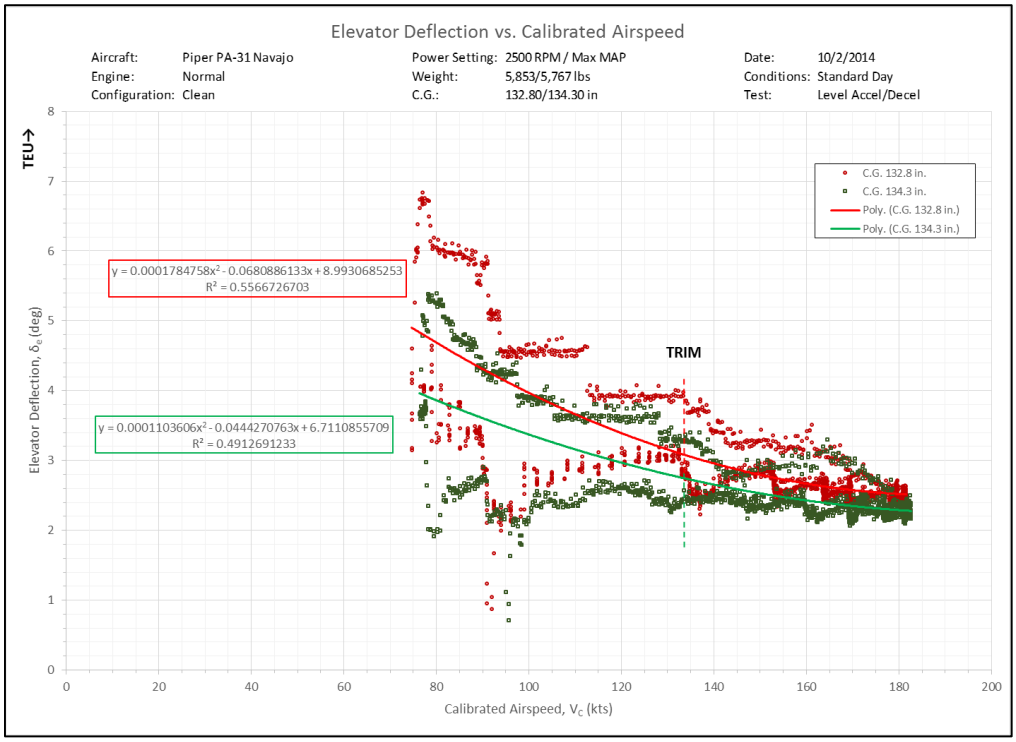


Figure 4.83 – Elevator Deflection vs. Calibrated Airspeed Using Level Accel/Decel for N11UT

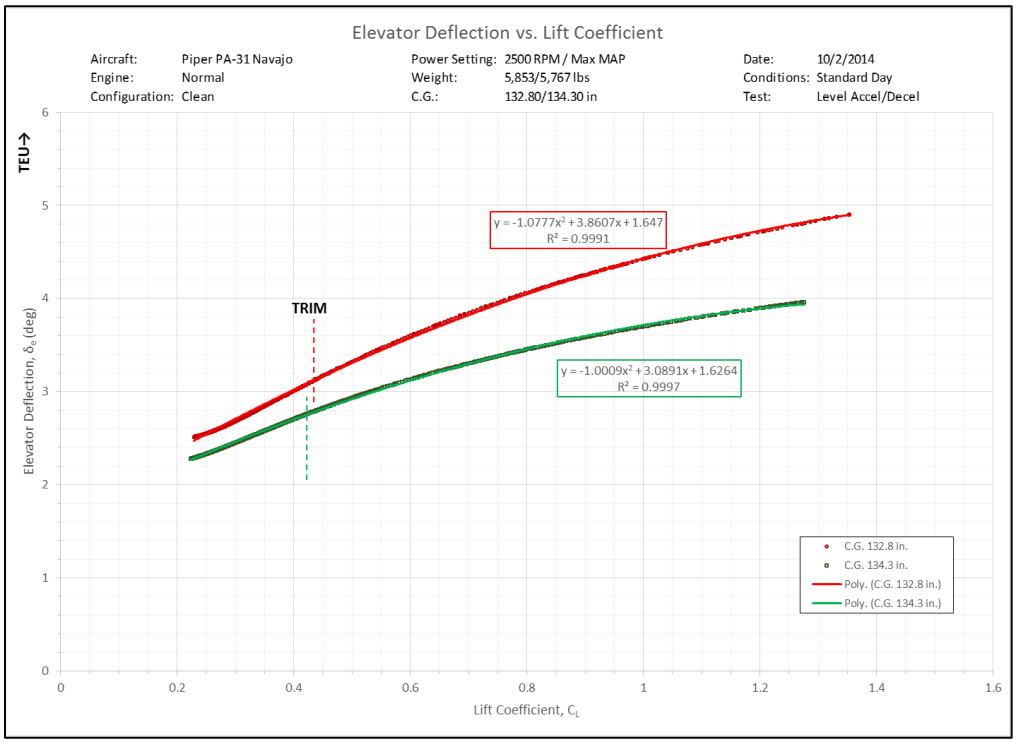


Figure 4.84 – Elevator Deflection vs. Lift Coefficient Using Level Accel/Decel for N11UT

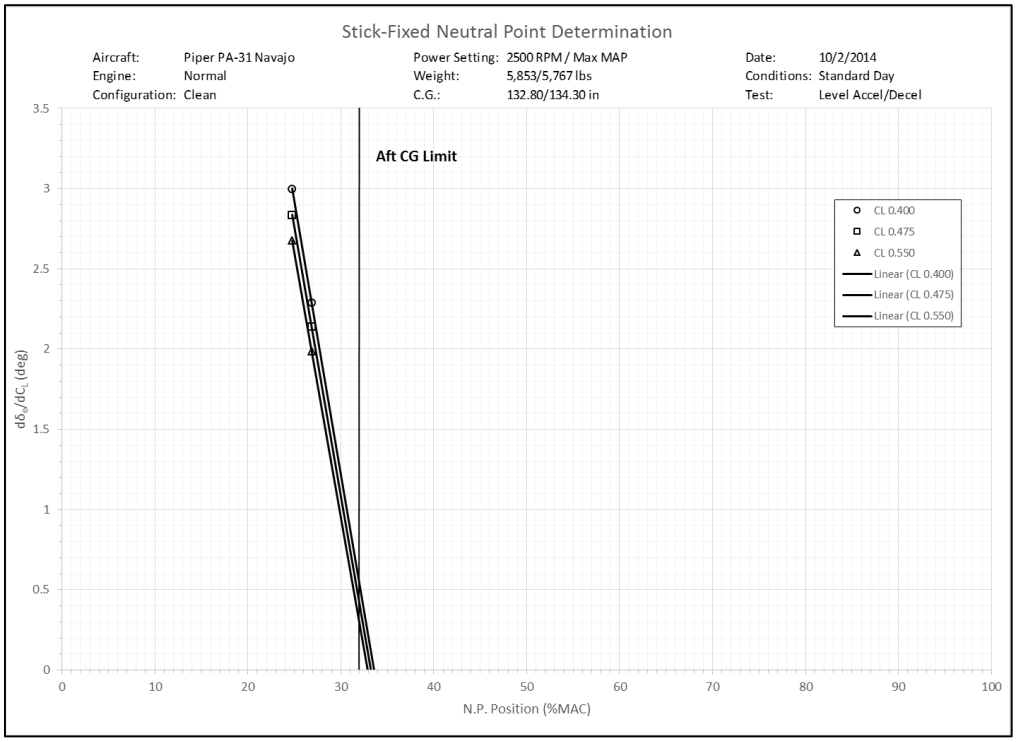


Figure 4.85 – Stick-Fixed Neutral Point Determination Using Level Accel/Decel for N11UT

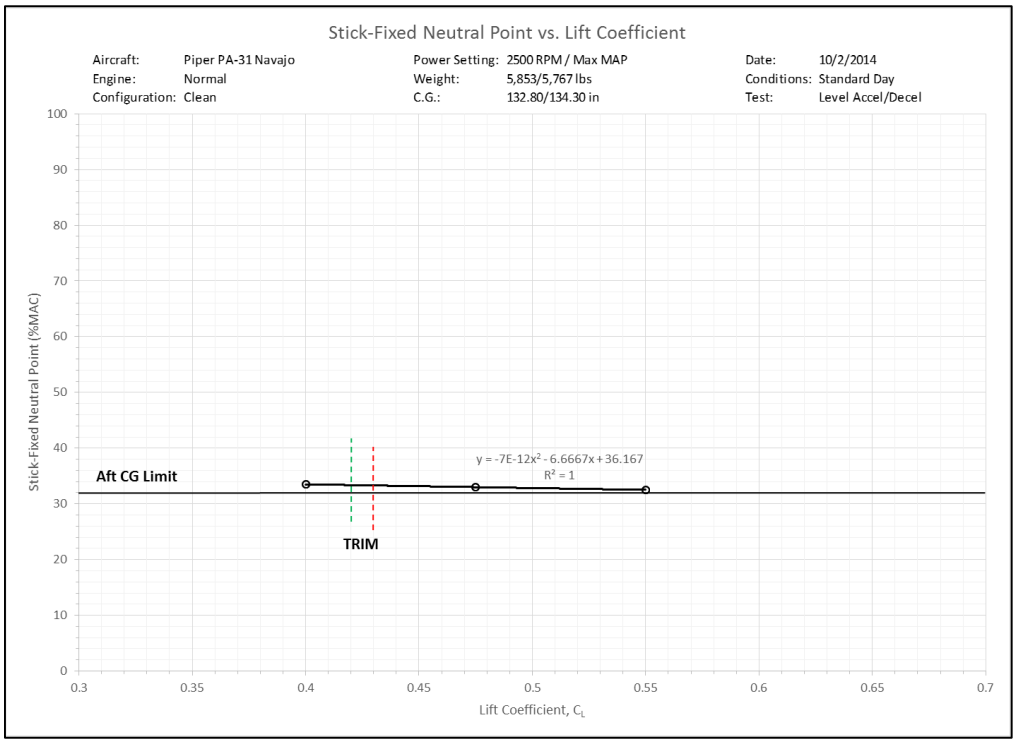


Figure 4.86 – Stick-Fixed Neutral Point vs. Lift Coefficient Using Level Accel/Decel for N11UT

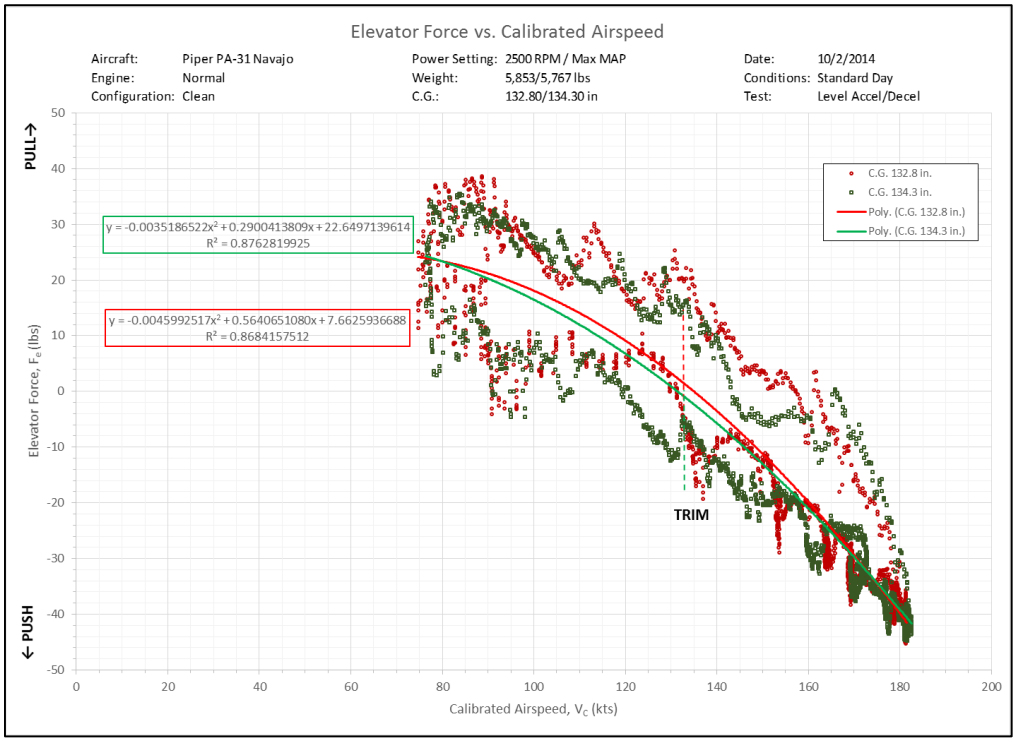


Figure 4.87 – Elevator Force vs. Calibrated Airspeed Using Level Accel/Decel for N11UT

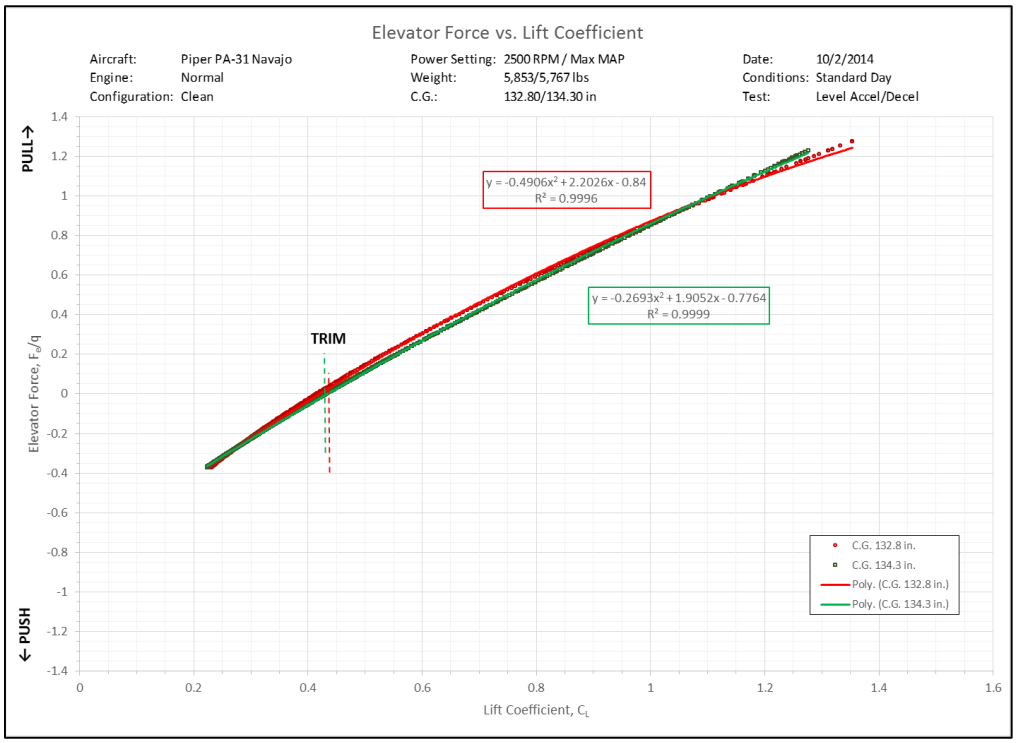


Figure 4.88 – Elevator Force vs. Lift Coefficient Using Level Accel/Decel for N11UT

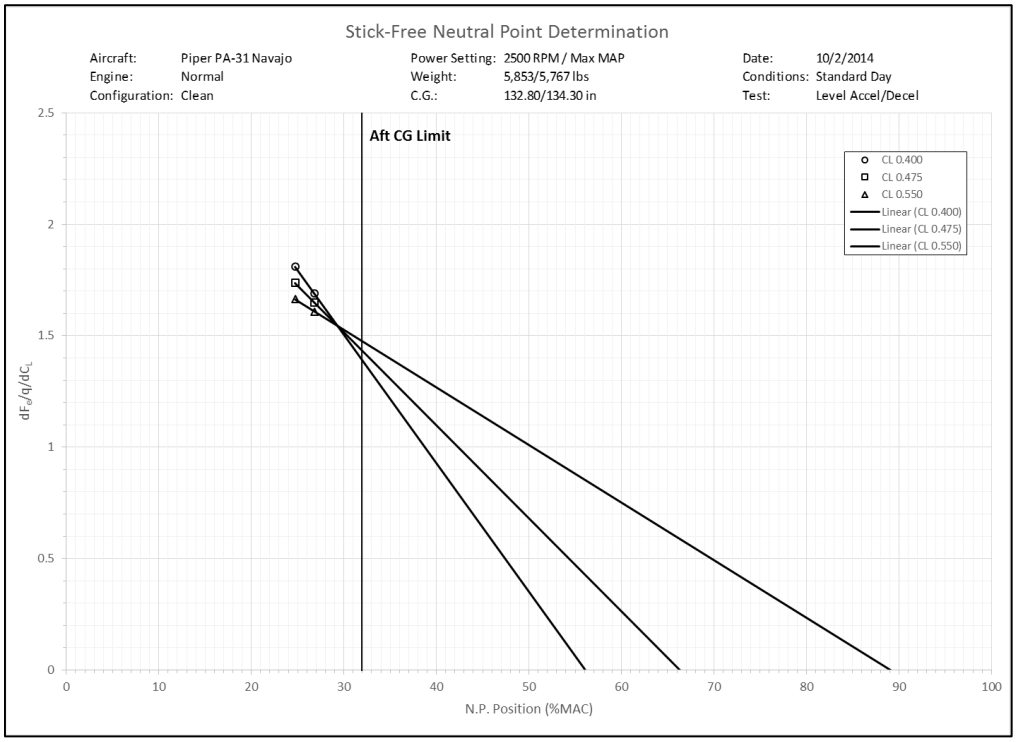


Figure 4.89 – Stick-Free Neutral Point Determination Using Level Accel/Decel for N11UT

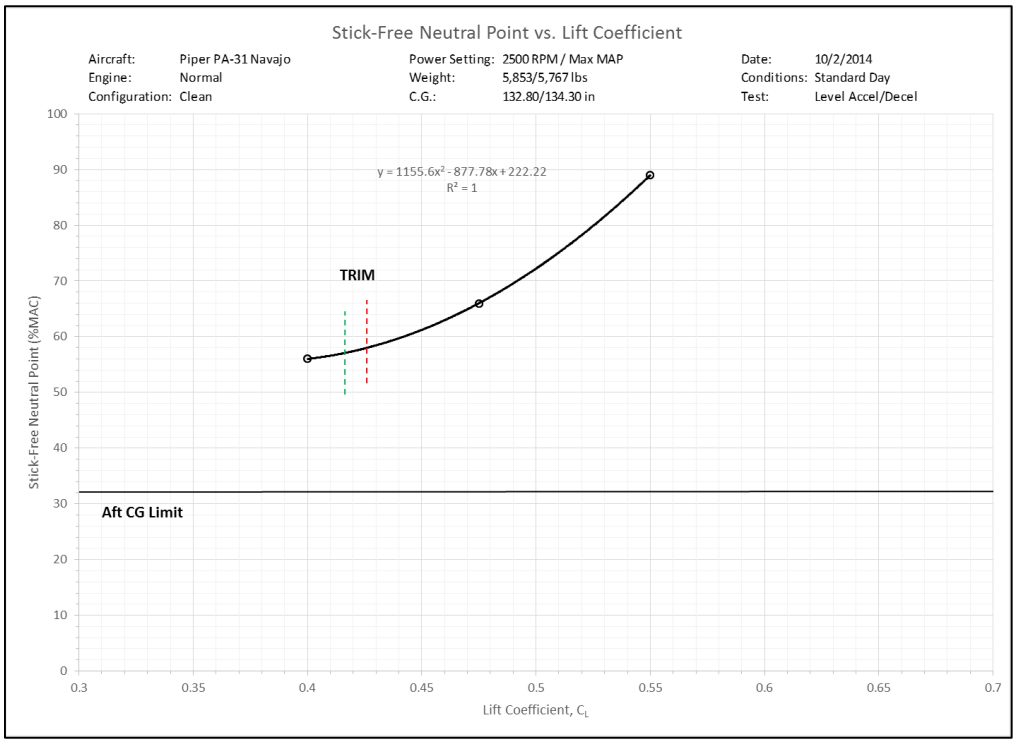


Figure 4.90 – Stick-Free Neutral Point vs. Lift Coefficient Using Level Accel/Decel for N11UT

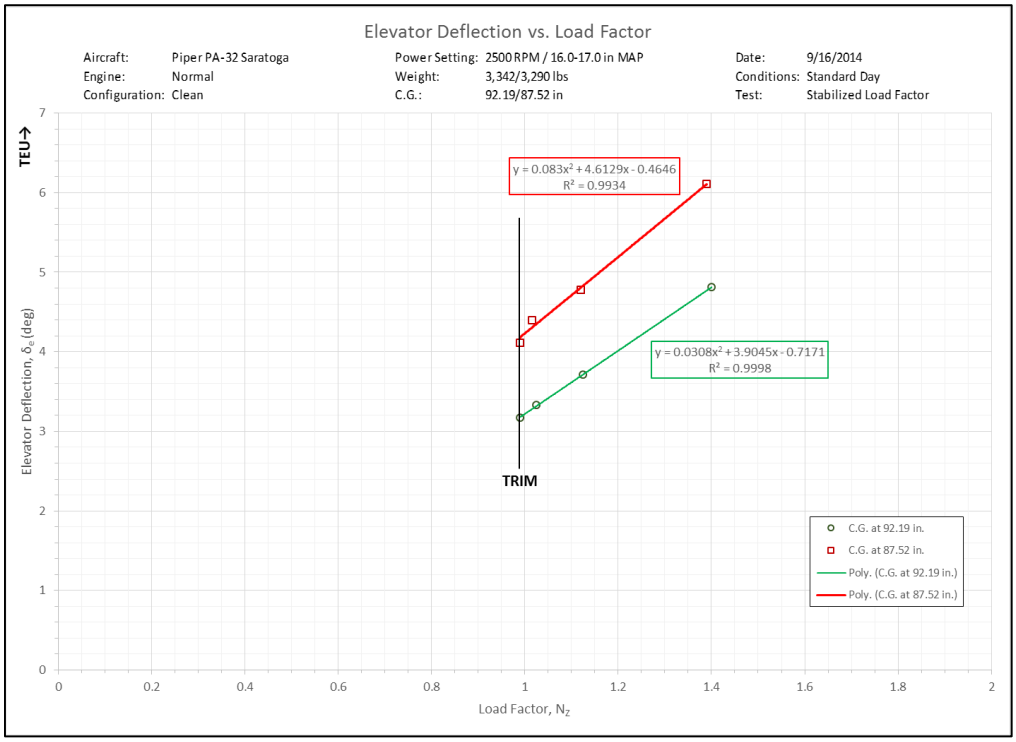


Figure 4.91 – Elevator Deflection vs. Load Factor for N22UT

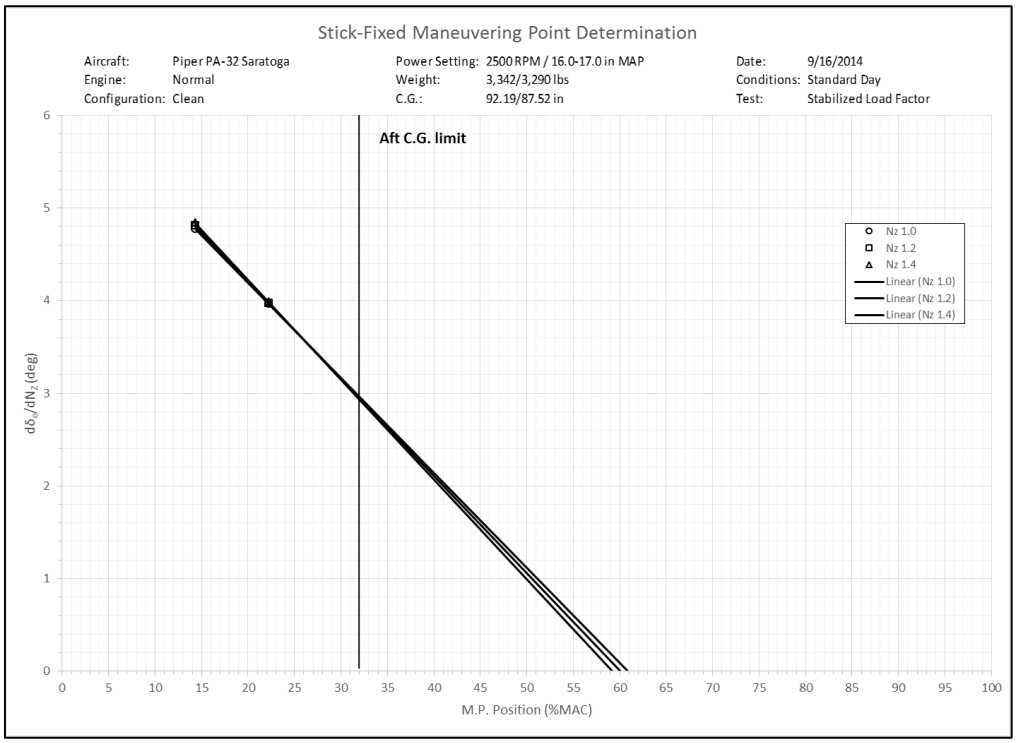


Figure 4.92 – Stick-Fixed Maneuvering Point Determination for N22UT

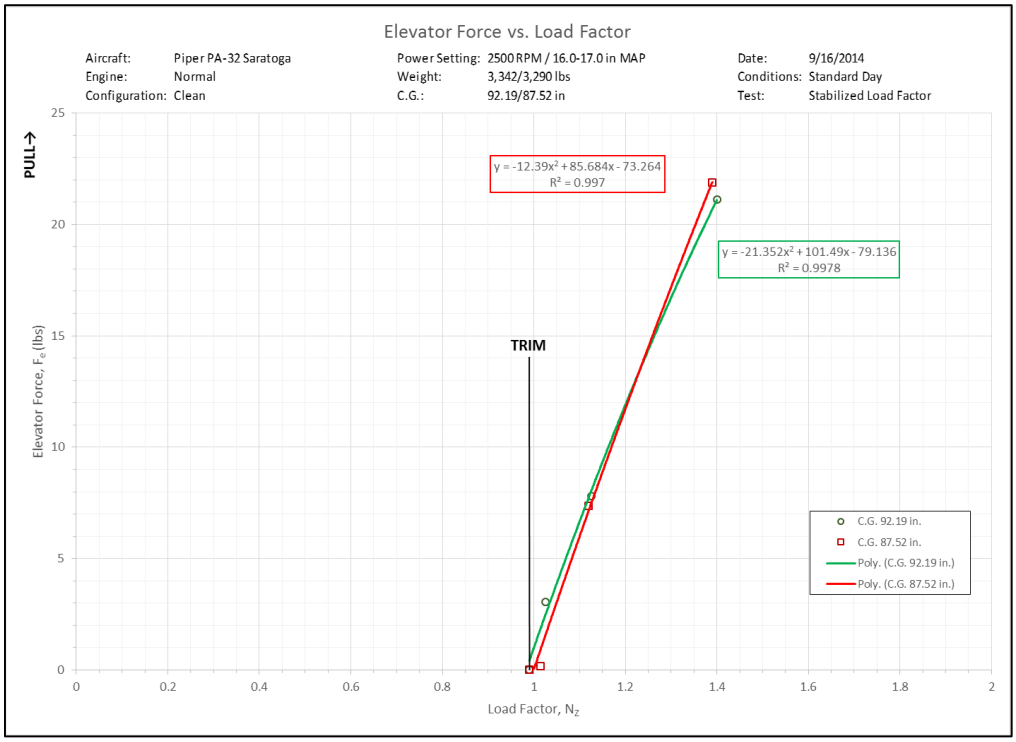


Figure 4.93 – Elevator Force vs. Load Factor for N22UT

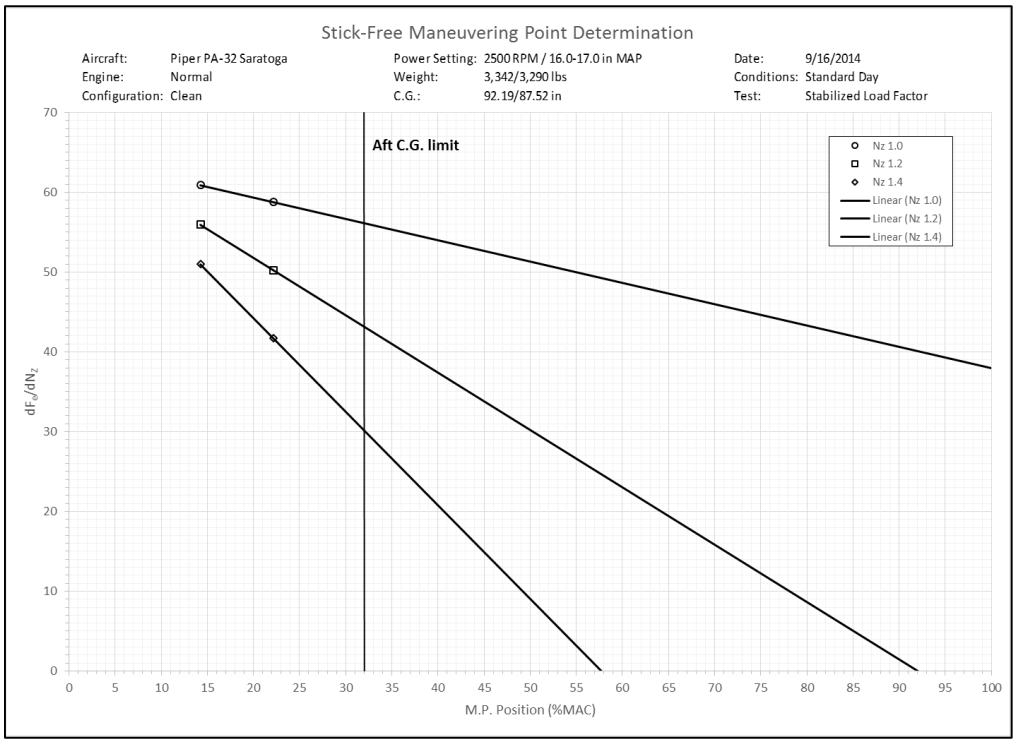


Figure 4.94 – Stick-Free Maneuvering Point Determination for N22UT

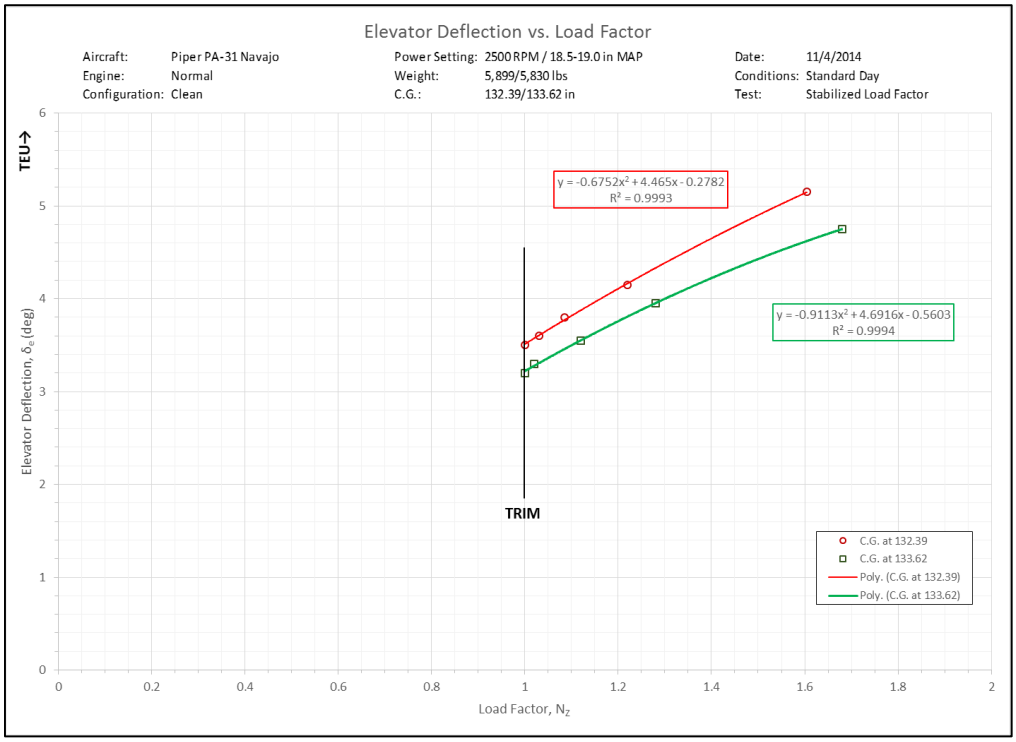


Figure 4.95 – Elevator Defection vs. Load Factor for N11UT

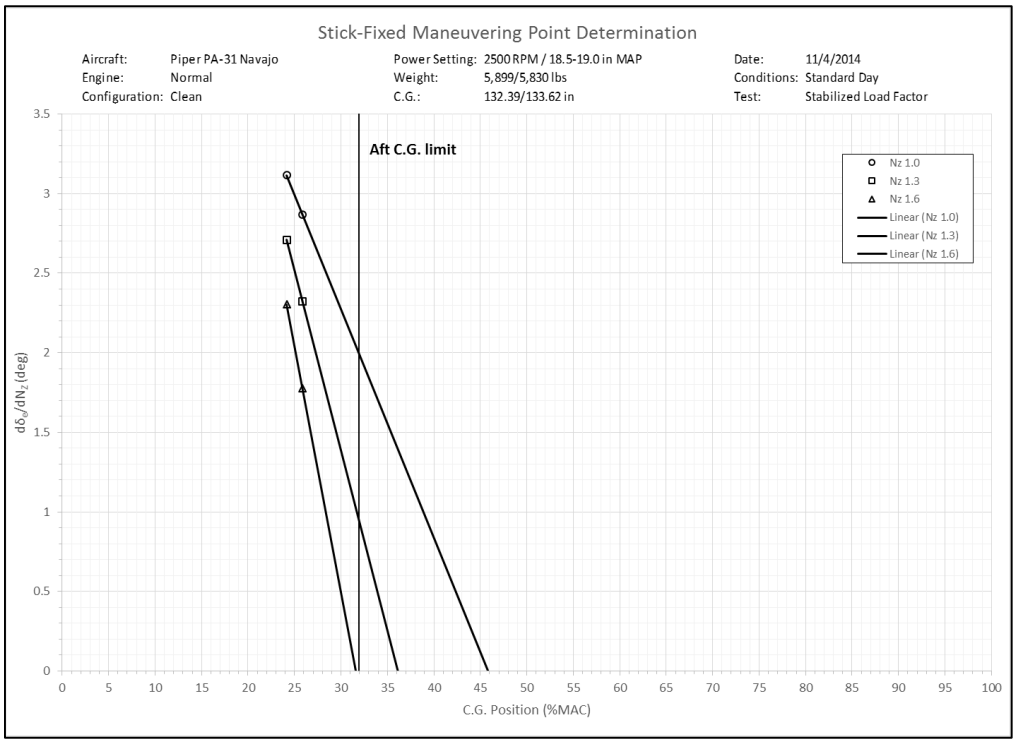


Figure 4.96 – Stick-Fixed Maneuvering Point Determination for N11UT

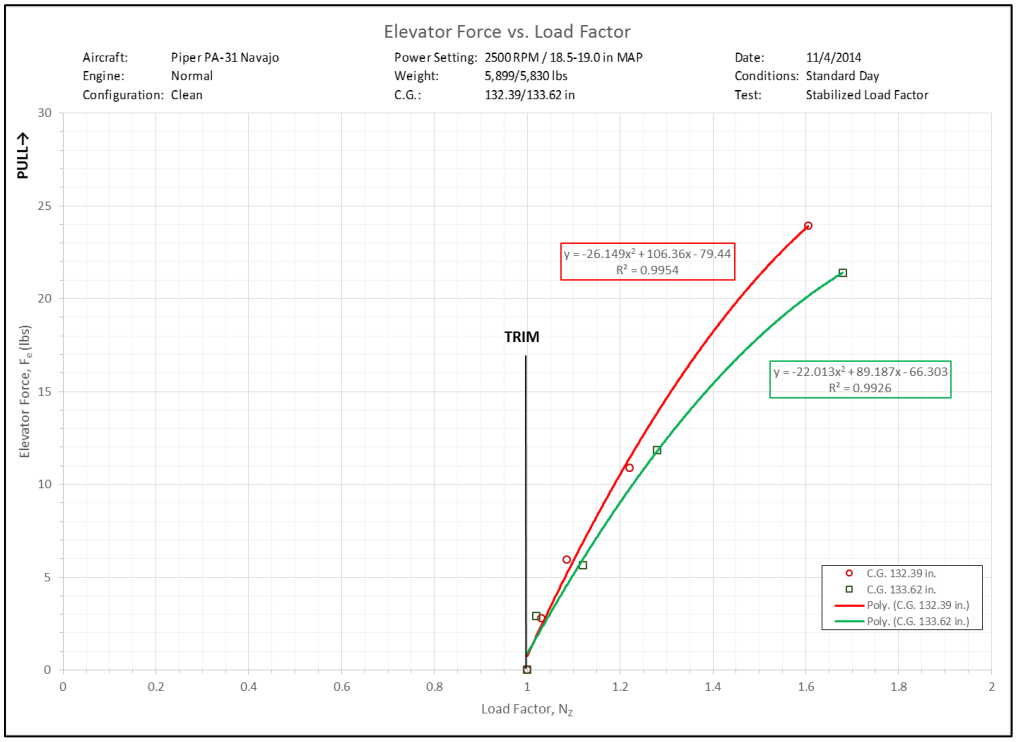


Figure 4.97 – Elevator Force vs. Load Factor for N11UT

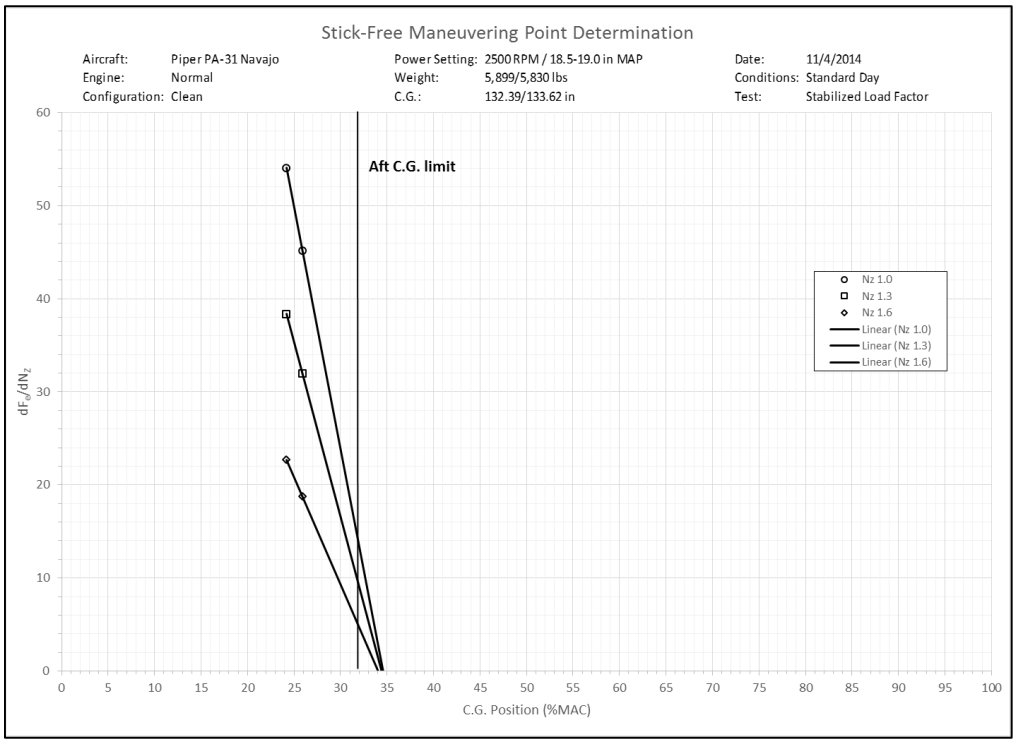


Figure 4.98 – Stick-Free Maneuvering Point Determination

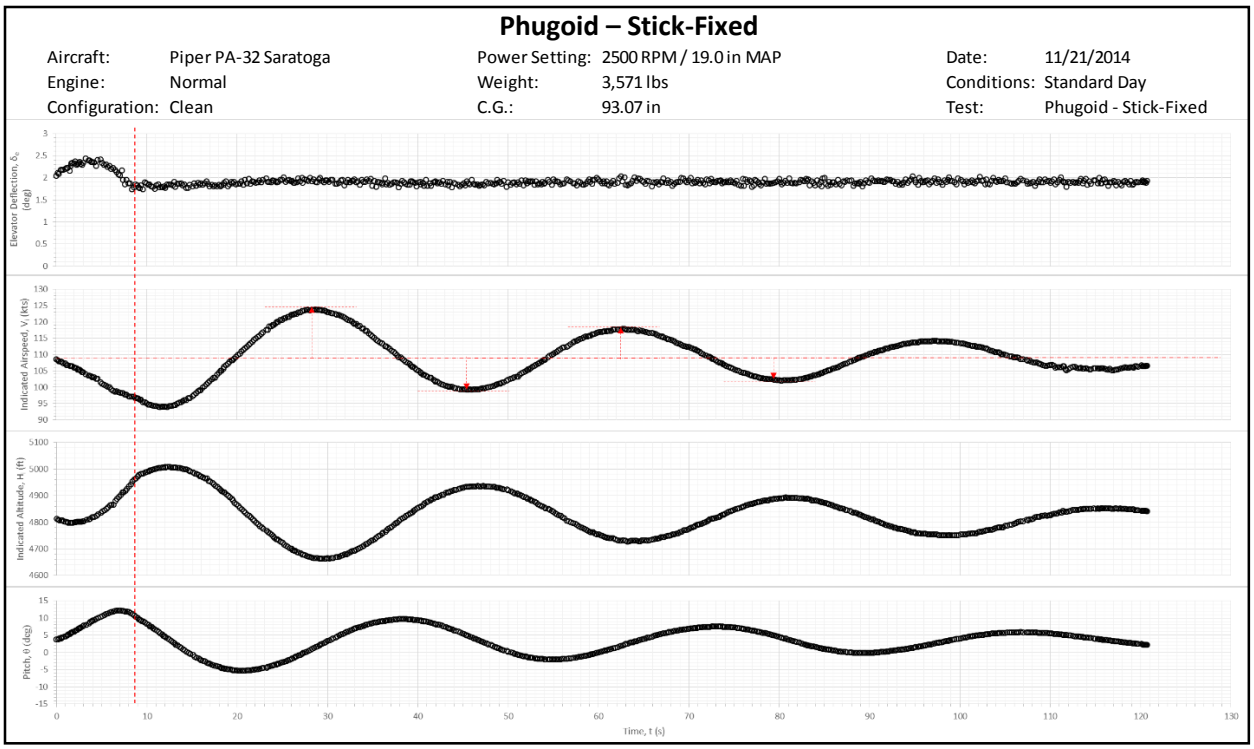


Figure 4.99 – Stick-Fixed Phugoid for N22UT

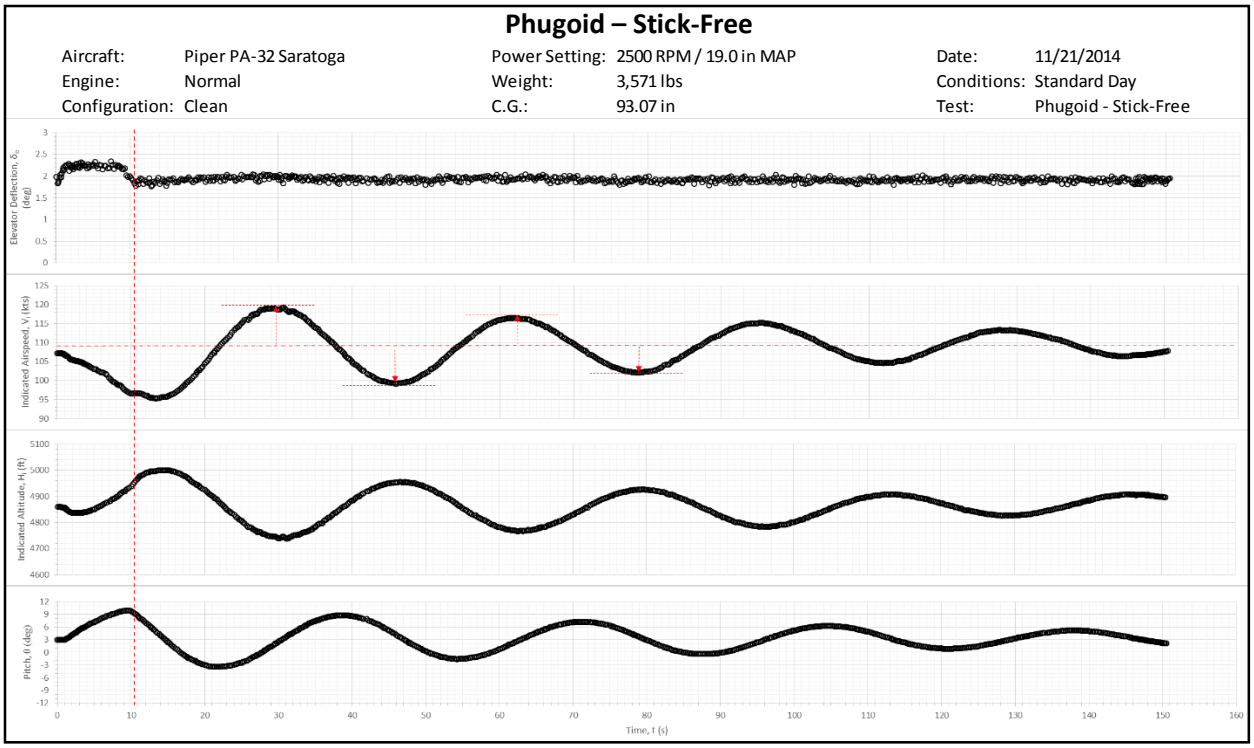


Figure 4.100 – Stick-Free Phugoid for N22UT

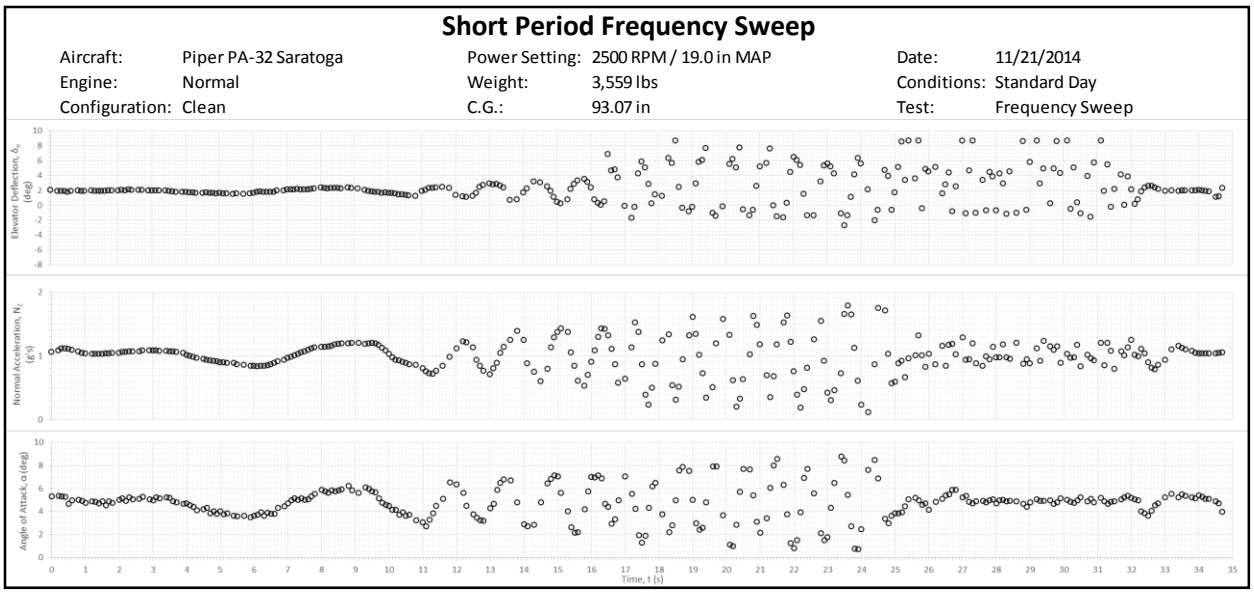


Figure 4.101 – Short Period Frequency Sweep for N22UT

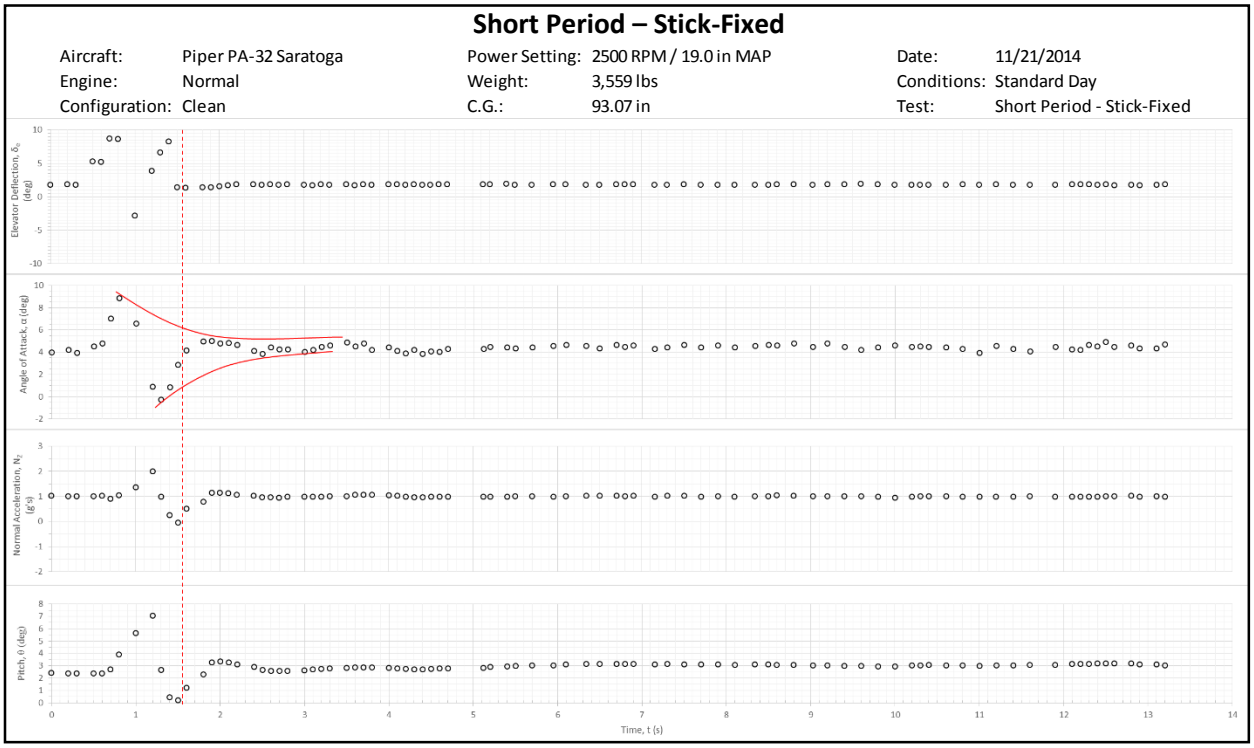


Figure 4.102 – Stick-Fixed Short Period for N22UT

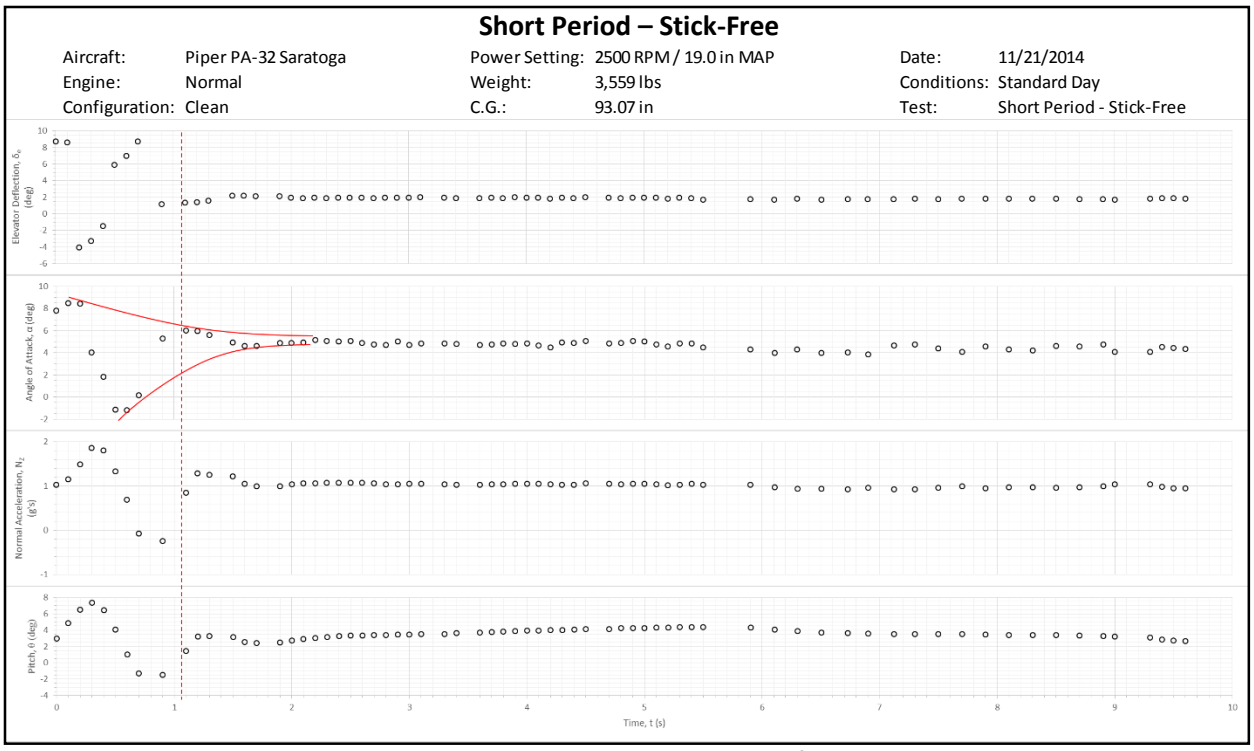


Figure 4.103 – Stick-Free Short Period for N22UT

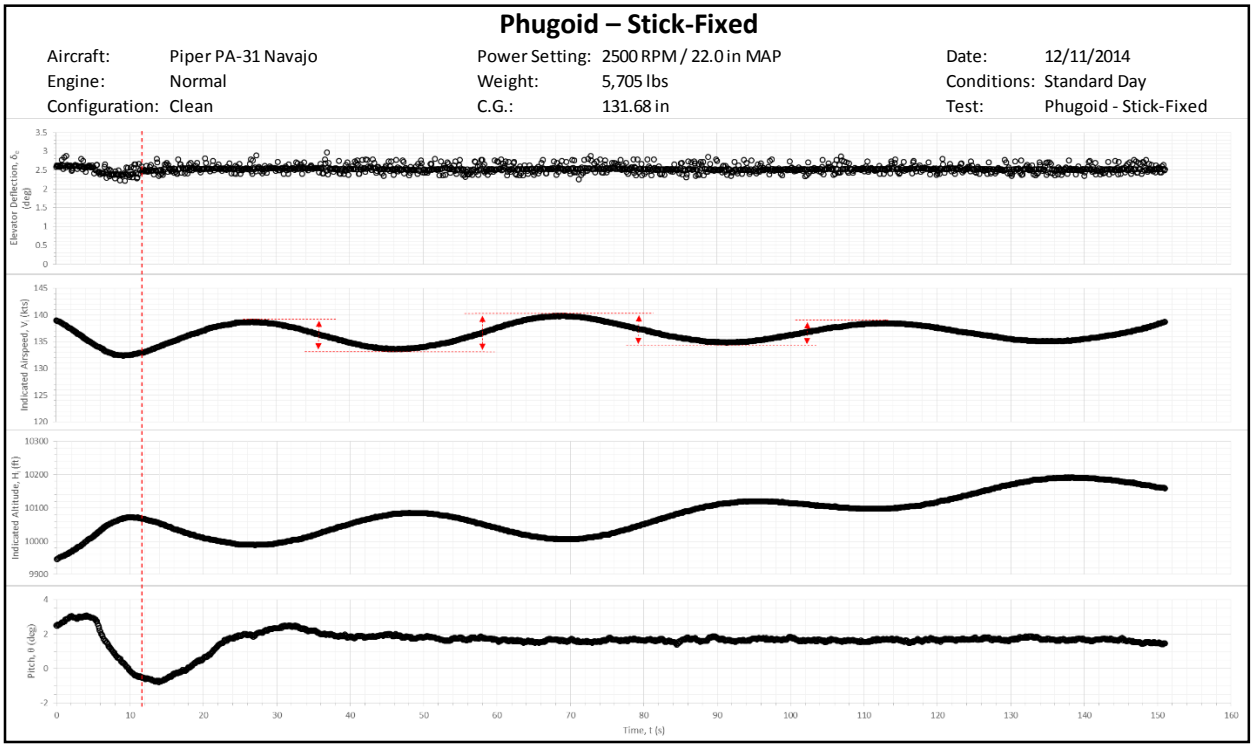


Figure 4.104 – Stick-Fixed Phugoid for N11UT

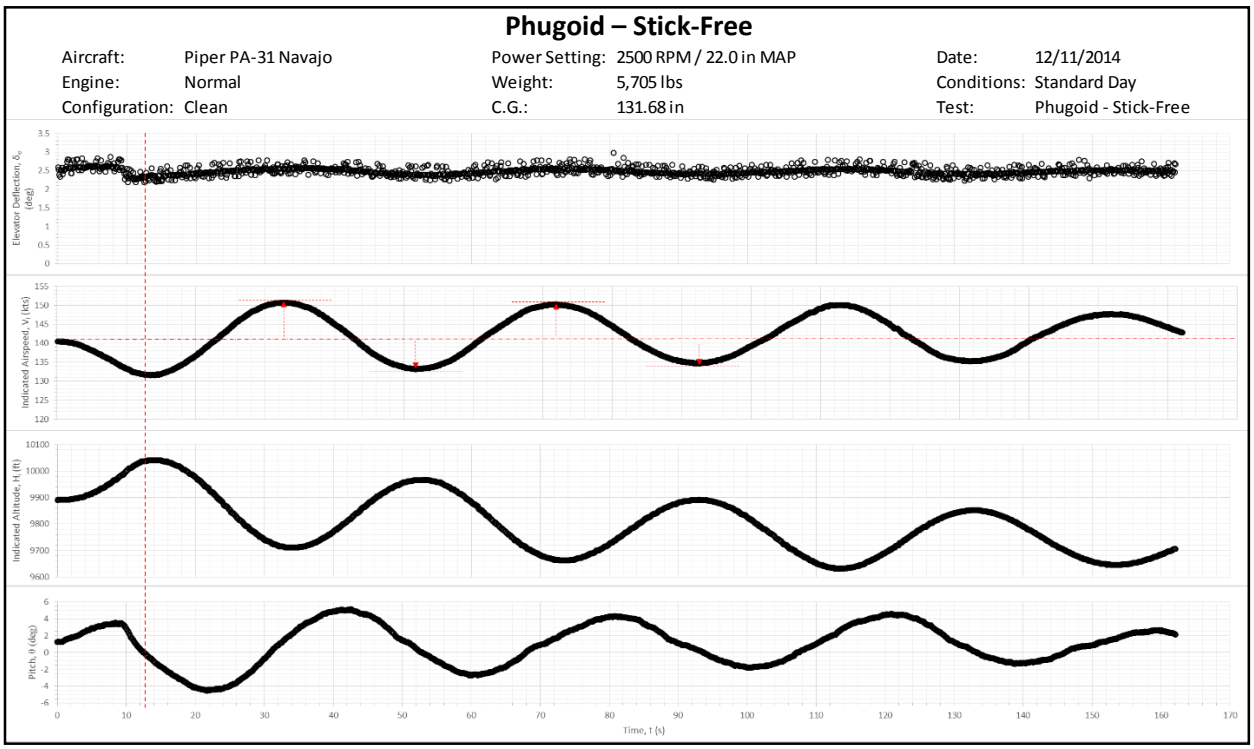


Figure 4.105 – Stick-Free Phugoid for N11UT

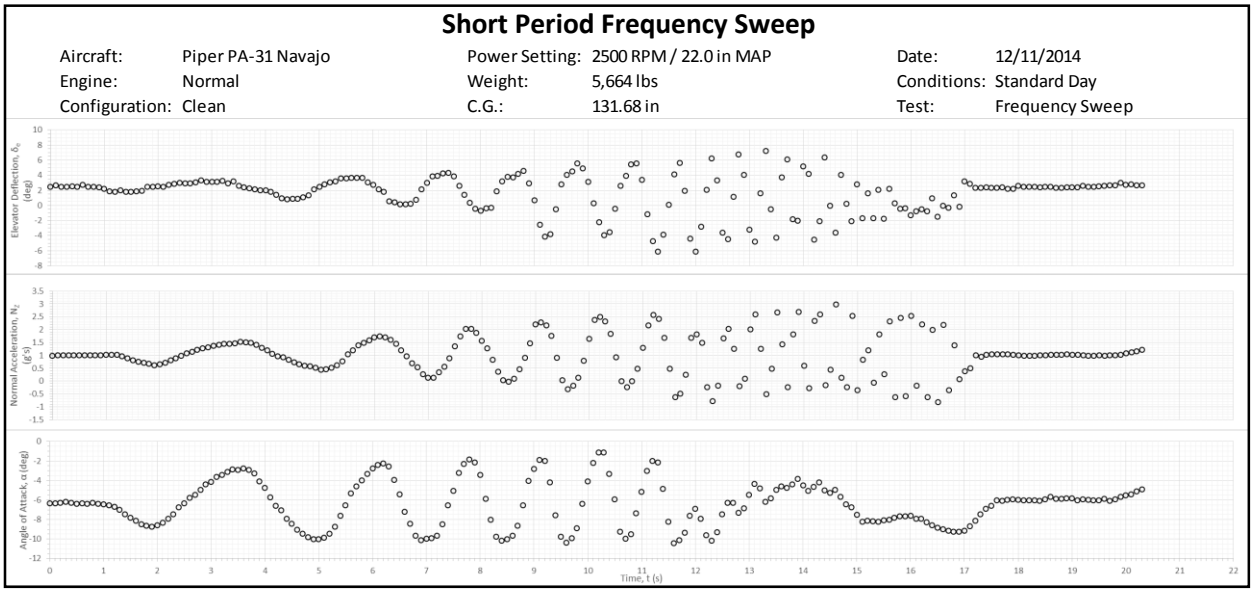


Figure 4.106 – Short Period Frequency Sweep for N11UT

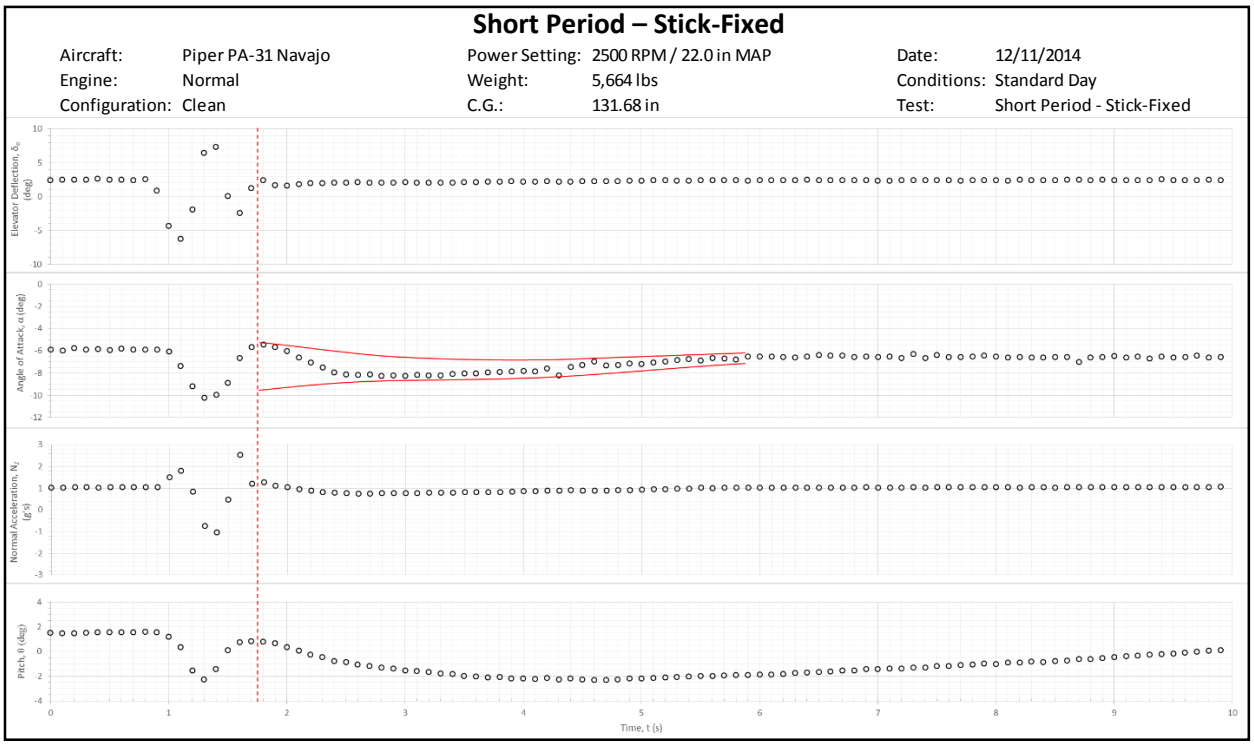


Figure 4.107 – Stick-Fixed Short Period for N11UT

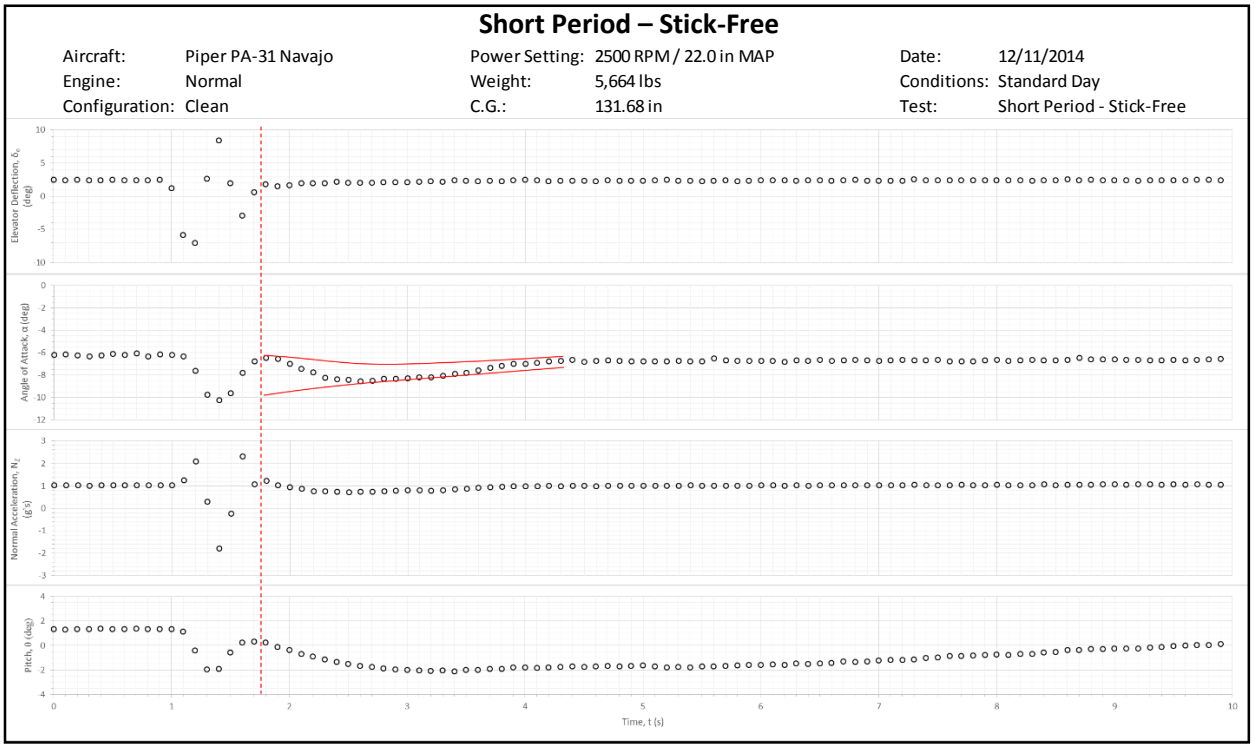


Figure 4.108 – Stick-Free Short Period for N11UT

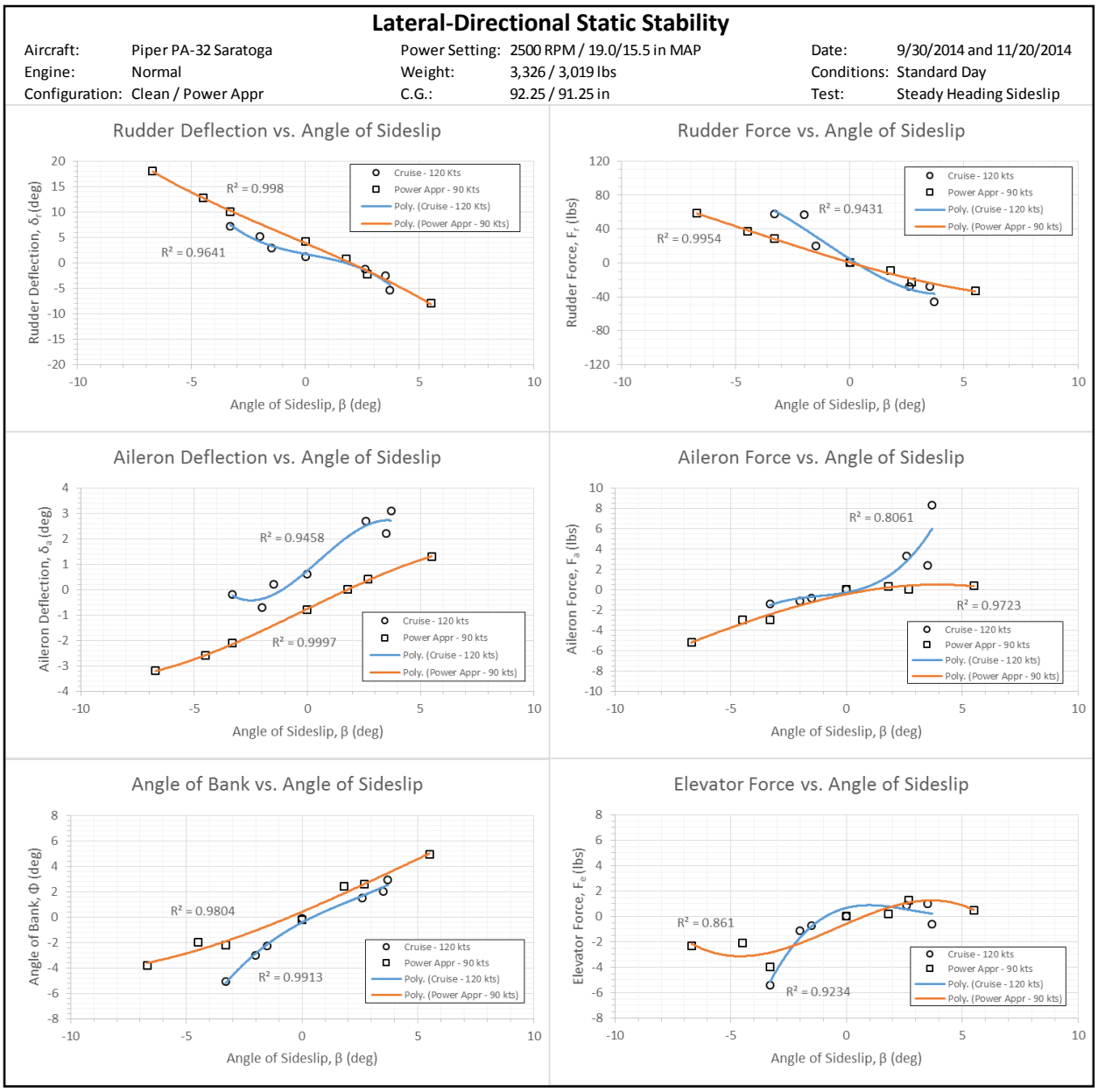


Figure 4.109 – Lateral-Directional Static Stability for N22UT

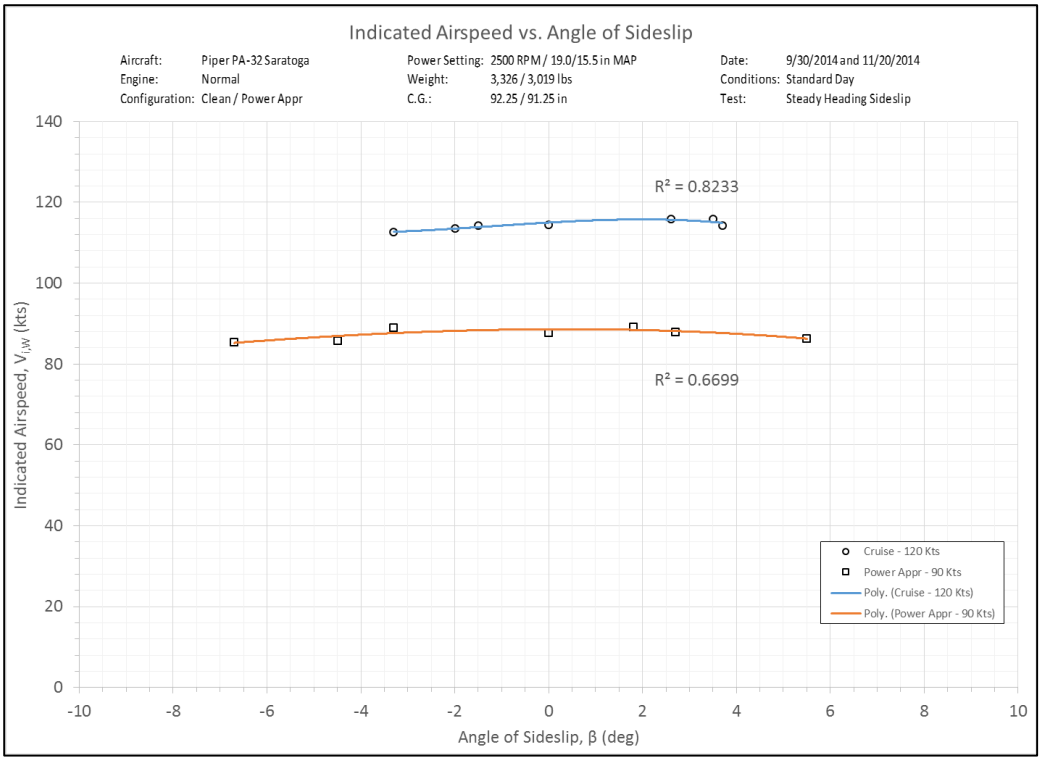


Figure 4.110 – Indicated Airspeed vs. Angle of Sideslip for N22UT

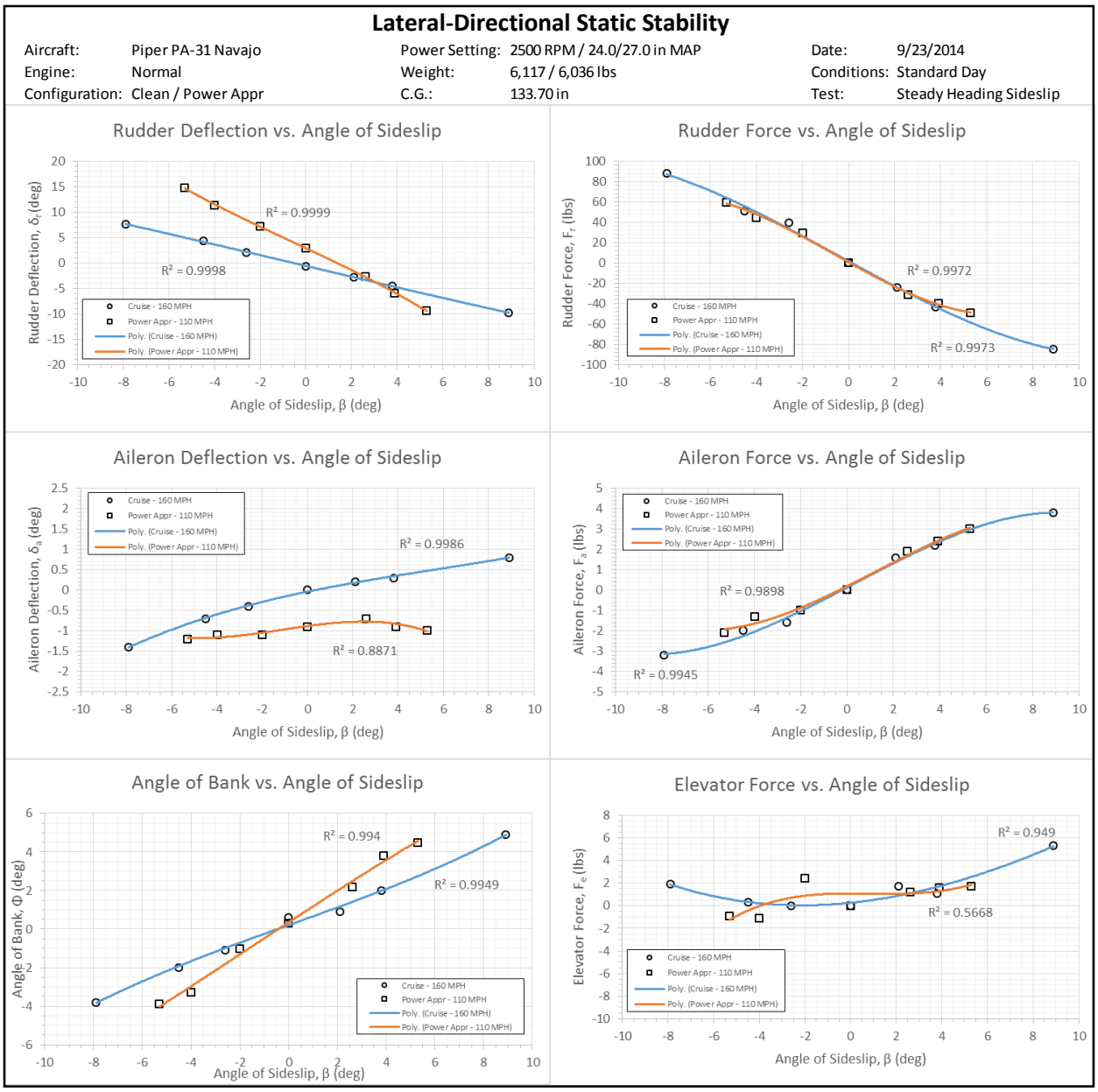


Figure 4.111 – Lateral-Directional Static Stability for N11UT

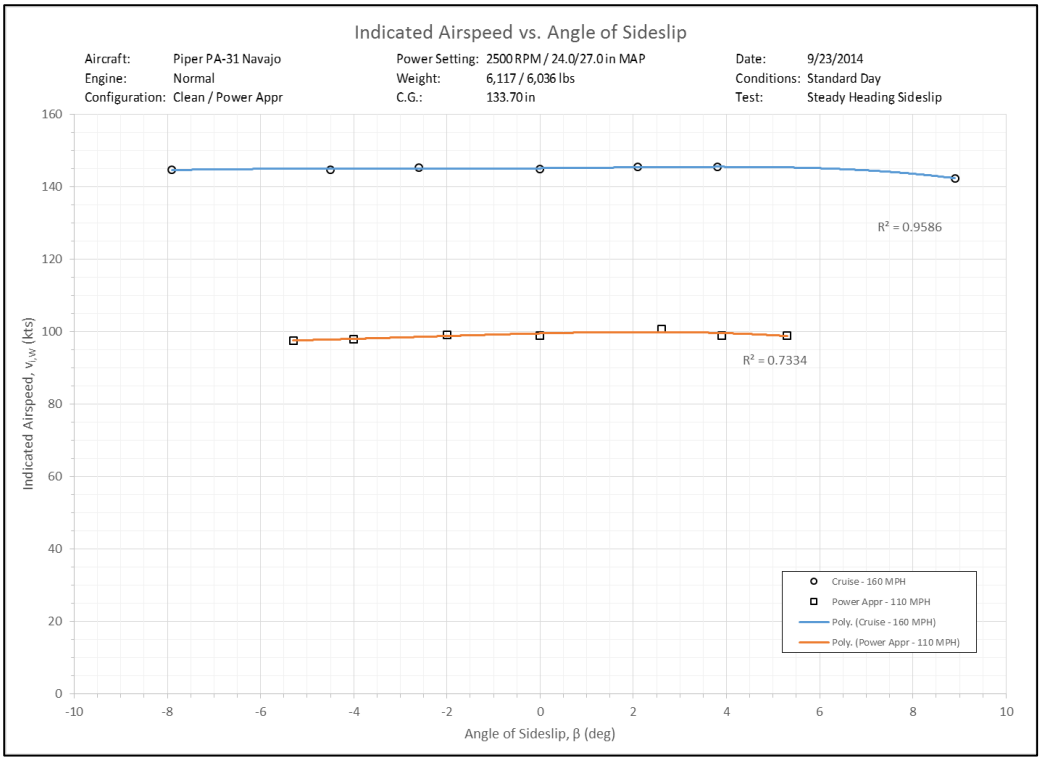


Figure 4.112 – Indicated Airspeed vs. Angle of Sideslip for N11UT

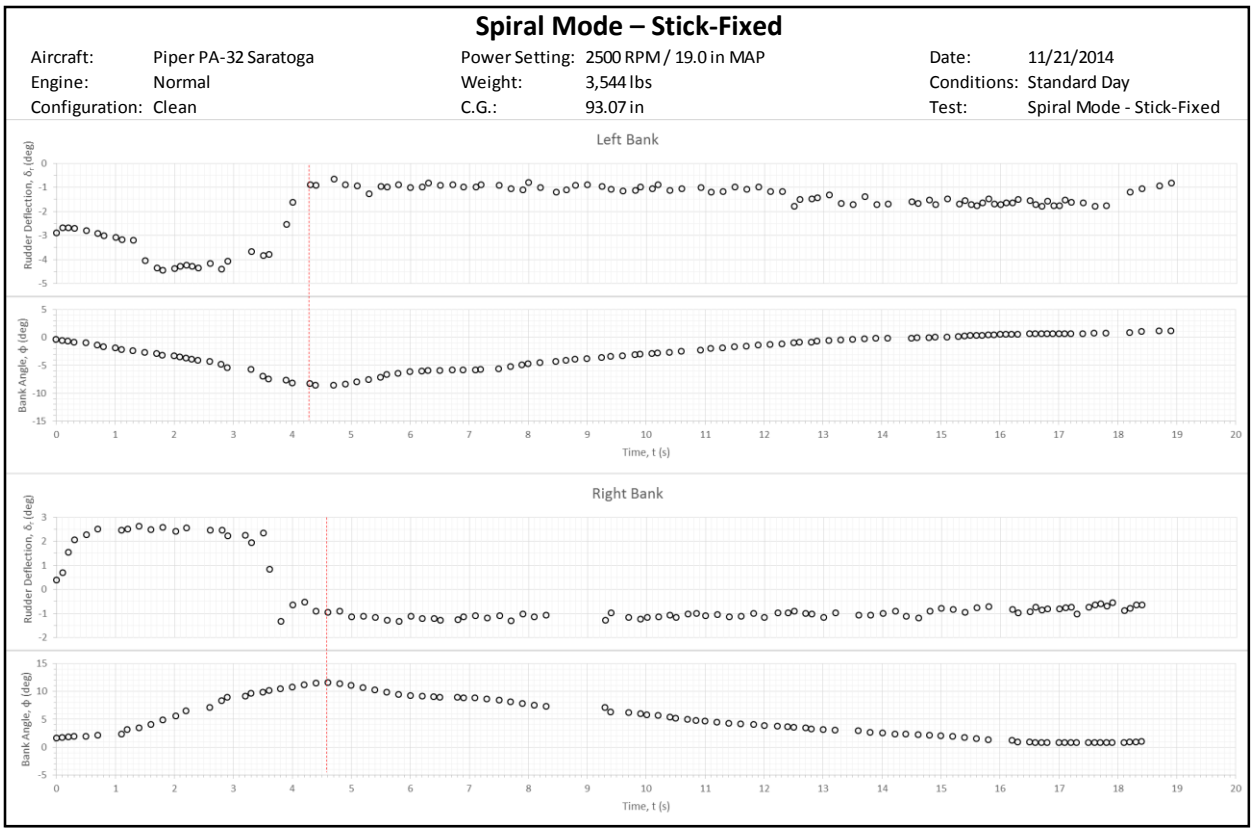


Figure 4.113 – Stick-Fixed Spiral Mode for N22UT

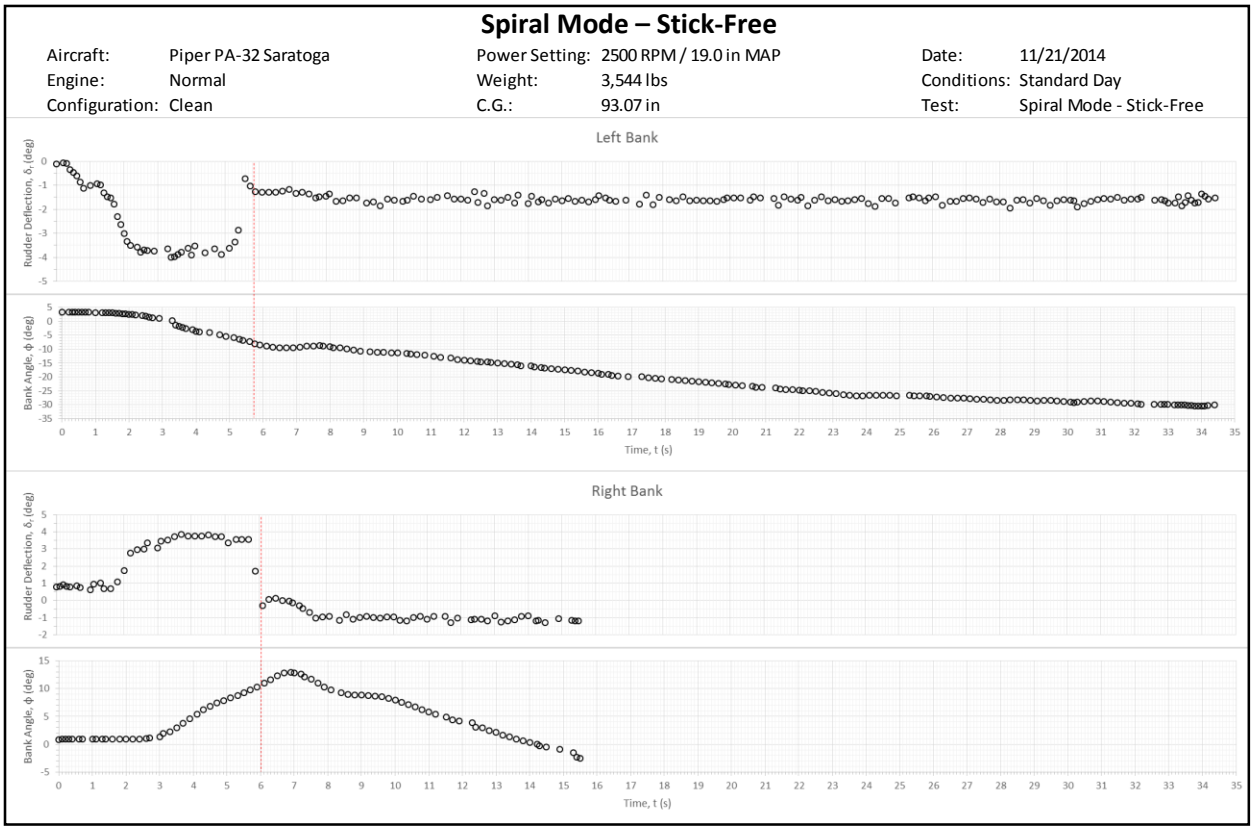


Figure 4.114 – Stick-Free Spiral Mode for N22UT

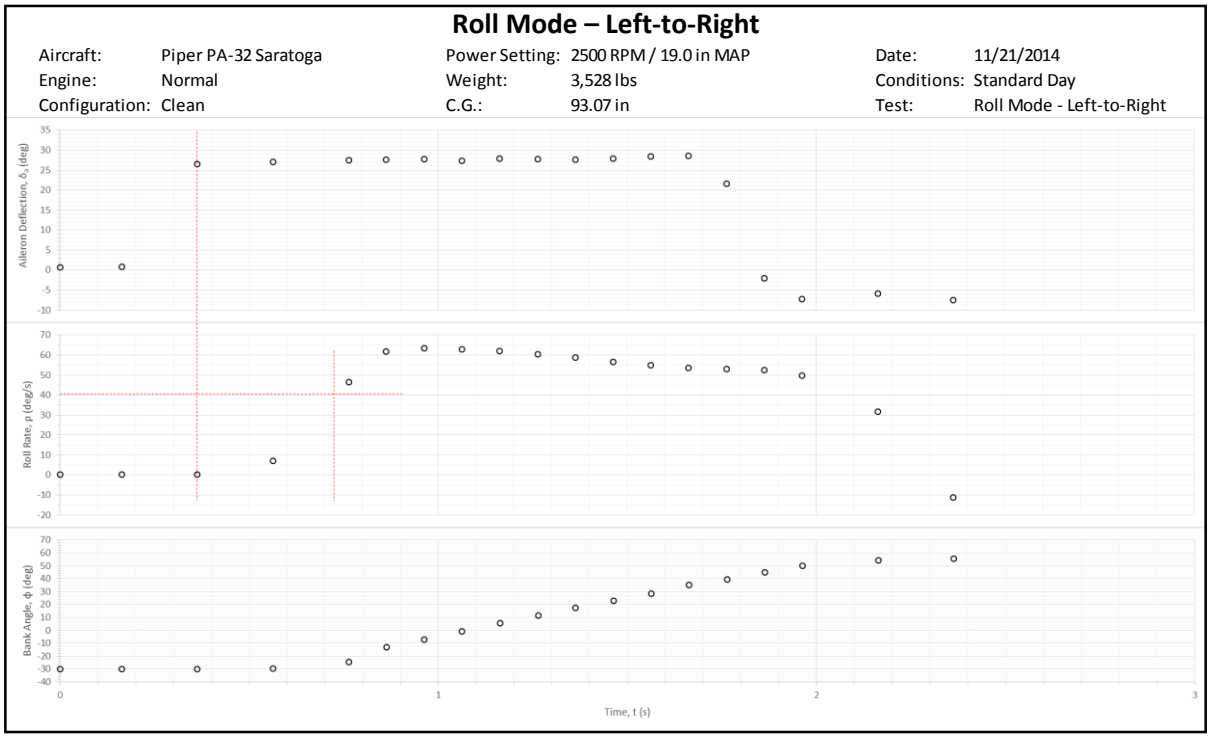


Figure 4.115 – Left-to-Right Roll Mode for N22UT

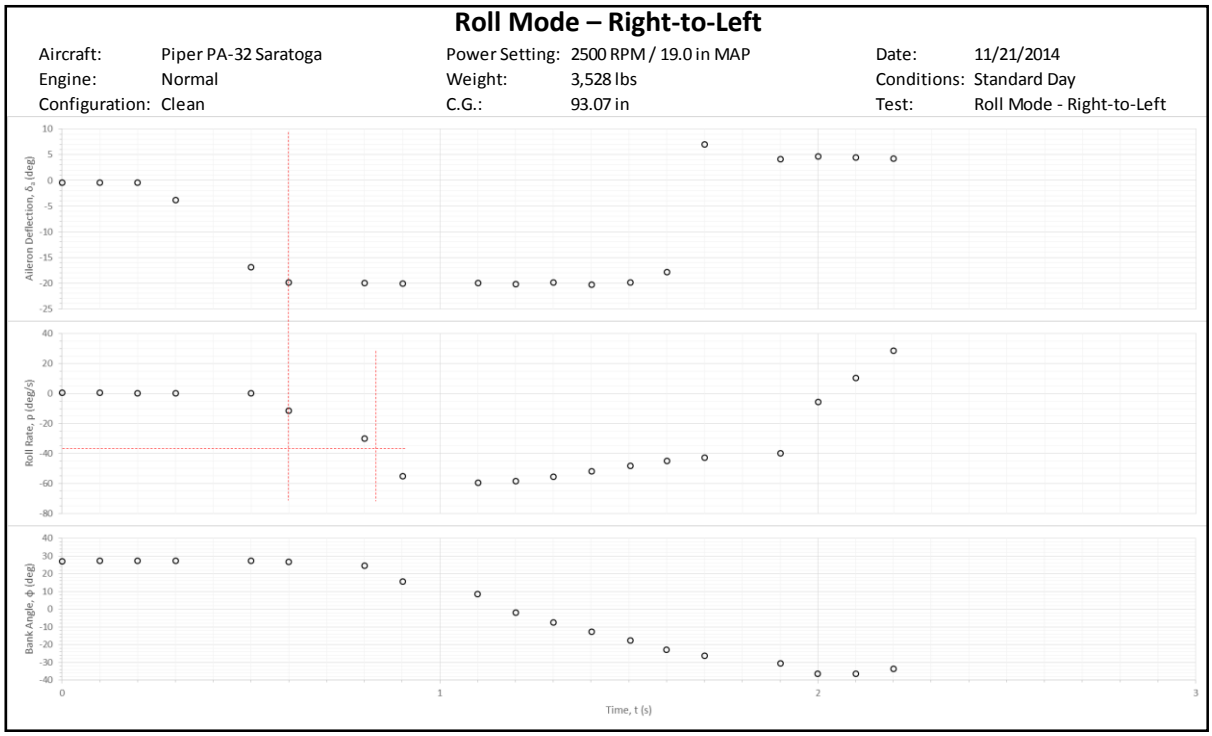


Figure 4.116 – Right-to-Left Roll Mode for N22UT

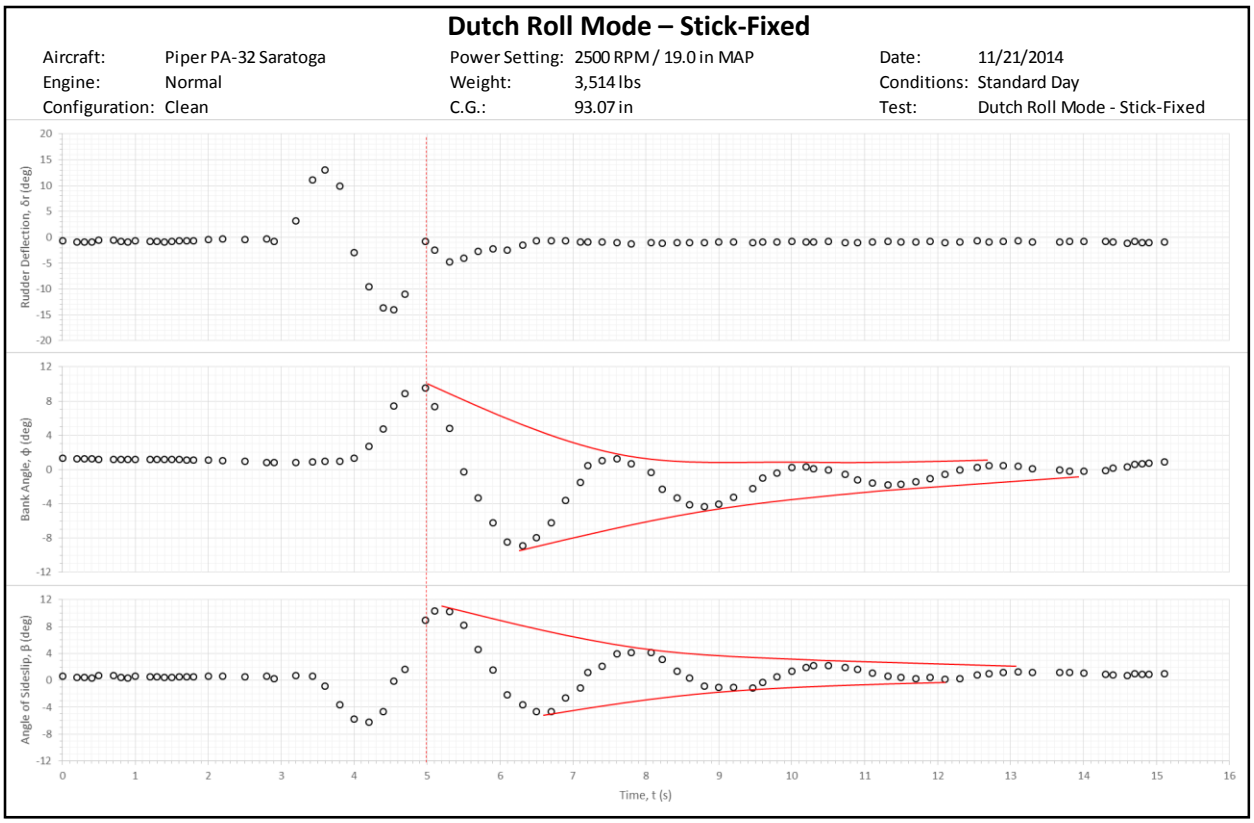


Figure 4.117 – Stick-Fixed Dutch Roll Mode for N22UT

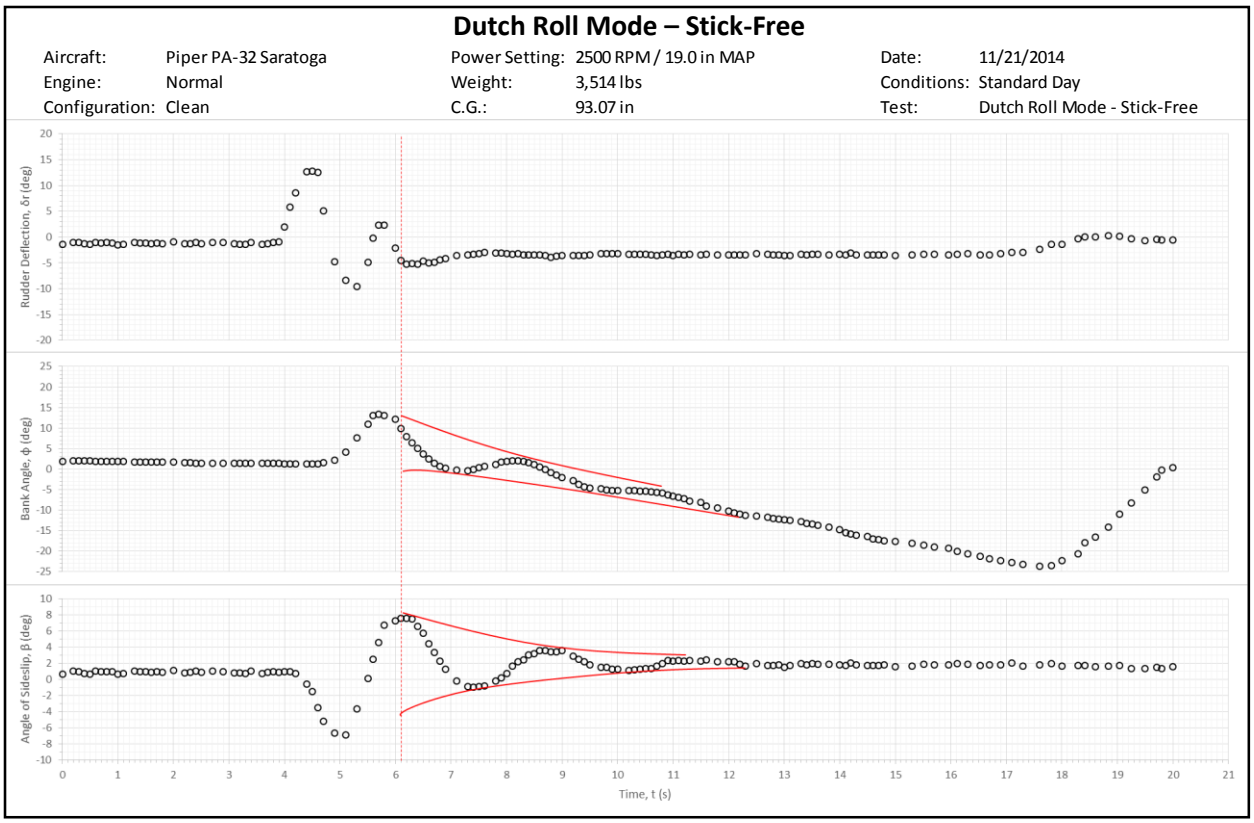


Figure 4.118 – Stick-Free Dutch Roll Mode for N22UT

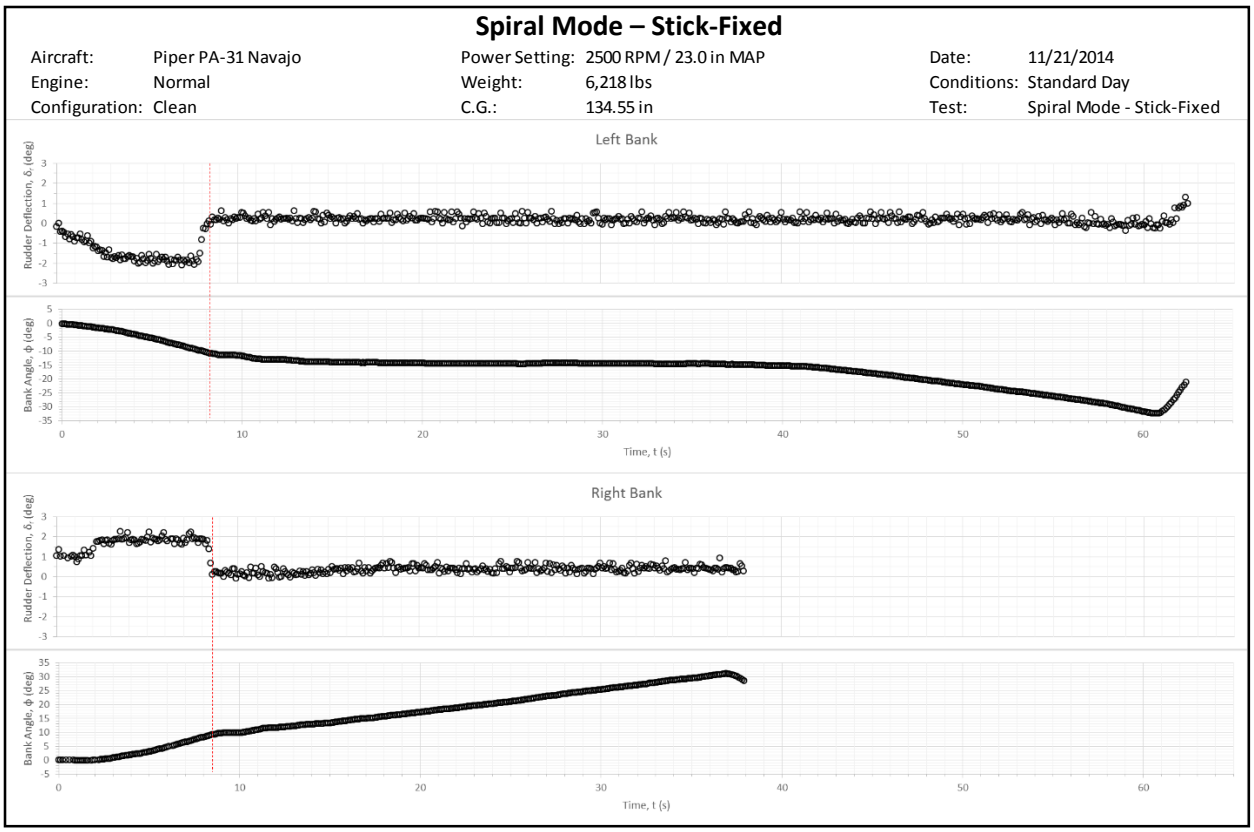


Figure 4.119 – Stick-Fixed Spiral Mode for N11UT

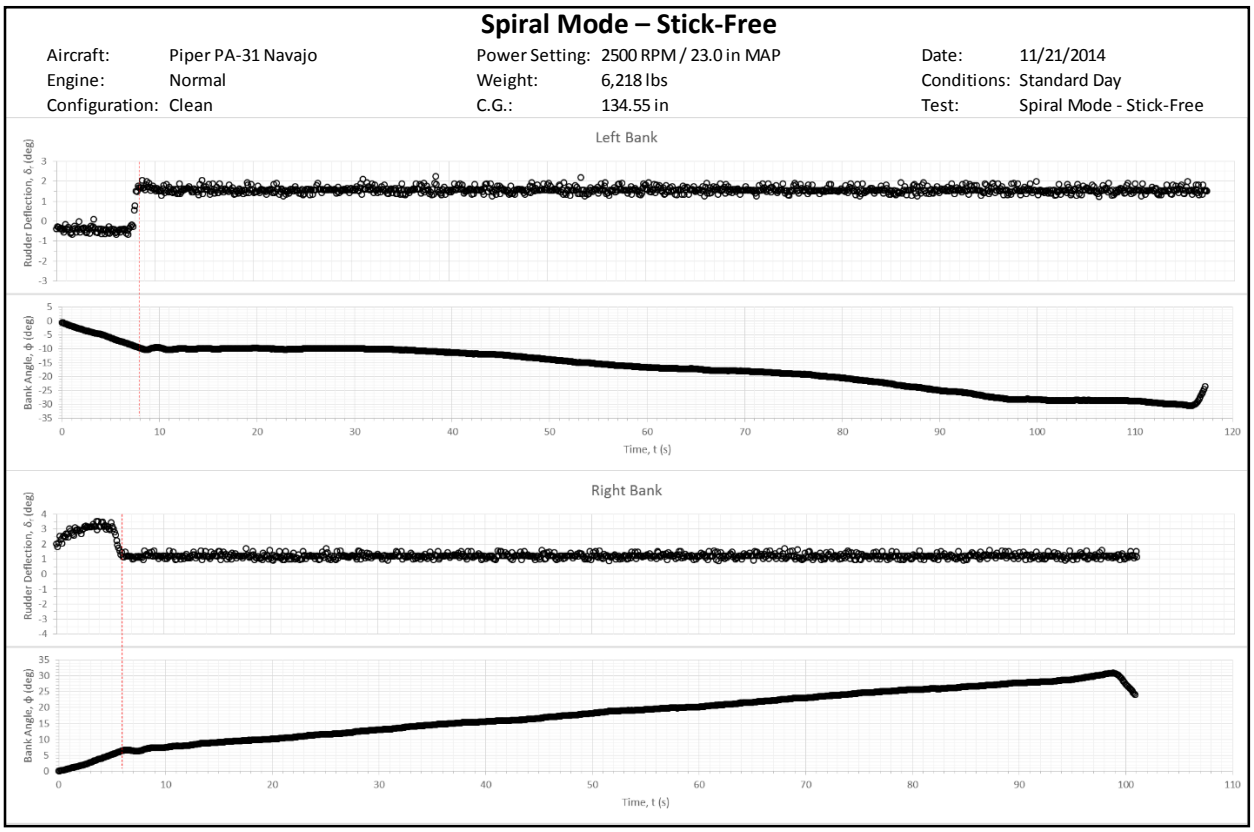


Figure 4.120 – Stick-Free Spiral Mode for N11UT

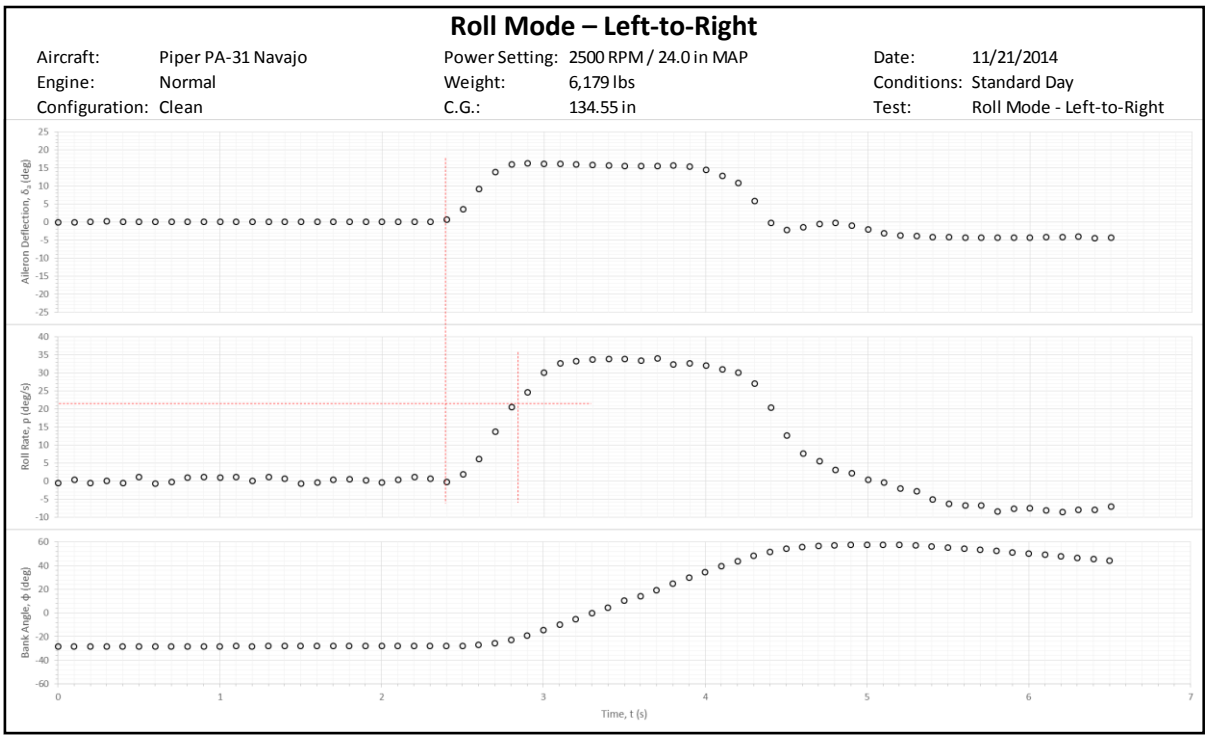


Figure 4.121 – Left-to-Right Roll Mode for N11UT

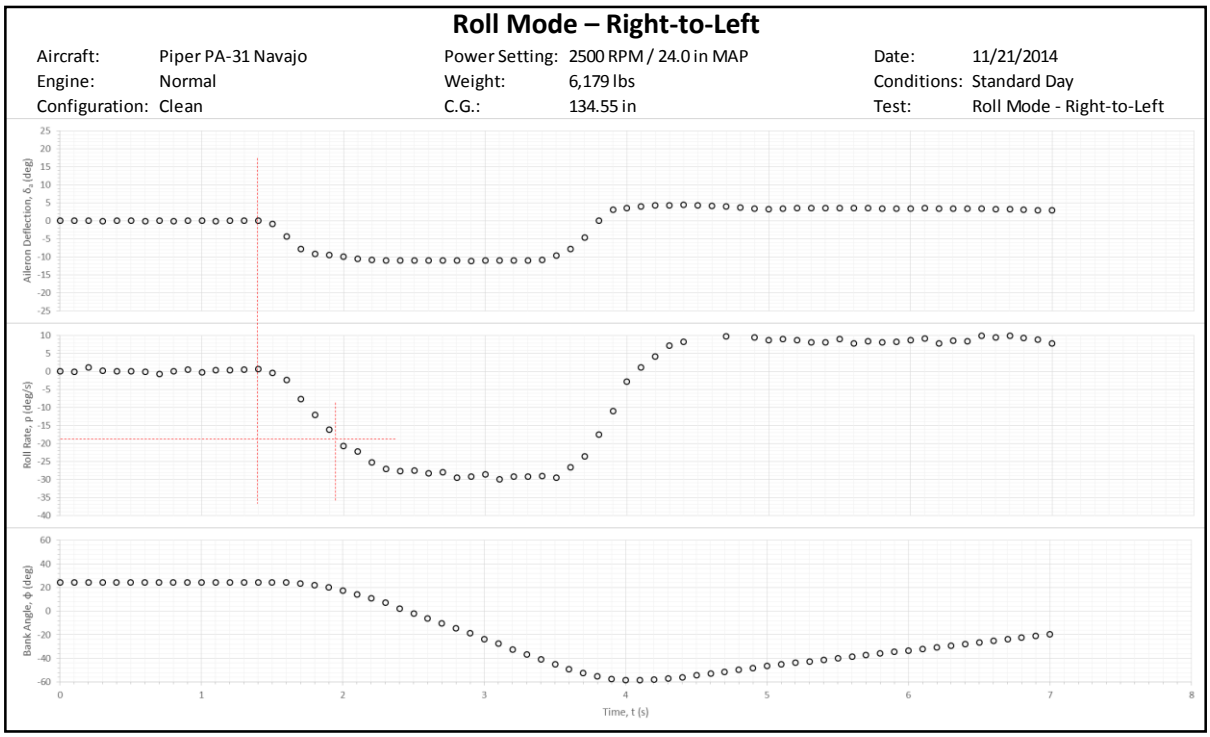


Figure 4.122 – Right-to-Left Roll Mode for N11UT

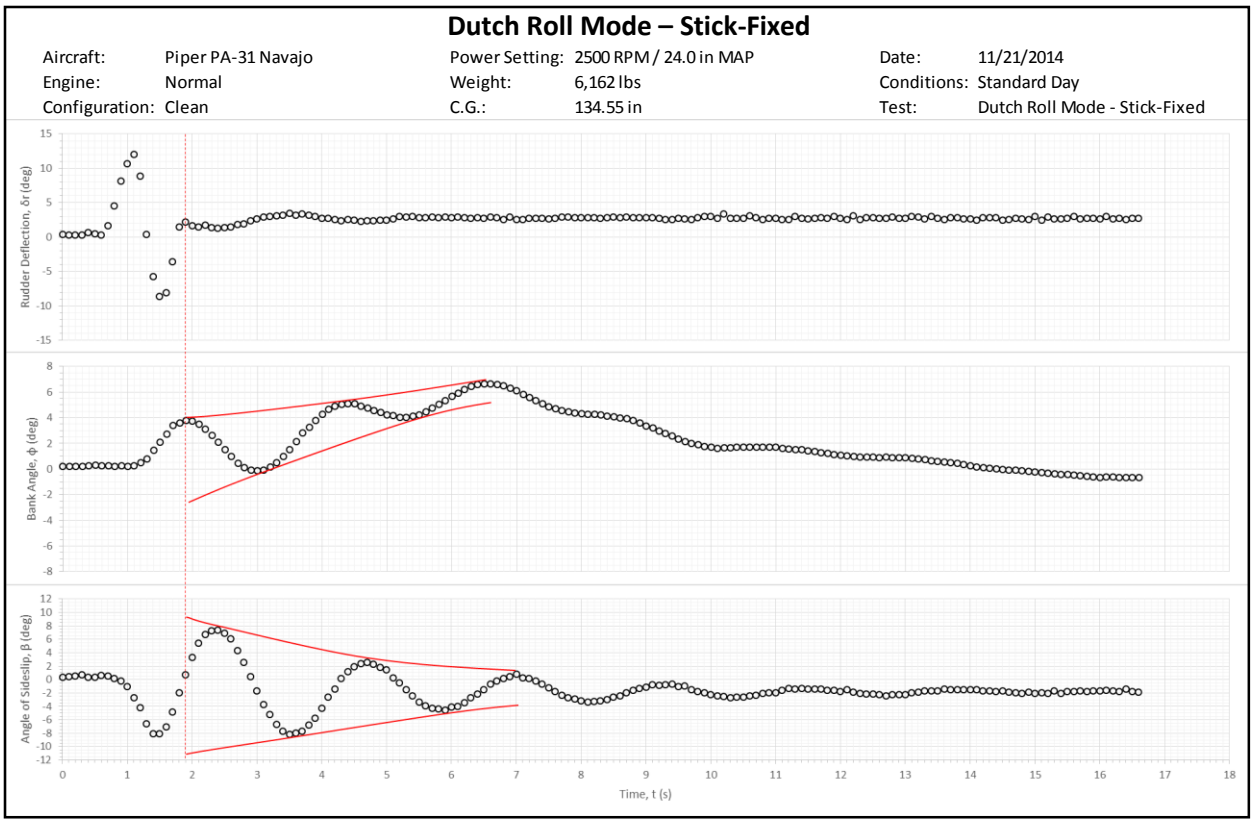


Figure 4.123 – Stick-Fixed Dutch Roll Mode for N11UT

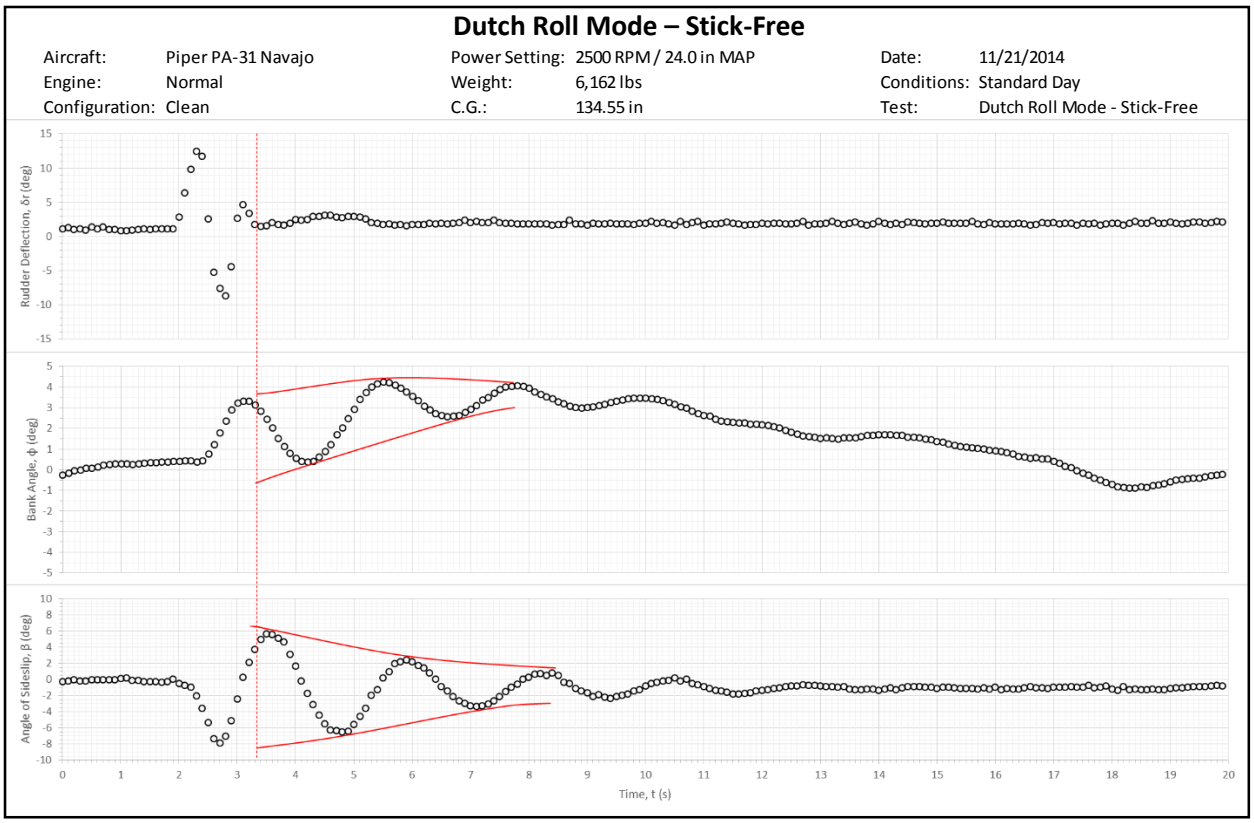


Figure 4.124 – Stick-Free Dutch Roll Mode for N11UT

APPENDIX B TABLES

Table 2.1 – Flight Test Parameter Details

Parameter	Units	Notes
Airspeed	Knots	
Altitude	Feet	Pressure altitude (29.92 inHg)
Outside Air Temperature	Saratoga - °F Navajo - °C	
Manifold Pressure	inHG	
RPM	RPM	
Fuel Quantity	Gallons	Not available in DAS
GPS Groundspeed	Knots	
GPS Track	Degrees	
Heading	Degrees	
Pitch	Degrees	Positive = Nose up
Roll	Degrees	Positive = Right
Angle of Attack	Degrees	Positive = Chordline leading edge above relative wind vector
Angle of Sideslip	Degrees	Positive = “Wind in right ear”
Aileron Deflection	Degrees	Positive = Right Trailing Edge Up
Aileron Force	Pounds	Positive = Right Yoke
Elevator Deflection	Degrees	Positive = Trailing Edge Up
Elevator Force	Pounds	Positive = Aft Yoke
Rudder Deflection	Degrees	Positive = Trailing Edge Right
Rudder Force	Pounds	Positive = Right Pedal Forward
Longitudinal Acceleration	G’s	Positive = Forward
Lateral Acceleration	G’s	Positive = Right
Normal Acceleration	G’s	Positive = Down (Saratoga) Up (Navajo)
Pitch Rate	Degrees/second	Positive = Pitch up
Roll Rate	Degrees/second	Positive = Roll right
Yaw Rate	Degrees/second	Positive = Yaw right

Table 4.1 – Comparison of Saratoga Values of Rate of Climb Using the Sawtooth Climb Method

	3,600 lbs		3,000 lbs	
Density Altitude (ft)	**Calculated ROC (ft/min)**	**Published ROC (ft/min)**	**Calculated ROC (ft/min)**	**Published ROC (ft/min)**
0	800	980	1,200	1,260
5,000	550	660	900	980
10,000	275	420	600	700

Table 4.2 – Comparison of Navajo Values of Rate of Climb Using the Sawtooth Climb Method

	6,500 lbs		5,500 lbs	
Density Altitude (ft)	**Calculated ROC (ft/min)**	**Published ROC (ft/min)**	**Calculated ROC (ft/min)**	**Published ROC (ft/min)**
0	1,075	1,250	1,550	1,650
5,000	975	1,150	1,450	1,550
10,000	875	1,050	1,375	1,450

Table 4.3 – Saratoga Stall Speeds in Clean Configuration

	V_{Siw} (kts)	V_{SC} (kts)	$V_{SC\text{-}CG}$ (kts)	$V_{Siw\text{-}CG}$ (kts)	Entry Rate (kts/s)
Stall A	50.3	63.1	65.8	56.9	-1.1
Stall A-1	48.3	61.8	64.4	55.2	-0.5
Stall A-2	46.6	60.7	63.4	53.9	-0.8
Stall A-3	46.9	60.9	63.8	54.3	-1.4
Average	**48.0**	**61.6**	**64.4**	**55.1**	**-1.0**

Table 4.4 – Saratoga Stall Speeds in Landing Configuration

	V_{Siw} (kts)	V_{SC} (kts)	$V_{SC\text{-}CG}$ (kts)	$V_{Siw\text{-}CG}$ (kts)	Entry Rate (kts/s)
Stall B	41.8	57.7	60.4	49.9	-0.8
Stall B-1	42.9	58.4	61.2	50.9	-0.7
Stall B-2	43.9	59.0	61.9	51.9	-0.6
Stall B-3	44.8	59.6	62.7	52.8	-0.6
Average	**43.3**	**58.7**	**61.6**	**51.4**	**-0.7**

Table 4.5 – Saratoga Stall Speeds in 30° Bank, Clean Configuration

	V_{Siw} (kts)	V_{SC} (kts)	V_{SC-CG} (kts)	V_{Siw-CG} (kts)	Entry Rate (kts/s)
Stall C	53.0	64.8	68.3	60.2	-1.0
Stall C-1	50.8	63.5	67.0	85.5	-1.3
Stall C-2	52.8	64.8	68.4	60.4	-0.6
Stall C-3	52.2	64.4	68.0	59.9	-0.5
Average	**52.2**	**64.4**	**67.9**	**59.7**	**-0.9**

Table 4.6 – Navajo Stall Speeds in Clean Configuration

	V_{Siw} (kts)	V_{SC} (kts)	V_{SC-CG} (kts)	V_{Siw-CG} (kts)	Entry Rate (kts/s)
Stall A	71.5	70.3	71.6	70.4	-0.9
Stall A-1	71.5	70.3	71.7	70.5	-1.1
Stall A-2	69.9	68.9	70.0	69.0	-0.9
Stall A-3	73.0	71.6	73.2	71.8	-0.8
Stall A-4	72.9	71.5	73.1	71.7	-0.7
Stall A-5	71.7	70.5	71.9	70.7	-0.9
Average	**71.8**	**70.5**	**71.9**	**70.7**	**-0.9**

Table 4.7 – Navajo Stall Speeds in Landing Configuration

	V_{Siw} (kts)	V_{SC} (kts)	V_{SC-CG} (kts)	V_{Siw-CG} (kts)	Entry Rate (kts/s)
Stall B	63.2	63.1	63.3	63.2	-1.6
Stall B-1	63.0	63.0	63.2	63.1	-1.4
Stall B-2	63.3	63.2	63.5	63.4	-1.8
Stall B-3	64.7	64.4	64.9	64.6	-0.9
Stall B-4	64.9	64.6	65.1	64.8	-0.9
Stall B-5	64.6	64.4	64.8	64.5	-0.8
Average	**64.0**	**63.8**	**64.1**	**63.9**	**-1.2**

Table 4.8 – Navajo Stall Speeds in 30° Bank, Clean Configuration

	V_{Siw} (kts)	V_{SC} (kts)	V_{SC-CG} (kts)	V_{Siw-CG} (kts)	Entry Rate (kts/s)
Stall C	79.0	76.8	79.2	77.0	-0.9
Stall C-1	74.9	73.2	75.1	73.4	-0.9
Stall C-2	79.4	77.2	79.6	77.4	-0.9
Stall C-3	79.7	77.5	79.9	77.6	-0.7
Average	**78.2**	**76.2**	**78.4**	**76.4**	**-0.9**

APPENDIX C LOCATION OF ADDITIONAL DOCUMENTATION

All standardized materials (i.e. flight data cards, reduction spreadsheets, and reduction procedures); video footage; thesis data (i.e. flight data, flight data cards, and reduction spreadsheets); engine power charts; and calibration files can be located on an external hard drive located at the Aviation System and Flight Research Department hangar.

APPENDIX D METHODS FOR DETERMINING DAMPING RATIO

D.1 Subsidence Ratio Method or Log Decrement Method

1) Determine airspeed deviations, X_n, from mean value using Figure D.1.

2) Calculate airspeed deviation ratios (minimum of 3).

$$m = \left|\frac{X_n}{X_0}\right| \tag{D.1}$$

3) Calculate m for each ratio (i.e. m=1,2,3,etc.).

$$m = i - j \; where \; ratio \; is \; \left|\frac{X_i}{X_j}\right| \tag{D.2}$$

4) Using Subsidence Ratio Plot, Figure D.2, determine ζ_m.

5) Calculate damping ratio.

$$\zeta = \frac{\sum \zeta_m}{n} \; where \; n \; is \; number \; of \; \zeta_m's \tag{D.3}$$

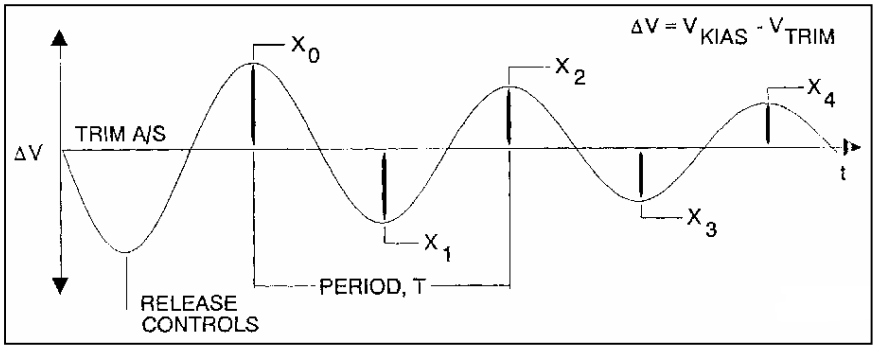


Figure D.1 – Airspeed Deviations

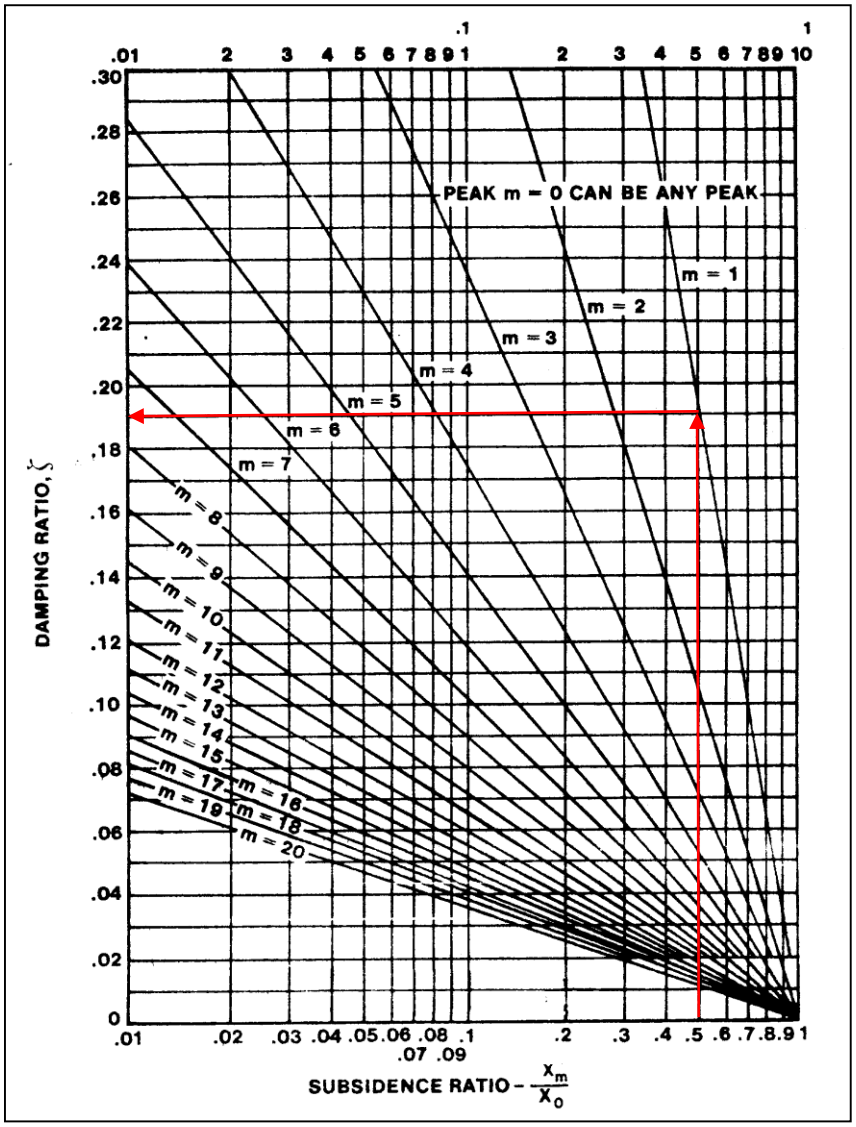


Figure D.2 – Subsidence Ratio Plot

D.2 Transient Peak Ratio Method

1) Determine peak-to-peak deviations, X_n, using Figure D.3.

2) Calculate airspeed deviation ratios (minimum of 3). Note: m=1 for all ratios.

$$m = \left|\frac{X_1}{X_0}\right|, \left|\frac{X_2}{X_1}\right|, \left|\frac{X_3}{X_2}\right| \tag{D.4}$$

3) Using Transient Peak Ratio Plot, Figure D.4 determine ζ_m.

4) Calculate damping ratio.

$$\zeta = \frac{\sum \zeta_m}{n} \; where \; n \; is \; number \; of \; \zeta_m's \tag{D.5}$$

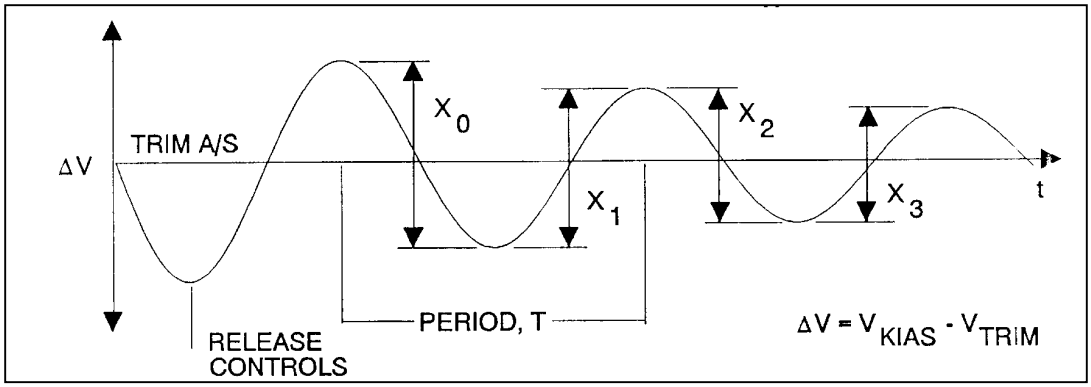


Figure D.3 – Peak-to-Peak Deviations

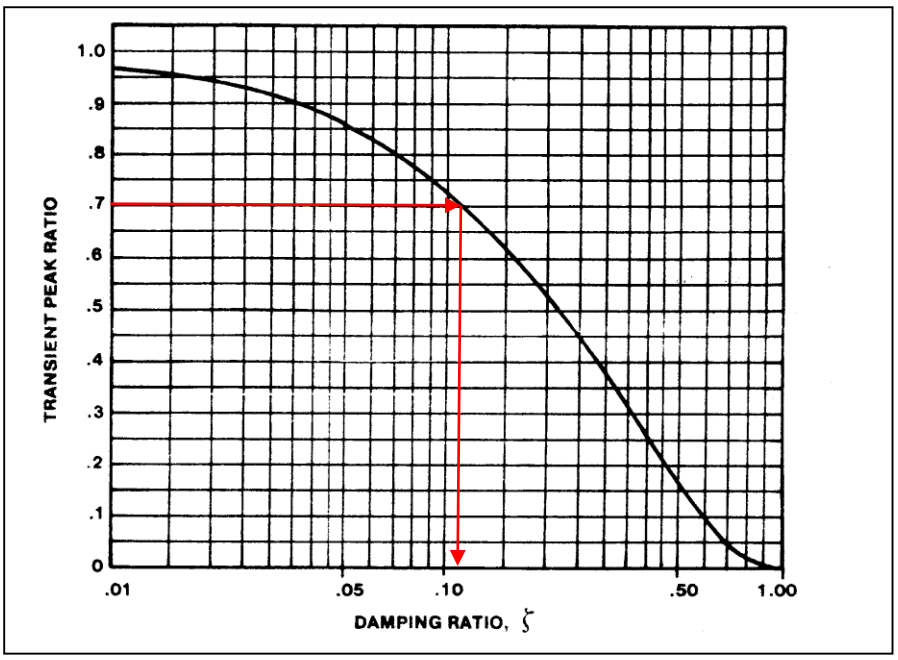


Figure D.4 – Transit Peak Ratio Plot

D.3 Time Ratio Method

1) Determine maximum value after controls are released.

2) Mark 100%, 73.6%, 40.9%, and 19.9% of max value as seen in Figure D.5.

3) Measure time from t_0=0 (at max value) to t_1, t_2, and t_3.

4) Calculate time ratios.

$$\frac{t_2}{t_1}, \frac{t_3}{t_1}, \frac{t_3 - t_2}{t_2 - t_1} \tag{D.6}$$

5) Using Time Ratios, determine ζ_t from Time Ratio Plot using dashed lines in Figure D.6.

6) Calculate damping ratio.

$$\zeta = \frac{\sum \zeta_m}{n} \; where \; n \; is \; number \; of \; \zeta_m's \tag{D.7}$$

7) Using ζ, determine Frequency Time Product, $\omega_n \Delta t_i$, from Time Ratio Plot using solid lines in Figure D.7.

8) Calculate $\omega_{n\text{-}i}$ for each Frequency Time Product.

$$\omega_{n_i} = \frac{\omega_n \Delta t_i}{t_i} \tag{D.8}$$

9) Calculate Average Undamped Natural Frequency, ω_n.

$$\omega_n = \frac{\sum_{i=1}^{3} \omega_{n_i}}{3} \tag{D.9}$$

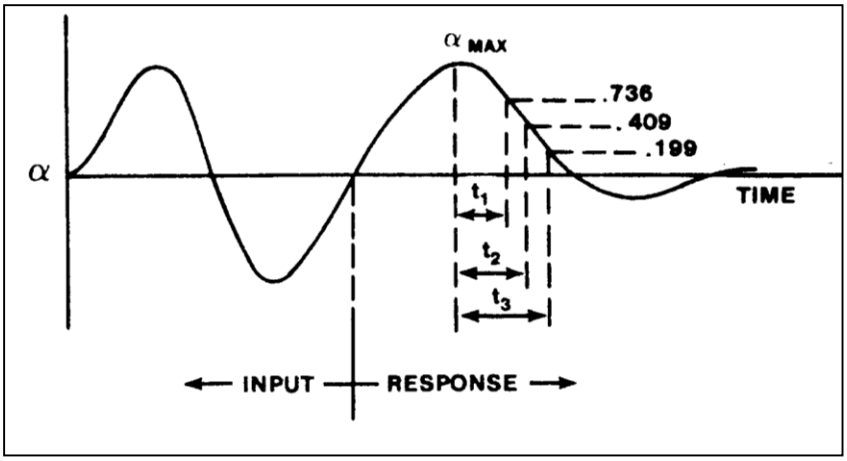


Figure D.5 – Maximum Parameter Value

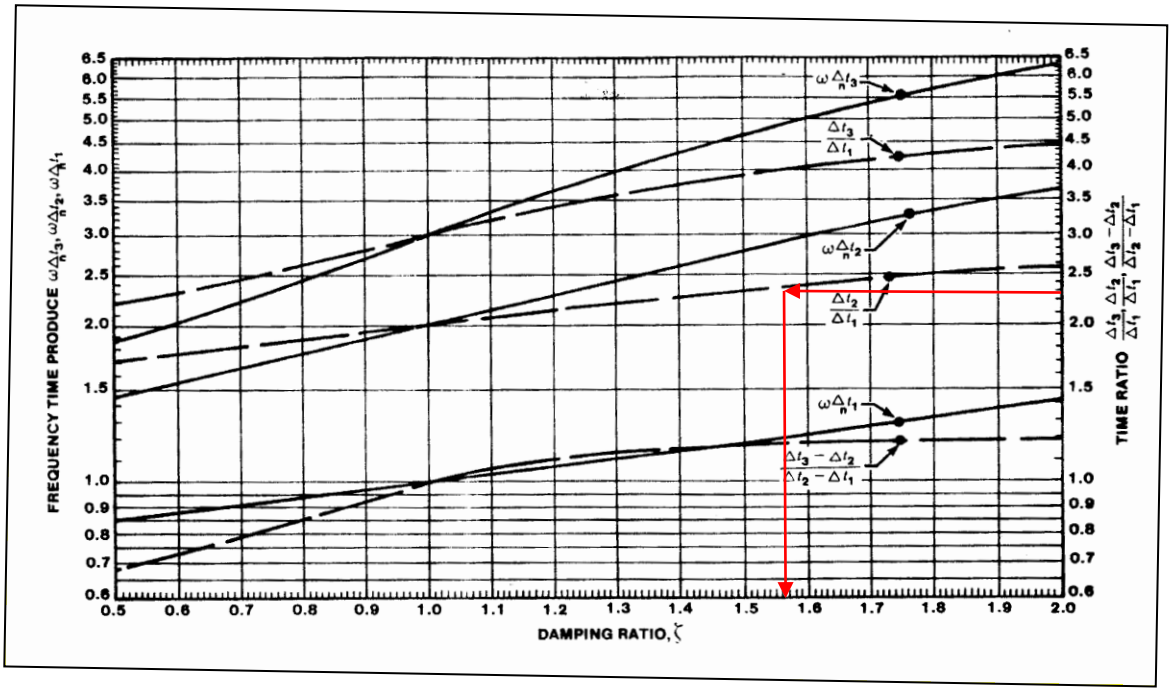


Figure D.6 – Time Ratio Plot – Determining Damping Ratio

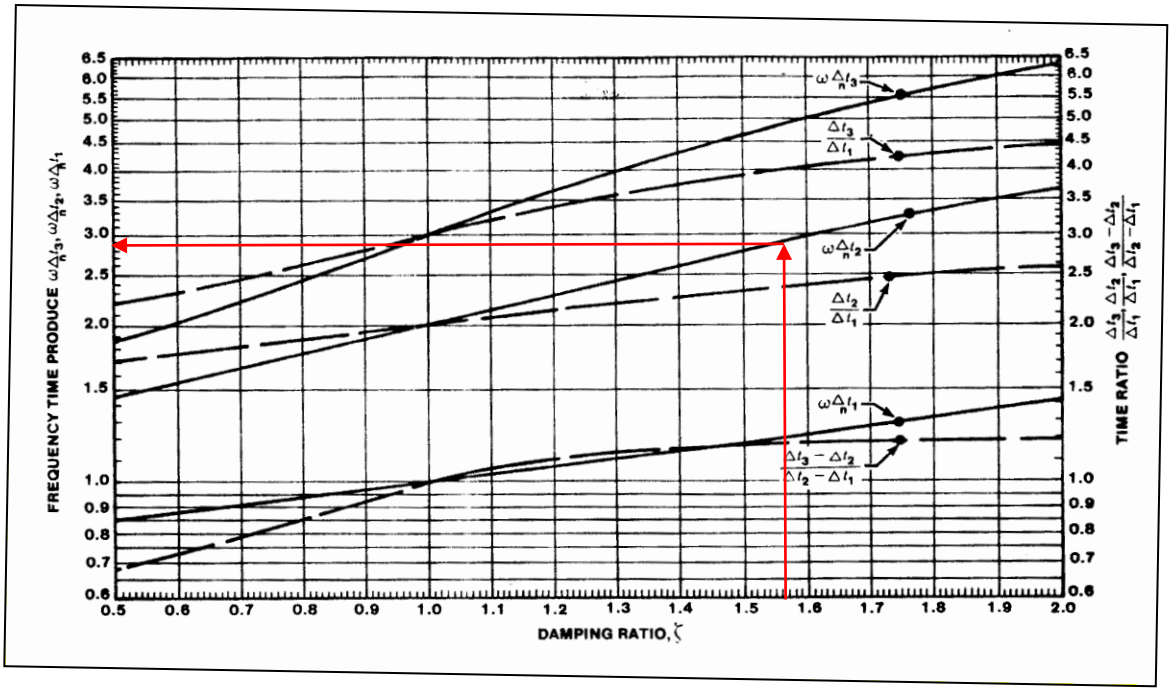


Figure D.7 – Time Ratio Plot – Determining Frequency

D.4 Log Decrement Equation Method

1) Determine values of X_0 and X_n as seen in Figure D.8.

2) Calculate δ.

$$\delta = \ln\left[\left(\frac{X_0}{X_n}\right)^{1/n}\right] \tag{D.10}$$

3) Calculate ζ.

$$\zeta = \frac{\delta}{\sqrt{\delta^2 + 4\pi^2}} \tag{D.11}$$

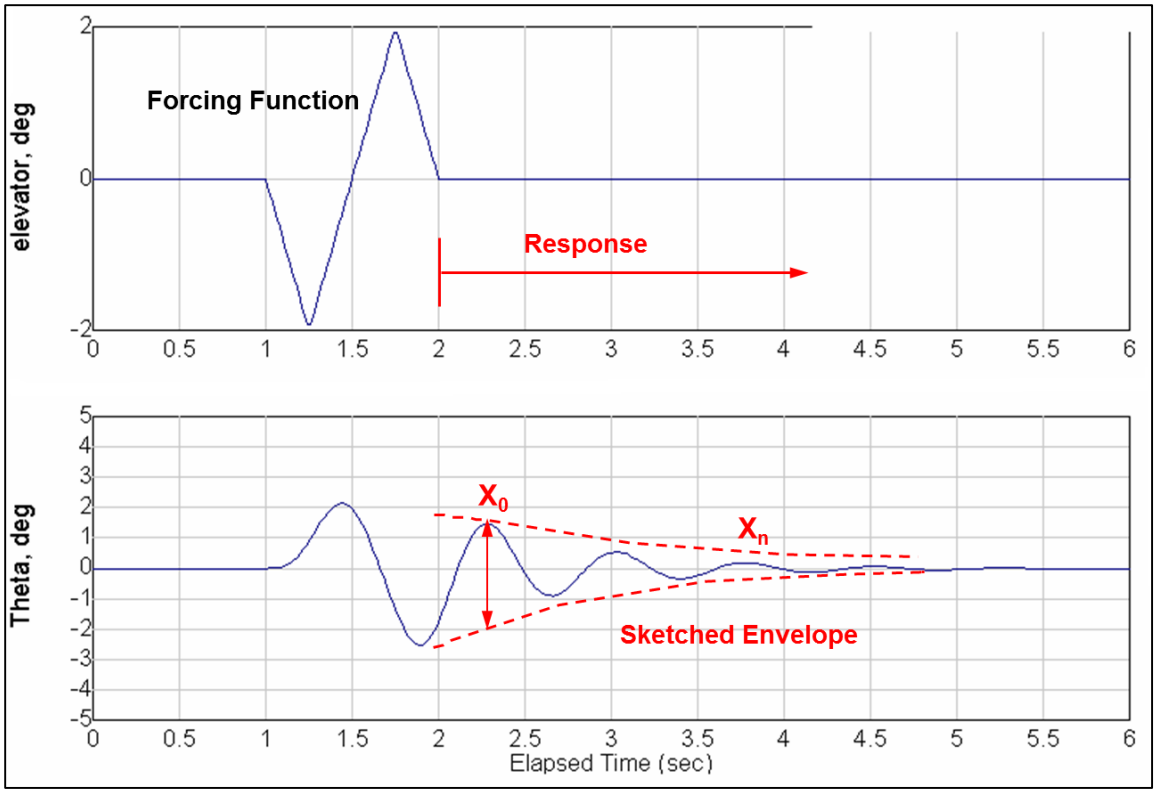


Figure D.8 – Determining X_0 and X_n

VITA

Matthew DiMaiolo was born in Trenton, NJ as the youngest of three. He grew up in Germantown, TN and graduated Houston High School in 2006. He attended Middle Tennessee State University with a major in Aerospace: Professional Pilot and a minor in Physics and in 2010 he graduated with a Bachelor of Science degree. After several years of working in aviation, he returned to school to pursue a master's degree in Aviation Systems at the University of Tennessee Space Institute. He graduated May 2015 with a Master of Science degree.